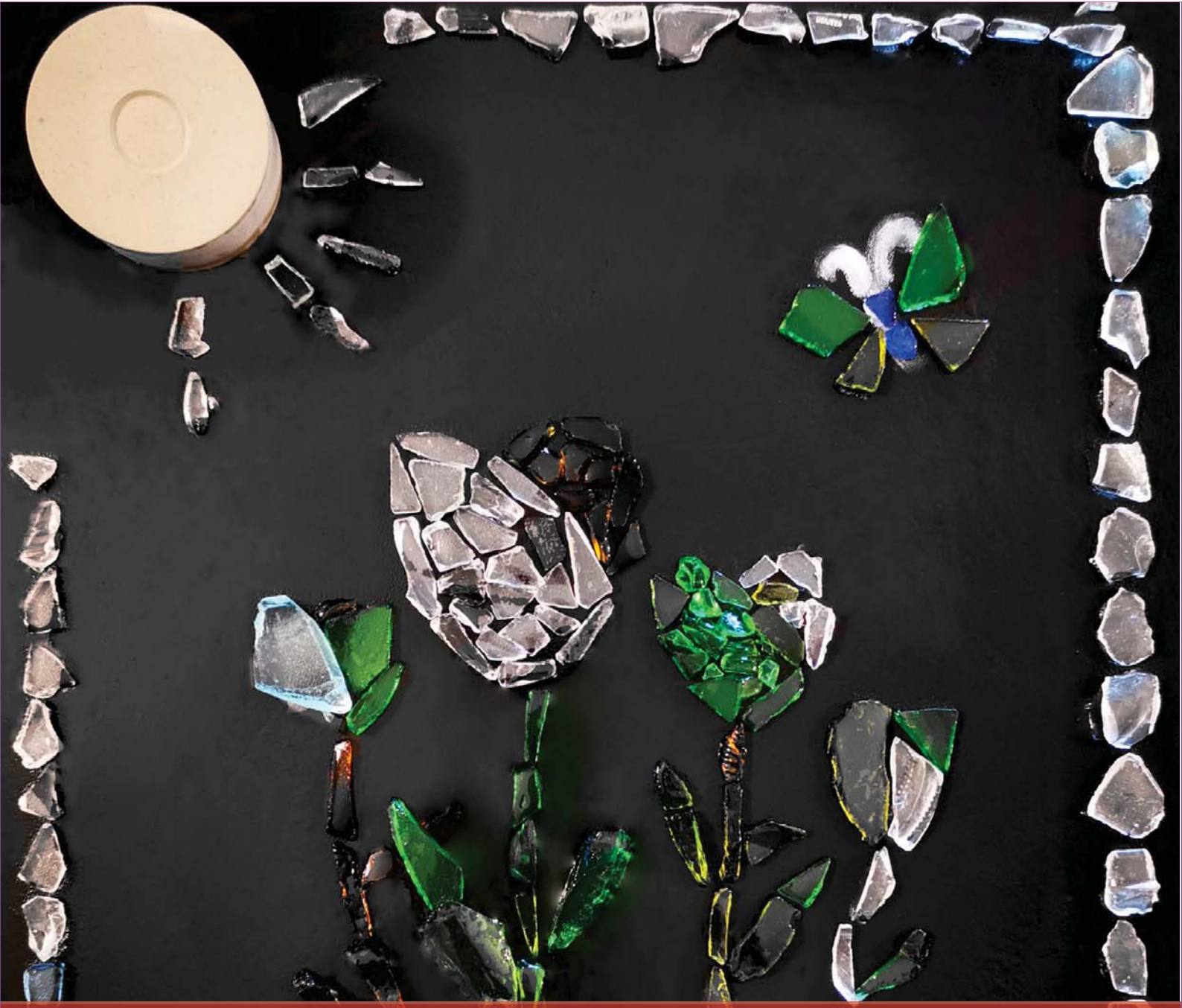

Valorization of Recycled Waste Glass and Converter Steel Slag as Ingredients for Building Materials

HYDRATION AND CARBONATION STUDIES

Gang Liu

Bouwstenen 304

Valorization of Recycled Waste Glass and Converter Steel Slag as Ingredients for Building Materials

Hydration and Carbonation Studies

PROEFSCHRIFT

ter verkrijging van de graad van doctor
aan de Technische Universiteit Eindhoven,
op gezag van de rector magnificus, prof.dr.ir. F.P.T. Baaijens,
voor een commissie aangewezen door het College voor Promoties,
in het openbaar te verdedigen op dinsdag 17 november 2020 om 16:00 uur

door

Gang Liu

geboren te Shaanxi, China

CIP-DATA LIBRARY TECHNISCHE UNIVERSITEIT EINDHOVEN

Valorization of Recycled Waste Glass and Converter Steel Slag as Ingredients for Building Materials: Hydration and Carbonation Studies/ by Gang Liu

A catalogue record is available from the Eindhoven University of Technology Library

ISBN: 978-90-386-5160-6

Bouwstenen 304

NUR 955

Cover design: Gang Liu & Xuan Ling

Ph.D. thesis, Eindhoven University of Technology, the Netherlands

Dit proefschrift is goedgekeurd door de promotoren en de samenstelling van de promotiecommissie is als volgt:

Voorzitter:	prof. dr. ir. T.A.M. Salet
Promotor:	prof. dr. ir. H.J.H. Brouwers
Copromotor 1:	dr. dipl.-Ing. M.V.A. Florea
Copromotor 2:	dr. K. Schollbach
Leden:	prof. dr. M. Illikainen (University of Oulu)
	prof. dr. W. Chen (Wuhan University of Technology)
	prof. dr.-Ing. P.M. Teuffel
	prof. dr. N. De Belie (Ghent University)
	prof. dr. S.R. van der Laan

Het onderzoek of ontwerp dat in dit proefschrift wordt beschreven is uitgevoerd in overeenstemming met de TU/e Gedragscode Wetenschapsbeoefening.

Dedicated to my parents

Preface

I started my research on 1st October 2016 in the group of Building Materials, Department of Built Environment, Eindhoven University of Technology (TU/e), in the Netherlands under the leadership of Prof. H.J.H. (Jos) Brouwers. This research is supported by China Scholarship Council and Eindhoven University of Technology. Since my PhD research is going to the end, I would like to express my sincere gratitude to people who helped and supported me on my 4 years' study.

Firstly, I would like to express my sincere appreciation to my promotor and supervisor Prof. H.J.H. (Jos) Brouwers. You provided me such a valuable opportunity to be a member of this group 4 years ago. A new research field was open for me by your guidance and support. During my PhD study, you offered me all the necessary conditions for my investigation, as well as enough trust. The suggestions from you always gave me new insights to improve my study and thesis. I had a chance to cooperate with excellent experts from industrial companies because of your recommendation, from which I learned and benefited a lot.

Secondly, I am grateful to my daily supervisor and co-promotor Dr. M.V.A. (Miruna) Florea. You helped me with the preparation of my proposal for the application of scholarship before I arrived here, which gave me a deep impression. I still remember the first day I met you in our office and you introduced everyone in our group to me. In that day, it rained five times, which also surprised me. You gave me enough freedom and trust to finish my research during my 4 years of PhD study. You always encouraged and inspired me when I was in trouble with my research. Optimism is such important for a researcher and I really learned it from you. The gratitude also goes to Dr. Katrin Schollbach, I cannot finish my PhD study and thesis without your help. You supported me with your professional knowledge and suggestions. You contributed a lot to my scientific paper writing and revising. I am so lucky to have had you as my daily supervisor.

I am sincerely thank to my master supervisor Prof. Henghui Fan, who guided me in the field of civil engineering. You taught me how to do research independently and gave me a lot of help with my CSC application. Prof. Jinqian Dang, Prof. Aijun Zhang and Prof. Yasheng Luo from Northwest A&F University, I appreciate to your high-quality education during my master study.

I also would like to extend my appreciation to my promotion committee, Prof. dr. M. Illikainen (University of Oulu), Prof. dr. W. Chen (Wuhan University of Technology),

Prof. dr.-Ing. P.M. Teuffel (Eindhoven University of Technology), Prof. dr. N. De Belie (Ghent University) and Prof. dr. S.R. van der Laan (Tata Steel and Eindhoven University of Technology) for accepting to be a member. Thanks for your reading and evaluation of my thesis.

Furthermore, the thesis cannot be finished without the efforts and help from my current and former colleagues. Thanks for the contributions from Ing. A.C.A Delsing and Mr. H.L.W Smulders for the tests and technical support during my research. Dr. Qadeer Alam, thanks for picking me up at Eindhoven Station on my first day in the Netherlands and kind help during my study. Dr. Veronica Caprai, thanks for your tutorials of test equipment in our lab and your suggestions on my experiments. Dr. Xu Gao, thanks for your encouragement and efforts at the beginning of my study, I still remember you revised my first journal paper for 3 times and gave me a lot of suggestions on paper writing. Dr. Bo Yuan, thanks for your advice on my experiments. Dr. Peipeng Li and Dr. Yangyueye Cao, it was my pleasure to cooperate with you, the experience of working together with you two is really unforgettable. Together with Anna, Kinga, Winnie, Kate, Zixiao, Xiaoxiao, Huarong, Fan, Zhengyao, Yuxuan, Yan, Tao, Xuan, Hoss, Jawad, Ce, Shaohua, Yuri and Perry. I wish you all the best in the future and have a wonderful life.

Moreover, I would like to give the most sincere appreciation to my Mum (Shuwen Guo) and Dad (Zhanliang Liu). Thanks for your support and encouragement on my every choice and decision. My thanks are also given to my brother (Jian Liu) and his wife (Yuqing Li), thanks for taking care of our parents during these years, and my lovely niece (Xiuyuan Liu). Finally, I would like to thank Dr. Meixia Li, thanks for your company and support since my master study, which is the most precious experience in my life.

Eindhoven, 8th August 2020

Gang Liu

Abbreviations

AAM	Alkali activated material
BET	Brunauer, Emmett and Teller method
BJH	Barrett-Joyner-Halenda method
CSS	Carbonated steel slag
EDX	Energy-dispersive X-ray spectroscopy
EMs	Effective modulus
FA	Fly ash
FTIR	Fourier-transform infrared spectroscopy
GGBS	Ground granulated blast furnace slag
IC	Ion chromatography
ICP	Inductively Coupled Plasma
ITZ	Interfacial transition zone
LOI	Loss on ignition
MIP	Mercury intrusion porosimetry
OPC	Ordinary portlandite cement
PONKCS	Partial or no known crystal structure
PSD	Particle size distribution
RCM	Rapid chloride migration
RGP	Recycled waste glass particles
RH	Relative humidity
SCMs	Supplementary cementitious materials
SEM	Scanning Electron Microscope
SS	Steel slag
TG	Thermal gravimetric
UHPC	Ultra-high performance concrete
XRD	X-ray diffraction
XRF	X-ray fluorescence

Cement chemistry notations

A	Al_2O_3
C	CaO
S	SiO_2
H	H_2O
N	Na_2O
C_3A	$3CaO \cdot Al_2O_3$
C_2S	$2CaO \cdot SiO_2$
C_3S	$3CaO \cdot SiO_2$
C_4AF	$4CaO \cdot Al_2O_3 \cdot Fe_2O_3$

Summary

The demand for solid wastes disposal such as industrial and domestic wastes, has gradually increased in recent years. As inorganic by-products, waste glass and steel slag cannot be used for energy recovery but only disposed in a landfill or applied in road constructions. For high-end application, it is desirable to use them as ingredients in building materials manufacture. In this thesis, recycled waste glass (RGP) and converter steel slag (SS) are the main objectives for the investigation of sustainable building materials design and performance evaluation with various application methods. The investigation aims to apply recycled waste glass in blended cement and alkali activated materials with a modified and improved performance, while steel slag is applied in CO_2 activated systems for low carbon footprint building materials manufacture.

The first section of this thesis illustrates the application of recycled waste glass as a supplementary cementitious material (SCM) in cement based building materials. Two different streams of recycled waste glass - organic contaminated waste glass and mixed color waste glass are studied. The sugar leaching from organic contaminated waste glass presents a significant reduction and delay of the cement hydration, and a consequence, the pozzolanic reaction of the glass phase is influenced. After pre-treatment such as washing and burning of organic contaminated waste glass, the delay in cement hydration can be effectively mitigated. On the other hand, the addition of chemical accelerators, for example, calcium chloride and nano-silica also can decrease the negative effect of sugar on cement hydration. The mixed color waste glass is hard to recycle for new container production due to the variation of chemical compounds. However, after milling, it can be used as a high volume cement replacement in high strength concrete. The high volume recycled waste glass in sustainable high strength mortars induces a high (Na+K)/Ca and low Ca/Si in reaction products, and recycled waste glass in high strength samples can result in a higher strength contribution compared to normal samples. To investigate the feasibility of combining recycled waste glass in blended cements, ternary binder systems are evaluated and discussed. The recycled waste glass incorporation results in the modification of the microstructure of blended mortars, which reduces the pore volume between 10 nm to 100 nm. In addition, a denser interfacial transition zone (ITZ) in glass blended samples can be observed. Therefore, waste glass powder modified slag or fly ash blended mortars exhibit a significant enhancement of resistance to chloride migration, as well as the strength performance.

The second section of this thesis explores the use of recycled waste glass as an amorphous silica source in alkali activated ground granulated blast furnace slag/fly ash

(GGBS-FA). The recycled waste glass exhibits a higher reactivity compared to fly ash in an alkali environment, which contributes to an increase of polymerization degree of reaction products due to the Si rich chemical composition. Furthermore, the resistance to aggressive carbonation is enhanced after the addition of recycled waste glass, especially for NaOH/Na_2CO_3 activated samples. To better understand the improvement in carbonation behaviour, recycled waste glass is used as the binder in Na_2CO_3 activated GGBS mortars, and compared to commercial water glass. The addition of 30% RGP in the GGBS binder system seems to significantly improve the resistance to carbonation. The carbonation shrinkage is also reduced after RGP incorporation; at the same time, a higher strength performance is observed. Samples containing RGP promote the formation of nahcolite, while less bound water loss and calcium carbonate formation are identified during the carbonation process. A high volume of gel pores (<10 nm) is formed in the RGP sample compared to specimens only containing GGBS. The recycled waste glass can also be used as a solid activator in one part concrete after alkali-thermal treatment. The alkali-thermal treatment of RGPs results in the formation of 2.2% to 45.8% Na_2SiO_3 based on the initial effective modulus of SiO_2/Na_2O (NaOH) ranging from 3.0 to 1.0. Compressive strengths of 55.8 MPa and 54.9 MPa are observed for mortars containing RGPs treated with EMs of 1.0 and 1.5, which is comparable to the performance of mortar prepared using CEM I 52.5 R.

The third section of the thesis discusses converter steel slag based building materials produced by CO_2 activation. Two application methods are investigated. The first application is to use fine converter steel slag as SCM in eco-ultra-high performance concrete (UHPC) after CO_2 pre-treatment at ambient conditions. The carbonation treatment is shown to modify the physical and chemical properties of converter steel slag particles, producing a rough and porous surface of slag particles because of the precipitation of calcium carbonate and amorphous silica gel as carbonation products. Consequently, the incorporation of carbonated steel slag improves the cement hydration, enhances the formation of ettringite and C-S-H, and densifies the microstructure compared to non-carbonated slag in eco-friendly UHPCs. The strength requirement (150 MPa) is satisfied when 15% to 45% of cement is replaced by carbonated converter steel slag. The second application is to use high volume converter steel slag as a binder to produce building materials by CO_2 activation. The steel slag particle size is found to influence the carbonation rate and speed during the CO_2 activation process, consequently, the strength performance and leaching properties can be affected. The application of an optimal size range of steel slag (21.75 to 24.13 μm) in blended mortars leads to a higher compressive strength (31.21 MPa), CO_2 uptake (15.9%), faster carbonation rate as well as sustainability efficiency (0.486 MPa/(kg CO_2/m^3 concrete)), which is superior compared to the steel slags mortars containing larger or smaller slag

particles. By using alkali activated GGBS/ steel slag system, cement-free mortars are produced, which exhibit a quick increase of strength during CO_2 activation. The GGBS part provides an initial strength of 1.5 to 8.1 MPa after 24 hours alkali activation. The final strength of 37.5 to 44 MPa are observed in activated mortars after 14 days CO_2 activation.

Contents

Chapter 1 Introduction

1.1 Background

Concrete is the most produced material worldwide, with more than 20 billion tons manufactured every year. As a necessary ingredient in concrete production, cement has been developed and applied for more than a hundred and fifty years. The reaction products of cement binds the aggregates in concrete together, while meeting the strength, durability, and economic requirements. Traditional cement production is an energy-intensive process (Feiz et al., 2015), and a large amount of limestone is calcined. Consequently, a huge amount of energy is needed (Andrew, 2018). Moreover, construction activity keeps increasing, which further enhances the demand for cement production. Therefore, the low costs and low environmental impacts building materials are getting more attention.

To reduce the demand and enhance the utilization efficiency of cement in concrete manufacture, supplementary cementitious materials (SCMs), for example, ground granulated blast furnace slag (GGBS), silica fume (SF), calcined clay (LC), incineration bottom ash and combustion fly ash (FA) have been applied in cement blends (Fernandez et al., 2011; Filipponi et al., 2003; Khatib, 2008; Lam et al., 1998; Li and Zhao, 2003). The valorization of these by-products in concrete production not only makes the recycling of industrial side products possible but also improves the performance of the concrete. The reaction of SCMs in cement based concrete promotes the densification of the microstructure, at the same time, the lower reaction heat reduces the potential risks of deformation. For instance, GGBS blended cement and FA blended cement have been commercially applied in constructions to achieve a superior durability performance compared to ordinary Portland cement (OPC). The pozzolanic reaction of SCMs can consume the calcium hydroxide from the hydration process of cement clinkers to form calcium silicate hydrate gel (C-S-H), filling pores and modifying pore size distribution. However, the presence of OPC is always a necessary part of the production of SCMs blended cement.

In recent decades, alkali activated materials (AAM) are getting more attention, which are Portland cement-free building materials. Two ingredients are necessary for AAM preparation, the activators, and precursors. The activators are usually alkali solutions, for example, sodium hydroxide, sodium silicate, sodium carbonate, and sodium sulfate. The most widely used precursors in AAM are rich in amorphous aluminosilicate such as GGBS and FA. The use of GGBS results in a high calcium binder system where the

main reaction product is C-A-S-H (Brough and Atkinson, 2002). Fly ash is usually used in low calcium geopolymer concrete production, where N-A-S-H is the main reaction production (Jeon et al., 2015; Škvára et al., 2009). In the future, less GGBS and fly ash will be available because the related industries (steel manufacture and coal power plants) will be reduced or stopped entirely. Therefore, other materials with the amorphous aluminosilicate structure such as (metakaolin) MK, SF, and nano-silica are investigated for AAM preparation (Bernal et al., 2011; Boddy et al., 2003; Gao et al., 2017). To manufacture a conventional alkali-activated concrete, the liquid activator needs to be prepared first, then mixed with the solids (binder and aggregates) as a 'two-part' concrete (Provis, 2014). However, the use of highly alkaline activator solutions poses an increased safety risk on construction sites (Kovtun et al., 2015). Therefore, the concept of 'one-part' alkali-activated mortar was proposed to reduce the potential hazards, which means 'just add water' like for an ordinary Portland cement (Duxson and Provis, 2008; Luukkonen et al., 2018; Sturm et al., 2016; Sturm, 2018). In general, AAM can be an alternative for OPC in some applications due to the fast strength development and similar performance compared to traditional OPC concrete. On the other hand, the absence of calcium hydroxide lowers the resistance to carbonation of AAM compared to normal OPC concrete. The C-(A)-S-H gel can be directly carbonated in which can result in a fast decrease of pH in a CO_2 rich environment (Bakharev et al., 2001). Consequently, the steel in building will lose the protection afforded by a high pH. Many studies revealed that the microstructure, activator type, and compositions of precursors can effectively influence the carbonation behaviour of AAM (Bernal et al., 2014, 2013; Li et al., 2017). Therefore, the carbonation behaviour becomes one of the most concerning factor for the durability of AAM and is getting more attention in recent years.

Besides the above mentioned applications, accelerated carbonation is also used to enhance performance and produce building materials with low environmental impacts and costs. For example, accelerated carbonation at high pressures and temperatures has been used as a method for special curing to enhance the early-age performance of normal Portland cement concrete (Zhan et al., 2013). The calcium silicate reactivity can be improved during carbonation curing, while the hydration products of cement such as calcium hydroxide and C-S-H carbonate and fill the pores and improve the microstructure of cement based concrete (Rostami et al., 2012). This contributes to a formation of high strength and low water absorption concrete at early ages. So, it is usually used as a pre-treatment method for pre-cast concrete (Ahmad et al., 2017; Shi et al., 2012; Zhang et al., 2017). The carbonation reaction also occurs at ambient conditions in construction materials. For example, the reaction between CO_2 and slaked lime has been used to produce building materials in early Greek times (Moorehead,

1986). Other natural minerals such as free-lime and calcium/magnesium silicate also show carbonation reactivity and are investigated in the context of CO_2 sequestration. Furthermore, it is identified that the process of mineral carbonation can play a role as cement hydration to bond filler and aggregates together. Besides, minerals with carbonation reactivity also can be found in many industrial by-products, for example, converter steel slag. This provides a chance to manufacture green building materials by using industrial waste with a further reduced CO_2 emission.

1.1.1 Recycled waste glass as the ingredients in building materials

The EU produces the most glass worldwide, which accounts for around 1/3 of global production. As shown in Fig. 1.1, the glass production in the EU keeps increasing in recent years. In 2018, the production of container glass and flat glass (soda-lime glass) accounted for more than 90% of all glass. Generally, glass wastes can be recycled and used for the manufacture of the new product. In the EU, the average recycling rate of glass is around 74%, because contaminated, broken, and mixed color waste glass is not easy to recycle and the costs for sorting and cleaning are high (Federico and Chidiac, 2009; Jani and Hogland, 2014). Therefore, a large amount of waste glass is landfilled ever year and other applications for this waste glass must be found.

The normal soda-lime glass is produced by heating silica sand, sodium carbonate, and limestone at a high temperature. The cooling process results in an amorphous structure as shown in Fig. 1.2, while different chemical additives are used to provide some specific properties, for example, color and resistance to thermal or chemical attack. The high content of amorphous silica in waste glass also makes it a potential SCM and precursor in AAM.

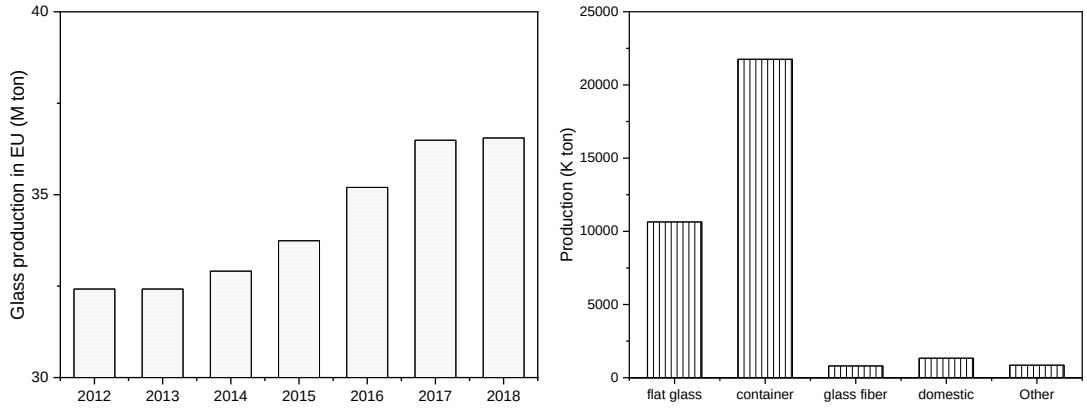

(a) (b)

Figure 1.1 (a) Glass production in EU in recent years, and (b) proportions of different glass products in 2018 (data source: glass alliance EU)

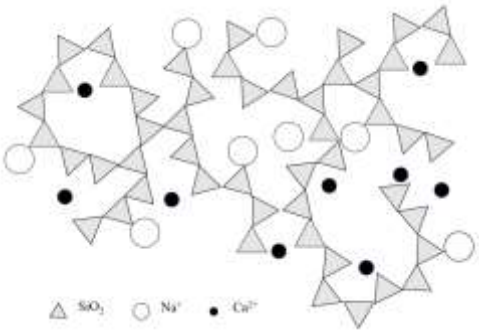

Figure 1.2 Amorphous structure of waste glass

- *Recycled waste glass as SCM in building materials*

The waste glass can be used as aggregates or a SCM/ precursor depending on its particle size. The large fractions of recycled waste glass were reported to have lower water absorption and higher reactivity compared to natural aggregates, which can provide better workability and mechanical performance for concrete (Soliman and Tagnit-Hamou, 2016; Vaitkevičius et al., 2014). However, the reactivity of amorphous silica in recycled waste glass induces a risk of alkali silica reaction (ASR), which can cause an expansion of concrete and effect the durability performance negatively (Lam et al., 2007). It was found that the ASR expansion caused by the waste glass in concrete is critically related to the particle size of glass particles (Du and Tan, 2014, 2013; Lee et al., 2011). When the waste glass particles are fine enough (< 75 μm), the ASR expansion of concrete reduces to a safe level (Shayan and Xu, 2004). It is also noticeable that the very fine glass powder can be used to reduce ASR expansion in concrete containing waste glass aggregates (Idir et al., 2010; Spiesz et al., 2016). Moreover, very fine glass powder (< 38 μm) can show a significant pozzolanic reactivity (Shao et al., 2000) at an equal to or even greater pozzolanic activity level than fly ash (Schwarz and Neithalath, 2008). During the pozzolanic reaction of fine recycled waste glass in cement based materials, the calcium hydroxide from cement hydration can be consumed to form Na rich C-S-H near the glass particles (Mejdi et al., 2019). It is reported that small addition of waste glass powder in concrete can improve the microstructure, enhance the strength performance and durability by improving the interfacial zone (ITZ) (Yazıcı, 2007). In many studies, 10% to 30% of fine recycled waste glass powder has been proved to be safe for blended concrete without deterioration of strength performance (Aliabdo et al., 2016; Omran and Tagnit-Hamou, 2016).

- *Recycled waste glass as binder in alkali activated materials*

As a silica-rich waste material with an amorphous structure, recycled waste glass can

dissolve and release silicate in an alkaline environment (Torres-Carrasco et al., 2014). Then, the dissolved silicate can contribute to the formation of N-A-S-H and C-A-S-H gels, which are the typical reaction products in AAM. Many studies have proven the feasibility of recycled waste glass in AAM in recent years (Torres-Carrasco and Puertas, 2017; Vafaei and Allahverdi, 2017). The incorporation of recycled waste glass in alkali activated GGBS mixtures results in increased polymerization of C-A-S-H due to the decreased Ca/Si ratio (Torres-Carrasco et al., 2014). In comparison with FA, recycled waste glass also shows a higher reactivity, which results in a better performance than GGBS/fly ash mixtures (Zhang et al., 2017). Besides, recycled waste glass can be used in the preparation of activator for AAM. In an alkaline environment, the dissolution of fine glass powder can reach 60% at 80 °C, which can produce a sodium silicate solution activator for AAM preparation. Samples activated with material prepared like this exhibited better mechanical performance than those prepared with NaOH only (Puertas and Torres-Carrasco, 2014). Afterward, the treated waste glass can be used for one-part alkali activated concrete manufacture.

1.1.2 Valorization of converter steel slag in building materials

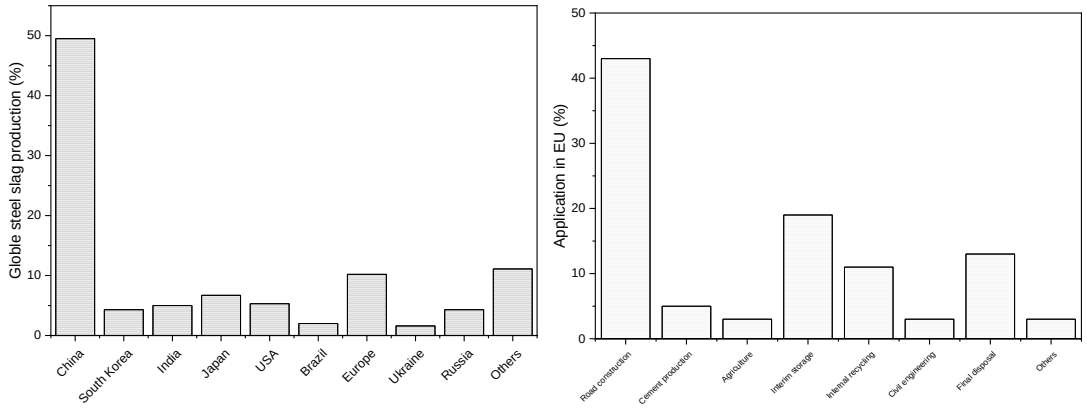

(a) (b)

Figure 1.3 (a) steel slag production worldwide and (b) in EU

Steel slags are by-products from the steel making process. Europe accounts for 10.2% of the total steel slag production worldwide. The EU alone produces about 110 million tons of raw steel, leading to approximately 10 million tons of steel slag annually (EUROFER, 2018). The amount of GGBS is the highest among the different kinds of steel slag, which accounts for around 60% of total slag, and has been commercially applied in blended cement production (CEM III) due to the high reactivity for a long time. Converter steel slag accounts for 20% of all steelmaking slag and is the second most common slag. For example, in Netherlands, 0.7 M tons converter steel slag are produced annually. Compared to GGBS, converter steel slag exhibits low reactivity, and is mostly used in road construction as aggregates (Qiang et al., 2016), because the

presence of free lime often prevents its use as aggregate in concrete. The main mineral phases in converter steel slag are larnite, wuestite and brownmillerite. Magnitite, and free lime are also found (Baciocchi et al., 2015; El-Naas et al., 2015; Reddy et al., 2019). The existence of calcium silicate phases results in the weak hydraulic reactivity of converter steel slag (Wang and Yan, 2010), which makes it possible to use it as binder in building materials.

- *Converter steel slag as SCMs in building materials*

The presence of dicalcium silicate (α-C_2S and β-C_2S) and brownmillerite phases contribute to the hydration reactivity of converter steel slag. However, the hydration reactivity of these minerals in steel slag is relatively low compared to cement clinkers and poorly understood. It is found that steel slag blended cement presents low early strength and the strength keeps decreasing with increasing steel slag content because of the relatively low reactivity of the calcium silicate phase (Kourounis et al., 2007). Only at a replacement ratio of less than 20%, are no negative effect on porosity and strength observed. The reactivity of steel slag was also shown to correlate to particle size (Qiang et al., 2016; Wang et al., 2012) and to improve the hydration reactivity of steel slag, extensive milling was tried to increase the surface area. The results showed that super fine steel slag can show a high reactivity at early age, while still being much lower than cement (Wang et al., 2013). Also, the energy costs during the mechanical activation process are increased. Therefore, more economic activation and application methods of steel slag in building materials are required.

- *CO_2 activation of converter steel slag*

In contrast to the low hydration reactivity, converter steel slag was show to have a high reactivity in a CO_2 rich environment (Huijgen and Comans, 2006) because it contains α-C_2S, β-C_2S, and free MgO/CaO that can carbonate and sequestrate CO_2 effectively according to related study (Reddy et al., 2019). EI-naas et al. also proposed a pre-hydration method for enhancing the carbonation degree of steel slag (El-Naas et al., 2015). A review by Humbert indicated that the CO_2 uptake ability of steel slag can be up to 200-400 g CO_2/kg depending on the carbonation conditions (Humbert and Castro-Gomes, 2019). The carbonation of steel slag can results in a decrease of density due to the presence of calcium carbonate, by utilization of the volume increase during carbonation process, it can be used as binding material for production of building materials by pressurized CO_2 curing (Moon and Choi, 2018). In Shao's study, a combination of poorly crystalline $CaCO_3$ and C-S-H was confirmed after steel slag carbonation, which provided a satisfactory strength (Shao et al., 2013). Most of the previous investigations were carried out using a pressurized and pure CO_2 environment

for fast strength development of steel slag concrete, conditions which add to the embodied energy of the products. On the other hand, the carbonation of steel slag was also confirmed to take place at ambient pressure and temperature (Ghacham et al., 2016). This provides a possible eco-treatment to activate steel slag blended concrete at ambient conditions using CO_2.

1.2 Motivation and objective

In recent years, industrial by-products and recycled wastes have been widely studied in order to be valorized in building materials. By introducing optimized utilization strategies (hydration, alkali activation, and carbonation), these by-products and recycled wastes can effectively reduce the amount of traditional Portland cement necessary in construction. As mentioned above, waste glass is one of them, a pozzolanic material in blended cement and a silica source in alkali activated materials, Another material is converter steel slag, whose carbonation reactivity provides a chance to produce CO_2-sequestrating building materials with low cost and carbon footprint. Therefore, the objectives of this study are as follows:

- Investigating the effect of high volume recycled waste glass as SCMs on hydration kinetics, reaction products, microstructure evolution, and durability performance of cement blends, which provide a comprehensive understanding of sustainable building materials containing high volume recycled waste glass.

- Evaluating the performance and carbonation behaviour of alkali activated materials containing recycled waste glass as silica source.

- Proposition of a low-temperature treatment method (80ºC) for producing solid activator from recycled waste glass and the application in one part concrete.

- Investigating the modification mechanism of converter steel slag fines after CO_2 pre-treatment and the application in ultra-high performance concrete (UHPC) design.

- Investigating the high volume converter steel slag based mortars activated by CO_2, and the effects of steel slag particle size on CO_2 activation process.

1.3 Outline of the thesis

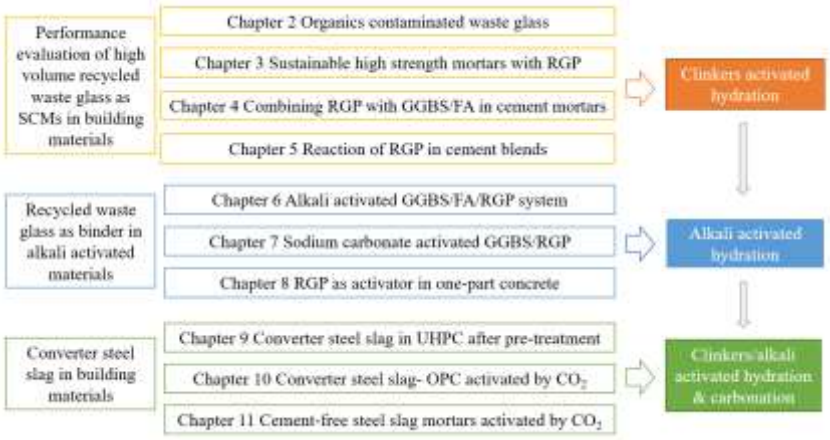

Figure 1.4 Outline of the thesis

The research framework is shown in Figure 1.4. The contents of chapters are briefly introduced in the following paragraphs.

In Chapter 2, a new stream of recycled waste glass with organic contaminations is studied as SCM in cement blends. The organic contaminations are characterized using high-performance anion exchange chromatography (HPAEC) and ion chromatography (IC). Their influences on cement hydration, reaction products and microstructure are identified by using isothermal calorimetry, X-ray diffraction (XRD) and scanning electron microscopy (SEM), respectively.

In Chapter 3, the high volume fine glass powder from mixed color recycled waste glass is used as SCM to produce high strength sustainable mortars. The fresh behavior and setting time are evaluated by mini-slump flow and Vicat test. The hydration behavior and products are analyzed by isothermal calorimetry, TG-DSC and SEM. The pore size characterization is performed by using N_2 absorption. The contribution of recycled waste glass to the strength and total shrinkage of high strength mortars is discussed.

In Chapter 4, the application of recycled waste glass powder in high volume (60%) ground granulated blast furnace slag (GGBS) or fly ash blended cement binder is investigated. The hydration kinetics, hydration products of different binder systems were studied by isothermal calorimetry and XRD tests. To investigate the microstructure properties of blended binders modified by glass powder, mercury intrusion porosimetry (MIP) tests are conducted. The resistance to chloride penetration was evaluated by the rapid chloride migration test.

Chapter 5 summarizes the reaction of recycled waste glass in cement based materials. By using the PONKCS method and Rietveld analysis, the reaction degree of recycled waste glass blended cement was determined. The reaction mechanism of recycled waste glass is proposed and discussed.

Chapter 6 illustrates the application of waste glass powder as part of the binder in slag-fly ash systems activated by NaOH and NaOH/Na_2CO_3 activators. To evaluate the reaction kinetics, reaction products, mechanical properties, and durability performance of glass powder modified alkali activated slag-fly ash systems, isothermal calorimetry, XRD, FTIR, strength test, drying shrinkage tests, and carbonation test are conducted.

In Chapter 7, the influences of recycled waste glass powder on the durability performance - resistance to carbonation of sodium carbonate activated ground granulated blast furnace slag (GGBS) mortars are studied. The effect of activator dosages, types and RGP addition on resistance to carbonation is evaluated. The modification mechanism of carbonation behaviour after incorporation of recycled waste glass are investigated and discussed.

In Chapter 8, an alkali-thermal treatment of recycled waste glass is applied to prepare one-part GGBS mortars. The recycled waste glass powder (RGP) is treated with NaOH and water at a temperature of 80°C for 24 hours and then dried at 105°C for producing a solid activator. Then the treated RGPs are used to prepare ground granulated blast furnace slag-based one-part GGBS mortars. The treated RGPs and the one part binders are characterized by XRD, FTIR and SEM. Furthermore, a quantitative analysis of the reaction products of RGP after alkali-thermal treatments is conducted by using Rietveld analysis and the PONKCS method. The hydration kinetics and mechanical performance of one-part GGBS mortars are evaluated by calorimetry and compressive strength test.

Chapter 9 deals with the modification of converter steel slag by an ambient CO_2 pre-treatment, and the application of modified converter steel slag as supplementary cementitious material (SCM) in the design of eco-friendly ultra-high performance concrete (UHPC) designed using a particle packing model.

In Chapter 10, low carbon footprint binders consisting of various fine converter steel slag powders (80%) and normal cement (20%) are applied to produce mortars using ambient carbonation. The variation of steel slag particle size influences gas transport and CO_2 uptake of carbonated steel slag blended mortars during the curing period, which affects microstructure, strength, and leaching.

In Chapter 11, the cement free - steel slag based green mortars activated by a

combination of alkalis and CO_2 are investigated. The GGBS accounts for 10%, 20%, 30%, 40% and 50% in steel slag based mortars, while sodium hydroxide solution (2M) is used as an activator in the preparation of mortars. The CO_2 uptake and mechanical performance are analyzed and discussed.

In Chapter 12, overall conclusions of the presented work are drawn, and recommendations for the future study are proposed.

Chapter 2 The hydration and microstructure characteristics of cement pastes with high volume organic-contaminated waste glass powder

This chapter investigates the influence of the organic-contaminated waste glass powder on cement hydration and the microstructure characteristics of the hydration products. In order to study the influences of organic contamination (mainly fibres and sugar), treated (washed) glass powder was used as reference addition. The incorporation of filter glass powder results in longer induction periods and lower reaction intensity compared to the samples with washed glass. The addition of chemical accelerators such as $CaCl_2$, nanosilica and microsilica can significantly improve the hydration of samples containing high volumes of filter glass powder. The organic contamination shows a negligible effect in terms of hydration products identified by XRD analysis. In mixtures with high volume filter glass powder (70%), the formation of calcium hydroxide was delayed at 3 and 7 days. Samples containing more than 50% waste glass present a higher pore volume in pore sizes lower than 15 nm and lower pore volume between 20 and 50 nm. It was observed from the SEM analysis that the organic contamination may slow the pozzolanic reaction of glass particles in mixes with 70% filter glass, because the reaction of cement is delayed.

This part is partially published elsewhere:

G. Liu, M.V.A. Florea, H.J.H. Brouwers. The hydration and microstructure characteristics of cement pastes with high volume organic-contaminated waste glass powder. Construction and Building Materials, 2018, Volume 187, Page 1177-1189.

2.1 Introduction

Recent studies about influences of contamination in waste glass usually focused on heavy metal contaminated waste glass, such as glass from cathode ray tubes (CRT), where cement could be used to immobilize the heavy metal in CRT glass (Hui et al., 2013). However, the waste glass fractions contaminated by organics (sugar, fiber) received less attention. This kind of waste usually combines with very fine glass particles and is mixed with organic matters from package and glue, making it difficult to clean and recycle for re-producing new glass products. For the sustainable use of this kind of organic containing glass fractions, it is desirable to use such filter glass as building material. However, the organic contamination will influence the application of the waste glass fractions in concrete. The waste glass in this study is a filter glass powder, which is filtered out of the drying furnace. It has a very fine particle size and contains considerable amounts of organic matters such as fibres and saccharides from labels and glue. Organic matter such as wood fibres and recycled waste paper fibre could be used to improve the performance of cement composites (Lin et al., 1994; Pehanich et al., 2004), but as an organic addition, fibres act as an inhibitor and show a negative effect on the cement hydration, because of the sugars, starches and tannins (Wei et al., 2000). Saccharides are mainly responsible for the inhibition of cement hydration in fibre-cement composites (Thomas and Birchall, 1983). Different organic compounds show different influences on retardation of cement hydration (Kochova et al., 2017). Saccharides could be absorbed on the surfaces of cement particles and hydration products, which inhibits the hydration process and hydration products growth (Juenger and Jennings, 2002; Young, 1972). The zeta potential of hydrating cement particles is positive and changed to negative after the incorporation of saccharides, which could be explained by the absorption of sugar on the cement particle surface (Neubauer et al., 1998).

This chapter aims to perform a comprehensive evaluation for a better understanding of the influencing of organic contaminated waste glass as supplementary cementitious material on cement hydration, products and microstructure, providing some theoretical basis for its application.

2.2 Materials and methods

2.2.1 Materials

The cement applied in this study is CEM I 42.5N supplied by ENCI, Netherlands. The used glass powder is a filter glass which was filtered out in a glass drying furnace, provided by a glass recycling plant. The micro silica (surface area 20 m^2/g) in this study was provided by Elkem, nano silica (surface area 234 m^2/g) was provided by AkzoNobel with a concentration of 50% and the calcium chloride dihydrate ($CaCl_2 \cdot 2H_20$) was provided by VWR international. The filter glass powder after washing was used as references. The washing process used L/S 2 and 250 rpm for 24 hours, then the floating impurities were poured out, the second washing used same process with a L/S 10. Then these two glass powders were milled, sieved and utilized as supplementary cementitious materials in present study. The specific surface area of milled filter glass powder is 0.65 m^2/g.

2.2.2 Methods

- *Sample preparation*

Different pastes were prepared with the water / binder ratio of 0.3, where cement was replaced by the filter glass or washed filter glass with 0%, 30%, 50% and 70% by mass. The mix designs are shown in Table 2.1. CF was prepared with only cement and filtrate (L/S 2) from first washing process.

Table 2.1 Sample mixtures

Sample	Filter glass powder (%)	Washed filter glass powder (%)	Cem (%)	W/B
C0	0	0	100	0.3
C3	30	0	70	0.3
C5	50	0	50	0.3
C7	70	0	30	0.3
CW3	0	30	70	0.3
CW5	0	50	50	0.3
CW7	0	70	30	0.3
CF	100% cement + filtrate (L/S 2) filtrate/cement 0.3			

- *Characterization of materials*

The particle size distribution (PSD) of materials were determined with laser particle size analyzer, Mastersizer 2000.

The specific density of materials were conducted by the gas pycnometer micrometrics, AccuPyc II 1340.

The sugar content of filter glass and ion concentration of filter glass and washed filter glass were measured with the high-performance anion exchange chromatography (HPAEC) as shown in (Kochova et al., 2017) and ion chromatography (IC).

- *Calorimetry test*

The calorimetry test was performed using an isothermal calorimeter (TAM Air, Thermometric). Cement was replaced by filter glass powder or washed filter glass with 0% to 70% by mass. Solid raw materials were firstly mixed with distilled water, then the mixed paste was injected into the ampoule and sealed by a lid and loaded into the calorimeter. All measurements were conducted for 160 h under a constant temperature of 20 °C. The duration of the calorimetry test for samples containing 70% waste glass was increased to 378 h because the induction period was relatively long. To study the influences of different chemical addition and treatment methods on the hydration of sample containing high volume of filter glass, additional samples for calorimeter were prepared as shown in Table 2.2.

Table 2.2 Samples for calorimeter test

Sample ID	Treatment Methods
B7	30% cement + 70% heat treatment filter glass powder (550°C for 4 hours)
DW7	30% cement + 70% second washing filter glass powder (L/S 2-L/S 10)
5% $CaCl_2$ dihydrate	C7 + 5% $CaCl_2$ dihydrate (by mass of binder)
5% nano silica	C7 + 5% nano silica (by mass of binder)
5% micro silica	C7 + 5% micro silica (by mass of binder)

- *Reaction products characterization*

The X-ray diffraction test was conducted with a Bruker D2 PHASER with a Co tube to study the hydration products of the paste samples. All samples were cured at ambient temperature and tested after 3, 7 and 28 days. After curing, all samples were crushed and immersed in acetone to cease further hydration. At last, all samples were milled into powder (< 300 um) for the XRD test.

The thermal-gravimetric (TG) analysis was conducted in a STA 449 F1 instrument, as follows: ground powder containing samples after 28 days and 90 days of ambient curing were heated up to 1000 °C from 40 °C at the rate of 10 °C/min with nitrogen as the carrier gas.

- *Microstructure*

Nitrogen sorption analysis was performed using a Brunauer-Emmett-Teller (BET) specific surface area and porosity instrument (TriStar II 3020, Micrometrics). Samples were milled (< 400 um) and dried at 105 °C in an oven until the mass was constant. The surface area was calculated by the Brunauer-Emmett-Teller method (Barrett et al., 1951) using the adsorption branch. The pore size distribution was determined by the Barrett - Joyner - Hallenda method (Brunauer et al., 1938) from the adsorption branch.

The microstructure of samples were observed by Scanning Electron Microscope with EDX detector (Phenom Pro). The EDX analyses were conducted at 10 kV accelerating voltage. Crushed samples were immersed in acetone and then dried in the oven at 40 °C to cease further hydration. After that, samples were used for SEM observation.

2.3 Results and discussion

2.3.1 Materials characterization

The chemical composition of raw materials is presented in the Table 2.3. It can be seen that the filter glass mainly contains sodium oxide, calcium oxide and silica with proportion of 11.4%, 14.2% and 67.0%, respectively, while a small quantity of MgO, Al_2O_3, K_2O and Fe_2O_3 can be observed. To wash out the contamination in filter glass, the washing treatment of 24 hours with L/S 2, 250 rpm on a shaker was conducted. As can be inferred that the filter glass contains 4.5% organic matter from the ignition loss at 550 °C, after the washing treatment, only 2.0% of organic matter is observed in the washed filter glass powder. Comparing the chemical composition of washed filter glass with untreated sample, a slight reduction of MgO, Al_2O_3, SO_3, CaO and Cl can be found. From the particle size distribution results shown in Fig. 2.1, washing treatment results in the slight decrease of volume around 40 μm, the d_{50} particle size of filter glass powder, washed filter glass powder and cement is 33.2, 31.4 and 22.1 μm, respectively. The specific density of cement, waste glass powder and washed glass powder are 3091 kg/m^3, 2421 kg/m^3 and 2429 kg/m^3, respectively.

Table 2.3 Chemical compositions of materials

Chemical composition	Filter glass (%)	Washed filter glass (%)	CEM I 42.5N (%)
Na_2O	11.38	11.47	/
MgO	1.42	1.37	1.55
Al_2O_3	2.75	2.58	3.44
SiO_2	66.97	68.29	14.38
SO_3	0.25	0.13	4.42
K_2O	0.84	0.80	0.45
CaO	14.25	13.61	69.24
TiO_2	0.19	0.14	0.38
Cr_2O_3	0.15	0.15	0.015
MnO	0.032	0.028	0.097
Fe_2O_3	0.95	0.79	3.86
ZnO	0.058	0.043	0.11
BaO	0.069	0.065	0.016
PbO	0.042	0.036	0.008
P_2O_5	/	/	0.31
Cl	0.21	0.061	0.073

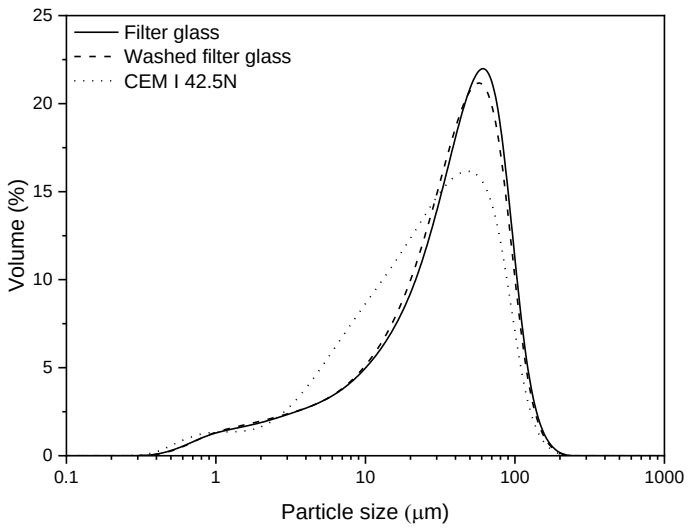

Figure 2.1 Particle size distributions

The results of the leaching test are presented in Table 2.4. Apparently, many kinds of saccharides are presented in the filter glass, such as galactose, glucose and mannose with leaching of 67.8 mg/kg, 91.8 mg/kg and 67.7 mg/kg, respectively. Additionally, high content of soluble salt also can be found, it can be observed that filter glass contains a relatively high leaching of Na^+ and Cl^- with a dosage of 1549 mg/kg and 540 mg/kg, respectively. After washing treatment, the residual Na^+ and Cl^- are 766 mg/kg and 191 mg/kg.

Table 2.4 Leaching properties of filter glass and washed filter glass

Filter glass			Filter glass	Washed filter glass
Sugar	mg/kg	Ion	mg/kg	mg/kg
Arabinose	12	Na^+	1549	766
Galactose	67.8	K^+	84	50
Glucose	91.8	Ca^{2+}	109	32
Xylose	14.8	Mg^{2+}	11	3
Mannose	67.7	NH_4^+	48	36
Galacturonic acid	31.3	Cl^-	540	191
Glucuronic acid	37	PO_4^{3-}	107	38
		SO_4^{2-}	235	72
		Organic Mass	4.5%	2.0%
		pH	9.807	9.704
		LOI 1000°C	2.5%	1.5%

Fig. 2.2 exhibits the morphology of filter glass particles and cement particles. The glass particles show smoother surface and sharp edges compared with the cement particles.

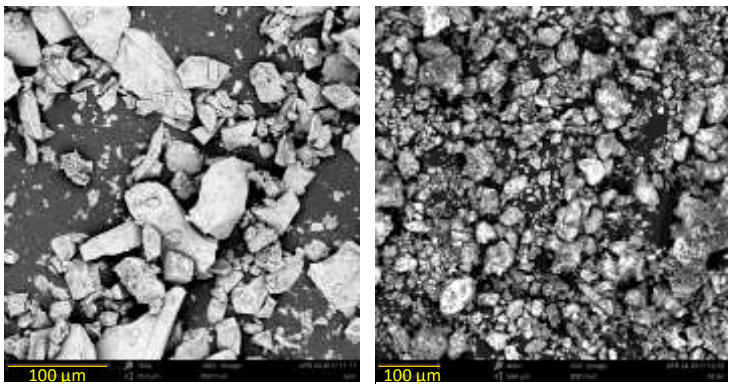

(a) (b)

Figure 2.2 SEM images of (a) filter glass and (b) cement particles

2.3.2 Early age hydration

The results of isothermal calorimetry test of pastes containing different amount of filter glass powder (C3, C5 and C7) and washed filter glass (CW3, CW5 and CW7) are shown in Figs. 2.3 to 2.4. It is apparent that all samples have the same general shape of heat flow curve as cement which contains five stages including initial reaction stage, induction stage, acceleration stage, reduction stage and long term reaction stage (Bullard et al., 2011).

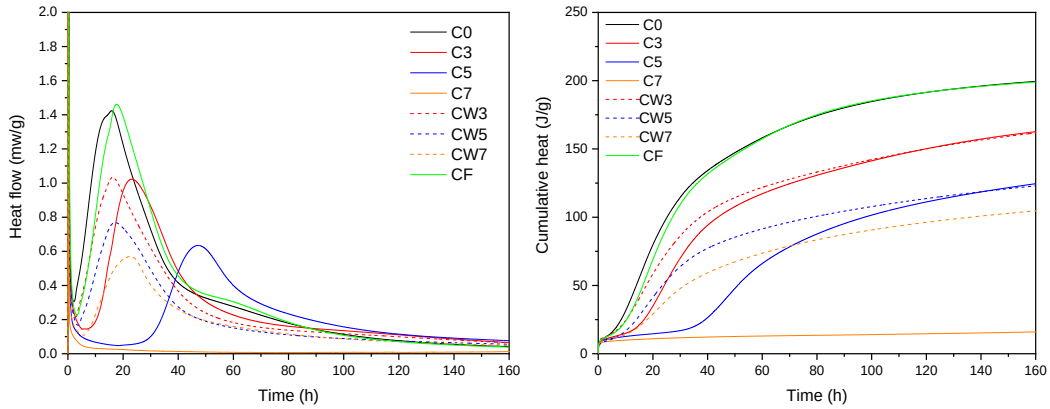

(a) (b)

Figure 2.3 Calorimetric results of different pastes: (a) heat flow and (b) cumulative heat

As shown in Fig. 2.3 (a), samples containing filter glass powder show longer induction periods than the reference sample (C0), and the intensity of heat flow was also reduced. It can be seen that the sample mixed with filtrate shows a weak delay effect on hydration. The addition of filter glass powder results in obviously reduced heat flow and prolonged hydration. Especially for the sample containing 70% filter glass powder (C7), it shows no obvious reaction after 160 hours of hydration. The increasing of the filter glass content obviously increases the time to achieve the peak of heat flow and reduces the intensity of hydration heat generation. Therefore, the cumulative heat was also decreased, which can be observed in Fig. 2.3 (b). Because no heat release was observed in the sample containing 70% filter glass powder, the cumulative heat of C7 shows almost no increase after 160 hours hydration.

As shown in Fig. 2.3 (a), samples containing washed filter glass show a lower intensity of heat flow than the reference sample. No significant delay in terms of the heat flow peak location is observed. The sample incorporating 70% washed filter glass powder shows the reaction peak around 20 h, which is slightly delayed compared to the reference. With the increasing of washed filter glass amount in the mixture, the intensity of reaction and the cumulative heat decreases continuously. It is noticeable that the cumulative heat of sample containing 30% filter glass (C3) presents at the same level as the washed contained sample (CW3) after 160 hours hydration, which also are presented by C5 and CW5, which indicates that the organic contamination in filter glass just increasing the induction period during the hydration but shows no effect on the cumulative heat of hydration.

In order to better understand the hydration process of mixtures with 70% filter glass powder, the testing duration was increased to 378 hours and the results are shown in Fig. 2.4. It is noticeable that the reaction starts from 170 hours and the peak of the acceleration stage is at 275 hours, so the hydration is delayed by almost 250 hours

compared to the mixtures with washed filter glass. The duration of the main reaction stage is longer, with lower reaction intensity.

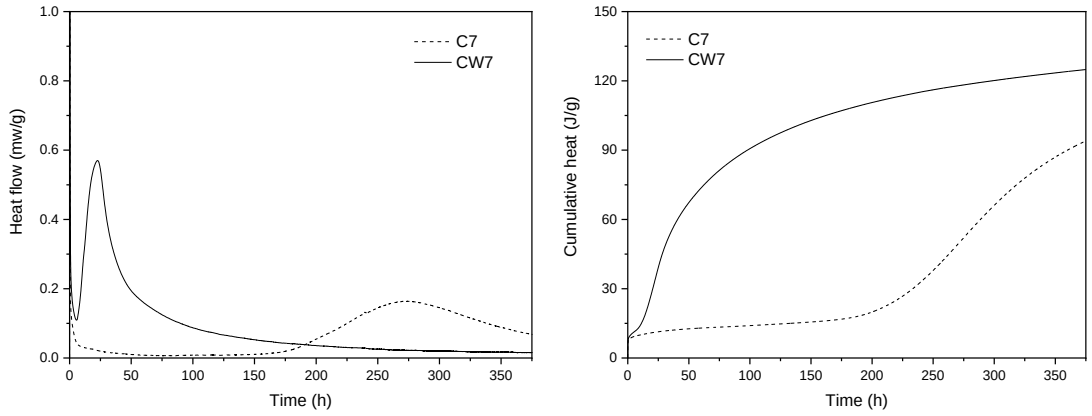

(a) (b)

Figure 2.4 Calorimetry results of 70% filter glass and 70% washed filter glass powder containing samples (a) heat flow (b) cumulative heat

It is believed that the fine glass powder can partially dissolve in the high pH environment and exhibit pozzolanic activity due to the high amorphous silica content (Vaitkevičius et al., 2014; Zheng, 2016). The pozzolanic reaction presents limited influence on early cement hydration, as it is a long-term reaction. With the increasing replacement of glass powder in pastes, less cement particles result in a lower concentration of ions due to the dilution effect (Du and Tan, 2017); as a consequence the intensity of hydration will be reduced but no influence will be shown concerning the reaction rate. When filter glass is incorporated, the sugars in it are responsible for the delay of the heat flow peak during the hydration. As an inhibitor of cement hydration, the sugars absorb on the surface of cement particles and the surface of hydration products, which slows down the growth of CH and C-S-H gels and inhibits the hydration of cement particles (Ataie et al., 2015; Bishop and Barron, 2006; Smith et al., 2012). The sugar in filter glass increases the duration of the induction stage, and the higher content of filter glass in pastes, the longer the induction period is. Eventually, the reaction suddenly begins again owing to the fact that the increasing number of nucleation sites overcome the barrier of limited sugar present in the pore solution (Juenger and Jennings, 2002).

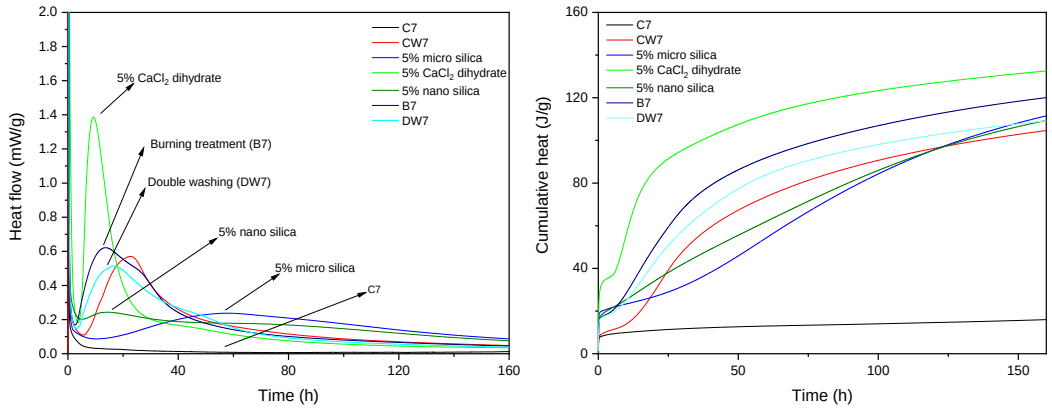

(a) (b)

Figure 2.5 Influences of different chemical addition on hydration of sample containing 70% filter glass (a) heat flow (b) cumulative heat

To improve the hydration of sample containing filter glass powder, different chemical additions were used to accelerate the reaction in C7, which can be seen in Fig. 2.5. It is clear that chemical additions improves the hydration of C7 significantly. The addition of 5% calcium chloride dihydrate by mass of binder enhances the reaction rate and cumulative heat, the peak of heat flow is brought forward to 9 h compared the 275 h of C7. The $CaCl_2$ can be used to improve the hydration of cement and the early strength of concrete. It is stated in literature that a dosage up to 3% to 4% could be used (Kourounis et al., 2007). The incorporation of micro silica and nano silica also improve the hydration of C7 with a dosage of 5% by mass of binder, and the peaks of heat flow take place after 56 h and 18 h respectively. Calcium chloride is a widely used chemical addition for the hydration acceleration of C_3S and Portland cement, as it can significant decrease the setting time and increase the early age strength. The Ca^{2+} from calcium chloride can absorb on the surface of C_3S and increase the zeta potential (Peterson and Juenger, 2006; Thomas et al., 2009). The additional Ca^{2+} from calcium chloride can form complexes with saccharides, which may reduce the effect of saccharides on cement particles surface (Ribeiro et al., 2011). This is different from the addition of nano silica and micro silica, which produce more nucleation sites for the cement hydration. As can be seen in Fig. 2.5 (a), the addition of micro silica and nano silica show no obvious influence on the intensity of heat flow peak but decrease the time to reach the heat flow peak. It was found that nano silica has more effective on accelerating hydration than micro silica with the same dosage (5%). Nano silica used in this study is a slurry with 50% concentration, it can fully disperse during the mixing, and while micro silica usually aggregates together. These result in different performances in the acceleration of hydration. The sample containing 70% double washing treatment filter glass (DB7) and sample containing 70% heating treatment filter glass (B7) also show no significant delay in hydration. After the double washing treatment, more saccharides

can be removed, as it can be observed that the heat peak of CW7 is slightly delayed compared with the DB7. After the heating treatment, the organic matter including saccharides were totally removed by burning at 550°C for 4 hours, while the salts were still kept which explains why B7 exhibits higher intensity and an earlier heat peak than CW7 and DB7 during the hydration.

Table 2.5 Summary of cumulative heat of samples at 160 h (see Table 2.1 and 2.2)

Sample	Cumulative heat at 160 h (J/g cement)	Heat change (J/g cement)
C0	199.5	/
CF	199	-0.5
C3	232.37	32.87
CW3	231.04	31.54
C5	249.08	49.58
CW5	245.94	46.44
C7	53.3	-146.17
CW7	348.83	149.33
C7+5%$CaCl_2 \cdot 2H_2O$	441.73	242.23
C7+5% microsilica	371.17	171.67
C7+5% nanosilica	363.93	164.43
B7	399.97	200.46
DW7	363.87	164.37

Table 2.5 illustrates the cumulative heat (normalized by the mass of cement) after 160 h hydration and the change in cumulative heat (normalized by mass of cement) compared the plain sample (C0). When the dosage of glass powder is less than 50%, there is no large difference between the samples containing filter glass and washed filter glass. This means the saccharides just retard the hydration, but have limited influence on the cumulative heat with the glass powder dosages of 30% and 50%. C7 shows a cumulative heat with 53.3 J after 160 h hydration, which is due to the serious delay caused by the saccharides. It can be seen that the increasing cement replacement ratio results in higher heat change, which may due to the increasing effective water/cement ratio. After the addition of accelerator such as nano particles and calcium chloride, the cumulative heat of samples is enhanced significantly. The burning treatment and the second washing treatment of the filter glass also can enhance the hydration of samples, which show higher cumulative heat than the CW7. More saccharides and organic matter can be removed during the treatment procedure, so consequently, less retardation is seen in B7 and DW7.

2.3.3 X-ray diffraction

Figure 2.6 illustrates the X-ray diffraction results of paste mixtures with different

compositions and curing ages. The XRD patterns results of samples containing 30%, 50% and 70% filter glass powder and washed filter glass powder are shown in Fig. 2.6 (a) and (b) respectively; these mixes were tested after 28 days of curing. It can be seen that after 28 days of hydration, typical hydration products are presented in all samples, such as ettringite that mainly from hydration of C_3A; quartz from the impurities; C-S-H and calcium hydroxide from the hydration of alite and belite; and calcium carbonate from the carbonation process during the cement hydration or curing. It should be noticed that the peak of hydrocalumite only shows in the samples with more than 50% waste glass. The intensity of the peak of unreacted calcium silicates decreases with the increasing amount of waste glass in the mixture, which is due to the dilution effects of glass powder addition.

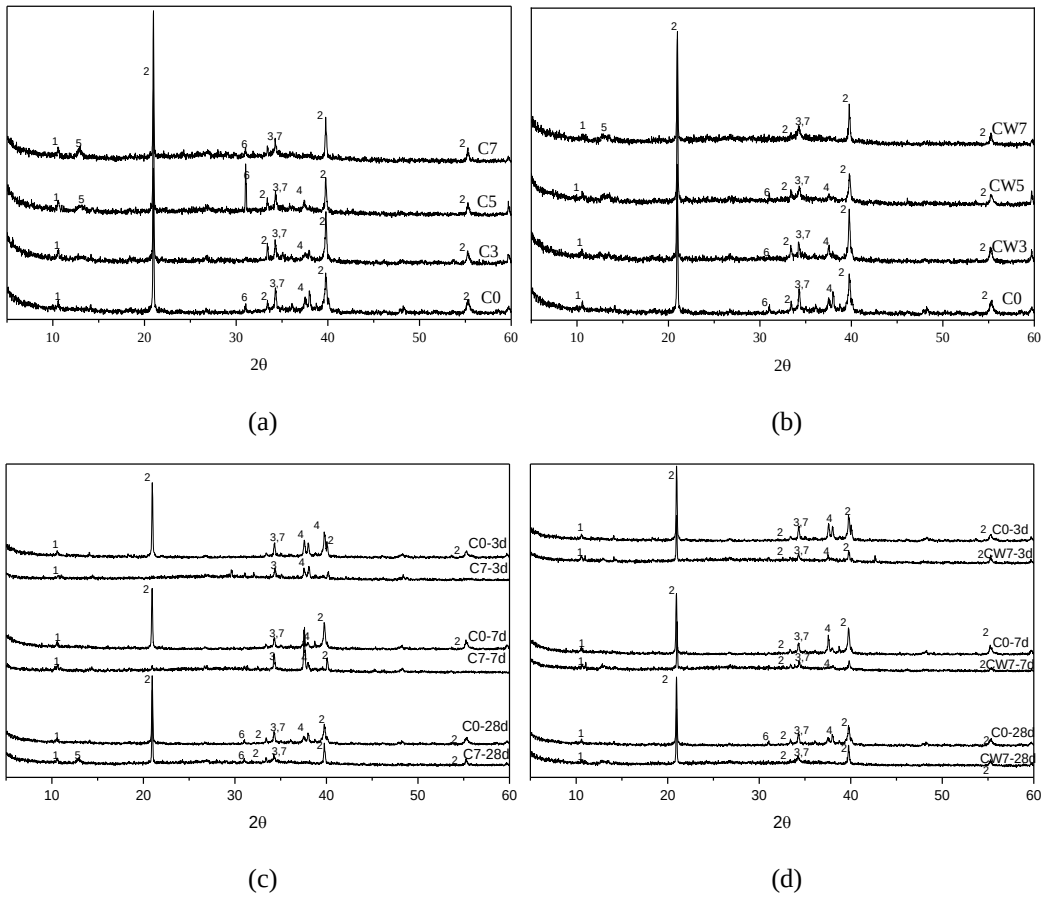

Figure 2.6 The XRD patterns of pastes mixtures: (a) with filter glass powder (b) with washed filter glass powder (c) 70% filter glass powder with age (d) 70% washed filter glass powder with ages (1-Ettringite, 2- calcium hydroxide, 3-calcite, 4-alite and belite, 5-hydrocalumite, 6-quartze, 7-C-S-H)

The effect of curing age on samples containing 70% filter glass powder and washed filter glass powder are presented in Fig. 2.6 (c) and (d). It can be observed from Fig. 2.6 (c) that the peak intensity of calcium hydroxide shown in mixes containing 70% filter glass is lower compared to the reference sample (C0) after 3 days curing. A similar

behaviour is also found in the same mixture after 7 days curing. After 28 days, the peaks of ettringite, calcium hydroxide, quartz and calcium carbonate are obviously observed in the XRD results, and the peaks of alite and belite show relatively low intensity. Compared to the filter glass powder based mixtures, the XRD results of 70% washed filter glass powder containing sample (CW7) show similar hydration products as the reference after 3 days of curing. As the curing aging increases, the peaks of alite and belite gradually decrease. After 28 days of curing, C7 and CW7 show a similar composition in terms of hydration products, which shows high intensity of calcium hydroxide peaks and relatively low intensity of alite and belite peaks.

The addition of filter glass as cement replacement shows significant effect on the hydration process. As shown in Table 2.2, the filter glass powder contains various kinds of saccharides such as galactose, glucose and mannose. The incorporation of large amount of filter glass powder (for instance C7) results in a high content of incorporated organic contaminations such as paper fibre and sugar. During the hydration, degradation also takes place on the paper fibre under the alkaline environment, which results in more released saccharides. As shown in Fig. 2.6 (c), the saccharides from filter glass exhibit a weaker effect on formation of ettringite and stronger effects on the formation of calcium hydroxide during hydration. The mechanism of saccharides on cement hydration was investigated in detail in previous research, which indicates that the presence of saccharides results in the retardation of cement hydration, due to surface absorption of retarders directly on the anhydrous surface; resulting in the nucleation and growth poisoning of hydrates including portlandite (Bishop and Barron, 2006). Actually the effect of saccharides is more evident on the hydration of C_3S and C_2S than C_3A (Ataie et al., 2015; Hong and Xiao-dong, 2014; Kochova et al., 2017). This explains why only the ettringite formation is not delayed from the XRD results. The increasing content of waste glass powder in the mixture leads to the reduced peak intensity of C_2S and C_3S. When the glass powder was used as cement replacement, the filler effects and heterogeneous nucleation (Xu et al., 2017) can be shown, similar to the role of applying fly ash or slag as cement substitute, thus more surface is available during the hydration. Besides, glass powder has a high content of amorphous silica, which will be dissolved in the alkaline environment and releases the silicates to the solution (Torres-Carrasco et al., 2014), increasing the consumption of C_3S and C_2S, and thus resulting in the reduced peak intensity of calcium silicate in high volume glass powder containing samples (Schwarz and Neithalath, 2008). Additionally, the peak of hydrocalumite is observed from the XRD results, especially in samples with high filter glass contents such as C5 and C7 after 28 days curing, while the hydrocalumite is also shown in the sample containing 70% washed filter glass powder, which may relate to the residue of chloride after the washing procedure. Ordinary Portland cement can bind

chloride through physical adsorption and chemical substitution (Florea and Brouwers, 2012). Hydrocalumite is a product from the hydration of calcium aluminate and, is a double layered hydroxide (Zhang et al., 2011). In ordinary cement paste, the ettringite will react with hydrocalumite to a calcium monosulfoaluminate hydrate. In the presence of Cl^-, SO_4^{2-} in the layered structure will be replaced by the Cl^- (Kourounis et al., 2007; Yu et al., 2010).

2.3.4 Thermogravimetric analysis

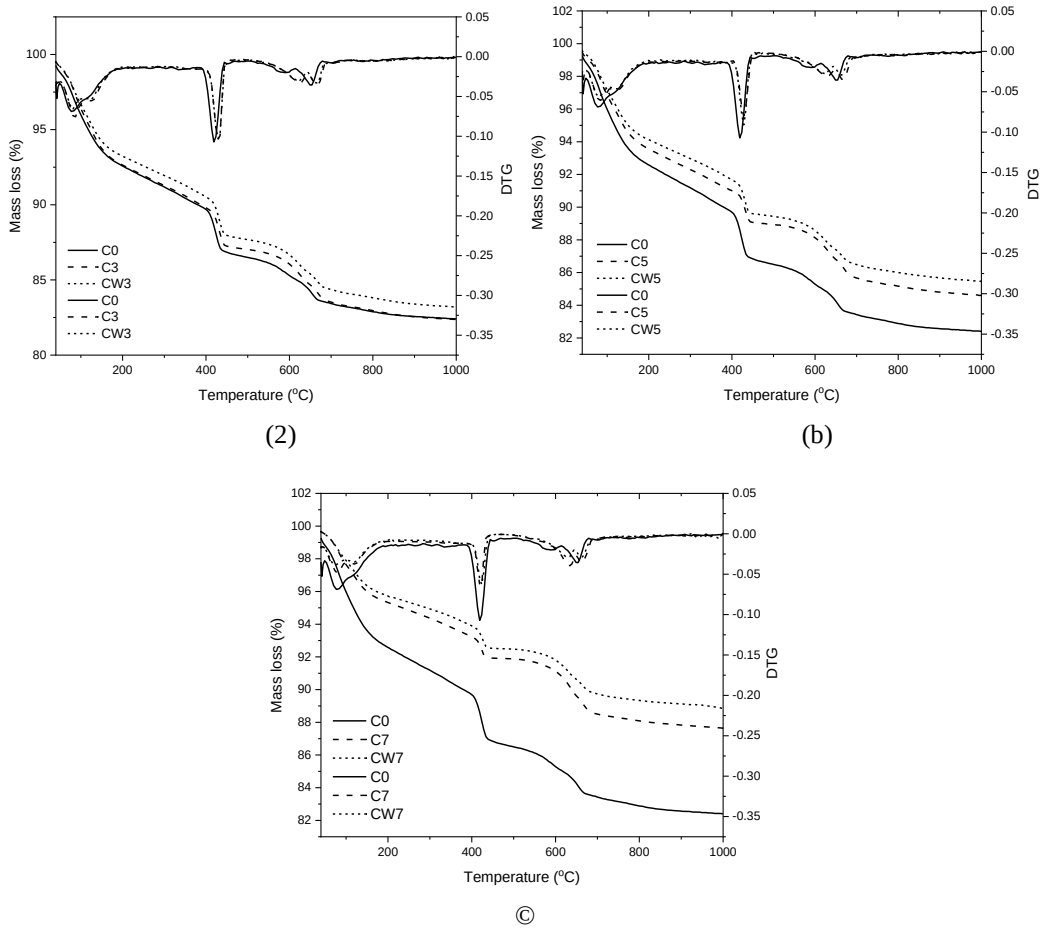

Figure 2.7 TG results of samples with different filter glass and washed filter glass content: (a) 30% (b) 50% (c) 70% after 28 days curing

The thermogravimetric results of different mixtures are shown in Fig. 2.7. The TG and DTG curves of samples containing 30%, 50% and 70% filter glass and washed filter glass powder are presented in Fig. 2.7 (a), (b) and (c) respectively. It can be seen that all samples present a significant mass loss from 40 °C to 105 °C. This mass loss is assigned to the physical bound water in mixtures. As the temperature increases, the mass loss is obviously increasing before 200 °C. After the evaporation of physically bound water, the C-S-H and Afm begin to lose the chemically bound water gradually at higher temperatures (Alarcon-Ruiz et al., 2005). The following two significant mass

losses are attributed to the decomposition of calcium hydroxide (400 °C-460 °C) and calcium carbonate (600 °C-700 °C). During the testing temperature range of 40 °C to 1000 °C, samples with waste glass powder show less total mass loss than the reference sample (C0). Additionally, the highest content of filter glass powder sample (C7) shows the least mass loss, which is also observed in washed filter glass containing samples. It is noticeable that washed filter glass samples show less total mass loss than the filter glass samples with the same replacing level after 28 days curing.

The calcium hydroxide content normalized by mass of cement are shown in Figs. 2.8. The content of calcium hydroxide is calculated from the TG results by applying the following equation:

$$W_{CH} = \frac{W_{400} - W_{460}}{M_{H_2O}} \times M_{CH} \quad (2.1)$$

$W_{400} - Mass\ loss\ at\ 400\ °C$

$W_{460} - Mass\ loss\ at\ 460°C$

$M_{H_2O} - Molar\ mass\ of\ water$

$M_{CH} - Molar\ mass\ of\ calcium\ hydroxide$

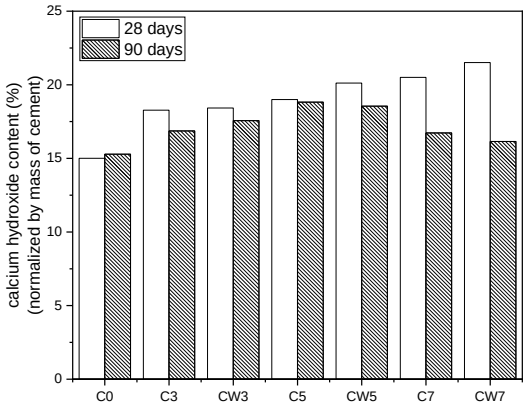

Figure 2.8 Calcium hydroxide contents

Fig. 2.8 shows the calcium hydroxide content (normalized by cement) after 28 days and 90 days curing in different samples. The addition of both filter glass and washed filter glass promotes the formation of calcium hydroxide. Filter glass powder containing samples, especially for high volume filter glass incorporation sample, present a slightly lower calcium hydroxide content after 28 days curing but higher after 90 days than samples containing washed filter glass. For the sample containing washed filter glass, calcium hydroxide consumption can be observed in all samples. Apparently, more calcium hydroxide is consumed in washed filter glass containing samples with the increasing of the replacement ratio compared with the sample containing filter glass powder. The lower calcium hydroxide consumption after 28 days and the delay of

calcium hydroxide formation in samples with filter glass addition may indicate that the pozzolanic reaction of glass powder is partially influenced by the retardation effect of saccharides.

2.3.5 N_2 adsorption analysis

Fig. 2.9 (a to c) present the nitrogen sorption and desorption isotherms of samples containing different dosage of filter glass powder and washed filter glass powder at various relative pressures (p/p^0). It is clear that the isotherm curves show similar type loop. A summary of the specific surface area results from the BET (Brunauer–Emmett–Teller theory) calculation is shown in Fig. 2.9 (d).

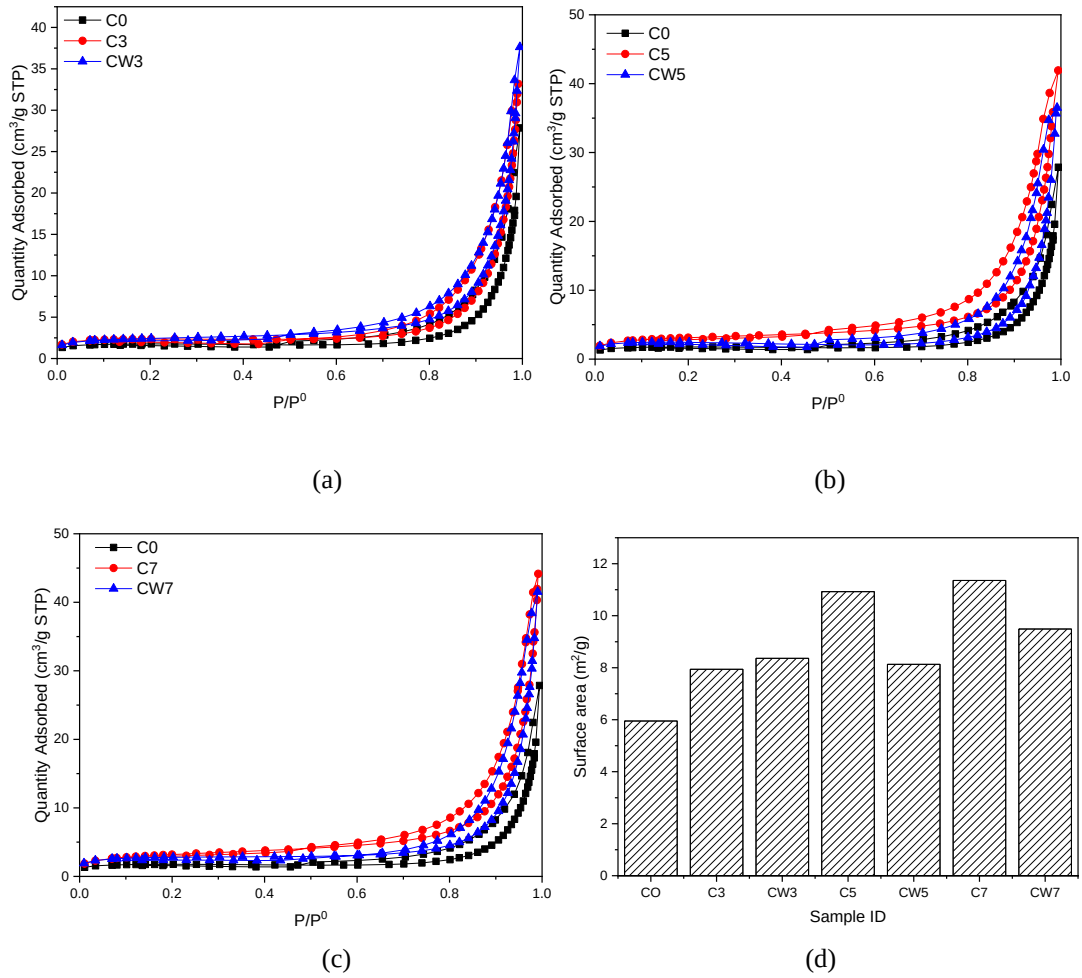

Figure 2.9 Nitrogen sorption isotherm curves (a) (b) (c) and (d) Bet surface areas

It can be seen that samples with filter glass and washed filter glass powder show higher quantity of adsorbents than the reference (C0) from the nitrogen adsorption branch. The washed filter glass containing sample (CW3) absorbs slightly more than the sample containing filter glass powder (C3) under the same replacement ratio of 30%, after the relative pressure reaches 0.4. When the dosage of filter glass and washed filter glass

powder increased to 50% and 70%, samples containing filter glass powder show higher absorption ability than the washed filter glass powder incorporated samples, from the very low relative pressure to high relative pressure.

It can be seen from Fig. 2.9 (d) that mixtures show different surface areas. The addition of filter glass and washed filter glass powder increases the specific surface area when compared with the reference (C0). It is noticeable that 70% filter glass powder containing sample (C7) presents the highest surface area around 11.36 m^2/g, while this value is 9.49 m^2/g in washed filter glass based samples. In addition, no significant difference in surface area is observed between filter glass and washed filter glass containing samples at low replacement level (30%).

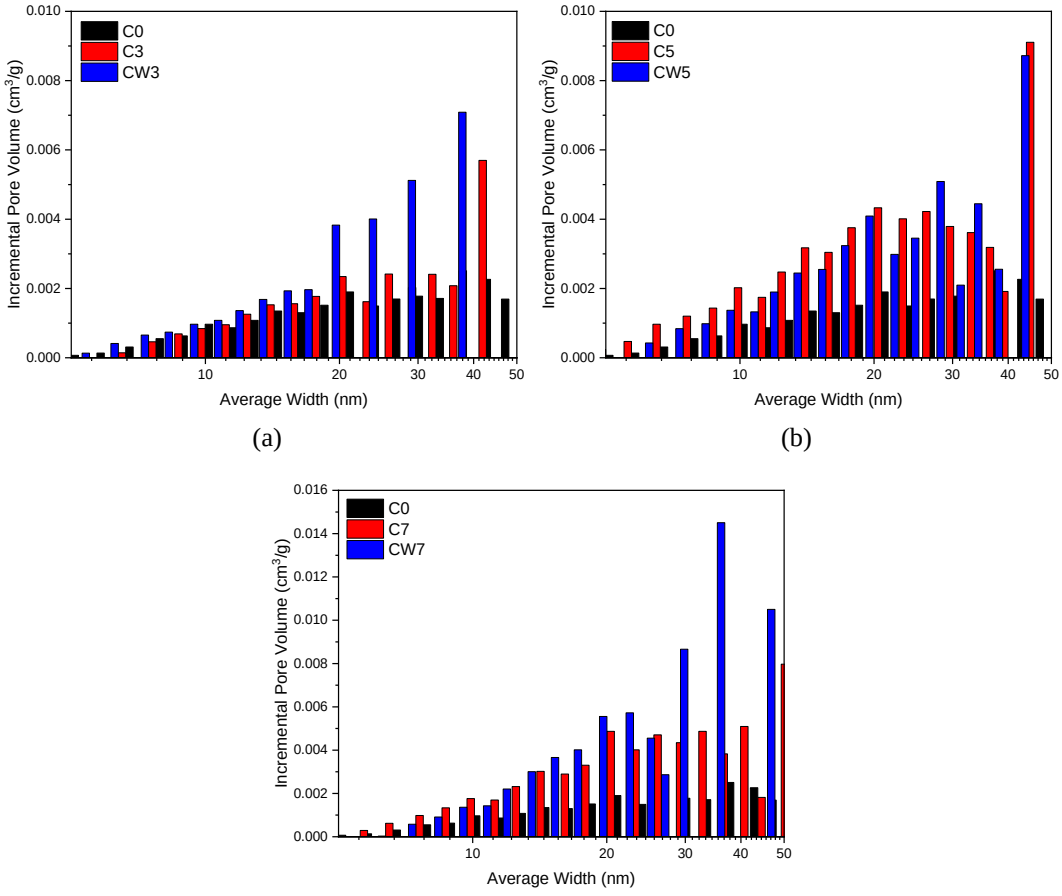

Figure 2.10 BJH pore distributions

The nitrogen sorption isotherm analysis was conducted through pore size distribution calculation by BJH (Barrett-Joyner-Halenda) method. The results of pore size distributions of mixtures are shown in Fig. 2.10. As can be seen, the addition of filter glass and washed filter glass powder leads to different pore structure changes on the hydration products. For samples containing 30% washed glass powder (CW3), a slightly higher volume of pores that less than 15 nm and relatively larger volume of

pores from 2 nm to 50 nm is observed in Fig. 2.10 (a), when compared with filter glass powder containing samples (C3). Further increasing the filter glass powder dosage to 50% and 70% leads to high porosity at low ranges (<15 nm), and low porosity at high ranges (> 20 nm) when compared with washed filter glass powder containing samples, as shown in Fig. 2.10 (b) and (c).

The addition of both filter glass and washed filter glass powder increase the surface area and results in reaction products with higher porosity. It is well known that the higher hydration degree of cement pastes contributes to the high specific surface area (Mikhail et al., 1964); and the water/cement ratio show limited influence on the surface area (Juenger and Jennings, 2001). As a consequence, the addition of glass powder could be the main reason for the increased surface area. Generally, the incorporation of glass powder lowers the overall Ca/Si atom ratio and increases Al/Ca in the pore solution, which causes the producing of C-S-H gel with low density as fly ash in early age (Goñi et al., 2012); additionally, the dissolving of glass powder in alkali environment releases silicate, which also promotes the hydration of the cement particle (Ben Haha et al., 2011). Comparing filter glass containing samples with washed filter glass containing ones, filter glass containing samples present higher surface area and larger pore volume. This indicates that the incorporation of filter glass produces C-S-H gels with lower density than washed filter glass incorporating samples. The retardation of the saccharide in filter glass powder containing samples induces the high initial dissolution of ions, while the long delay period demonstrates that the many ions could migrate to the sites far from the reaction particle (Juenger and Jennings, 2002). These result in the formation of C-S-H gel in the open pore spaces and higher surface area in terms of the microstructure, which is also due to the more porous structure.

2.3.6 SEM

The SEM- EDX are used together to determine the micro-structure and chemical composition of hydration products of pastes containing filter glass powder and washed filter glass powder. The results are shown in Fig. 2.11.

(a) 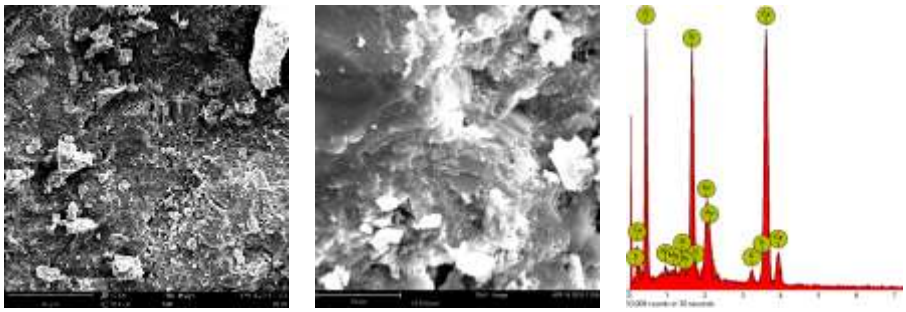

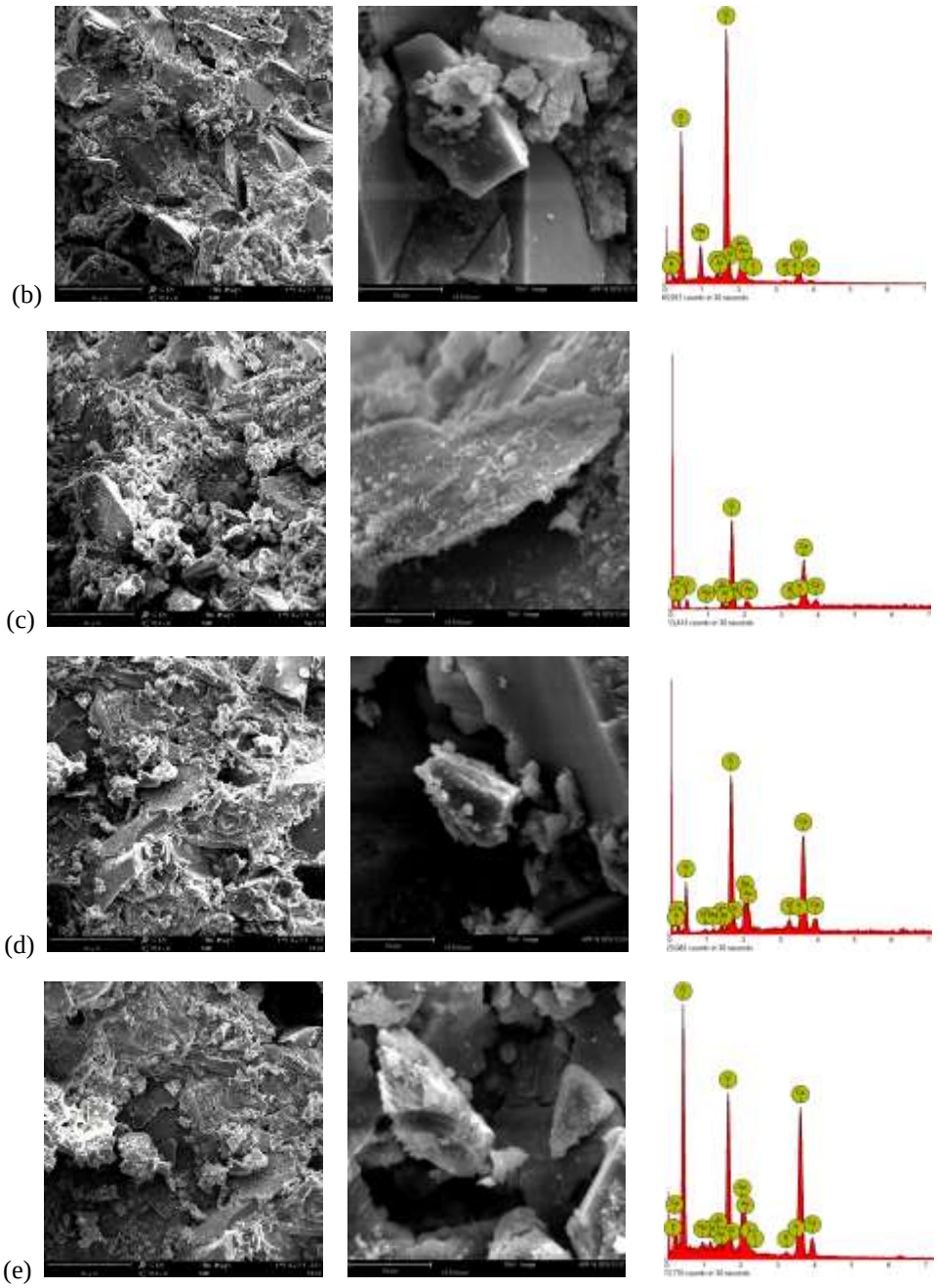

Figure 2.11 SEM images (left ×1000, right ×5000)and EDX results: (a) plain sample C0 (b) 70% filter glass sample C7 (c) 70% washed filter glass sample CW7 (d) 30% filter glass sample C3 (e) 30% washed filter glass sample CW3

It can be observed that the plain cement paste (C0) shows a relatively dense microstructure. The hydration products ideally fill the space between the unreacted cement particles and show a homogeneous structure. The result of EDX obtained around the unreacted cement particle shows a Ca/Si ratio of 2.02, which is a typical C-S-H produced by cement hydration (Richardson and Groves, 1993; Rodger and Groves, 1989).The filter glass and washed filter glass incorporation leads to a more porous structure at micro scale. As can be seen in Fig. 2.11 (d) and (e) that 30% filter glass (C3)

and washed filter glass (CW3) samples shows more porosity than the plain sample, and EDX and SEM images with 8000 × exhibit that the glass particles around 10 μm are covered by the C-S-H gel with a low Ca/Si ratio. For example, Ca/Si with 1.09 and 1.67 are observed in C3 and CW3, respectively. At the same time, most of the glass particles around 10 μm in C7 show clean and smooth surface with a Ca/Si with 0.14, which is due to the largely unreacted glass particles. These may indicate that a limited pozzolanic reaction occurred on the surface of these glass particles, and the products from cement hydration fill the pores between glass particles with weak binding forces. The EDX result of the glass particles surface in sample C7 also presents high Si and O content, which can be referred to the raw glass phase, while the morphological image of sample containing 70% washed filter glass powder exhibits a rough surface of glass particle. As can be seen from the SEM picture Fig. 2.11 (b) and (c), the glass particles in CW7 are covered by the reaction products. The EDX result of the gel on the surface of glass particle shows a low Ca/Si of 0.93, which can be considered as the products from the pozzolanic reaction of glass powder.

Compared with the glass particles in high volume filter glass and washed filter glass containing samples, it is obviously that the washed filter glass particles show a clear sign of pozzolanic reaction. The glass particle could be dissolved in the alkaline environment and the silicate released from glass phase reacts with the calcium hydroxide from cement hydration. The filter glass powder contains organic matter and saccharides contamination, which poisons the surface of cement particle and the growth of calcium hydroxide. Consequently, the dissolution of glass particles is inhibited, which limits the pozzolanic reaction on the surface of glass particles. Combining with the results of BET, it can be suggested that the samples containing washed filter glass show higher volume pore between 20-50 nm, which could be related to the C-S-H from pozzolanic reaction.

2.4 Conclusions

1. The leaching results indicate that the filter glass contains saccharides and high dosage of Na^+ and Cl^-. After washing treatment, the soluble salts and organic matter can be removed efficiently.

2. The addition of filter glass powder significantly retards the hydration process. The incorporation of filter glass powder also decreases the heat flow peak and cumulative heat during hydration. After washing, filter glass powder shows a limited influence of retardation on the cement hydration, which indicates that the organic contamination in filter glass is the main reason for the retardation of hydration.

3. The addition of the hydration accelerator such as $CaCl_2$, nano-silica and micro silica can significantly improve the hydration process and reduce the retardation of sample containing high volume filter glass. Burning treatment and second washing treatment for filter glass also can obviously reduce the retardation effect.

4. The saccharides in filter glass powder show significant influence on the hydration of high volume filter glass containing samples during different ages. After 28 days curing, the high volume filter glass powder containing samples show peaks of hydrocalumite which is related to the chloride in raw material. Also, the high volume filter glass powder and washed filter glass powder incorporation improve the consumption of tricalcium silicate and dicalcium silicate.

5. The filter glass powder containing samples show lower calcium hydroxide consumption than washed filter glass powder containing samples. However, the amount of generated portlandite suggests that the glass undergoes a pozzolanic reaction.

6. The filter glass powder incorporation increases the specific surface area, which is attributed to the increasing pore volume. The saccharides in filter glass powder contributes to the higher pore volume of less than 15 nm and lower pore volume of more than 20 nm when compared to the filter glass after washing.

7. High volume filter glass powder and washed filter glass powder containing samples result in porous microstructure. From the SEM images, the washed filter glass powder shows higher activity of pozzolanic reaction than the filter glass powder.

Chapter 3 Performance evaluation of sustainable high strength mortars incorporating high volume waste glass as binder

This chapter investigates the performance of sustainable high strength mortars incorporating recycled waste glass as a supplementary cementitious material (SCM) to replace cement with low (10%) to high (60%) replacement ratios, while normal mortars with high water to binder ratio (0.5) design were used as reference. The addition of the recycled waste glass significantly improves the slump-flow of fresh mortars with superplasticizer (SP). The increase of the recycled waste glass dosage contributes to a longer initial and final setting time compared to the plain cement sample, and shows an obvious delay of hydration compared with others incorporating the same amount of SP. The high strength series samples containing various contents of recycled waste glass show similar total gel porosity, but a significant increase of gel porosity was observed in normal strength series samples containing recycled waste glass. The addition of high volume waste glass results in a higher mesopore volume, then introduceing higher drying shrinkage in sustainable mortars. The mechanical performance tests show that sustainable high strength mortars containing 60% recycled waste glass can achieve a satisfactory strength (99 MPa) compared to the plain cement sample (115 MPa).

This part is partially published elsewhere:

G. Liu, M.V.A. Florea, H.J.H. Brouwers. Performance evaluation of sustainable high strength mortars incorporating high volume waste glass as binder. Construction and Building Materials, 2019, Volume 202, Page 574-588.

3. 1 Introduction

For the sustainable application of solid wastes, and reducing the energy consumption associated with cement production, high volume of SCMs (supplementary cementitious materials) from solid wastes such as ground granulated blast furnace slag (GGBS) and coal fly ash have been studied for high volume cement replacement. For example, high volume fly ash in conventional concrete and high strength concrete has been generally studied for several years (Jeong et al., 2015; Kim and Lee, 2013; Siad et al., 2018). But for waste glass, most of the existing studies focused on a cement replacement ratio of less than 30%.

From a value and sustainable application point of view, it can be desirable to incorporate high volume waste glass powder in high-strength concrete. It has been addressed that a low water to binder ratio is beneficial to reduce the strength loss and environmental impact when high volume pozzolanic material is incorporated as cement replacement (Poon et al., 2000). High-strength concrete also has a high durability (Ghafari et al., 2015) due to the very low water to binder ratio. Different industrial wastes in sustainable high strength concrete, such as slag, fly ash etc. have been widely studied (Chen et al., 2018; Ghafari et al., 2016; Kim et al., 2016). The addition of pozzolanic material contributes to a better workability and an improved microstructure of high performance concrete due to the pozzolanic reaction and filler effect (Cheyrezy et al., 1995). The reactivity of fine waste glass fractions' and their benefits on the workability of concrete, by applying it in ultra-high performance concrete to replace quartz powder and micro sand in high-strength concrete were also reported (Soliman and Tagnit-Hamou, 2016; Vaitkevičius et al., 2014). Drying shrinkage and strength are important parameters to evaluate the performance of high strength concrete (Li and Yao, 2001), but for sustainable high performance concrete containing recycled waste glass, the available studies are limited, and the influence on hydration kinetics, mechanical performance, shrinkage properties and especially microstructure still need further study for the high-value applications.

This chapter evaluates the fresh and hardened behaviour, hydration kinetics and hydration products, drying shrinkage, strength properties and microstructure of high strength and normal strength mortars containing high volume recycled waste glass as a SCM. The aim is to assess the performance of sustainable high strength mortars incorporating a high volume of recycled waste glass as binder and to investigate the different effects of glass powder on strength development, drying shrinkage and gel structure between sustainable high strength and normal strength mortars.

3.2 Materials and methods

3.2.1 Materials

The cement used in this study is a CEM III/A 52.5 N and is provided by ENCI. The waste glass powder was acquired from milled mixed coloured waste glass (soda-lime glass) fractions, and ground by ball milling with 300 rpm for 30 minutes. The superplasticizer used in this study is polycarboxylic ether based, with a concentration of 35%, provided by Sika. The sand used in this study is the CEN-Standard sand (0-2 mm) according to EN 196-1 provided by Normensand.

3.2.2 Methods

- *Mortars and pastes preparation*

Table 3.1 Mixtures design (1 m^3)

Sample ID	Cement (kg)	Glass powder (kg)	Water (kg)	Sand (kg)	SP (kg)
R-N	565.1	0	282.6	1412.8	0
GP10-N	506.4	56.3	281.3	1406.6	0
GP30-N	390.4	167.3	278.9	1394.5	0
GP60-N	220.3	330.4	275.3	1376.6	0
R-H	658.1	0	150.4	1645.2	18.8
GP10-H	589.3	65.5	149.7	1636.9	18.7
GP30-H	453.7	194.4	148.2	1620.5	18.5
GP60-H	255.4	383.1	145.9	1596.4	18.2

N-normal strength series H-high strength series

As shown in the Table 3.1 mixtures for 1 m^3, a low water / binder (cement + waste glass) ratio of 0.25 and superplasticizer (SP) were selected for the high strength series sample. The same dosage of SP for all high strength samples was conducted for investigating the influence of recycled waste glass on the workability of different components. The normal series mortars were prepared with the water / binder ratio of 0.5. The sand / binder ratio is 2.5 for all mortars. The cement was replaced by recycled waste glass from 0%, 10%, and 30% up to 60% by mass. Superplasticizer was used to get the desired flowability of high strength mortars. The mixing of mortar was done by using a 5-liter Hobart mixer. At first, mixing the dry binder (cement and waste glass powder) and fine aggregate (standard sand) were mixed for 30 s under low speed. Then water and superplasticizer were added and mixed for 120 s at low speed and 120 s at medium speed. At last, the fresh mortars were filled into the plastic mould of 40 mm × 40 mm × 160 mm and vibrated for 60 s and covered with the plastic film for 24 hours. After

the first 24 h, the mortar prisms were demoulded and covered by plastic film for ambient curing until further testing.

- *Flowability and setting time*

The slump-flow of fresh mortar was measured using the flow table test (EN 1015-3) (DIN EN, 2007). The fresh mortars were filled into a standard conical ring and a flow with 15 impacts was measured. Two diameters were recorded and the average value was used as the slump flow. The setting time of pastes was measured according to the Vicat needle method as described in EN 196-3 (EN, 2009).

- *Characterization methods for raw materials and reaction products*

The calorimetry test, X-ray diffraction, XRF, specific density, thermogravimetric test, SEM and N_2 absorption test were performed as the described in Chapter 2.2.2.

- *Mechanical performance*

The strength tests were carried out according to EN 196-1 (BS EN, 2005). Prism samples with a size of 40 mm × 40 mm × 160 mm were prepared and tested after 7 days, 28 days, 56 days and 90 days. An average value of flexural strength was calculated by testing 3 prism samples. In addition, compressive strength tests were conducted by 6 specimens. The drying shrinkage tests were conducted using prisms of 40 mm × 40 mm × 160 mm. After 24 hours sealed curing, the specimens were moved to an environment with 50% RH and a temperature of 20 °C. Then the length of different samples were measured and recorded after a given time.

3.3 Results and discussion

3.3.1 Characterization of the raw materials

The chemical composition of recycled waste glass and cement conducted by using XRF are shown in Table 3.2. It can be seen that the recycled waste glass accounts for 68.33% of SiO_2, 11.9% of CaO, and 14.65% of Na_2O.

Table 3.2 XRF of materials

Chemical composition	Recycled Waste glass (%)	Cement (%)
Na_2O	14.65	/
MgO	1.29	5.35
Al_2O_3	1.93	7.63
SiO_2	68.33	22.27
SO_3	0.086	5.52
K_2O	0.7	0.42
CaO	11.9	54.54
TiO_2	0.062	0.83
Cr_2O_3	0.12	0.005
MnO	0.022	0.19
Fe_2O_3	0.36	1.61
ZnO	0.009	0.027
BaO	0.061	0.031
PbO	0.05	0.002
Cl	0.019	0.023
P_2O_5	/	0.15
Specific density	2.50 g/cm^3	3.10 g/cm^3

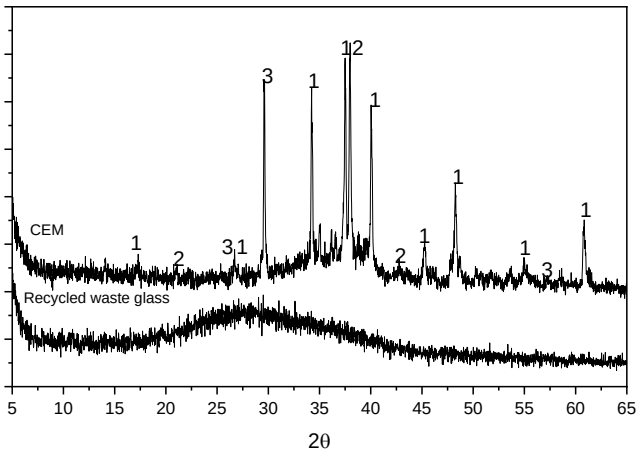

Figure 3.1 XRD patterns of cement and recycled waste glass (1-C_3S, 2-C_2S, 3-$CaSO_4$)

Their X-ray diffraction patterns and particle size distributions are shown in Fig. 3.1 and Fig. 3.2. The recycled waste glass powder milled from mixed colour waste glass fractions is shown in Fig. 3.3. The average particle size of glass powder and cement is 10.97 μm and 8.23 μm, respectively. It can be seen from the XRD patterns that recycled waste glass shows no distinct peaks but a relatively wide peak, which is related to the amorphous structure. The cement presents typical peaks related to dicalcium silicate, tricalcium silicate and calcium sulphate.

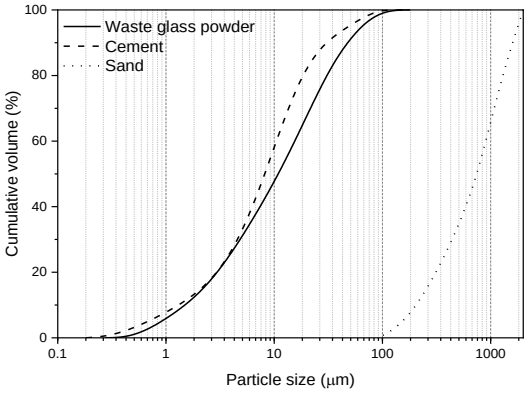

Figure 3.2 Particle size distributions

Figure 3.3 Recycled waste glass fractions before and after milling

3.3.2 Fresh behaviour of sustainable mortars

- *Slump flow and density*

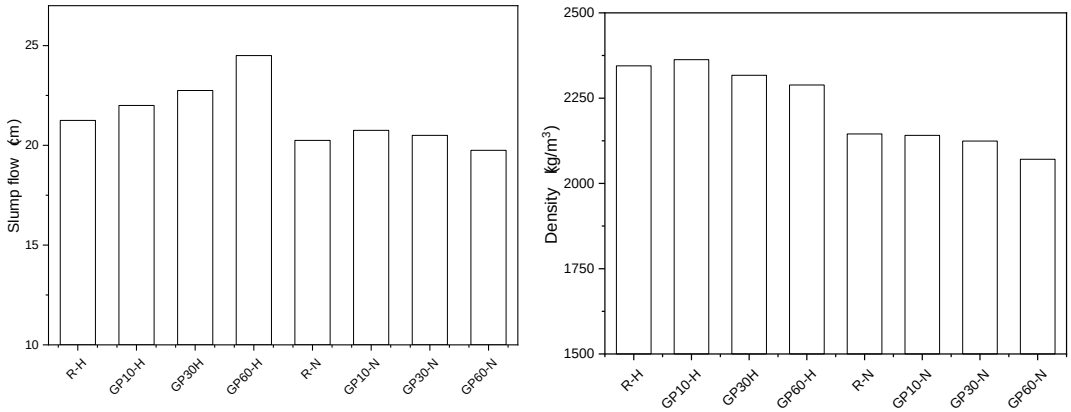

(a) (b)

Figure 3.4 (a) Slump flow and (b) density

The slump flow and density of mortars are shown in the Fig. 3.4. It can be seen that the slump flows of high strength mixtures are enhanced by the increase of the recycled waste glass incorporation. The plain high strength mixture (R-H) has a slump flow of

21.25 cm. Compared with the plain sample, the high strength sample mixing with 60% recycled waste glass exhibits a 15.3% higher flowability with 24.5 cm, while the normal mixtures present no significant change on the flowability or even a slight decrease when high volume recycled waste glass was incorporated.

It can be observed from Fig. 3.4 (b) that the density of mortar keeps decreasing with the increase in recycled waste glass dosage, in both of high strength series or normal strength series. Recycled waste glass has a lower density (2.5 g/cm^3) than the cement (3.1 g/cm^3). The higher content of glass powder in mortar results in a lower density. The decreasing density of mortar incorporating waste glass was also reported by other studies (Yu et al., 2016).

The addition of superplasticizer can efficiently improve the flowability of mixtures with very low water / binder ratios. The superplasticizer used in this study shows higher effects on the flowability on recycled waste glass-containing samples than on the plain samples (R-H), at the same dosage (SP/binder). This polycarboxylate-based superplasticizer has long chains and side chains can adsorb on the surface of the cement particle (Yamada et al., 2000), and produce an electrostatic repulsive effect, which causes the dispersing of cement particles (Zingg et al., 2009). The dosage of superplasticizer causes a significant influence on the flowability and hydration kinetics (Li et al., 2017). For a cement replacement ratio from 0% up to 60% by recycled waste glass, the lower cement proportion increases the SP/cement ratio. These all contribute to a better flowability of high strength mixtures with the increase of glass powder incorporation.

- *Setting time*

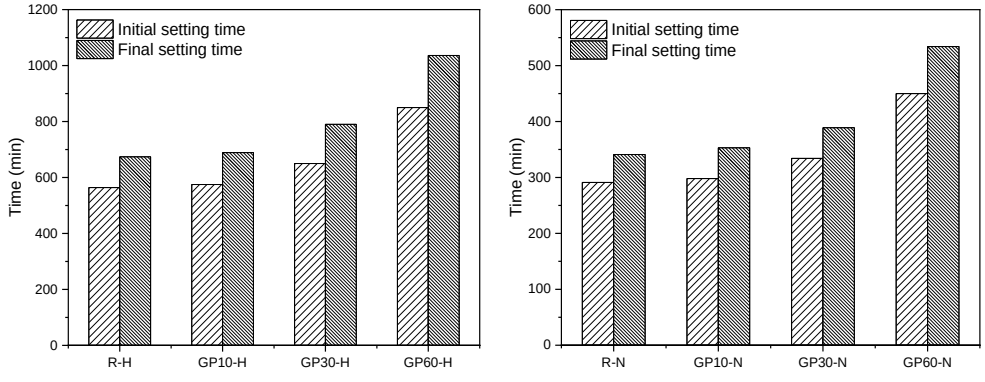

(a) (b)

Figure 3.5 Setting time of mixtures

For the high strength mixtures, the setting time is almost 2 times longer than for the

normal strength sample due to the addition of superplasticizer. The initial setting time of the plain sample with high strength is 564 min and 674 min to reach the final setting after mixing. When the amount of recycled waste glass increases up to 60%, the initial setting is retarded to 850 min while the final setting takes place after 1036 min. Normal strength samples show a shorter setting time than the high strength mixtures. The initial setting time of the plain sample (R-N) is 291 min and 341 min for final setting. High volume glass-containing normal strength sample presents an initial setting time of 450 min and the final setting time of 534 min.

A high alkalis content usually results in flash setting (Xie and Xi, 2002), but in this case, no flash setting was observed. This may be due to the fact that the alkali dissolution is not fast enough from waste glass just induces a limited influence on the hardening process (Schwarz and Neithalath, 2008). The setting behaviour is related to the dispersion of cement grains and hydration (Hwang and Shen, 1991). Since the cement is substituted by recycled waste glass, the decreased cement mass in pastes results in less hydrates formation. On the other hand, the cementitious effects caused by the pozzolanic reaction shows limited influences at early ages. In addition, with the increasing glass powder incorporation, the effective water to cement ratio keeps increasing, a higher water to cement ratio inducing a longer duration to achieve setting. As consequence, the addition of recycled waste glass increases both initial and final setting times.

3.3.3 Hydration kinetics and products analysis of sustainable mortars

- *Hydration kinetics*

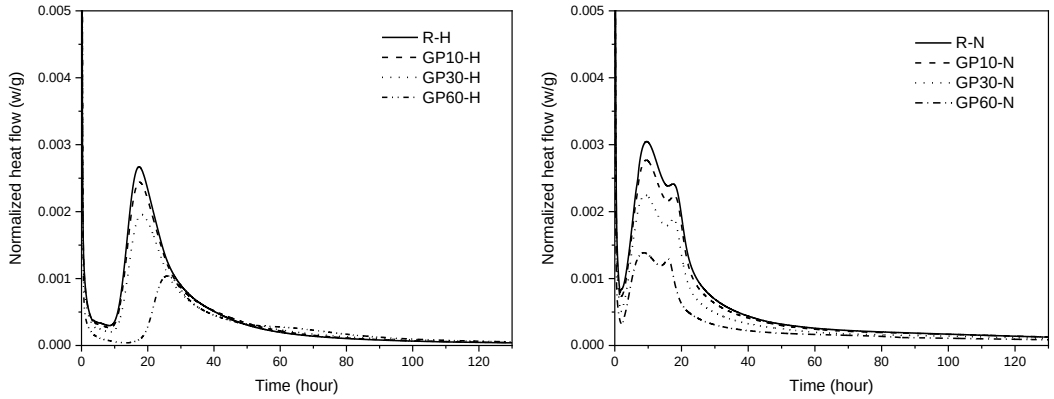

(a) (b)

Figure 3.6 Heat flow during the early hydration

As shown in Fig. 3.6 (a), all samples show one peak of heat flow during the hydration with different intensities. The heat flow peak intensity decreases gradually by the

increasing of glass powder dosage. It is noticeable that the hydration of paste containing high volume glass powder is delayed significantly compared with other samples with the same superplasticizer dosage.

The heat flow curves of normal samples with no superplasticizer and high water to binder ratio show two peaks and shorter time to reach the first peak during hydration, which can be seen in Fig. 3.6 (b). The first peak is related to the hydration of C_3S, and the second peak corresponds to conversion of ettringite to monosulfate (Mostafa and Brown, 2005). As shown in the Fig. 3.6 (b), the high-volume recycled waste glass-containing sample (GP60-N) takes a shorter time to reach the first and second peak, which means that the addition of a high amount of recycled waste glass improves the reaction rate.

Fine waste glass powder has been shown to have a pozzolanic activity in an alkaline environment because of the high amorphous silica content (Shi et al., 2005). In addition, the dissolution of fine glass powder in an alkaline environment is accompanied by the release of sodium ions (El-Shamy et al., 1972). For samples containing superplasticizer, the cement particle's dissolution and reaction in the pore solution are delayed. As a consequence, the pH of the pore solution increases with a slow rate, and subsequently, the dissolution of fine glass powder is inhibited. On the other hand, the SP to cement ratio is increased with the increase of the waste glass powder content. Generally, the higher SP to cement ratio results in a more significant retardation effect on sample hydration. However, for the samples without SP, there is no delay on the dissolution of waste glass powder, which releases sodium and silica to the pore solution and causes the acceleration of hydration rate (Nocuò-Wczelik, 1999).

Table 3.3 Cumulative heat (normalized by cement) and acceleration index

	Cumulative heat (J/g)				Acceleration index			
Sample ID	Total heat	1 day	3 days	5 days	1 day	3 days	5 days	Total heat
R-H	211.40	117.00	196.70	210.60	0.00%	0.00%	0.00%	0.00%
GP10-H	231.22	123.33	213.44	230.11	5.41%	8.51%	9.26%	9.38%
GP30-H	264.00	130.00	237.14	262.43	11.11%	20.56%	24.61%	24.88%
GP60-H	319.25	69.00	263.25	316.25	-41.03%	33.83%	50.17%	51.02%
R-N	294.90	188.00	259.70	292.20	0.00%	0.00%	0.00%	0.00%
GP10-N	302.67	190.56	264.22	299.56	1.36%	1.74%	2.52%	2.63%
GP30-N	315.14	198.43	274.14	311.86	5.55%	5.56%	6.73%	6.86%
GP60-N	365.25	214.00	307.50	360.25	13.83%	18.41%	23.29%	23.86%

To investigate the influence of recycled waste glass on the hydration of cement, the summary of the calorimeter result (normalized by mass of cement) of different samples is shown in Table 3.3. As can be seen in the high strength samples, the addition of waste

glass can improve hydration of cement significantly. The acceleration index of different samples during calorimeter test is calculated by the following equation:

$$Acceleration\ index = \frac{H_{GP} - H_C}{H_C} \times 100\% \quad (3.1)$$

$H_{GP} - normalized\ cumulative\ heat\ of\ samples\ by\ mass\ of\ cement$
$H_C - normalized\ cumulative\ heat\ of\ plain\ cement\ sample$

The acceleration index of high volume waste glass containing sample (GP60-H) is negative at 1 day, which is due to the highest SP/cement ratio. From the heat flow curve, it can be seen that the same dosage SP in high volume waste glass sample causes longer duration to reach the heat peak. However, after the induction period, the acceleration index enhances dramatically. Compared to the normal strength samples with the same waste glass dosage, high strength samples show a higher acceleration index. This can be explained by the strong dilution effect and heterogeneous nucleation (Lawrence et al., 2003) by increasing waste glass proportion in such a low water to binder ratio system. In general, a higher acceleration effect (as described in Equation 3.1) on cement hydration is observed in the high strength samples compared to the normal strength samples by the incorporation of recycled waste glass.

- *XRD of reaction products*

The mineral composition of the high strength series and normal strength series samples containing different amount of recycled waste glass after 90 days curing are shown in Fig. 3.7. It can be seen that all samples exhibit common peaks of ettringite, portlandite, C-S-H and tricalcium silicate and dicalcium silicate, which were produced by the cement hydration, but with different peak intensities.

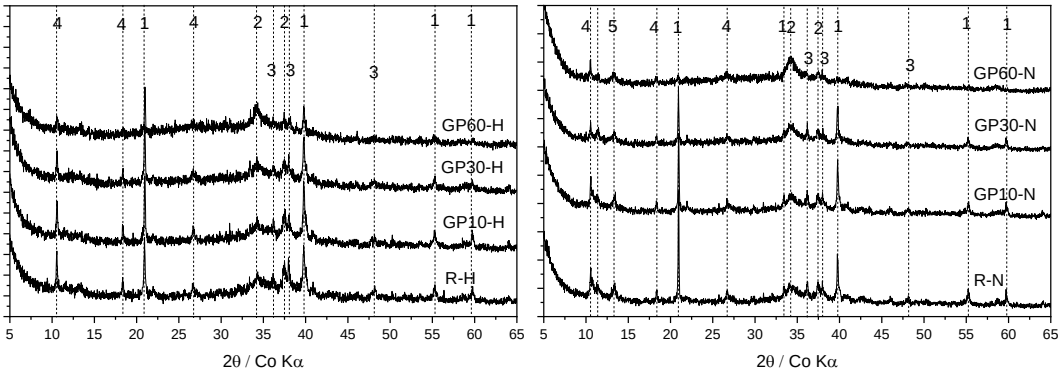

(a) (b)

Figure 3.7 XRD patterns of samples of (a) high strength series and (b) normal strength series (1- calcium hydroxide, 2- C-S-H, 3- alite and belite, 4- ettringite, 5- hydrocalumite)

The peaks of ettringite come from the hydration of C_3A; peaks of portlandite mainly come from the hydration of C_2S and C_3S; peaks of C-S-H are generated combining from the hydration of C_2S, C_3S and the pozzolanic reaction of glass powder. The addition of recycled waste glass reduces the peak intensity of portlandite, ettringite and C_2S, C_3S with the increasing glass powder amount, while the peaks of C-S-H become clearer and of higher intensity. The pozzolanic character of waste glass can also enhance the consumption of calcium hydroxide and calcium silicate, which is related to the reduced peak intensity.

It is interesting to notice that the peaks intensity of portlandite in the high strength sample and normal sample show a significant difference. In the high strength sample (GP60-H) containing high volume of recycled waste glass, the peaks of portlandite are weak but still can be observed clearly, while an extremely low peak intensity of portlandite can be observed in normal strength sample (GP60-N). These may indicate that the normal strength sample modified by high volume recycled waste glass contains less portlandite compared to the high strength sample containing same dosage of recycled waste glass.

- *Thermogravimetric study of hydration products*

The results of the thermogravimetric test of all samples after 90 days curing are show in Fig. 3.8. All samples show a significant mass loss from 40°C to 1000°C due to the loss of physically bound water, the loss of chemically bound water, decomposition of C-S-H gel, decomposition of calcium hydroxide and decomposition of calcite.

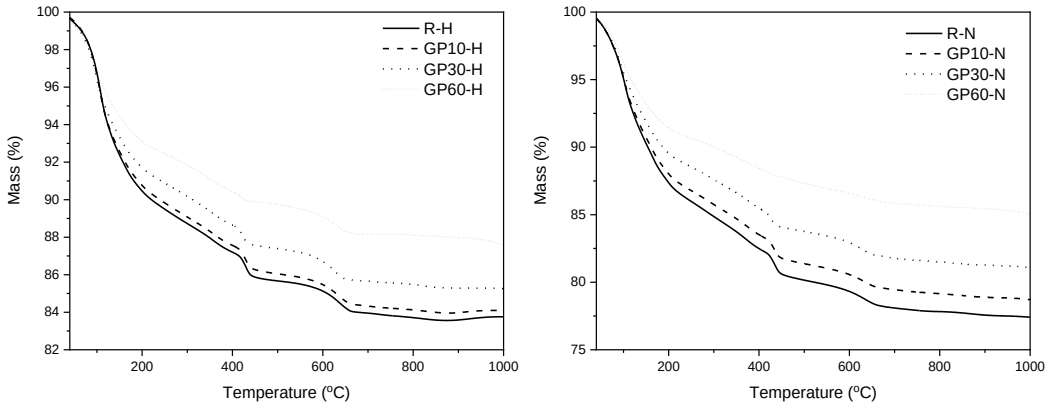

(a) (b)

Figure 3.8 The thermogravimetric curves of (a) high strength mixtures and (b) normal strength mixtures

As can be seen in Fig. 3.8 (a), the addition of recycled waste glass results in a decreasing mass loss for high strength samples during the whole TG test. The remaining mass of plain sample after heating to 1000°C is about 83.75%, which is the lowest compared to

84.08%, 85.26% and 87.59% for 10%, 30% and 60% recycled waste glass containing samples, respectively. The high strength specimens exhibit lower mass loss than the normal strength samples during the test. As shown in Fig. 8 (b), 60% recycled waste glass-containing sample (GP60-N) presents a remaining mass of 85.05%. The plain sample (R-N) has the remaining mass of 77.4% and 10% waste glass-containing sample (GP10-N) remains 78.72% of mass after heating to 1000 °C.

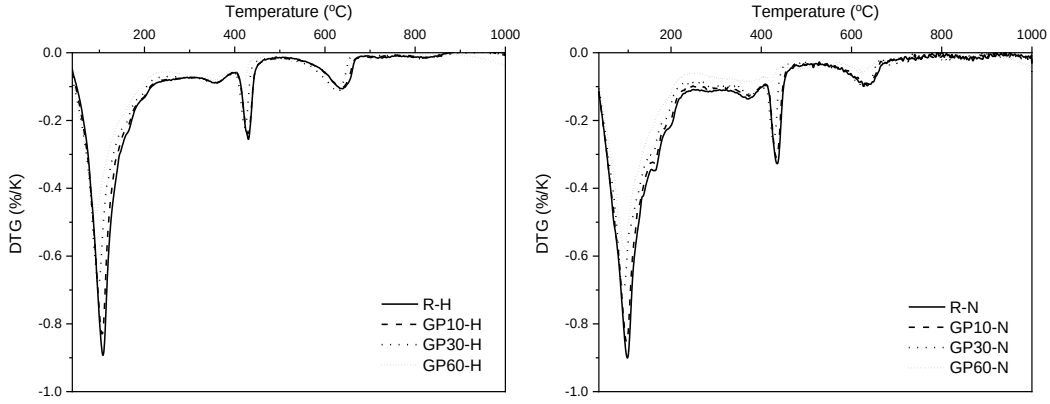

(a) (b)

Figure 3.9 DTG curves of samples with (a) high strength and (b) normal strength series

Table 3.4 Calcium hydroxide content (normalized by cement mass)

	CH content (%)				CH content change from 7 day		
Sample ID	7 days	28 days	56 days	90 days	28 days	56 days	90 days
R-H	5.96	5.84	5.59	5.71	-2.07%	-6.21%	-4.14%
GP10-H	6.30	6.30	5.94	6.21	0.00%	-5.80%	-1.45%
GP30-H	7.40	7.28	6.70	6.58	-1.59%	-9.52%	-11.11%
GP60-H	9.76	8.02	6.68	5.24	-17.89%	-31.58%	-46.32%
R-N	8.63	8.39	8.43	8.26	-2.86%	-2.38%	-4.29%
GP10-N	8.86	8.63	8.59	8.45	-2.58%	-3.09%	-4.64%
GP30-N	10.04	9.69	8.57	8.63	-3.51%	-14.62%	-14.04%
GP60-N	10.07	10.18	7.09	4.83	1.02%	-29.59%	-52.04%

The DTG results of different samples are shown in Fig. 3.9 (a) high strength series and (b) normal strength series. All DTG curves show three main peaks during the test. The first peak around 105 °C indicates the evaporation of physically bound water. The second peak around 400-460 °C is related to the decomposition of calcium hydroxide, the last peak from 600-700 °C corresponds to the decomposition of calcium carbonate. It is obvious that all peak intensities gradually decrease with the increasing amount of recycled waste glass in samples. This also indicates that the addition of recycled waste glass reduces the physically bound water and calcium hydroxide content of specimens. Recycled waste glass is believed to show pozzolanic activity in an alkali environment. The silica dissolved from the glass phase can react with calcium hydroxide to form C-S-H, which reduces the CH content in samples.

To further understand the consumption of calcium hydroxide by recycled waste glass, the calcium hydroxide content of different samples with various curing duration are summarized and shown in Table 3.4. It is clear that in normal strength samples, recycled waste glass shows a higher CH consumption after 7 days compared to high strength samples. The pozzolanic reaction of waste glass powder mostly relies on the amount of CH. In normal strength samples, high water to cement ratio contributes to the higher hydration degree of the cement part, in other words, more CH is produced by cement hydration. On the contrary, low water to binder ratio in high strength samples results in a lower hydration degree. As a consequence, the CH content change in the high strength samples is lower compared to normal strength samples. This is similar to the CH consumption in high volume fly ash concrete (Poon et al., 2000).

3.3.4 Microstructure characterization of sustainable mortars

- *SEM and EDX analysis*

Fig. 3.10-13 show the SEM images of unpolished pastes and polished mortar samples. As shown in Fig. 3.10 (a) and Fig. 3.11 (a), the normal strength sample containing 60% recycled waste glass (GP-60N) presents a more porous microstructure compared to the plain sample (R-N). As well as in the images of the polished mortar samples, the plain sample shows a denser structure than the sample with high volume glass powder (Fig. 3.10 (b) and Fig. 3.11 (b)). The aggregated glass particles (red circle) can be observed in GP-60N, which shows a loose packing. This may be caused by low gel / space ratio and the high amount of glass addition; as a consequence, the limited products of hydration and pozzolanic reaction are not enough to fill the volume of the pores. On the contrary, the high strength plain sample and sample containing 60% recycled waste glass show no significant differences in morphology of microstructure; as shown in Fig. 3.12 (a) and Fig. 3.13 (a), a dense gel structure can be found in these two samples. From the mortar samples, the dense packing and compact interfacial transition zone (ITZ) can be observed. No aggregated glass particles are observed in GP-60H, which is due to the effect of dispersion effect of SP. In addition, the high gel / space ratio (Lam et al., 2000) of GP-60H induces less space for hydration and pozzolanic reaction products. Consequentlly, a dense microstructure is formed.

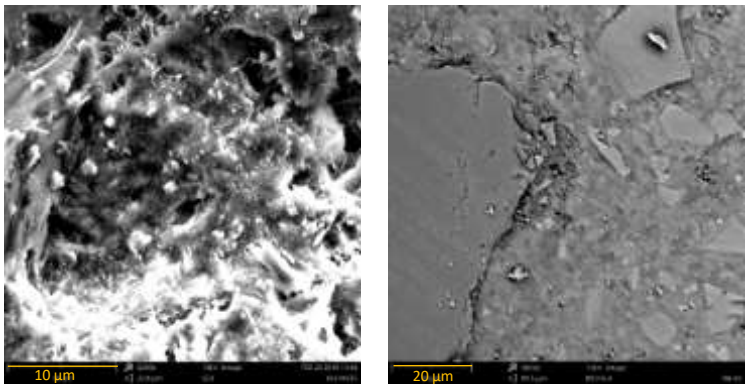

(a) (b)

Figure 3.10 SEM images of normal strength plain sample (a) paste (b) mortar cured for 90 days

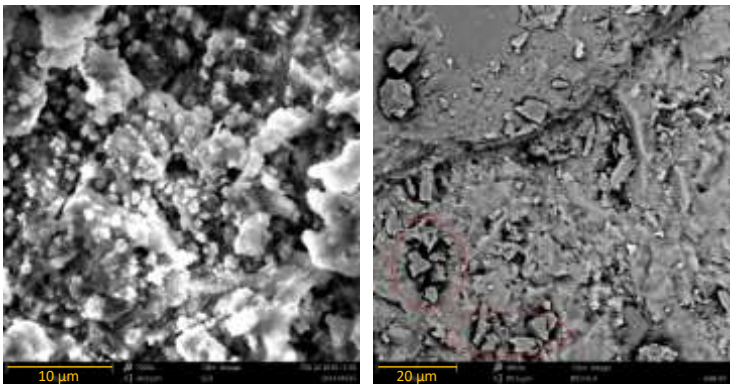

(a) (b)

Figure 3.11 SEM images of normal strength sample containing 60% waste glass powder (a) paste (b) mortar cured for 90 days

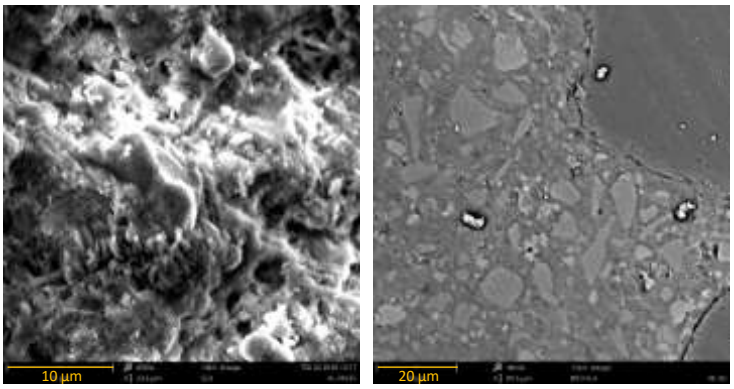

(a) (b)

Figure 3.12 SEM images of high strength plain sample (a) paste (b) mortar cured for 90 days

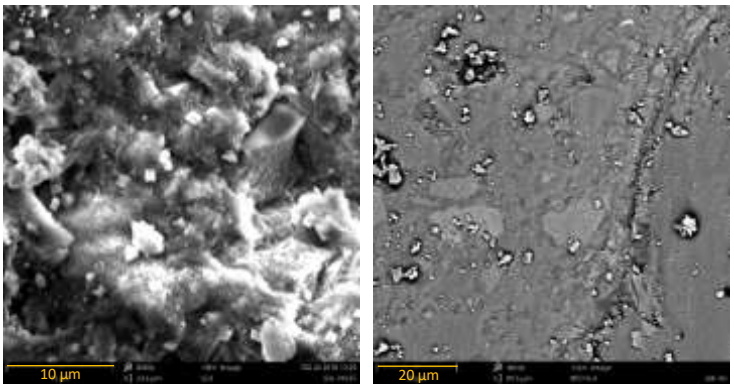

(a) (b)

Figure 3.13 SEM images of high strength sample containing 60% waste glass (a) paste (b) mortar cured for 90 days

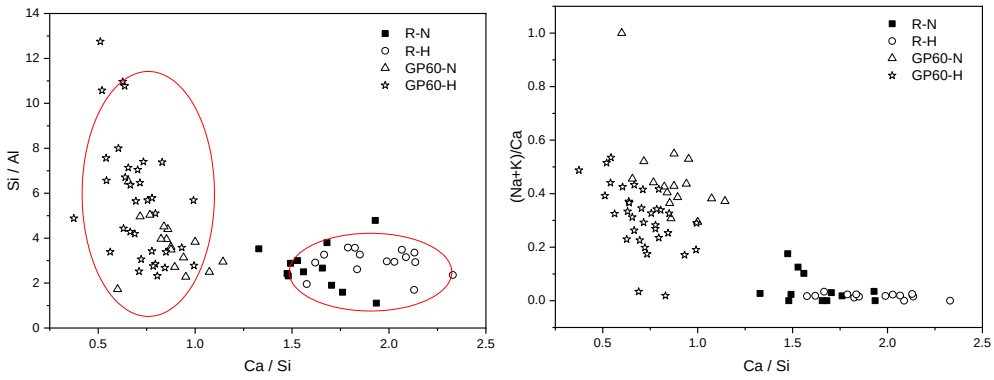

(a) (b)

Figure 3.14 EDX results of different samples

Fig. 3.14 illustrates the summary data from EDX analysis, which presents the relationship between Ca/Si, Si/Al and (Na+K)/Ca ratios in formed gel. As it can be seen in Fig. 3.14 (a), after the high volume recycled waste glass was incorporated, the Ca/Si ratio of C-S-H decreases significantly compared to the reference samples. In addition, a higher Si/Al ratio is exhibited by high volume glass containing samples. This is due to the recycled waste glass, which is a SiO_2 rich material; as the consequence, the total Al and Ca are reduced. Generally, the decreasing Ca/Si ratio can improve the alkali binding ability of C-S-H or C-A-S-H gel as shown in the studies by Brouwers (Brouwers and vanEijk, 2003), Chen (Chen and Brouwers, 2010) and Yoon Hong (Hong and Glasser, 1999). It can be seen in Fig. 3.14 (b) that high volume recycled waste glass containing samples have a slightly higher (Na+K)/Ca compared to the plain sample. Moreover, the (Na+K)/Ca in GP60-N is higher than in GP60-H, this may be related to the high porosity gel structure in GP60-N, which can result in a higher physical adsorption ability.

- *Gel structure- N_2 adsorption analysis*

Fig. 3.15 (a) and (b) illustrate the cumulative pore volume of different paste samples by N_2 adsorption test. The recycled waste glass incorporation in the high strength series samples shows no significant change on the total pore volume from the adsorption branch of N_2 adsorption test. High volume recycled waste glass-containing sample (GP60-H) shows a slight increase in total pore volume compared with the plain sample. For the normal strength series samples, the addition of recycled waste glass obviously enhances the pore volume.

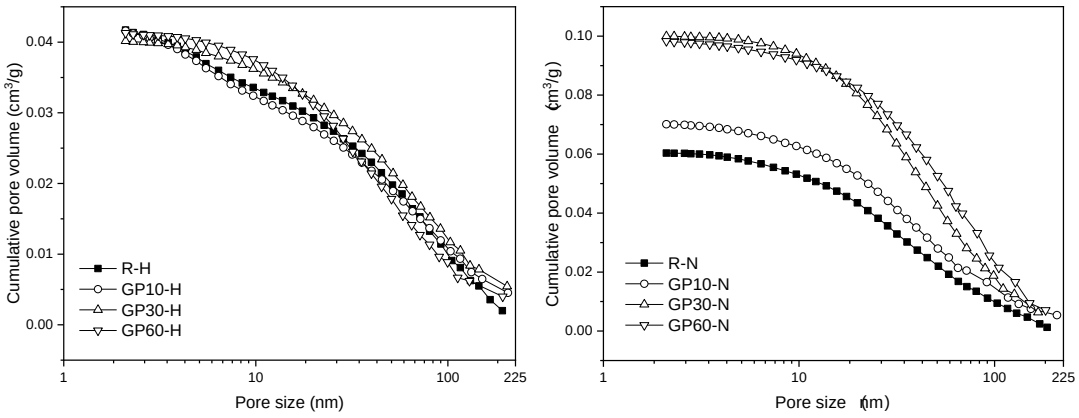

(a) (b)

Figure 3.15 Cumulative pore volume of various samples from BJH adsorption branch: (a) high strength samples and (b) normal strength samples after 90 days

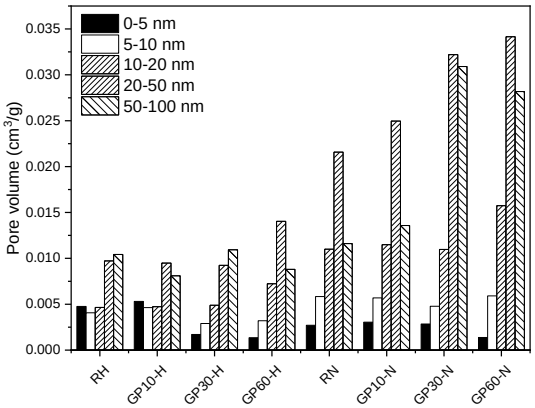

Figure 3.16 Pore size distribution of mixtures after 90 days

The pore size distribution of different samples is illustrated in Fig. 3.16. The pore volume of the range of 0-5 nm, 5-10 nm, 10-20 nm, 20-50 nm and 50-100 nm were summarized from the data of the BJH adsorption branch. The addition of recycled waste glass results in the variation of pore volume in different size ranges of all samples. For the high strength series specimens, the addition of 10% recycled waste glass slightly increases the pore volume between 0 to 20 nm compared to reference sample. On the contrary, a higher amount of recycled waste glass incorporations (30% and 60%)

decrease the volume in this range obviously by more than 50%. The pore volume between 20 to 50 nm is enhanced by the increasing of the recycled waste glass addition. In the normal strength series samples, the incorporation of recycled waste glass significantly increases the pore volume between 10 to 20 nm, 20 to 50 nm and 20 to 100 nm.

Comparing the total pore volume and pore size distribution between the high strength and normal strength series samples, it is clear that the addition of recycled waste glass induces a limited influence on total pore volume of high strength series samples, but significantly enhances the total volume of normal strength series samples. At the same time, the pore volume between 0 to 5 nm in the high strength series samples are higher than the normal series, while large size pore (10-50 nm) in normal strength series samples are definitely higher. The gel porosity and structure is greatly influenced by many aspects, such as water to binder ratio (Atahan et al., 2009), curing conditions (Odler and Rößler, 1985) and mineral composition (Alderete et al., 2017) of the binders. Firstly, the addition of low dosage (10%) recycled waste glass in samples induces the filler and nucleation effects, which can result in the denser microstructure of hydration products, this can explain why the GP10-H and GP10-N exhibit a higher pore volume of 0-5 nm. However, with the increasing recycled waste glass dosage, the dilution effects become prominent and lead to a highly porous microstructure (Schwarz and Neithalath, 2008). As a consequence, the pore volume in the range of 10-50 nm was enhanced significantly, which agrees with the studies of water adsorption of pastes with different water to cement ratios by Powers and Brownyard (Powers, 1958). Secondly, a low water to binder ratio in the high strength series samples provides less space for cement hydration products and pozzolanic reaction products, which results in a lower pore volume and denser microstructure (Cook and Hover, 1999). On the contrary, due to the high water to binder ratio in normal strength series sample, a significant increase of gel porosity was observed. Thirdly, as a pozzolanic material, the reaction of recycled waste glass mostly relies on the calcium hydroxide from cement hydration, subsequently, C-S-H gel with low Ca/Si ratio is formed with the alkali incorporation on the surface of the glass particles. In case of the low Ca/Si ratio, this C-S-H gel presents a higher porosity structure compared with the C-S-H gel from cement hydration (Goñi et al., 2012). Especially, according to the study of Lam that low water-to-cement ratio not only results in lower hydration degree, but also the lower reaction degree of pozzolanic material (Lam et al., 2000), this also was verified by the results of calcium hydroxide development of low replacement ratio (< 30%) samples. For high volume recycled waste glass containing samples, the dilution effect dominates the hydration and similar amount calcium hydroxide consumption was observed. Subsequently, the significantly higher porosity of normal strength sample containing 60% recycled waste

glass is mostly caused by the lower gel to space ratio which is related to the water to binder ratio.

3.3.5 Mechanical performance of sustainable mortars

- *Drying shrinkage*

The drying shrinkage behaviour of high strength and normal strength mortars containing various recycled waste glass up to 90 days of curing are shown in Fig. 3.17. It can be seen that all specimens present an obvious deformation over the period. For the high strength series samples, the shrinkage is strongly affected by the early period (before 10 days), and shows a slow increase in the later period, while in the normal strength series mixtures, the shrinkage of samples shows a distinct difference after about 28 days and higher drying shrinkage than the high strength series samples. It is clear that the addition of high volume recycled waste glass as cement replacement induces the higher shrinkage after 28 days.

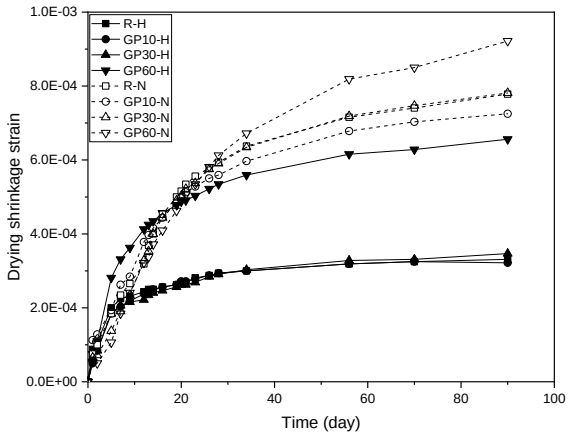

Figure 3.17 Drying shrinkage of mixtures

As shown in Fig. 3.17, the high volume recycled waste glass-containing sample (GP60-H) presents the highest drying shrinkage among the high strength samples during the whole test period. Apparently, the addition of 10% recycled waste glass slightly reduces the drying shrinkage compared to the reference sample. When the amount of recycled waste glass is increased to 30%, the sample (GP30-H) shows a slight increase in shrinkage. During the first 3 days, all samples show a similar development of shrinkage, while after 5 days, the high volume of glass powder-incorporating sample exhibits a significant acceleration on shrinkage development.

The normal strength series show a similar trend as the high strength samples in development of drying shrinkage. The 60% recycled waste glass-containing sample exhibits the highest dry shrinkage. The addition of 10% recycled waste glass presents

a lower shrinkage with 7.25×10^{-4}, which is reduced by 6.8% compared to the reference, and the addition of 30% recycled waste glass shows almost the same drying shrinkage as the reference. It is noticeable that all normal strength samples present similar shrinkage development during the period of the first 28 days. After that, the high volume recycled waste glass containing sample (GP60-N) presents a higher increasing rate of shrinkage.

It is well known that the chemical composition, curing conditions and water/binder ratio have effects on the shrinkage behaviour (Bentz, 2006; Khokhar et al., 2010). Based on the results of drying shrinkage, the normal series samples exhibit significantly high drying shrinkages than the high strength series samples due to the higher water/binder ratio. Generally, a higher water to binder ratio can enhance the total drying shrinkage due to the water loss during the drying period (Shi et al., 2015; Zhang et al., 2003). The slight lower drying shrinkage of 10% glass powder containing samples can be explained by the decreasing of autogenous shrinkage. It has been identified that the small addition of supplementary cementitious materials, for example, GGBS and FA, can increase the volume of large pores, then induce a lower capillary pressure; eventually, the autogenous shrinkage can be mitigated (Cheah and Ramli, 2012; Ghafari et al., 2016).

Table 3.5 Drying shrinkage and mesopore volume

	RH	GP10-H	GP30-H	GP60-H	RN	GP10-N	GP30-N	GP60-N
Drying shrinkage ($\times10^{-6}$)	330	322	347	656	778	725	781	922
Mesopore volume (mm^3/g)	14.37	14.23	14.12	21.27	32.57	36.46	43.17	49.9

It is believed that the pore size distribution is related to the drying shrinkage behaviour (Juenger and Jennings, 2002), especially for the mesopore volume (Collins and Sanjayan, 2000). Table 3.5 illustrates the total drying shrinkage and mesopore volume from the N_2 adsorption test. The drying shrinkage of high strength samples shows a positive correlation with the mesopore volume. High volume waste glass incorporation in high strength sample induces higher mesopore volume, which also shows higher drying shrinkage among all samples. The high volume of mesopore results in a high capillary pressure, consequently, a high drying shrinkage can be induced, this is also confirmed in a previous study (Collins and Sanjayan, 2000). Moreover, from the EDX results of high volume waste glass containing samples, it can be concluded that high volume waste glass incorporation can result in a low Ca/Si and high (Na+K)/Si. The decreasing Ca/Si ratio usually increases the porosity of C-S-H, as well as a high drying

shrinkage, this is also observed in the study of Gao (Gao et al., 2016).

In addition, when a high amount of recycled waste glass is applied in the mortar, the lower cement content results in a low content of bound water, which means more evaporable water is present; on the other hand, the reduction of cement cannot produce enough calcium hydroxide for the pozzolanic reaction of glass powder, which produces a lower amount of C-S-H gel. As a consequence, the water loss of samples containing high dosage recycled waste glass in dry air condition also contributes to the high total drying shrinkage

- *Strength properties*

The compressive strength of mortars containing various amount of recycled waste glass were measured after 7 days, 28 days, 56 days and 90 days curing and the results are shown in Fig. 3.18.

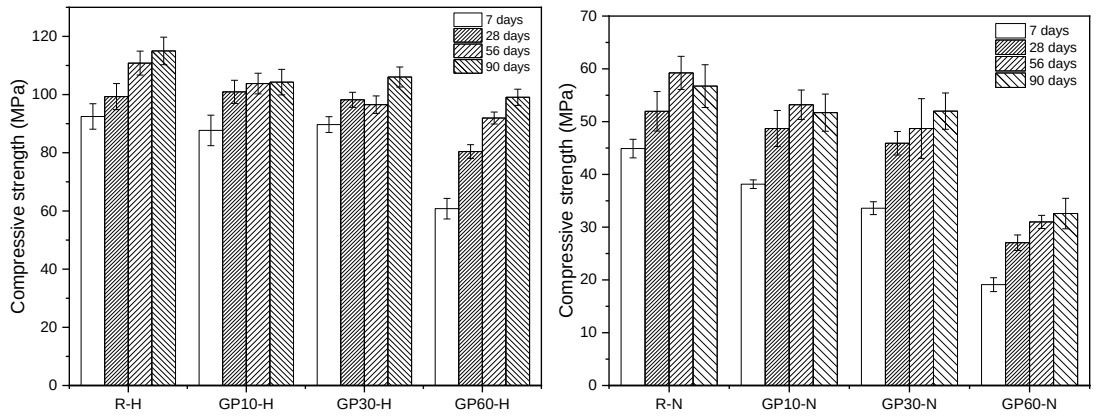

(a) (b)

Figure 3.18 Compressive strength of (a) high strength mortars and (b) normal strength mortars in different curing ages

It can be seen in Fig. 3.18 (a) that the high strength mortars containing 0%, 10%, 30% and 60% glass powder as cement replacement present compressive strength of 115 MPa, 104.3 MPa, 106 MPa and 99.07 MPa, respectively, after 90 days curing. In the early age, the sample containing 60% recycled waste glass shows a relatively low early compressive strength at 7 days with 60.78 MPa compared with 92.47 MPa, 87.69 MPa and 89.69 MPa for samples incorporating 0%, 10% and 30% recycled waste glass. This indicates that the sample containing 60% recycled waste glass exhibits higher strength increasing rate during the curing period than other samples.

The compressive strength of the normal strength series mortars are shown in Fig. 3.18 (b); it is clear that the addition of waste glass significantly decreases the compressive strength with the increasing of the glass powder amount at all curing period. The

reference, 10%, 30% and 60% recycled waste glass containing samples show 44.9 MPa, 38.15 MPa, 33.6 MPa and 19.11 MPa, respectively, at the early age (7 days curing). After 90 days of curing, the normal strength reference achieves the compressive strength of 56.73 MPa, while 32.58 MPa is reached by the sample containing 60% recycled waste glass. High volume glass powder results in a more significant strength loss at early ages compared to the reference sample and samples containing low dosage of recycled waste glass.

Table 3.6 Increasing and relative strength contribution index

	Strength contribution I_{GP}				Strength increase from 7 days (Mpa)		
Sample ID	7 days	28 days	56 days	90 days	28 days	56 days	90 days
R-H	0.0%	0.0%	0.0%	0.0%	6.85	18.35	22.53
GP10-H	5.4%	12.9%	4.1%	0.8%	13.26	16.11	16.59
GP30-H	38.6%	41.3%	24.4%	31.7%	8.52	6.85	16.36
GP60-H	64.3%	102.4%	107.4%	115.4%	19.64	31.16	38.29
R-N	0.0%	0.0%	0.0%	0.0%	7.06	14.34	11.83
GP10-N	-5.6%	4.1%	-0.2%	1.3%	10.55	15.05	13.56
GP30-N	6.9%	26.2%	17.4%	30.9%	12.30	15.09	18.39
GP60-N	6.4%	30.2%	30.8%	43.6%	7.96	11.89	13.48

To compare and estimate the strength activity degree of the different amount of recycled waste glass in high strength and normal strength mortars, the relative strength contribution index by addition of recycled waste glass is calculated as the following equation,

$$I_{GP} = \frac{f_c - f_{ref} \times (1-R)}{f_{ref} \times (1-R)} \times 100\% \quad (3.2)$$

$f_c - compressive\ strength\ of\ mortars\ containing\ recycled\ waste\ glass$
$f_{ref} - compressive\ strength\ of\ plain\ cement\ sample$
$R - cement\ replacement\ ratio$

The strength contribution index and strength increase from 7 days are illustrated in Table 3.6. It is clear that the increase of recycled waste glass proportion induces higher strength contribution index during all ages. For samples containing high volume recycled waste glass, the strength contribution index are higher compared to other samples. After 90 days curing, samples containing low dosage recycled waste glass show a strength contribution index less than 31.7%, while 43.6% and 115.4% for GP60-N and GP60-H, respectively. Apparently, high volume recycled waste glass contributes higher strength activity to high strength sample during all ages. The results of strength increase from 7 days also indicate that GP-60H exhibits the highest strength

development among all samples after 90 days of curing by 38.29 MPa. The mineral addition in binder system usually induces two effects on strength development, they are pozzolanic reaction effect and filler effect, such as the addition of silica fume, rice husk ash and quartz powder (Dembovska et al., 2017; Schwarz and Neithalath, 2008). The secondary products from the pozzolanic reaction can reduce the CH content and results in small CH crystals, which refines the pore and produces less harmful voids. From the results of CH content change in Table 3.4, it is clear that the pozzolanic reaction of recycled waste glass is more significant in normal strength samples than high strength samples, which means more secondary C-S-H can be produced in normal strength samples containing same dosage of recycled waste glass. However, high volume recycled waste glass presents a significantly higher strength contribution index in the high strength sample. This indicates that another factor-filler effect- may be the main reason for the better performance of high strength sample containing high volume waste glass. In addition, the results of N_2 adsorption also indicates that normal strength samples have a higher porosity microstructure compared to the high strength sample containing waste glass. The denser microstructure of high strength sample containing high volume waste glass also identifies the more significant filler effect. In Isaia's study, a less pozzolanic reaction and more significant filler effect was observed in higher strength mixtures incorporating pozzolanic materials (Isaia et al., 2003), which is also accorded with the results in this paper. These all explain the better performance of high volume recycled waste glass in high strength mortars.

3.4 Conclusions

1. Increasing the amount of recycled waste glass from 0% to 60% increases the flowability of fresh mortar containing a same superplasticizer amount. Samples containing recycled waste glass have longer initial setting time and final setting times.

2. The addition of a constant dosage of superplasticizer results in a longer delay of hydration with higher waste glass dosage in high strength mixtures.

3. High strength mortar containing high volumes of recycled waste glass exhibits a better strength performance (99 MPa) than normal strength mortar (20 MPa) with the same dosage of recycled waste glass after 90 days. A low early age strength (60 MPa at 7 days) can be observed in high volume waste glass mortars. The addition of recycled waste glass results in less strength loss in high strength mortars, at the same time, can result in higher drying shrinkage compared to the plain sample and samples containing low volume of recycled waste glass.

4. The addition of recycled waste glass shows no significant influence on the total gel volume of high strength samples by using N_2 absorption test, but induces the increase of total gel porosity in normal strength samples. The addition of high volumes of recycled waste glass results in less pore porosity between 0-5 nm and higher pore volume between 10-50 nm of blended samples compared to the plain sample.

5. High strength mortar containing high volume recycled waste glass shows a denser microstructure than the plain sample. Normal strength mortars containing high volume of recycled waste glass exhibits a loose packing of microstructure compared with the normal plain sample. A low Ca/Si and high (Na+K)/Ca C-S-H gel is observed in high volume recycled glass containing samples.

Chapter 4 Characterization and performance of high volume recycled waste glass and ground granulated blast furnace slag or fly ash blended mortars

Combining various SCMs properly in cement blends can result in a superior mechanical or durability performance. This chapter illustrates the application of recycled waste glass powder in high volume (60%) of ground granulated blast furnace slag (GGBS) or fly ash blended cement binder. The hydration kinetics, hydration products of the different binder systems were studied by calorimetric and X-ray diffraction test. To investigate the microstructure properties of bended binders modified by glass powder, the mercury intrusion porosimetry test and scanning electron microscopy were conducted. The resistance to chloride penetration was evaluated by the rapid chloride migration test. The incorporation of recycled waste glass in slag or fly ash blended cement improves the intensity of heat flow peak while decreasing the duration of the induction period. The addition of recycled waste glass in GGBS or fly ash blended cement promotes the consumption of calcium hydroxide. Consequently, a densification effect on the capillary pores (10-100 nm) and the total porosity of waste glass containing ternary binders were observed. From the SEM analysis, a dense microstructure and inter transition zones can be found in recycled waste glass blended samples. The waste glass powder modified slag or fly ash blended mortars exhibit a significant enhancement of resistance to chloride migration. Furthermore, a synergistic effect on the mechanical performance of large volume GGBS blended mortars containing recycled waste glass was identified, which presented the highest compressive strength among all waste blended samples.

This part is partially published elsewhere:

G. Liu, M.V.A. Florea, H.J.H. Brouwers. Characterization and performance of high volume recycled waste glass and ground granulated blast furnace slag or fly ash blended mortars. Journal of Cleaner Production, 2019, Volume 235, Page 461-472.

4.1 Introduction

The application of GGBS and fly ash as SCMs in concrete has attracted more focus for the purpose of CO_2 reduction and sustainable application of industrial by-products in the past decades (Crossin, 2015). Generally, a low replacement ratio of cement by GGBS or fly ash can significantly enhance the compressive strength compared to plain cement. In addition, the microstructural densification of blended concrete is observed due to the products of pozzolanic reaction, and low permeability can be achieved (Häkkinen, 1993; Leng et al., 2000). Regarding hydraulic and pozzolanic activity of GGBS in concrete (Bijen, 1996; Bouikni et al., 2009; Chen and Brouwers, 2007), many studies investigated various replacement ratios of GGBS in concrete production from a low level (10%-30%) to high level (50%-80%) with less strength reduction in early age compared to OPC (Mo et al., 2015). Compared to GGBS, fly ash exhibits a lower reactivity in concrete. The high volume fly ash blended cement usually shows a lower mechanical performance at the early age (Kurda et al., 2018; Rashad, 2015) and a poorer resistance for chloride migration than the low replacement level sample (Ranjbar et al., 2016). In some studies, combining fly ash and GGBS resulted in a superior mechanical performance and durability compared to applying these materials alone (Gholampour and Ozbakkaloglu, 2017; Rashad, 2015). However, in some cases with high replacement ratio, the total pore volume increased compared to plain cement samples, and as a consequence, a decrease of compressive strength was observed (Kayali and Sharfuddin Ahmed, 2013; Zeng et al., 2012). Fine glass particles exhibited a higher pozzolanic activity than that of fly ash (Schwarz and Neithalath, 2008). However, the high volume addition of waste glass in cementitious system still shows a poor mechanical performance even if it can reach a comparable strength to OPC after 1 year (Du and Tan, 2017). Unlike GGBS and fly ash, there is a limited research related to large volume addition of waste glass as a binder in concrete (Du and Tan, 2014; Liu et al., 2019).

In addition, reports of combining waste glass powder with slag or fly ash are rare. The waste glass addition can improve the mechanical performance of high volume fly ash blended concrete (Siad et al., 2018). In addition, an improvement of the mechnical properties of GGBS concrete containing recycled waste glass powder also was reported (Ramakrishnan et al., 2017). These limited studies indicate that the combined application of recycled waste glass with other SCMs is beneficial for the concrete performance. However, the modification mechanism and durability performance of waste glass powder blended ternary cement binders are still not clear. To optimize the performance of sustainable concrete containing recycled waste glass, GGBS and fly ash

as binders, many related aspects, such as hydration kinetics, durability performance, and microstructure characterization need further study.

In Chapter 3, recycled waste glass is studied in the manufacturing of sustainable mortars combined with commercial CEM III (slag cement). In this chapter, recycled waste glass is combined with other SCMs, for example GGBS and fly ash. This chapter includes a comparative evaluation of the mechanical performance, resistance for rapid chloride migration and microstructure between different binary mortars containing recycled waste glass, GGBS or fly ash. The aim is to optimize the large volume application by combining recycled waste glass with GGBS and fly ash in concrete.

4.2 Materials and methods

4.2.1 Materials

The cement in this study was CEM I 52.5 R which produced by ENCI, Netherlands. The recycled waste glass powder, ground granulated furnace slag (GGBS), and fly ash were selected as the SCMs in this study. The recycled mixed color glass fractions supplied by a glass recycling plant were grounded into powder by ball milling. Ground granulated blast furnace slag (GGBS) was provided by ENCI. The fly ash was provided by Vliegasunie, the Netherlands. The chemical composition of raw materials are shown in Table 4.1 and the mineral composition of materials are exhibited in Fig. 4.1. The d_{50} particle size of cement, waste glass powder, GGBS, and fly ash were 8.08 μm, 10.97 μm, 19.38 μm and 23.27 μm respectively. The particle size distribution of raw materials are shown in Fig. 4.2.

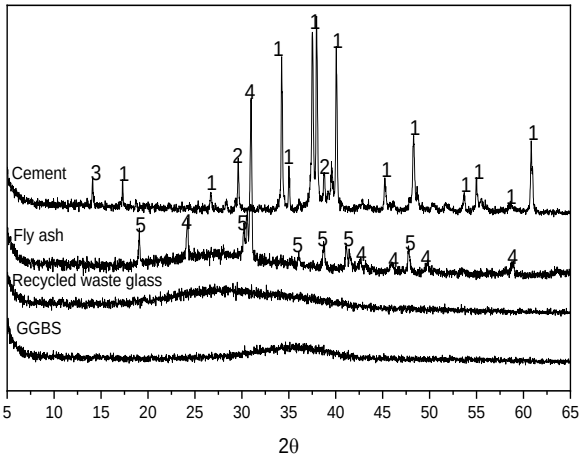

Figure 4.1 XRD of materials (1-C_3S+C_2S, 2-$CaSO_4$, 3-CAF, 4- quartz, 5- mullite)

Table 4.1. Chemical composition and physical properties of cement, waste glass, GGBS and fly ash

Chemical composition	CEM I 52.5 R (%)	Waste glass (%)	GGBS (%)	Fly ash (%)
Na_2O	/	14.65	/	/
MgO	1.71	1.30	8.57	1.14
Al_2O_3	3.79	1.93	13.21	26.98
SiO_2	16.19	68.33	29.41	51.44
SO_3	4.05	0.086	2.64	1.12
K_2O	0.19	0.70	0.42	1.84
CaO	67.97	11.90	42.67	5.83
TiO_2	0.28	0.062	1.49	1.78
Cr_2O_3	0.01	0.12	0.001	0.034
MnO	0.094	0.022	0.40	0.057
Fe_2O_3	3.59	0.36	0.37	8.27
ZnO	0.1	0.009	/	0.022
BaO	0.005	0.061	0.08	/
PbO	0.005	0.05	/	0.009
P_2O_5	0.42	/	/	0.849
Cl	0.041	0.019	0.011	/
LOI	0.72	1.34	1.15	2.27
Specific density (g/cm^3)	3.10	2.51	2.93	2.30
Specific surface area (m^2/g)	1.004	0.992	0.365	0.815

4.2.2 Methods

- *Mortars preparation*

The mixtures design of mortars is shown in Table 4.2. The different binders were mixed with water and sand by a Hobart mixer. Then the fresh mortars were filled into the plastic mould of 40 mm × 40 mm × 160 mm and vibrated for 60 s and covered with the plastic film for 24 hours. After that, the prisms were demoulded and covered by plastic film for ambient curing until further testing.

- *Raw material characterization*

The characterization of raw materials and hydration products have been described in Chapter 2.2.2.

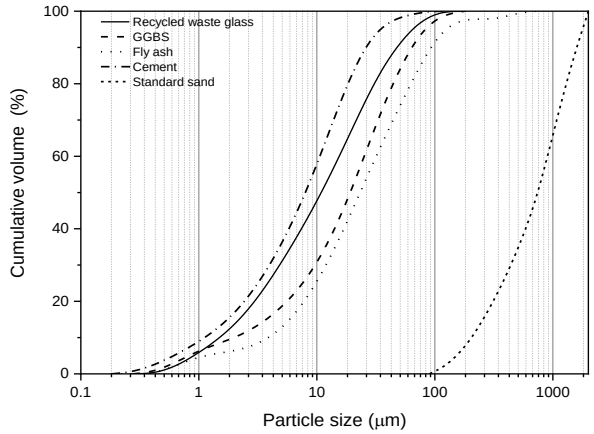

Figure 4.2 PSD of applied materials

Table 4.2. Mixture design of mortars

Sample ID	Cement (%)	Fly ash (%)	GGBS (%)	Glass powder (%)	w/b	Sand/binder	
OPC	100	0	0	0	0.5	2.5	Reference
G60	40	0	0	60	0.5	2.5	
S60	40	0	60	0	0.5	2.5	Binary
F60	40	60	0	0	0.5	2.5	sample
S10G50	40	0	10	50	0.5	2.5	
S30G30	40	0	30	30	0.5	2.5	
S50G10	40	0	50	10	0.5	2.5	Ternary
F10G50	40	10	0	50	0.5	2.5	sample
F30G30	40	30	0	30	0.5	2.5	
F50G10	40	50	0	10	0.5	2.5	

- *Fresh behaviour and mechanical properties*

The slump-flow test, density, compressive strength of mortars have been described in Chapter 3.2.2.

- *Rapid chloride migration test*

Cylindrical cores with a diameter of 100 mm were cut from the cubes after 91 days curing. Then the cylindrical cores were sliced into specimens with 50 mm height for the RCM test. Before the test, each sample was vacuumed and saturated with lime water. The vacuum-saturation was conducted as follows: specimens were placed in a desiccator connected to a vacuum pump, then pressure was kept constant at 40 mbar for 3 hours. After that the lime water was filled in the desiccator slowly until the specimens were immersed completely. After this, the vacuum was maintained for one more hour, then turned off and the drilled cores were kept in solution for 18 hours. The equipment for RCM test is shown as Fig.4.3. A 0.3 M NaOH solution and the 10% (wt.)

NaCl solution were prepared .The voltage of the test used in this study was selected according to the previous research (Spiesz and Brouwers, 2012). The D_{RCM} (chloride diffusion coefficient) was calculated by the equation:

$$D_{RCM} = \frac{RTL}{zF(U-2)} \times \frac{x_d - \alpha\sqrt{x_d}}{t_{RCM}} \quad (4.1)$$

$$\alpha = 2\sqrt{\frac{RTL}{zF(U-2)}} \times erf^{-1}(1 - \frac{2c_d}{c_0}) \quad (4.2)$$

R-universal gas constant (8.314 $Jmol^{-1}K^{-1}$), T-temperature (293 K), L-thickness of the sample (0.05 m), U -applied external voltage (V), z - ion valance, F -Faraday constant (96.485 C/mol), x_d -average chloride penetration depth, α -laboratory constant, t_{RCM} -duration of the test, erf^{-1} -inverse of error function, c_d -chloride concentration at which the colour changes (0.07 N), c_0-chloride concentration in the catholyte solution (2 N) .

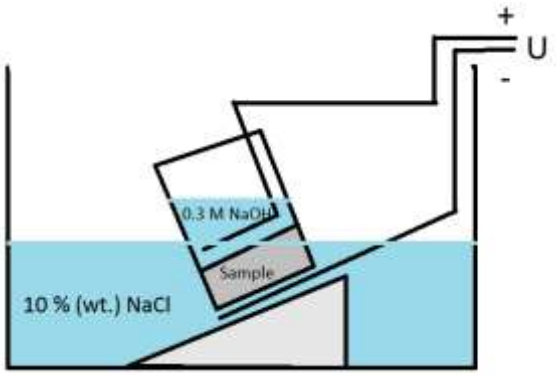

Figure 4.3 Sketch representation of RCM test (Spiesz and Brouwers, 2012)

- *Mercury intrusion porosimetry*

The mercury intrusion porosimetry (Micromeritics) was conducted to study the pore size distribution of mortars. The mortars after 90 days curing were crushed into small fractions (2 mm-4 mm) for analysis. The intrusion pressure is from 0 to 227 MPa.

4.3 Results and discussion

4.3.1 Fresh properties and density of blended mortars

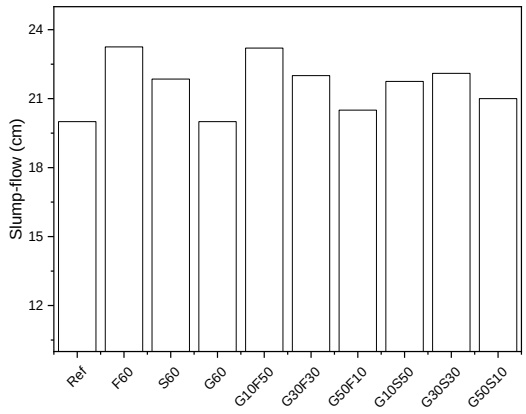

Figure 4.4 Slump-flow of mixtures

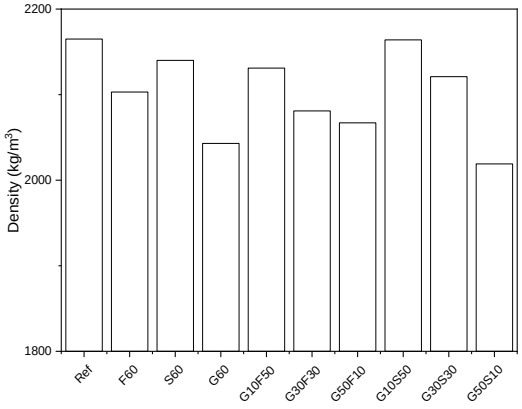

Figure 4.5 Density of mixtures

The slump-flow results of fresh blended mortars are shown in Fig. 4.4. It is observed that the fresh plain sample (OPC) presents a slump flow of 20 cm; when 60% cement was replaced by fly ash, slag, or waste glass powder, the slump flow was 23.25 cm, 21.85 cm, and 20 cm, respectively. Samples containing a combination of recycled waste glass powder and fly ash show a decreasing slump flow with the increase of the glass powder proportion, as well as the samples containing the combination of recycled waste glass powder and GGBS. The high surface area and fine particle size of waste glass powder (as shown in Table 4.1 and Fig. 4.2) induced a higher water absorption compared to fly ash and GGBS, and as a consequence, a low flowability was observed.

It can be seen from Fig. 5.5 that the mortar containing 60% slag (S60) shows the highest density, while the sample incorporating fly ash (F60) presents higher density than the waste glass powder sample (G60). Fly ash exhibits a lower specific density and specific surface area than the recycled waste glass powder. However, due to its spherical shape, fly ash contributes to a better compactibility and therefore particle packing, as a result, increasing the density of the mortar. For the waste glass containing GGBS or fly ash blended samples, the increase of waste glass amount results in a lower density; however, 10% of waste glass powder containing ternary mortars shows an enhancement on the density of samples compared to using fly ash and slag only. This indicates that 10% of recycled waste glass powder results in an improvement on packing of mortars containing GGBS or fly ash.

4.3.2 Hydration behaviour and production of blended cement

- *Hydration behaviour*

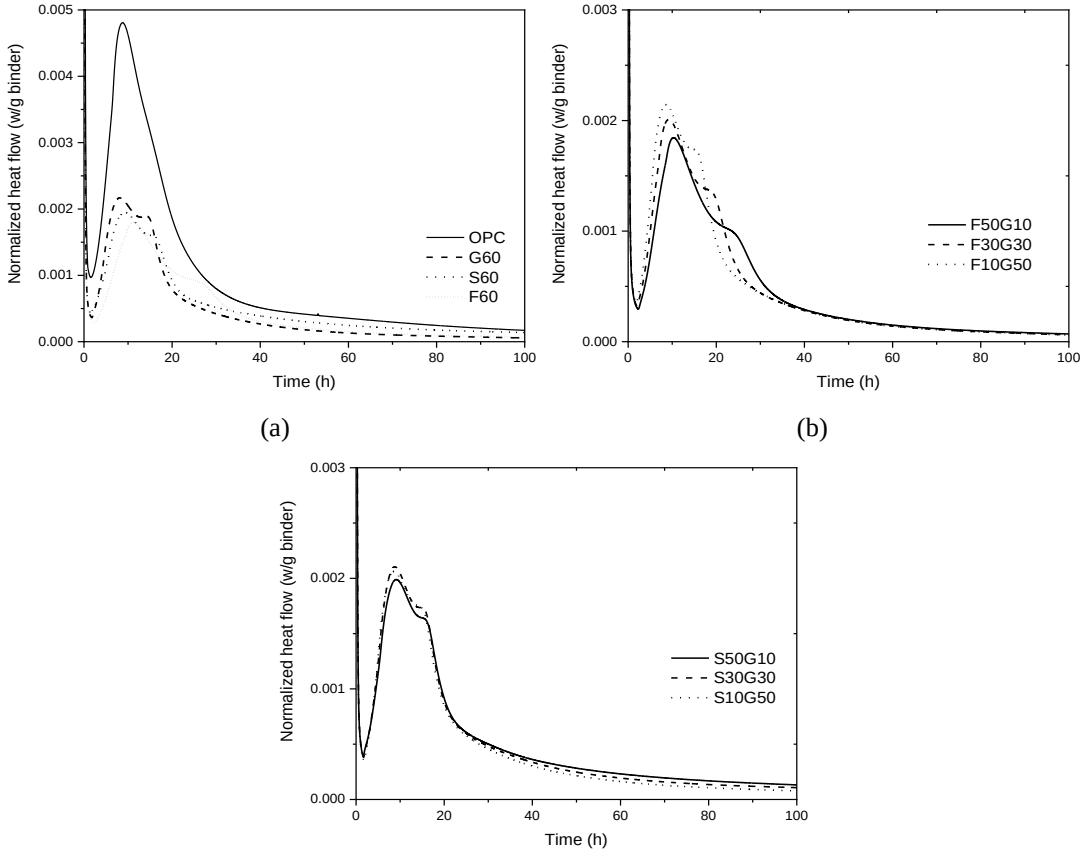

Figure 4.6 Heat rate development of different mixtures (a) binary binders, (b) OPC-waste glass-fly ash ternary binders and (c) OPC-waste glass-GGBS ternary binders

The reaction heat development of various pastes during the early hydration period are shown in Fig. 4.6. It can be seen in Fig. 4.6 (a) that all binary binders (G60, S60 and F60) show two main peaks of heat flow, and the intensity of these peaks are relatively low compared to the OPC sample.

The 60% of recycled waste glass powder binder (G60) takes a shorter duration to reach the first heat flow peak by 0.7 h, and the high volume fly ash prolongs the duration of induction period in comparison with OPC. It is reported that the fly ash can remove the calcium ions from the pore solution, so, the concentration of calcium becomes lower in the first hours, and the formation of calcium hydroxide and C-S-H is delayed, therefore the hydration is retarded (Jun-yuan et al., 1984; Ogawa et al., 1980; Plowman and Cabrera, 1984). Generally, the first heat flow peak of blended cement is induced by the reaction of C_3S and the following shoulder relates to the transfer of AFt to AFm (Mostafa and Brown, 2005). Apparently, the G60 exhibits a higher reactive intensity,

featuring higher and earlier peaks compared to high volume GGBS and fly ash binary samples. Fine glass particles have been observed providing the additional Si and sodium source due to the amorphous structure of silica (Shi et al., 2005). As a consequence, a shorter induction period and higher reaction intensity in large volume waste glass powder binder (G60) can be observed by the increasing alkali and silica in pore solution (Nocuò-Wczelik, 1999).

In the heat flow result of OPC-fly ash-waste glass ternary samples, the heat generation of different samples is controlled by the different fly ash/waste glass proportion as shown in Fig. 4.6 (b). With the increase of the waste glass/fly ash ratio, the reaction rate and intensity are all enhanced. The lower waste glass/fly ash ratio is related to the longer induction period. The increasing proportion of waste glass powder decreases the retardation effect caused by fly ash. This improvement is probably induced by the acceleration effect of glass powder as shown above and the reduction of fly ash content.

The heat flow of OPC-GGBS-waste glass ternary binders are shown in Fig. 4.6 (c). The incorporation of glass powder reduces the time to reach the first heat flow peak. The increase of glass powder/GGBS proportion increases the reaction intensity of heat flow slightly.

- *Hydration products characterization*

The hydration products of mixtures identified by XRD after 91 days are exhibited in Fig. 4.7 (a)-(c). Samples with different proportions of waste glass powder, GGBS and fly ash show different compounds and peaks. When waste glass, GGBS and fly ash are used individually as 60% cement replacement in samples, all binary mixtures show weak peaks of calcium hydroxide compared to the reference sample (OPC). Among the blended samples, G60 exhibits the lowest peaks of calcium hydroxide. Meanwhile, a significant and wide peak can be found around 34°, which is induced by the poorly ordered C-S-H (Garbev et al., 2008). The S60, F60, and OPC all present distinguishable peaks of ettringite, contrary to G60. In addition, the peaks of hydrotalcite are observed just in F60 and S60, which is a typical product during the reaction of GGBS and fly ash under alkali activation (Oh et al., 2010; Puertas and Fernández-Jiménez, 2003; Song and Jennings, 1999).

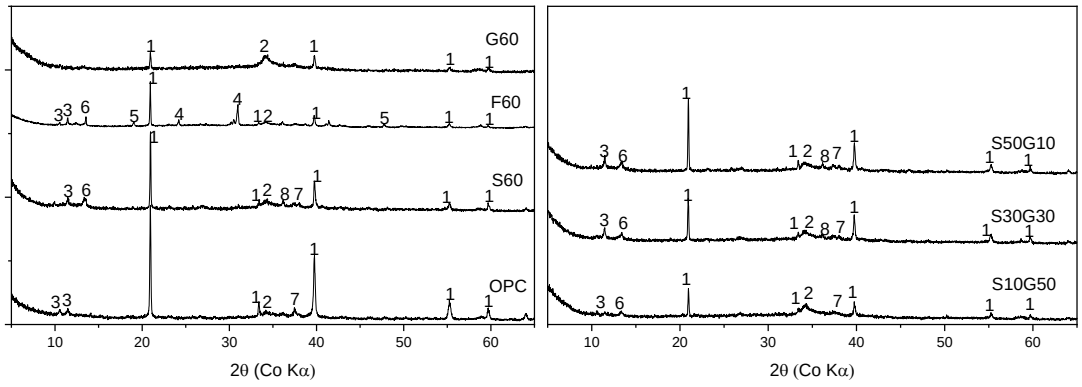

(a)

(b)

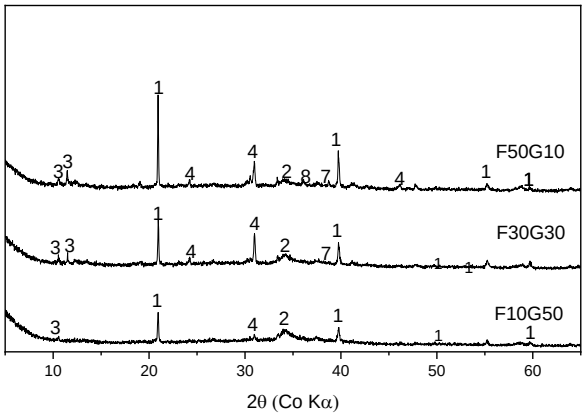

(c)

Figure 4.7 XRD patterns of samples after 91 days curing (a) OPC and binary samples (b) cement-recycled waste glass-GGBS samples (c) cement-recycled waste glass-fly ash samples (1-CH, 2-C-S-H, 3-Ettringite, 4-Quartz, 5-Mulite, 6-Hydrotalcite, 7-Dicalcium silicate, 8-Dolomite)

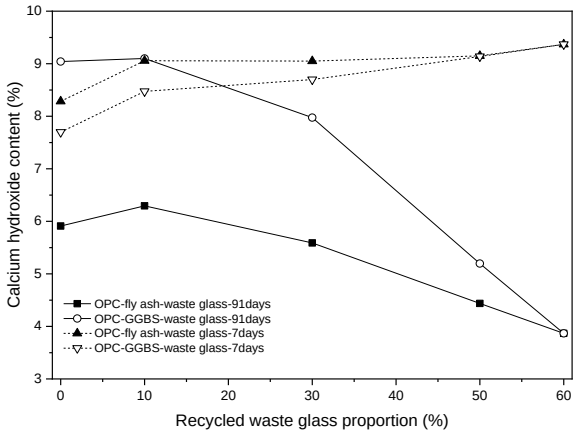

Figure 4.8 Calcium hydroxide content of different mixtures after 7 days and 91 days

After the waste glass powder was incorporated with GGBS or fly ash, the peaks correspond to C-S-H are wider and more intense with higher waste glass powder amount in ternary systems; moreover, the intensity of calcium hydroxide peaks decrease significantly. The GGBS and fly ash ternary binders containing recycled waste glass powder show a significant influence on the residual calcium hydroxide of mixtures after

91 days. As the results illustrate in Fig. 4.8, 60% recycled waste glass powder sample (G60) exhibits the lowest CH content compared to high volume of GGBS (S60) or fly ash samples (F60). Compared to the CH in mixtures after 7 days curing, the higher proportion of recycled waste glass powder in binders is related to more CH reduction. It can be seen that the higher waste glass powder proportion enhances the consumption of CH from cement hydration, which is due to the pozzolanic reaction of SiO_2 from the glass particles. Meanwhile, the increase of SiO_2 content in samples results in a lower Ca/Si ratio, leading to a poorly crystallized C-S-H (Garbev et al., 2008; Kumar et al., 2017), which shows a wild hump peak in X-ray diffraction.

4.3.3 Microstructure characterization of blended cement mortars

- *Pore structure*

Fig. 4.9 (a) shows the cumulative pore volume of mortars containing 60% waste glass powder (G60), fly ash (F60) and slag (S60) compared with the plain cement sample (OPC). The large pore (> 1000 nm) only contributes to a limited pore volume, the contribution of smaller pore (< 1000 nm) increases quickly. High volume fly ash mortar shows the highest total pore volume compared with other samples. This is due to the slow pozzolanic reaction of fly ash particles (Yu and Ye, 2013; Zeng et al., 2012). Also the high volume of GGBS sample presents a higher porosity than the OPC, which can also be found in related studies (Li et al., 2014, 2010; Moon et al., 2006). On the contrary, the mortar (G60) shows a reduction of its total pore volume compared to the OPC sample, which indicates 60% of recycled waste glass powder results in no negative effect on the pore volume of mortar.

The cumulative pore volume of combining waste glass powder with fly ash or GGBS are shown in Fig. 4.9 (b) and Fig. 4.9 (c). It is interesting to notice the higher amount of recycled waste glass powder in ternary binders enhances pore volume of cement-GGBS-recycled waste glass powder mortars but decreases the total pore volume of cement-fly ash-recycled waste glass powder samples. However, all ternary binder mortars still show a lower pore volume compared to the sample containing high volume GGBS or fly ash alone. This indicates a synergistic effect on total pore volume reduction was induced by the incorporation of waste glass powder with GGBS or fly ash.

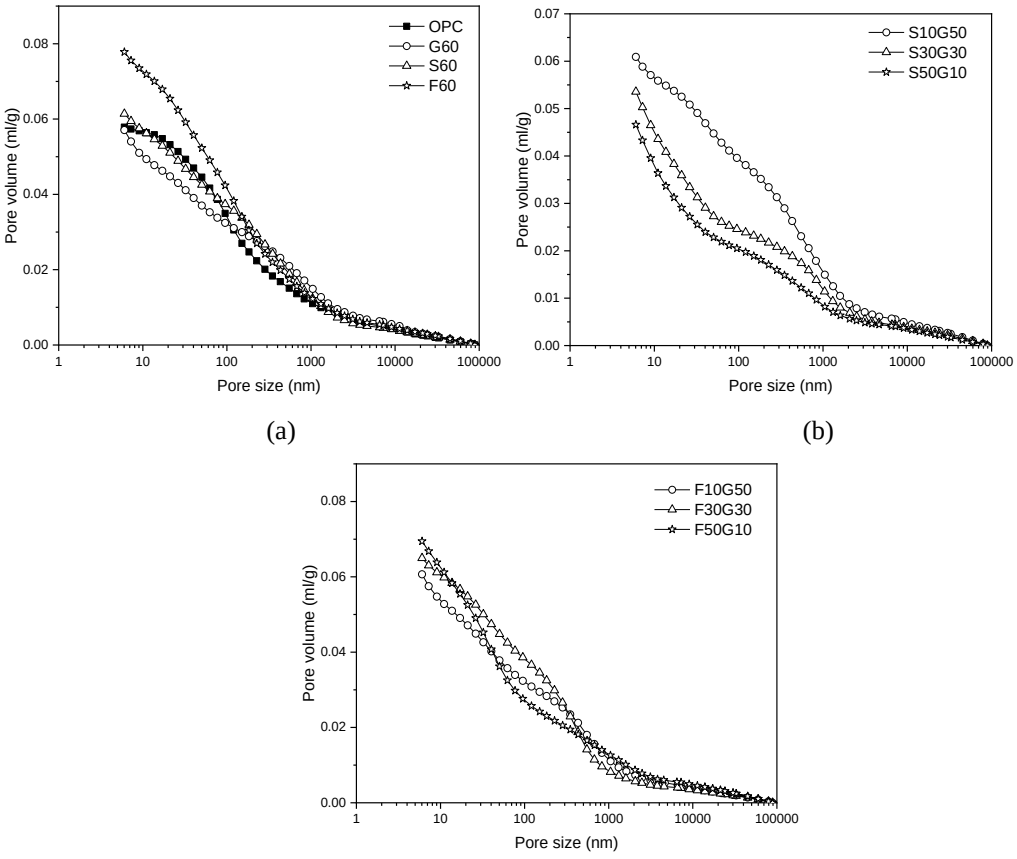

Figure 4.9 Total pore volume results (a) OPC and binary samples (b) OPC-GGBS-waste glass samples (c) OPC-fly ash-waste glass samples

Generally, a limited addition of GGBS and fly ash is helpful for reducing of the concrete porosity (Leng et al., 2000; Zuquan et al., 2007). However, the high volume SCMs in concrete results in higher total porosity and a limited improvement of durability (Zeng et al., 2012), and even the deterioration of mechanical performance of concrete (Kim and Lee, 2013). In the present study, 60% fly ash and 60% GGBS binary samples show higher porosity than the OPC, which also agrees with other studies (Gholampour and Ozbakkaloglu, 2017). Nevertheless, when the recycled waste glass is incorporated, some samples exhibit a reduction of porosity compared to OPC, for example, all cement-GGBS-recycled waste glass binder specimens and F10G50. This indicates that recycled waste glass powder not only exhibits less deterioration in total porosity but also shows a synergistic effect with GGBS and fly ash on the improvement microstructure of concrete. The porosity reduction of blended concrete can be induced by several effects, among which the pore refinement by the C-S-H of the pozzolanic reaction. The products from the pozzolanic reaction gradually fills the volume of voids and contributes to the concrete strength. Another is the micro filler-effect: when the CH from cement hydration is insufficient for the reaction of the large volume pozzolanic materials, some unreacted particles can be the micro-filler in voids. These particles

block the connection between pores as micro-aggregates and induce an effect on water penetration and ion transportation (Wongkeo et al., 2014). Furthermore, since the pozzolanic materials show different particle size and morphology, a specific mix design can introduce a dense packing for concrete, which presents a denser microstructure and a better mechanical performance (Brouwers, 2016).

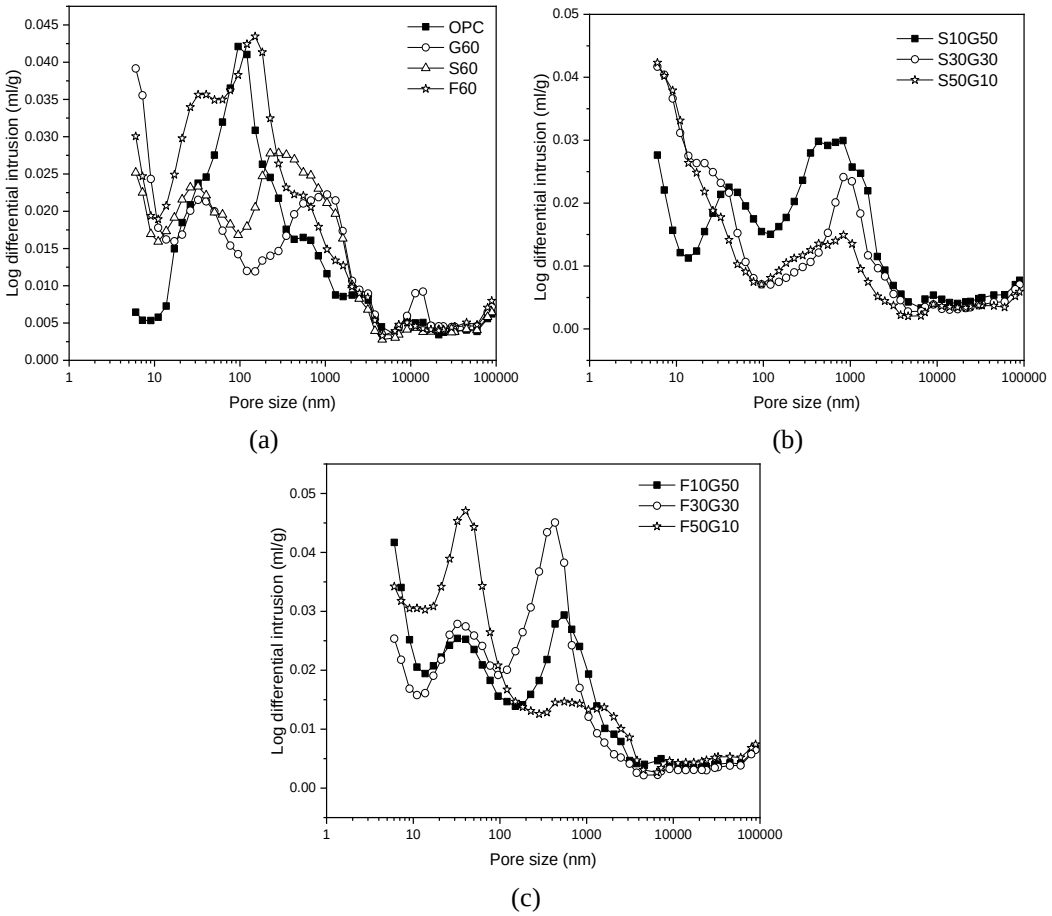

Figure 4.10 Pore size distribution of different samples (a) OPC and binary samples (b) OPC-GGBS-waste glass samples (c) OPC-fly ash-waste glass samples

The pore size distribution of mortars containing 60% recycled waste glass powder (G60), GGBS (S60), fly ash (F60) and the plain sample (OPC) are shown in Fig. 4.10 (a). It can be seen that the OPC shows a main peak and continuous pore distribution, and F60 exhibits a similar shape of pore size distribution as OPC, but a higher volume of pores less than 10 nm, and a small second peak between 10 nm – 100 nm. For the sample G60 and S60, two clear peaks can be found from results, the first peak is located in the range of 10 nm – 100 nm and the second peak around 1000 nm.

Fig. 4.10 (b) exhibits the pore size distribution curves of combining waste glass powder and GGBS with different proportions in mortars. The different recycled waste glass/GGBS ratio induces variation in the peak location and pore volume. The sample

containing waste glass powder and GGBS with a proportion of 5:1 shows a higher and significant peak around 1000 nm compared to samples with waste glass/GGBS of 3:3 and 1:5. When recycled waste glass powder and fly ash were used together, the change of the pore volume around 40 nm and another peak around 1000 nm can be found as shown in Fig. 4.10 (c). All samples show the similar shape of a peak around 40 nm, especially, F50G10 shows the highest peak here. After a higher waste glass powder proportion was conducted, this peak turns into weaker. These indicate that the increasing proportion of waste glass powder can reduce the pore volume around 40 nm. From the other side, the increase of waste glass powder amount enhances the pore volume from 100 nm to 1000 nm.

- *SEM*

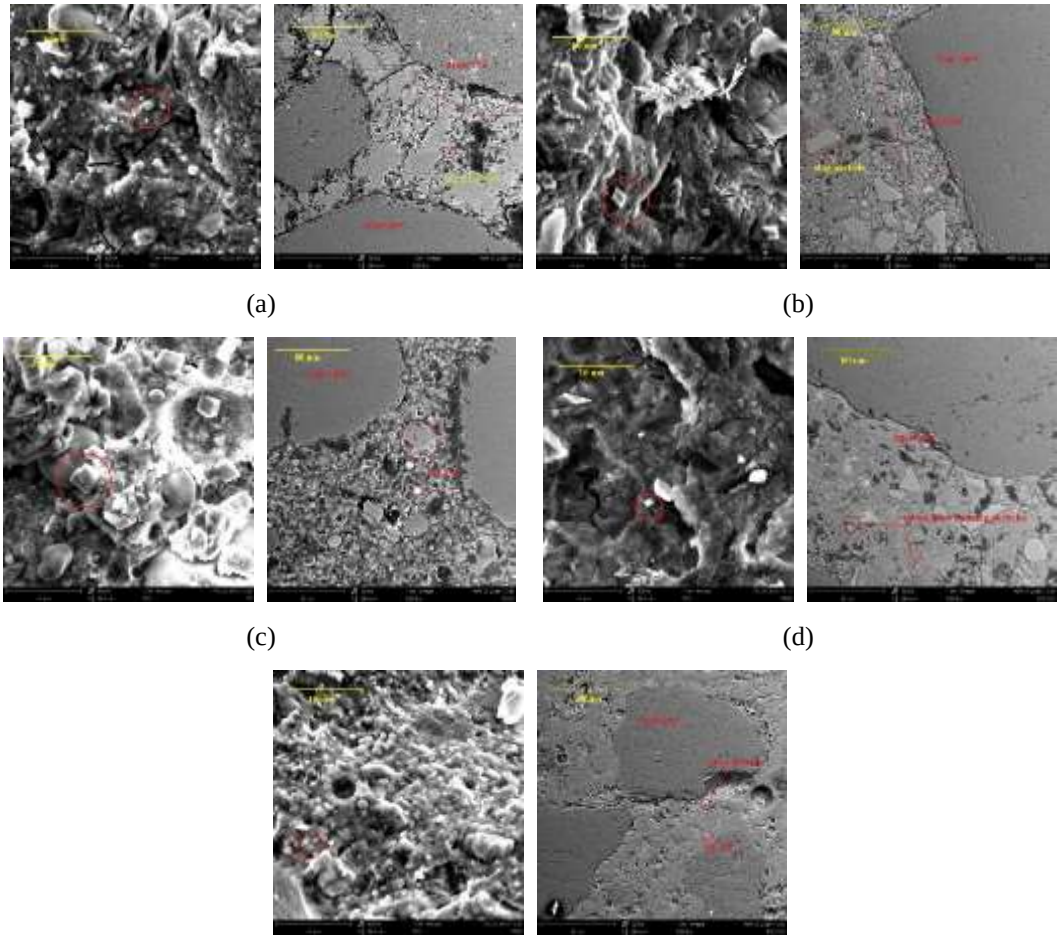

(a) (b) (c) (d) (e)

Figure 4.11 SEM images of (a) G60, (b) S60, (c) F60, (d) S30G30 and (e) F30G30 (left ×8000, right×1000)

Fig. 4.11 presents the microstructure of different mortars. The left side is related to the pastes, while the right side is related to polished mortar samples. The improvement of the microstructure of pozzolanic materials blended concrete has been addressed in may

studies (Li and Zhao, 2003; Shayan and Xu, 2006; Zong et al., 2014). As shown in Fig. 4.11 (a), a dense structure is observed in the sample G60. The small amount of cubes in the red circle are corresponded to the residual calcium hydroxide (Li and Zhao, 2003). In the case of high volume addition of waste glass powder, there are micro crack and an aggregation of unreacted glass particles, which are located between sand particles. This may relate to the higher porosity around 1000 nm. In addition, a thick ITZ is presented between the aggregate and the matrix, and a dense ITZ can also be found in high volume of GGBS sample as shown in Fig. 4.11 (b). In Fig. 4.11 (c), the unreacted fly ash sphere is covered by the loosely packed matrix, and a number of large calcium hydroxide crystals can be clearly identified. Compared to the other samples, the high volume fly ash sample presents a porous structure of polished mortar sample. The larger calcium hydroxide crystal size and porous microstructure of high volume fly ash sample are responsible for the high D_{RCM}. This increase in calcium hydroxide crystal size in fly ash blended cement was also observed in Hu's study (Hu, 2014). When the recycled waste glass powder is incorporated with GGBS or fly ash, a denser microstructure is clearly exhibited as shown in Fig. 4.11 (d) and (e). In addition, a better compacting ITZ indicates that an improvement of microstructure occurred after the incorporation of recycled waste glass powder.

4.3.4 Rapid chloride migration of blended cement mortars

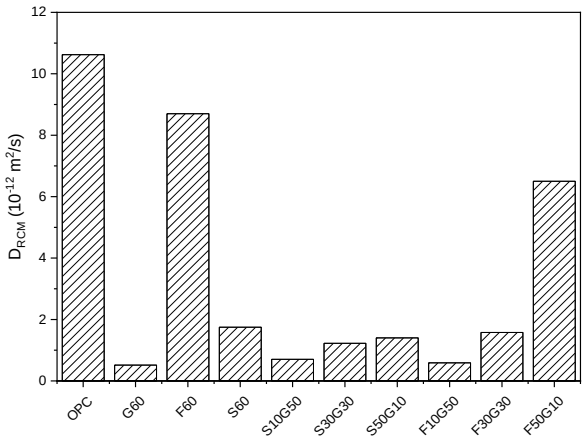

Figure 4.12 Rapid chloride migration coefficient of mortars

The results of rapid chloride migration of different mortars (aged 91 days) are shown in Fig. 4.12. The plain OPC mortar shows the highest D_{RCM} among all samples. For binary binder samples, after cement was replaced by the high volume of recycled waste glass, GGBS or fly ash, these samples (G60, S60 and F60) all show a lower D_{RCM} compared to the OPC. Especially for the G60 and S60, the D_{RCM} are reduced dramatically by 95% and 83.5%, respectively. At the same time, the D_{RCM} of the specimen incorporating high volume of fly ash (F60) only shows a reduction of 18.1%

compared to the OPC. The incorporation of 60% recycled waste glass provides an excellent resistance to chloride migration compared to the GGBS and fly ash samples. In ternary binders, combining use recycled waste glass with GGBS or fly ash also exhibit better performance than only using GGBS or fly ash. In addition, it is interesting to notice that when the recycled waste glass is combined with fly ash in binders, the D_{RCM} presents a significant reduction with the increased amount of recycled waste glass.

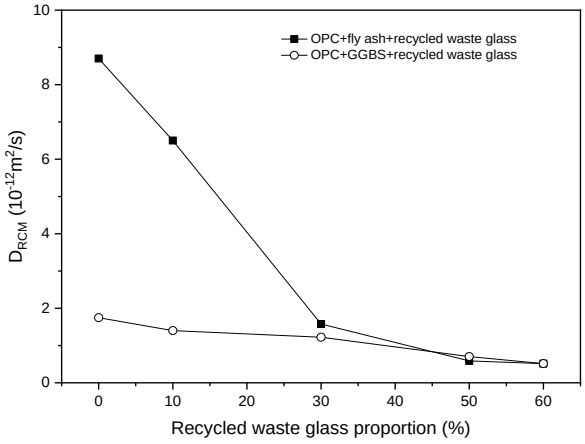

Figure 4.13 The correlation between recycled waste glass content and rapid chloride migration coefficient

The relationship between recycled waste glass content and rapid chloride migration coefficient in two different ternary binder is illustrated in Fig. 4.13. With the increase of the recycled waste glass amount in binders, cement-fly ash-recycled waste glass mixtures exhibit a drastic drop of D_{RCM}. At the same time, the reduction of D_{RCM} for OPC-GGBS-recycled waste glass mortars with increasing glass powder content is limited. This indicates that the incorporation of waste glass powder in fly ash blended mixtures present a more significant improvement of resistance to chloride migration than in GGBS blended mixtures. Generally, the interfacial transition zone (ITZ) of OPC concrete is rich in calcium hydroxide, which is the weak area in concrete for ion transportation. The addition of pozzolanic material consumes CH and then provides a dense ITZ, which is beneficial for the concrete. Furthermore, the RCM test is based on the electric conductivity method, which can be affected by the conductivity of the concrete pore solution. Meanwhile, the ion dosage in the pore solution depends on the chemical composition of different binder systems. For example, in concrete containing pozzolanic materials, the change of chemical composition can be induced by the consumption of calcium hydroxide during pozzolanic reaction (Jain and Neithalath, 2010). As shown in Fig. 8, the increase of waste glass powder proportion in blended binders results in a decrease of calcium hydroxide content after 91 days, which is accompanied by the reduction of D_{RCM}.

However, when comparing CH contents in GGBS ternary binders and fly ash ternary binders, it can be observed that although the GGBS ternary binders exhibit a higher CH content, it still presents a lower D_{RCM} compared to fly ash ternary binders. High volume fly ash sample (F60) shows a lower CH content compared to the high volume slag sample (S60), but a significantly higher D_{RCM}. This may be induced by the different microstructure of mixtures, for example, pore size structures, which will be discussed in the following.

The difference of pore size distributions can result in the observed variation in the chloride migration. It has been identified that using SCMs in concrete cause changes in concrete pore structure, which result in different resistance to chloride penetration (Liu et al., 2017; Shi, 2004; Zong et al., 2014). The previous research shows that the pore between 10-100 nm is mostly related to the coefficient of rapid chloride migration. The relationship between the volume of the capillary pores and the transport property of concrete has been addressed in many studies (Yu et al., 2017; Yu and Ye, 2013). For example, in Wu's study about microstructure and ITZ of blended cement, a reduction of chloride transport correlated with the decrease of the pore volume between 10-100 nm (Wu et al., 2016), which is also in agreement with the present data. As described in microstructure-property on pozzolan-containing concrete by Paiva et al., the pozzolanic reaction occurred inside the capillary pores, as a consequence, a densification of micro pores was observed by the results of MIP (Paiva et al., 2017). This conclusion also supports the MIP results as previously discussed.

In this study, the G60 shows a great modified effect on mixtures microstructure. An obvious densification has been exhibited by MIP results. It is interesting to notice that the G60 shows a similar pore size distribution as the S60. This indicates that the addition of 60% of waste glass particles has a potential to build similar microstructure as GGBS in concrete. On the contrary, although the 60% fly ash mortar exhibits a lower D_{RCM} than OPC, it displays an analogous pore size distribution curve to the OPC mortar. The reduction of D_{RCM} of high volume fly ash containing sample is mainly due to the decrease of electrical conductivity caused by lower the alkalinity of the pore solution of concrete compared to OPC sample, which is related to the reduction of alkaline ions and hydroxyl ions (Shehata et al., 1999). In addition, due to the alumina rich in fly ash blended cement, the Friedel's salt formation during test also contributes to the enhancement of the chloride binding capacity (Jain and Neithalath, 2010).

4.3.5 Mechanical performance of blended cement mortars

The compressive strength of mortars is shown in Table 4.4. High volume of glass powder, GGBS, and fly ash in binary binders result in different compressive strength at

various ages. It is clear that the plain mortar (OPC) exhibits the higher compressive strength at early age and late age than the sample containing 60% glass powder, GGBS or fly ash. The best mechanical performance of mortar in binary binder system after 91 days curing is presented by G60, which is higher than the slag sample (S60) by 10.4% and the fly ash sample (F60) by 18%. However, the glass powder sample presents a poor mechanical performance at early ages, such as 7 days, compared to other specimens. The compressive strength of G60 after 7 days curing shows a reduction of 47% and 26.4% compared to S60 and F60, respectively. However, the poor strength performance of G60 is improved significantly after prolonged curing . For example, after 56 days, the strength of G60 is higher than that of S60 and F60.

Table 4.4 Strength performance of mortars

Sample	Flexural strength (MPa)				Compressive strength (MPa)			
	7 days	28 days	56 days	91 days	7 days	28 days	56 days	91 days
OPC	6.74	7.60	8.39	8.47	41.91	51.84	55.25	57.72
F60	3.89	5.07	6.08	6.26	14.96	22.47	32.63	36.99
S60	5.07	6.13	6.16	6.31	20.79	36.15	38.15	39.54
G60	3.08	5.12	6.29	6.69	11.01	29.08	38.91	43.65
F10G50	3.86	5.47	5.95	5.55	13.66	31.39	33.78	41.04
F30G30	3.73	5.64	6.27	6.26	14.14	32.60	34.18	39.68
F50G10	3.80	6.00	7.25	6.88	14.66	27.79	37.91	41.53
S10G50	3.92	5.54	7.40	7.63	13.81	33.64	36.59	41.30
S30G30	4.23	6.49	8.19	8.34	17.27	38.29	49.85	51.18
S50G10	4.77	6.83	7.69	7.95	20.48	39.43	48.09	51.11

In OPC-GGBS-recycled waste glass powder ternary samples, an obvious enhancement of strength at later ages can be observed compared to binary sample G60 and S60. Ternary samples S30G30 and S50G10 achieve the highest compressive strength after 91 days. At the early age, combining GGBS and glass powder improves early strength (7 days) gradually with the increasing of GGBS/glass powder ratio. The slag proportion contributes to the better performance at early age, which is due to the higher reactivity of GGBS.

The glass powder in OPC-fly ash-glass powder binder results in fewer effects on strength development. The increasing fly ash/glass powder ratio shows almost no influence on the early age strength but increases the strength after 28 days. Eventually, F50G10 achieves the highest compressive strength, which is higher than the fly ash binary sample (F60) by 12.3%.

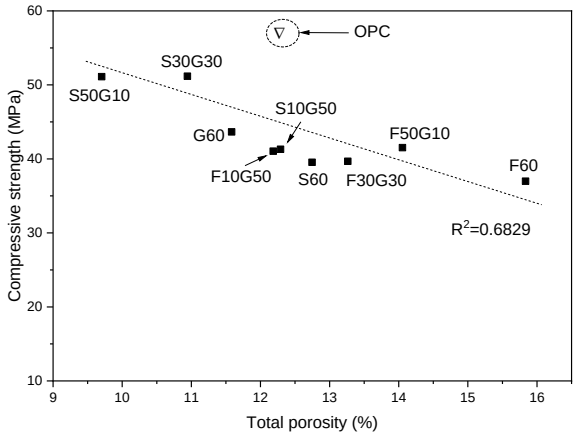

Figure 4.14 The total porosity and compressive strength of blended samples after 91 days

In general, the high volume glass powder, slag and fly ash in ternary and binary binders result in lower strength compared to the plain OPC sample until 91 days. The low early strength can be found in all samples, especially for G60. After combining glass powder with GGBS or fly ash, the early strength can be improved, as well as the better performance at late age, for example, S50G10 and S30G30. The OPC-GGBS-glass powder binder exhibits significant better performance than the cement-fly ash-glass powder binder on compressive strength development. In many studies, the mechanical performance of blended concrete has been confirmed to correspond to the microstructure (Jeong et al., 2015; Lavergne et al., 2018; Yang et al., 2018). Fig. 4.14 exhibits the correlation between compressive strength and total porosity. It can be seen that the compressive strength performance of blended mortars depends on the variation of total porosity. A low porosity corresponds to the high compressive strength of blended mortars. From MIP results, S50G10 and S30G30 show a very low porosity compared to other samples, whereas exhibiting the highest compressive strength. A conclusion of combining application of small amounts of glass with GGBS can significantly enhance the mechanical performance of OPC-GGBS-recycled waste glass powder mortars can be addressed. However, the OPC sample shows a medium total porosity, while the highest compressive strength compared to blended mortars. This is induced by the unique pore size distribution, which is different from the blended samples.

4.4 Conclusions

1. The isothermal calorimetry results indicate that combining recycled waste glass powder in GGBS or fly ash blended binders improve early reaction intensity and accelerate the hydration process.

2. The 60% recycled glass binary binder presents the lowest calcium hydroxide after 91 days curing compared to 60% GGBS and 60% fly ash blended samples. The combination of recycled waste glass powder in GGBS or fly ash blended system results in a reduction of the residual calcium hydroxide amount and a denser microstructure of mortar samples.

3. Combining recycled waste glass powder with GGBS and fly ash provides a significantly better performance of resistance for rapid chloride migration compared to samples only blended with high volume GGBS or fly ash. A densification of capillary pores (10 nm – 100 nm) is observed after blending recycled waste glass powder with GGBS or fly ash in binder system. Furthermore, a decrease of total pore volume can be induced by adding recycled waste glass powder in GGBS or fly ash blended mortars.

4. Combining recycled waste glass powder with GGBS or fly ash contributes to a better mechanical performance of mortars compared to samples containing waste glass powder only. The incorporation of 10% and 30% recycled waste glass powder in GGBS ternary binder can markedly decrease the total porosity of samples, which produces a comparable compressive strength of 51.11 MPa and 51.17 MPa, respectively, compared to 57.52 MPa of a plain OPC mortar.

Chapter 5 Hydration of recycled waste glass blended cement

In this chapter, a combination of Rietveld analysis and PONKCS (partially or unknown crystal structure) is employed to study the hydration behaviour of recycled waste glass blended cement. The ordinary Portland cement is replaced by 20%, 40%, and 60% recycled waste glass powder by mass. Paste samples of blended cement are characterized after 1, 3, 7, 28, and 91 days of hydration. The reaction degree of recycled waste glass powder after various curing ages is identified by using the PONKCS method. The total reaction degree in blended cement keeps decreasing from 93% to 53%, when the waste glass content increases from 0% to 60%. The reaction degree of recycled waste glass achieves from 24.6% to 37.8% after 91 days. Therefore, most of the recycled waste glass act as filler in blended cement. The formed reaction product from waste glass has a Ca/Si of 0.6 to 0.8, while a (Na+Ca)/Si of 1.0-1.3.

5.1 Introduction

To obtain a clear understanding of the hydration of SCMs blended cement, more focus has been placed on the study of reaction kinetics in recent years. The determination of the reaction degree of SCMs in cement systems is important to guide the application and optimization of blended cement. In previous studies, SCMs such as ground granulated blast furnace slag (GGBS), fly ash (FA), silica fume (SF) and metakaolin (MK) have been studied by various test methods in the lab using hydrated SCMs blended cement samples (Deschner et al., 2012; Pane and Hansen, 2005; Wan et al., 2018; Zeng et al., 2012). Generally, thermal gravimetric (TG) analysis, scanning electric microscopy (SEM), selective dissolution, and quantitative XRD analysis (QXRD) are combined for the identification of reaction products and reaction degree of SCMs. However, it is difficult to quantify SCMs by using XRD because it cannot differentiate between amorphous phases, and both the unreacted SCMs and the cement hydration products are largely amorphous.

The PONKCS (partially or no known crystal structure) method is an efficient way to do a quantification analysis for materials with amorphous or poorly crystalline structures (Scarlett and Madsen, 2006). In recent studies, it has been used for the determination of GGBS and fly ash in unhydrated blended cement (Naber et al., 2019; Stetsko et al., 2017). The PONKCS method is also used on hydrated cement with amorphous SCMs (Snellings et al., 2014). This way the reaction degree of SCMs and cement can be successfully described compared to other independent methods, which is helpful for a better understanding of the hydration process. The only requirement for this method is an XRD measurement of the pure, unreacted SCM.

As a material with a highly amorphous structure, waste glass has been applied as an SCM in the preparation of blended cement (Bignozzi et al., 2015; Bueno et al., 2020; Liu et al., 2019; Shayan and Xu, 2006). Many studies revealed that the incorporation of recycled waste glass contributes to a better durability performance of concrete by modifying the reaction products by changing the (Na+Ca)/Si ratio of C-S-H and the microstructure (Bignozzi et al., 2015; Bueno et al., 2020; Liu et al., 2019; Shayan and Xu, 2006b; Topçu and Canbaz, 2004). However, only rare studies mentions the reaction mechanism of recycled waste glass in cement blends, which is still not clearly understood. By using the combination of PONKCS and Rietveld methods, it is possible to estimate the reaction process clearly and to give a better understanding of kinetics.

This chapter illustrates the investigation of waste glass blended cement hydration using the PONKCS and Rietveld methods to determine the reaction degree of various

amounts of recycled waste glass in cement. The results can contribute to a better understanding of the application of recycled waste glass in building materials.

5.2 Materials and Methods

5.2.1 Characterization of materials and sample preparation

The results of the characterization of recycled waste glass and cement are shown in Chapter 3.2.2 and Chapter 4.2.2.

The pastes samples are prepared with CEM I 52.5 R and 0%, 20%, 40% and 60% of recycled waste glass powder (RGP) by mass. The samples are called OPC, G20, G40 and G60, respectively. The water to binder ratio is 0.5. After 1 day, 3 days, 7 days, 28 days and 91 days, the hydrated samples are crushed and mixed with isopropanol to cease hydration. Then samples are dried at 40^{o} C for 48 hours for further analysis.

5.2.2 Quantification of reaction products in recycled waste glass blended cement

- *Quantification of recycled waste glass with PONKCS*

TOPAS V5 from Brucker was used for all quantifications. The building of the structure file for the amorphous phases using TOPAS has been described in many previous studies (Mehdi Mejdi et al., 2019; Naber et al., 2019; Scarlett and Madsen, 2006). The quantification of recycled waste glass with the PONKCS method includes 3 steps. At first, a crystalline standard is measured with XRD (in this case Si) to determine the background level. In a second step, the pure recycled waste glass powder (RGP) is measured. In TOPAS the previously refined background level is applied, and an hkl phase is added with a space group of P4, lattice parameter a=1, and c=70, and refined to fit the amorphous hump of recycled waste glass. Then, the phase constant (ZM) is calculated by the following equation:

$$(ZM)_{RGP} = \frac{W_{RGP}}{W_{silicon}} \times \frac{S_{silicon}}{S_{RGP}} \times \frac{(ZM)_{silicon} \times V_{silicon}}{V_{RGP}} \quad (5.1)$$

W_{RGP} and $W_{silicon}$ are the mass ratio (%) for recycled waste glass and silicon, respectively.
S_{RGP} and $S_{silicon}$ are the refined scale factors.
$(ZM)_{silicon}$ is the Cell Mass of silicon.
V_{RGP} and $V_{silicon}$ are the refined Cell Volumes.

At last, the phase constant is used as the cell mass of the hkl phase of recycled waste glass. Then the structure file is used for all following Rietveld calculation. To test the

accuracy of the hkl phase of recycled waste glass, mixtures of recycled waste glass and silicon are prepared (90% RGP-10% Si, 70% RGP-30% Si, 50% RGP-50% Si, and 20% RGP-80% Si) and waste glass content calculated. The result is shown in Fig. 5.1. The calculated phase content of recycled waste glass powder (RGP) is slightly higher than the true content in the raw mixtures (around 1% to 2%), which is still acceptable. The calculation errors shown in Fig. 5.1 are from TOPAS, and it can be seenthat the decrease of RGP content results in a larger error. However, it is still acceptable for phase content determination of RGP.

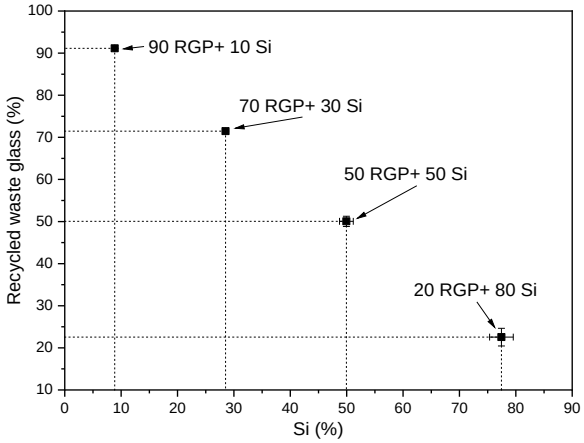

Figure 5.1 The calculated RGP contents using PONKCS method of know RGP-Si mixtures

- *Quantification of hydrated blended cement*

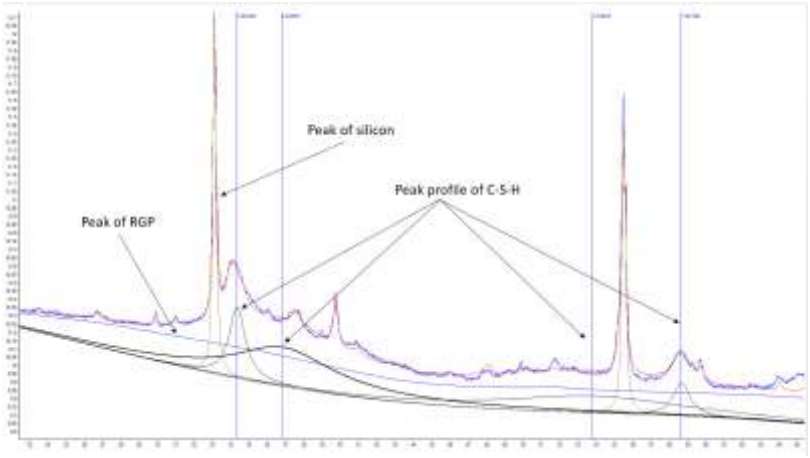

Figure 5.2 An example of the refinement with hkl phase (RGP)

A Bruker D4 with a Co tube was used for all measurements (10^{o} to 90^{o}, step size 0.018 ^{o}, time 1.5 s, 40 kV). The XRD mill (Retsch McCrone Micronizer mill) was used to mill the crushed samples into powder for quantification after stopping hydration. The Si was used as the internal standard (10%) to conduct the Rietveld quantification for mixtures by using TOPAS V5. The selected quantification results of clinkers, calcium hydroxide and waste glass content are shown in Table 5.1. The mass of clinker includes

C_3S, C_2S, C_3A, and C_4AF. The bound water is related to the mass loss from 105° C to 600° C by TG test, and normalized to the mass of dry mixtures. In the following discussion, all results are normalized to the mass of initial dry mixtures (mass at 600° C during TG test). An example of an XRD pattern of a hydrated sample is plotted as Fig. 5.2, refined with the built hkl phase of RGP, peaks of Si and used C-S-H profile. The data of C-S-H profile is derived from the research of (Snellings et al., 2014), which can fits the peaks of C-S-H of 7 years hydrated OPC.

Table 5.1 The selected quantification and TG results

	Age (day)	Clinkers (%)	CH (%)	RGP (%)	Amorphous (%)	Bound water $(\%)_{105°C\text{-}600°C}$
OPC	1	32.1	10.5	0.00	49.6	13.3
	3	18.2	13.1	0.00	62.1	18.6
	7	11.1	14.0	0.00	68.7	20.7
	28	5.4	16.7	0.00	73.4	23.2
	91	4.4	16.6	0.00	76.5	25.2
GP20	1	22.5	9.4	16.3	45.8	11.5
	3	13.6	11.6	14.6	56.3	15.7
	7	8.7	13.0	13.7	60.3	17.0
	28	4.1	14.3	12.7	65.2	19.0
	91	3.4	11.3	9.9	72.2	20.8
GP40	1	14.2	7.7	35.4	38.3	9.5
	3	9.3	10.5	33.4	42.3	12.5
	7	5.9	10.5	33.1	46.9	13.3
	28	3.4	10.9	31.2	51.0	15.4
	91	2.6	6.7	23.3	64.1	16.9
GP60	1	9.3	5.4	54.6	27.4	6.8
	3	5.5	7.3	51.0	33.4	9.2
	7	3.2	7.1	50.4	36.7	9.7
	28	1.6	5.6	49.4	40.1	11.4
	91	1.3	1.3	38.4	55.8	13.8

5.3 Results and discussion

5.3.1 Cement clinker hydration degree in blended cement

Generally, the incorporation of SCMs can promote the cement hydration by several mechanisms as shown in Chapter 3 and Chapter 4. Firstly, the addition of SCMs effectively reduces the mass of cement, which results in an increased water to cement ratio. Thus, more water is available for the reaction of cement particles. Secondly, the SCM particles also provide more sites for the growth of the hydration products of cement, which is the effect of nucleation. Thirdly, the chemical properties of SCMs can

also influence the cement hydration by releasing various ions. The hydration degree of cement clinkers (C_3S, C_2S, C_3A, and C_4AF) is calculated by the Equation 5.2. The clinkers in the OPC sample exhibits a hydration degree of 58% and 75% at 1 day and 3 days, respectively. After 20% of cement was replaced by RGP, the hydration degree of clinkers at 1 day and 3 days was 64% and 77%, respectively. G40 and G60 show a clinker hydration degree of 70% and 71% after 1 day hydration. The addition of recycled waste glass enhances the hydration of cement clinkers significantly, which is due to the dilution effect and nucleation effect. Thus, the hydration degree of cement clinkers increases quickly after the addition of more recycled waste glass.

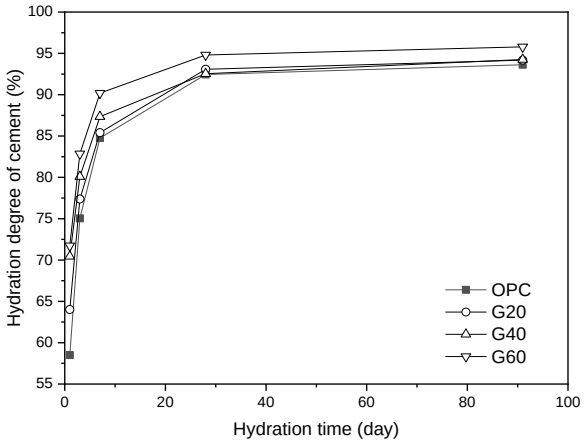

Figure 5.3 Hydration degree of cement clinker in different mixtures

5.3.2 Reaction degree of recycled waste glass in blended cement

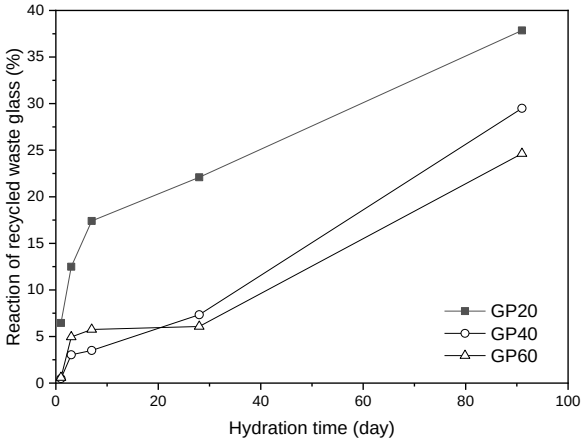

Figure 5.4 Reaction degree of recycled waste glass

The reaction degree of recycled waste glass at different ages is shown in Fig. 5.4, and was calculated by the Equation 5.3. It can be seen that the reaction degree of recycled waste glass is increased with increasing curing duration. G20 exhibits the highest reaction degree during all ages, and reached 37.8% after 91 days. At the same time, the reaction degree of glass particles in G40 and G60 shows a relatively slower increase,

and achieved 29.5% and 24.6% after 91 days, respectively. This indicates that the amount of recycled waste glass can influence the final reaction degree, which is probably due to decreasing amounts of calcium hydroxide and lower pH with increasing waste glass content. This is in agreement with the observation in a related study of mixing calcium hydroxide and waste glass powder, where the higher calcium hydroxide to waste glass ratio resulted in a higher reaction degree of waste glass particles (Mehdi Mejdi et al., 2019).

5.3.3 Total reaction degree of blended cement

The hydration degree of cement can be described using the following equation:

$$Dc_{(t)} = \left(1 - \frac{mC_3S_{(t)} + mC_2S_{(t)} + mC_3A_{(t)} + mC_4AF_{(t)}}{mC_3S + mC_2S + mC_3A + mC_4AF}\right) \times 100\% \quad (5.2)$$

$Dc_{(t)}$ - Hydration degree of cement clinkers
$mC_3S_{(t)} + mC_2S_{(t)} + mC_3A_{(t)} + mC_4AF_{(t)}$ - Mass of clinker from Rietveld quantification in hydrated samples normalized by mass at 600ºC
$mC_3S + mC_2S + mC_3A + mC_4AF$ - Mass of clinker from Rietveld quantification in unhydrated cement

Then, the reaction degree of recycled waste glass blended cement can be expressed as follows:

$$Dgp_{(t)} = \left(1 - \frac{mgp_{(t)}}{m_{gp}}\right) \times 100\% \quad (5.3)$$

$$Dgpc_{(t)} = M_c Dc_{(t)} + M_{gp} Dgp_{(t)} \quad (5.4)$$

$$Dgpc_{(t)} = M_c \left(1 - \frac{mC_3S_{(t)} + mC_2S_{(t)} + mC_3A_{(t)} + mC_4AF_{(t)}}{mC_3S + mC_2S + mC_3A + mC_4AF}\right)$$

$$\times 100\% + \left(1 - \frac{mgp_{(t)}}{m_{gp}}\right) \times 100\% \quad (5.5)$$

$Dgp_{(t)}$ - Reaction degree of recycled waste glass
$Dgpc_{(t)}$ - Reaction degree of blended cement
$mgp_{(t)}$ -Mass of recycled waste glass in hydrated samples normalized by mass at 600ºC
m_{gp} -Original mass of recycled waste glass in dry mixtures
M_c - Mass ratio of cement in dry mixtures
M_{gp} - Mass ratio of recycled waste glass in dry mixtures

After the calculation, the total hydration degree of recycled waste glass blended cement

is shown in Fig. 5.5.

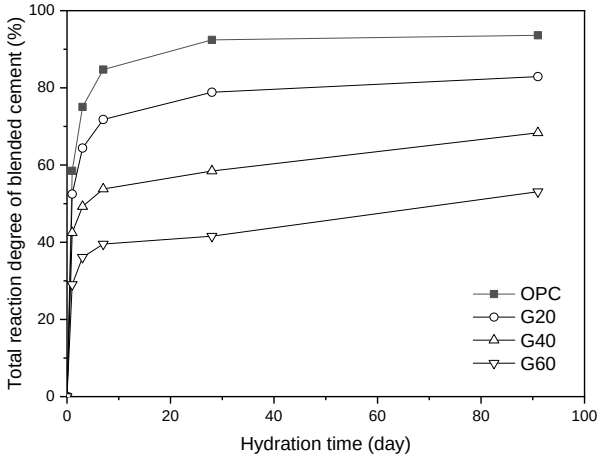

Figure 5.5 Total reaction degree of recycled waste glass blended cement

It can be seen that the total reaction degree of blended cement (reaction degree of cement and recycled waste glass) keeps decreasing with the increase of recycled waste glass in mixtures. The plain cement samples can achieve a total reaction degree of 93% at 91 days, while GP20, GP40, and GP60 only show a total reaction degree of 82%, 68%, and 53%, respectively. This indicates that the high amount of recycled waste glass results in a lower reaction degree of blended cement, which is in agreement with other SCMs blended cement, for example, coal fly ash (Skibsted and Snellings, 2019). The low reaction degree in high volume recycled waste glass (40% and 60%) blended cement also indicates that a relatively high volume of glass particles are remaining unreacted, and then only plays a role as filler. Such a low total reaction degree may result in a low amount of bound water, and as a consequence, the compressive strength can be reduced compared to plain OPC as shown in Chapter 3 and Chapter 4. However, the reduction of strength can be compensated by using a low initial water to binder ratio, which has been discussed in Chapter 3. Nevertheless, in Chapter 4, the high volume waste glass samples exhibit a superior performance of resistance to chloride penetration compared to other samples, the related effects of microstructure modification have been discussed, and from the results in this chapter, the unreacted waste glass may also contribute to the resistance to chloride from the physical aspect explained as follows. It needs to be noted that the recycled waste glass particles are covered by the outer reaction products (from cement hydration or pozzolanic reaction), while the inner part remains unreacted and can play the role of fine aggregates during chloride migration test. Thus, the path for chloride migration can be significantly increased, also for other ions or cations migration.

5.3.4 Bound water and calcium hydroxide content in blended cement

- *Bound water in recycled waste glass blended mixtures*

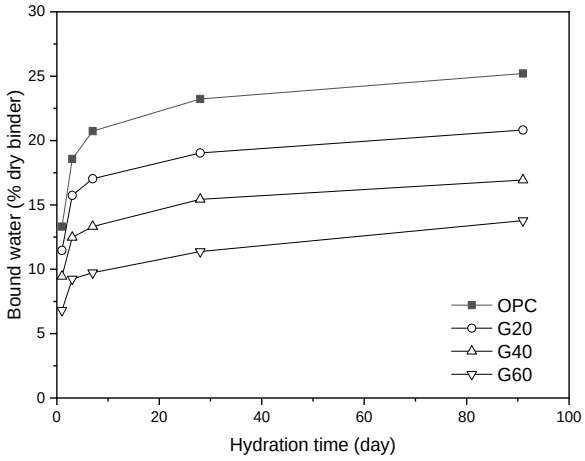

Figure 5.6 The bound water content in different blended cement

According to some studies, the bound water content can also indicate the hydration degree of mixtures (Parrott et al., 1990). The bound water contents of recycled waste glass blended cement are shown in Fig. 5.6, which were determined by TG from 105° C to 600° C. The OPC sample exhibits the highest bound water content among all samples. The addition of recycled waste glass keeps decreasing the bound water content with the increase of recycled waste glass proportion. This observation is in agreement with the results in Fig. 5.5 (total reaction degree of blended cement). Water can be bound by the hydration of the cement part and the pozzolanic reaction of waste glass. Depending on the bound water in a pure cement sample (0.2693 g/ g of cement in this study), the water bound by the pozzolanic reaction of recycled waste glass can be calculated by the following equation,

$$\frac{M_{H_2O}}{M_{SiO_2}} = \frac{(m_{bw} - 0.2693 \times Dc_{(t)} \times M_c \times 100)/18g/mol}{(Dgp_{(t)} \times M_{gp} \times 100) \times \frac{0.6833}{60g/mol}} \quad (5.6)$$

$\frac{M_{H_2O}}{M_{SiO_2}}$ - *molar ratio of combined water to reacted amorphous SiO_2 from recycled waste glass*

m_{bw} - *bound water content by mass at 600ºC,* $Dc_{(t)}$ - *hydration degree of cement*

M_c - *mass ratio of cement in dry mixtures,* 0.2693 - *bound water per gram of cement in present study*

$18g/mol$ - *molar mass of water,* $Dgp_{(t)}$ - *reaction degree of recycled waste glass*

M_{gp} - *mass ratio of recycled waste glass in dry mixtures,*

0.6833 - *mass of SiO_2 per gram of recycled waste glass,* $60g/mol$ - *molar mass of SiO_2*

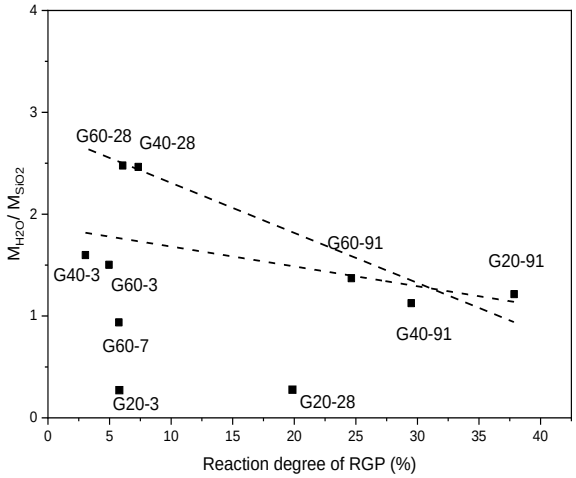

Figure 5.7 The reacted water to SiO_2 ratio during the pozzolanic reaction

The results are shown in Fig. 5.7. It can be seen that the water to SiO_2 (molar ratio) is variable between 1 and 2.5, and that the water to SiO_2 ratio shows a decrease with the reaction degree of recycled waste glass. This could be induced by the increasing Si released from the waste glass with higher reaction degrees. Furthermore, it should be noted that the differences in the calculated results are extremely large for samples with early ages and samples with low amounts of waste glass. This is induced by the calculation error of Rietveld and PONKCS method. From the refinement of Si-RGP mixtures, it is clear that a decreasing RGP content leads to a larger error. For a content of 20% the absolute error is around 2-3%. However, in the hydrated blended cement sample with low RGP contents, the glass is partially reacted which decreases its contents even more and therefore increases the error of results up to 50%. Therefore, for samples containing a low content of RGP or with a low RGP reaction degree, the calculation is not accurate enough to get reliable results of consumed water/CH to reacted RGP ratio. So, the results at high reaction degree and high volume waste glass samples are more reliable, for examples, G20, G40 and G60 at 91 days. This also indicates that the PONKCS and Rietveld still need to be improved to get a reasonable results for hydrated blended samples with low RGP content and at early ages.

- *Calcium hydroxide in recycled waste glass blended mixtures*

As a material with high amorphous silica, recycled waste glass has a pozzolanic reactivity, it even shows a higher reactivity than fly ash as shown in Chapter 4. It can be seen in Fig. 5.8 that the recycled waste glass samples contain lower calcium hydroxide content compared to OPC. The reduction of calcium hydroxide can be explained by the reduced cement amount and the consumption of the pozzolanic reaction. A theoretical pozzolanic reaction, for example, pure silica fume, can be described as follows:

$$S + 1.7CH + 2.3H \rightarrow C_{1.7}SH_4 \quad (5.7)$$

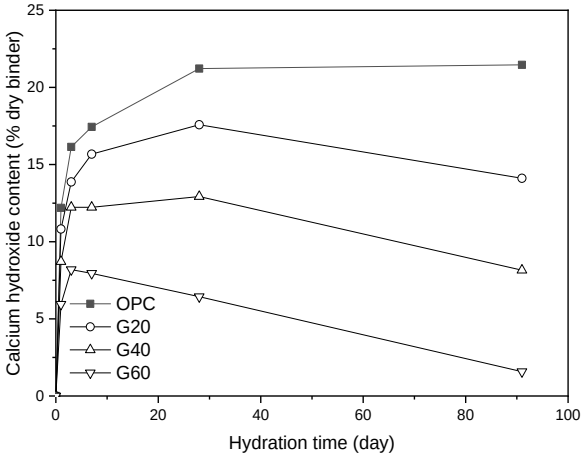

Figure 5.8 Calcium hydroxide content in dry mixtures

However, the ratio of Ca/Si of the C-S-H could be variable due to ion diffusion (Ca and Si), chemical composition and the particle size of SCMs. As shown in Chapter 3, the recycled waste glass consists of 68.3% SiO_2, 11.9% CaO, and 14.65% Na_2O and the presence of Na and Ca in waste glass may alter the Ca/Si ratio in the reaction products. For a better understanding of the influences of reacted recycled waste glass on products, the Ca/Si and (Na+Ca)/Si are calculated based on the calcium hydroxide consumption and reaction degree of glass particles for G20, G40, G60 at 91 days and G60 at 28 days, and the results are shown in Fig. 8. The Ca/Si 1 indicates the Ca/Si ratio in reaction products without including Ca from reacted waste glass. The Ca/Si 2 is the Ca/Si including Ca from reacted waste glass. The (Na+Ca)/Si includes Ca and Na from reacted waste glass. The results are calculated as follows:

$$Ca/Si\ 1 = \frac{(m_{CH} - 0.2198 \times Dc_{(t)} \times M_c \times 100)/74g/mol}{(Dgp_{(t)} \times M_{gp} \times 100) \times \frac{0.6833}{60g/mol}} \quad (5.8)$$

$$Ca/Si\ 2 = \frac{(m_{CH} - 0.2198 \times Dc_{(t)} \times M_c \times 100)/74g/mol + Ca\ from\ RGP}{(Dgp_{(t)} \times M_{gp} \times 100) \times \frac{0.6833}{60g/mol}} \quad (5.9)$$

$$(Na + Ca)/Si = \frac{(m_{CH} - 0.2198 \times Dc_{(t)} \times M_c \times 100)/74g/mol + Ca\ from\ RGP + Na\ from\ RGP}{(Dgp_{(t)} \times M_{gp} \times 100) \times \frac{0.6833}{60g/mol}} \quad (5.10)$$

$$Ca\ from\ RGP = (Dgp_{(t)} \times M_{gp} \times 100) \times \frac{0.1190}{56g/mol} \quad (5.11)$$

$$Na\ from\ RGP = (Dgp_{(t)} \times M_{gp} \times 100) \times 0.1465 * \frac{2}{62g/mol} \quad (5.12)$$

m_{CH} - calcium hydroxide content in dried mixtures, $Dc_{(t)}$ - hydration degree of cement

M_c - *mass ratio of cement in dry mixtures,*
0.2693 - *grams of bound water from per gram of cement in present study*
$Dgp_{(t)}$ - *reaction degree of recycled waste glass,* M_{gp} - *mass ratio of recycled waste glass in dry mixtures,*
0.6833 - *mass of SiO_2 per gram of recycled waste glass,* 60 - *molar mass of SiO_2*
0.2198 - *grams of calcium hydroxide from per gram of cement in this study*
$74 g/mol$ - *molar mass of calcium hydroxide,* $56 g/mol$ - *molar mass of CaO,* $62 g/mol$ - *molar mass of Na_2O,* 0.1190 - *mass of CaO per gram of recycled waste glass*
0.1465 - *mass of Na_2O per gram of recycled waste glass*

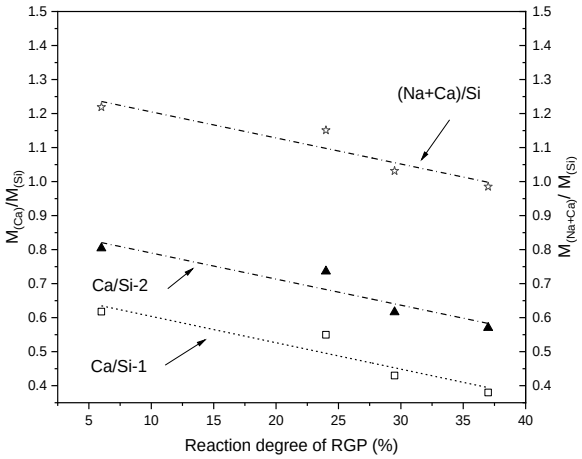

Figure 5.9 The calcium hydroxide to SiO_2 ratio during the pozzolanic reaction (Ca/Si-1 Ca/Si ratio from consumed calcium hydroxide and silica, Ca/Si-2 Ca/Si ratio after combining the Ca from reacted waste glass, (Na+Ca)/Si after combining the Na from reacted waste glass)

It can be seen that Ca/Si-1, which is calculated based on the consumption of calcium hydroxide and silica from reacted recycled waste glass, ranges from around 0.4 to 0.6. The Ca/Si ratio keeps decreasing with the increasing reaction degree of waste glass, which is a similar trend as the bound water in Fig. 5.7 shows. This Ca/Si 1 is extremely low compared to the EDX results in Chapter 2 and Chapter 3 (0.7-1.2). However, after adding the Ca from reacted waste glass (Ca/Si-2), a more reasonable Ca/Si ratio can be observed of around 0.6 to 0.9. This indicates that the Ca from the dissolution of recycled waste glass can also take part in the formation of secondary C-S-H during the pozzolanic reaction. Furthermore, the Na from the reacted waste glass can also be incorporated into the C-S-H gel as (N)-C-S-H, which is similar to alkali activated materials. The (Na+Ca)/Si ratio in the present results is around 1.0 to 1.3. The Ca/Si and (Na+Ca)/Si ratio is also in agreement with the results in a previous study from EDX, which is observed in reacted mixtures of calcium hydroxide and waste glass powder (Mehdi Mejdi et al., 2019). Besides, the increase of reaction degree of recycled waste glass powder also shows a reduction on the Ca/Si, (Na+Ca)/Si, and the H_2O/Si in the reaction products. This could be induced by the slow diffusion of Si with the increase of the waste glass reaction degree.

5.3.5 Reaction process of recycled waste glass in cement blends

The recycled waste glass can be described as follows depending on the main chemical compositions (Na_2O, CaO, and SiO_2 in XRF):

$$(Na_2O)_{0.2075}(CaO)_{0.1866}(SiO_2)_1 = N_{0.2075}C_{0.1866}S \quad (5.13)$$

Then, depending on the above results and discussion, the reaction of recycled waste glass in cement blends can be described as follows:

$$N_{0.2075}C_{0.1866}S + (0.38\sim0.62)CH + (1\sim2.5)H$$

$$\rightarrow N_{0.2075}C_{(0.57\sim0.80)}SH_{(1\sim2.5)} \quad (5.14)$$

The variation of consumed CH and bound water can be explained by the reaction degree of recycled waste glass, which is discussed in the following part.

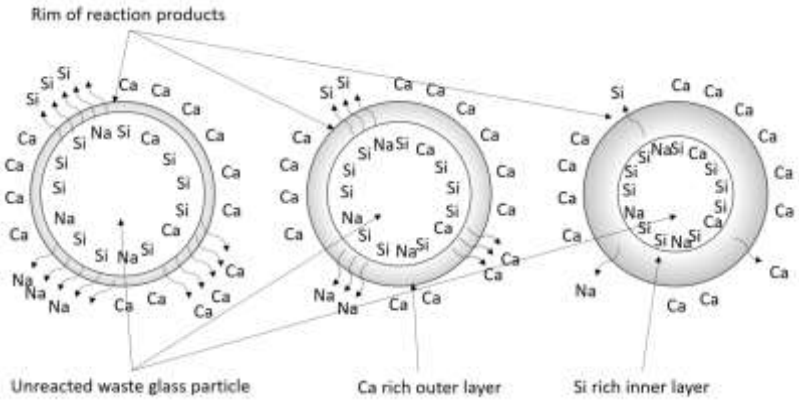

Figure 5.10 The reaction of recycled waste glass in cement blends

The reaction process of a recycled waste glass particle is described in Fig. 5.10. The reacted rim is gradually growing with the increase of the glass reaction degree. The curved arrows represent the diffusion of elements from the waste glass surface, and the Ca around the glass particle is related to the hydrated cement matrix. The waste glass particle keeps dissolving due to the high pH provided by calcium hydroxide from cement hydration. At the same time, Na, Ca and Si are gradually diffused from the surface of the glass particle into the cement matrix. At the beginning of the reaction, the reaction products with high Ca/Si can be formed on the surface of the glass particle due to the Ca-rich environment around the glass particle and limited Si dissolving. Before the calcium hydroxide is totally consumed, the pH is still high enough for the dissolving of waste glass particles. However, the formed rim of reaction products could be an inhibitor for Na, Ca and Si transportation from the unreacted glass surface.

Therefore, the lower Ca/Si layer can be formed in the inner layer compared to the outer layer with the increase of glass reaction degree. Depending on this process, the reaction degree of recycled waste glass in cement blends could be affected by several factors. Firstly, the cement replacement ratio can effectively control the amount of available calcium hydroxide, it is clear to see the low cement replacement ratio results in a high reaction degree of waste glass. Secondly, the particle size of waste glass, the high surface area is expected to contribute a high reaction degree.

5.3 Conclusions

1. In the recycled waste glass blended cement, the reaction degree of cement clinkers can be significantly enhanced by the increase of substitution ratio. However, the total reaction degree of blended cement gradually decreased with the increase of recycled waste glass substitutions because of the low reaction degree of glass particles.

2. The reaction degree of recycled waste glass in cement blends is for 24.6% to 37.8%. The highest reaction degree is observed in G20, while the lowest reaction degree is found in G60.

3. The reaction degree of recycled waste glass controls the Ca/Si and (Na+Ca)/Si ratio in the reaction products. The increase of waste glass reaction degree contributes to a lower (Na+Ca)/Si and Ca/Si ratio in products due to higher amounts of dissolved Si in the inner layer of reaction rim.

4. In the recycled waste glass blended cement, every mole of waste glass can consume 0.38 to 0.62 mole of calcium hydroxide and bind 1 to 2.5 molar of water during the pozzolanic reaction.

Chapter 6 Waste glass as binder in alkali activated blast furnace slag-fly ash mortars

This chapter illustrates the application of waste glass powder as part of the binder in slag-fly ash systems activated by NaOH and NaOH/Na_2CO_3. To evaluate the reaction kinetics, reaction products, mechanical properties, and durability performance of glass powder modified alkali activated slag-fly ash systems, calorimetry test, X-ray diffraction, FTIR, strength test, drying shrinkage tests, and carbonation test were conducted. From the isothermal calorimetry results, glass powder shows a higher reactivity compared to fly ash but still lower than GGBS. The reaction products of glass powder modified samples exhibit a higher of polymerization degree of Si-O-T, observed in FTIR. Furthermore, a higher drying shrinkage exists in glass modified mortars. The mechanical performance of different samples is mostly controlled by the Ca/Si ratio of the dry mixtures and activator type. After the slag-fly ash binder system was modified by the waste glass, a significant enhancement of resistance to carbonation was identified, especially for NaOH/Na_2CO_3 activated mortars, which show an increase of 300% in their resistance to carbonation compared to the reference sample. The Na/(Si+Al) ratio of dry mixtures exhibits a positive correlation with carbonation resistance.

This chapter is partially published elsewhere:

G. Liu, M.V.A. Florea, H.J.H. Brouwers. Waste glass as binder in alkali activated slag–fly ash mortars. Materials and Structures, 2019, Volume 52, Page 1-12.

6.1 Introduction

In Chapter 2 to Chapter 5, the recycled waste glass is investigated as SCMs in cement based building materials. It is clear, that the reaction of recycled waste glass is strongly affected by the cement hydration. Specially, the presence of calcium hydroxide, which provides a high enough pH for glass dissolution. Consequently, the microstructure can be modified. On the other hand, alkali activated materials are also potential systems for the application of recycled waste glass. Usually, ground granulated blast furnace slag (GGBS) and fly ash are used. For example, GGBS can be used for providing Ca and Si in the high calcium binder system in normal alkali activated materials, the reaction product being mainly C-(A)-S-H (Brough and Atkinson, 2002). Combining GGBS and fly ash in alkali activated binder systems is helpful to compensate their individual negative effects induced by each other. Some studies revealed that the incorporation of fly ash in alkali activated slag samples can significantly improve the shrinkage during the reaction (Kumarappa et al., 2018; Gao et al., 2016; Lee et al., 2014). Furthermore, the blended binder exhibits an excellent performance of strength and durability (Sugama et al., 2005).

Waste glass is also reactive in alkali activated system and shows a higher dissolution rate in a NaOH/Na_2CO_3 solution compared to NaOH solution at the same sodium concentrations (Torres-Carrasco and Puertas, 2017). In addition, the blended activator NaOH/Na_2CO_3 was reported to results in better performance of GGBS-glass systems (Martinez-Lopez and Escalante-Garcia, 2016). In some reports, the waste glass powder in alkali activated concrete plays a role similar to water glass in microstructure enhancement (Puertas and Torres-Carrasco, 2014). In general, the selection of binder composition and activator of alkali activated concrete has a huge influences on the concrete durability performance.

This chapter evaluates the application of waste glass in slag-fly ash alkali activated binder systems. The waste glass was used to replace slag, fly ash or a total of binder of 20% by mass, to study the influences of waste glass on slag-fly ash binder system. Two kinds of activators (NaOH and NaOH/Na_2CO_3) were selected. The reaction kinetics, reaction products, strength performance and durability properties are studied. The purpose is to optimize the application of waste glass in a slag-fly ash binder.

6.2 Materials and methods

6.2.1 Materials characterization

The recycled waste glass, ground granulated blast furnace slag (GGBS), fly ash and fine aggregate (standard sand) are same as the materials in Chapter 4. The characterization results have been shown in Chapter 4.2.1.

6.2.2 Test methods

- *Activators and mortars preparation*

The NaOH activator solution was prepared using sodium hydroxide pellets (NaOH) and distilled water to achieve a concentration of 8M. The blended NaOH-Na_2CO_3 (50:50 by mass) activator was prepared from sodium hydroxide pellets (NaOH), sodium carbonate (Na_2CO_3) and distilled water, which results in the same Na concentration of 8M. The sample mix design and the initial Ca/Si and Na/(Si+Al) of dry mixtures are shown in Table 6.1. The equivalent Na_2O% for all binders is kept at a constant dosage of 10%.

The mixing of mortars was done by using a 5-liter Hobart mixer. At first, the dry slag-fly ash-waste glass binders and fine aggregate (standard sand) were mixed for 30 s at low speed. Then activator was added and mixed on medium speed. Lastly, the fresh mortars were filled into the plastic mould of 40 mm × 40 mm × 160 mm and covered with plastic film for the first 24 hours curing. After that, the mortar prisms were demoulded and covered by plastic film for ambient curing until further testing.

- *Fresh behaviour, mechanical performance and reaction kinetics*

The slump flow, setting time, calorimeter, XRD, drying shrinkage strength tests have been described in Chapter 3.2.2.

- *FTIR*

The Fourier transform infrared spectroscopy (FTIR) measurement was performed in a Varian 3100 instrument with the wavenumbers ranging from 4000 to 400 cm^{-1} with a resolution of 1 cm^{-1}.

- *Aggressive carbonation test*

Carbonation curing was conducted in a carbonation chamber. The relative humidity was

set as 65% (in the range of the optimal value for carbonation test from previous studies (Leemann and Moro, 2017)), the temperature was set at 25 °C, and the CO_2 gas dosage kept a constant of 20% at ambient pressure. Samples were moved to the carbonation chamber for the test after 28 days normal curing. The phenolphthalein solution was sprayed on the fracture surface of samples after different time of carbonation to test the uncarbonated area. Then the fractions of uncarbonated area was identified and quantified by using Image J.

Table 6.1 Mix design for 1 m^3

Sample	GGBS (kg)	FA (kg)	RGP (kg)	Sand (kg)	Activator (kg)	w/b	Flowabilty (cm)	Ca/Si	Na/(Si+Al)
NH1	251.5	251.5	0	1509.0	265.6[a]	0.4	15.5	0.64	0.30
NH2	252.4	151.4	100.9	1514.3	266.5[a]	0.4	16.0	0.62	0.40
NH3	150.0	250.0	100.0	1500.1	264.0[a]	0.4	15.8	0.40	0.36
NH4	200.9	200.9	100.5	1507.2	265.3[a]	0.4	16.5	0.51	0.38
NC1	251.5	251.5	0	1509.0	274.6[b]	0.4	15.3	0.64	0.30
NC2	252.4	151.4	100.9	1514.3	275.5[b]	0.4	14.5	0.62	0.40
NC3	150.0	250.0	100.0	1500.1	272.9[b]	0.4	15.8	0.40	0.36
NC4	200.9	200.9	100.5	1507.2	274.3[b]	0.4	14.8	0.51	0.38

a – NaOH activator, b – NaOH-Na_2CO_3 activator

6.3 Results

6.3.1 Reaction kinetics and products characterization

- *Isothermal calorimetry test*

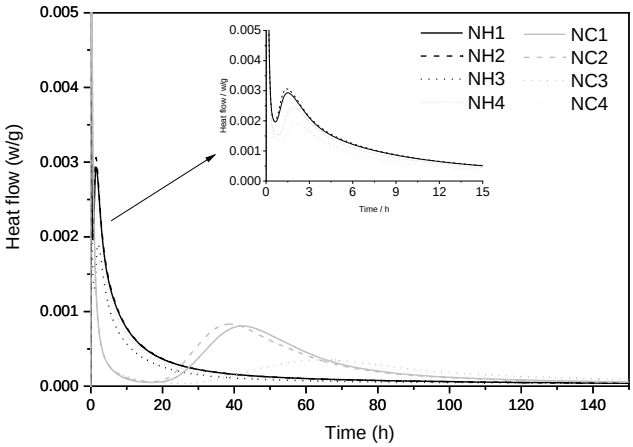

Figure 6.1 Reaction heat development of various binders

Isothermal calorimetry tests were conducted for the different mixtures activated by NaOH type and NaOH/Na_2CO_3 type activator. As shown in Fig. 6.1, all mixtures exhibit

a typical four-stage heat evolution curve of initial dissolution, induction, acceleration to deceleration and stable period (Fang et al., 2018; Gao et al., 2015; Puertas et al., 2018). It can be identified that different mixtures show a variation of peak intensity and acceleration/deceleration period. The different parts of slag-fly ash binder replaced by waste glass induce the enhancement or reduction of the reaction intensity and reaction rate. For NaOH activated mixtures, NH2 shows the highest peak intensity and shortest induction period compared to the reference (NH1). NH3 and NH4 exhibit a significant lower heat peak intensity and a longer induction period. Binders activated by NaOH/Na_2CO_3 blended activator exhibit a relatively longer induction period and lower reaction intensity compared to NaOH series samples. However, a similar influence of waste glass incorporation on the reaction kinetics of slag/fly ash system is observed. NC2 (glass replacing fly ash part) shows the shortest induction period and highest reaction intensity compared to other blended activator activated binders, while NC3 (glass replacing slag part) exhibits the slowest reaction rate.

For all NaOH and NaOH/Na_2CO_3 series samples, the highest reaction intensity and reaction rate is observed in NH2 and NC2, respectively, which is related to mixtures containing 50% of GGBS, 30% of fly ash and 20% of waste glass powder. On the contrary, the binder exhibiting the lowest reactivity is found in NH3 and NC3, mixtures containing 30% of GGBS, 50% of fly ash and 20% waste glass. These results indicate that the waste glass powder may show a lower reactivity than GGBS, while higher reactivity than fly ash when activated by NaOH or NaOH/Na_2CO_3 type activator.

This difference of heat flow is induced by the significant higher pH provided by the NaOH, which accelerates the dissolution of Al and Si during the induction period (Song and Jennings, 1999). As higher reaction rate and reaction intensity can be observed in the first hours as shown in Fig. 6.3. On the contrary, the Na_2CO_3 shows a limitation on providing a high pH environment in the first hours. This is also the reason why NaOH/Na_2CO_3 activated samples show a relatively long duration to reach the setting compared to NaOH activated specimens. In some cases, the reaction heat flow peak of Na_2CO_3 activated slag binder was presented after 50 to 60 hours of reaction (Bernal et al., 2015; Yuan et al., 2017). In the present study, the heat flow peaks of binders activated by NaOH/Na_2CO_3 locate in the range of from 35 h to 60 h, which is faster compared to previous studies. This is induced by combining NaOH and Na_2CO_3 as activator.

- *XRD and FTIR analysis*

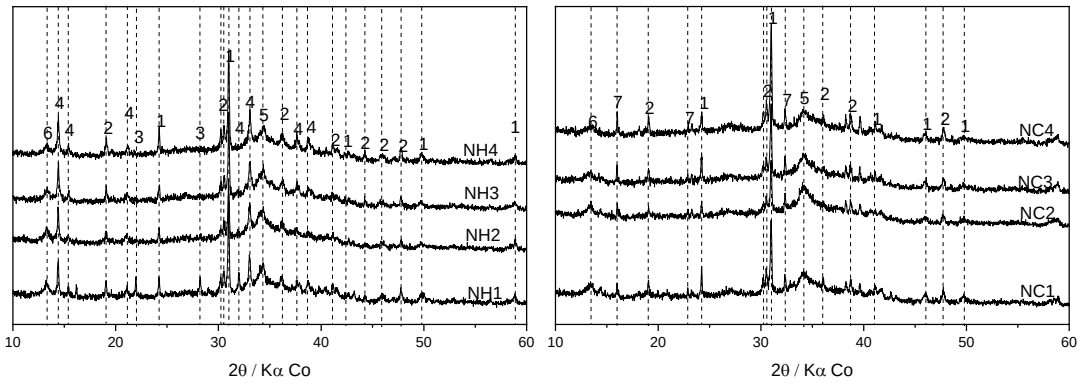

(a) (b)

Figure 6.2 XRD patterns of different mixtures (a) NaOH activated binders and (b) NaOH-Na_2CO_3 activated binders (1-quartz, 2-mullite, 3-cancrinite, 4-garronite, 5-C-(A)-S-H, 6-hydrotalcite, 7-gaylussite)

The XRD patterns of the paste samples are shown in Fig. 6.2. As can be seen, some minerals are found in all mixtures, regardless of the activator types. For example, quartz and mullite, which are the residual minerals in fly ash. In comparison to the XRD data of raw materials (shown in Chapter 4.2.1), many new peaks were formed after 28 days reaction by the activation of NaOH or NaOH-Na_2CO_3. In NaOH activated samples, a peak with broad hump and low intensity can be identified between 33° to 35°, which is related to the formation of C-S-H with a low degree of crystallinity (Garbev et al., 2008; Kumar et al., 2017). In addition, hydrotalcite, garronite and cancrinite also can be found in all samples as the usual products in similar binder systems (Toniolo et al., 2018; Ismail et al., 2014). For the samples activated by NaOH-Na_2CO_3, a different phase-gaylussite was formed. The addition of waste glass in binders shows no significant effect on the variation of reaction products. It is interesting to notice that the peaks of cancrinite in NaOH activated binders are relatively weak after the incorporation of waste glass. This may be caused by the change in the SiO_2/Al_2O_3 ratio after the addition of waste glass.

To further study the reaction products of different mixtures, FTIR was employed as shown in Fig. 6.3. The location of the dashed line is determined by the peak of Si-O-T in reference samples, which contain 50% slag and 50% fly ash as a binder (shown as NH1 and NC1, repectively). For all alkali activated samples, the main peaks shown in the present range are around 870 cm^{-1}, 960 cm^{-1}, and 1406 cm^{-1}. The peaks located around 870 cm^{-1} and 1406 cm^{-1} are related to the C-O bond (Bernal et al., 2011a), with appearances of carbonate in samples. It can be hydrotalcite, which has been identified in the XRD patterns. The appearance of carbonate in NaOH activated samples might

be caused by the carbonation during the sample preparation, while for the NaOH-Na_2CO_3 activated specimens, it results in the formation of gaylussite ($Na_2Ca(CO_3)_2 \cdot 5H_2O$), which also has been found with XRD. As it can be seen, the sodium hydroxide activated slag-fly ash binder system shows its main peak around 964 cm^{-1}, and at 957 cm^{-1} in sodium hydroxide-sodium carbonate activated slag-fly ash. This band is related to the υ_3 vibration of Si-O-T bond, which generally exists in N-A-S-H and C-A-S-H gel in alkali activated slag-fly ash systems(Gao et al., 2016). After 20% of waste glass powder was introduced in the slag-fly ash binder, the Si-O-T peaks in all waste glass mixtures exhibits a slight shift to higher wavenumbers. The addition of waste glass powder introduced an additional Si source to the reaction system; as a consequence, more Si could be incorporated in to the gel network to form a Si-rich structure (Zhang et al., 2017), which can generate a higher polymeriziation degree of reaction products.

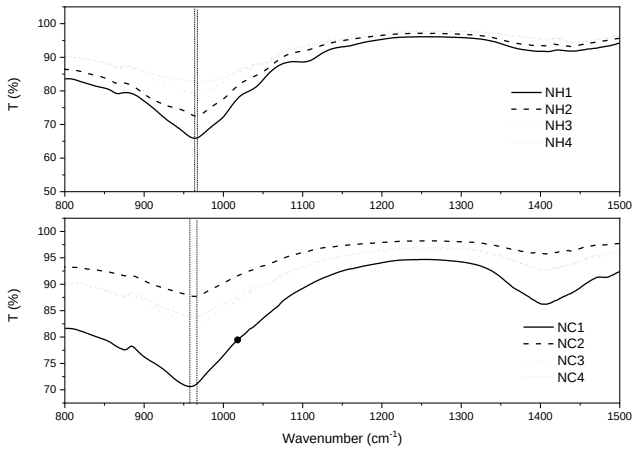

Figure 6.3 FITR of different mixtures after 28 days curing

6.3.2 Setting and mechanical behaviours

- *Setting time*

The setting behaviour of various binder systems is shown in Table 6.2. As it can be seen, the significant differences are observed between different binders, as well as between samples with different activators. For NaOH activated binders, the reference sample, NH1, reaches the initial setting at 89 min, while the final setting at 139 min. Comparing to NH1, NH2 shows a slightly shorter initial and final setting time of 85 min and 129 min, respectively. On the contrary, NH3 experiences a longer duration to reach the initial and final setting, of 116 min and 163 min, respectively. For NaOH-Na_2CO_3 activated binders, all samples show a relatively longer duration for the setting than NaOH activated samples. NC2 and NC4 exhibit almost the same duration to the setting, which is shorter than the reference NC1. The longest setting time is shown by NC3.

This observation is in accordance with the results of the calorimetry test.

Table 6.2 Setting and mechanical performance of mortars

Sample ID	Initial setting (min)	Final setting (min)	Flexural strength (MPa)		Compressive strength (MPa)	
			7 days	28 days	7 days	28 days
NH1	89	139	2.67±0.07	4.21±0.04	8.34±0.11	12.77±0.36
NH2	85	129	3.03±0.07	4.11±0.01	8.34±0.10	10.82±0.18
NH3	156	206	1.52±0.03	2.89±0.05	4.16±0.09	9.73±0.25
NH4	116	163	2.16±0.04	3.38±0.18	6.16±0.12	9.78±0.28
NC1	320	410	5.20±0.08	6.29±0.09	16.38±1.16	25.68±0.17
NC2	306	380	4.84±0.11	5.30±0.22	16.09±0.76	23.89±0.30
NC3	370	470	3.23±0.06	5.12±0.24	12.38±0.23	17.99±0.64
NC4	307	379	4.18±0.01	5.13±0.05	14.00±0.22	21.62±0.85

- *Mechanical performance*

The mechanical performances of different alkali activated mortars are shown in Table 6.2. The incorporation of waste glass in binders reduces the strength performance of mortars activated by NaOH or NaOH-Na_2CO_3 after 28 days. For NaOH activated mortars, fly ash-slag samples (NH1) exhibit an average compressive strength of 12.76 MPa. After the waste glass was used to replace the fly ash part, slag part or all binder, the compressive strength of 28 days are 10.82 MPa, 9.73 MPa, and 9.78 MPa, respectively. The reduction of mechanical performance is mostly caused by the decreasing of the slag proportion, for example, NH3 (30% slag) exhibits the lowest strength performance.

The obvious higher strength performance can be found in NaOH-Na_2CO_3 activated mortars. The reference sample (NC1) achieves a compressive strength of 25.68 MPa, while 23.89 MPa, 17.98 MPa and 21.62 MPa for waste glass containing samples NC2, NC3 and NC4, respectively. The addition of waste glass in NaOH-Na_2CO_3 activated mortars shows a similar effect on the strength development as NaOH activated mortars. The slag component is a critical parameter of strength behaviour for alkali activated slag based materials (Marjanović et al., 2015). The difference in mechanical performance is possibly induced by the chemical composition of binders, which will be discussed in the following part.

The compressive strength of NaOH/Na_2CO_3 activated mortars are obviously higher than the mortars activated by NaOH at 7 days and 28 days only. As it is well known, the mechanical performance of alkali activated concrete is influenced by the type and the concentration of activator (Fernández-Jiménez et al., 1999). In the previous research,

NaOH activator helped to form C-S-H containing high Q_2 value of Si, while no Q_3 value was found, this kind of long chains indicate a low strength performance of samples. However, the application of Na_2CO_3 induced more Q_3 value of Si and very low Q_2, which indicates a cross-linked structure of C-S-H (Fernández-Jiménez et al., 2003). As a consequence, the mechanical performance will be higher. In addition, the existence of long chains in NaOH activated samples was also identified by the FTIR results in Fig. 5 that NaOH activated slag-fly ash binders shows a higher wavenumber of Si-O-T than NaOH/Na_2CO_3 activated samples.

6.3.3 Shrinkage and carbonation resistance performance evaluation

- *Drying shrinkage*

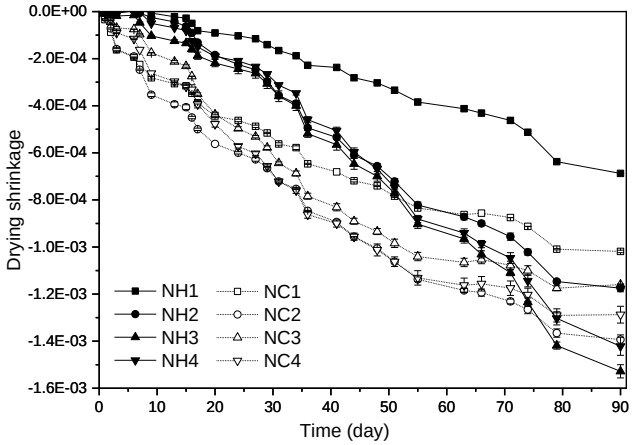

Figure 6.4 Drying shrinkage of different mortars

The change in length during the drying shrinkage test (90 days) is shown in Fig. 6.4. The addition of waste glass in slag-fly ash binders both increases the final drying shrinkage of both NaOH and Na_2CO_3-NaOH activated mortars. For NaOH activated binders, the highest drying shrinkage is observed in NH3, which contains 30% slag, 20% waste glass, and 50% fly ash. At the same time, sample NH1 (50% slag and 50% fly ash) exhibits a significantly lower drying shrinkage compared to other samples. On the contrary, when blended activator was used, NC2 (50% slag, 30% fly ash and 20% waste glass) presents the highest drying shrinkage during the test. In addition, as the fly ash proportion increases, the drying shrinkage of mortars keeps decreasing, which agrees with the previous study (Lee et al., 2014).

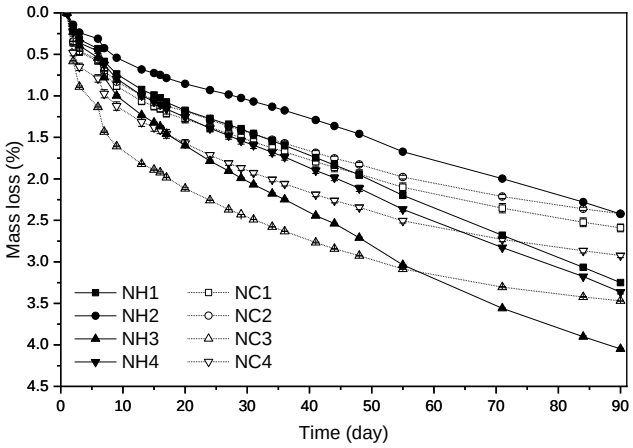

Figure 6.5 Mass loss during shrinkage test

The mass change of all mixtures was recorded during the shrinkage test and is shown in Fig. 6.5. It is noticeable that the results of mass change can not totally agree with the drying shrinkage data. For sodium hydroxide activated samples, NH3 presents the highest mass loss, while NH2 exhibits the lowest mass loss. A similar trend also can be found in sodium hydroxide-sodium carbonate activated mortars of the same dry mixtures design. Furthermore, mortars activated by sodium hydroxide present an overall higher mass loss compared to the sample activated by sodium hydroxide-sodium carbonate. These indicate that samples activated by blended activators have less content of evaporable water than samples activated by NaOH.

- *Resistance to aggressive carbonation*

The uncarbonated area of mortars by different duration of CO_2 penetration is shown in Fig. 6.8. As it can be seen, the application of waste glass as part of the binder in slag-fly ash binders induces the difference of the resistance to carbonation for both for NaOH and NaOH-Na_2CO_3 series. NH1 shows an uncarbonated area of 94.8% after 3 days carbonation; this value is reduced to 70.0% after 8 weeks. When the waste glass was added as part of binders, NH2 (replacing fly ash), NH3 (replacing slag), and NH4 (replacing all binder) exhibit the uncarbonated area of 95.9%, 94.7% and 91.9%, respectively after 3 days carbonation. After 8 weeks carbonation, they present the uncarbonated area of 78.8%, 73.0%, and 73.6%, respectively. This indicates that the addition of waste glass as part of binders improved the resistance to carbonation of sodium hydroxide activated binder systems.

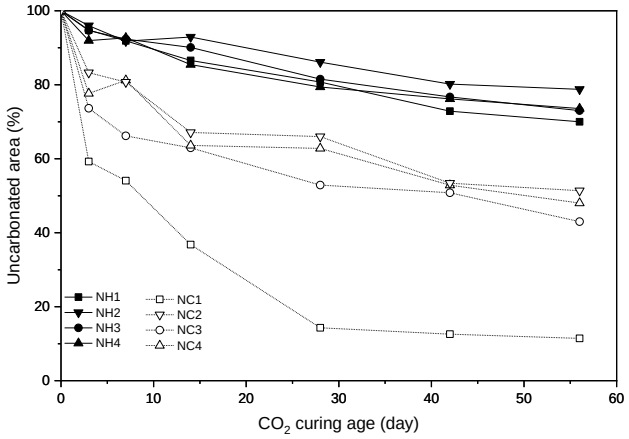

Figure 6.6 Uncarbonated area of samples subjected to various duration of CO_2 penetration

In the comparison to NaOH activated series samples, blended activator-NaOH-Na_2CO_3 -activated samples all exhibit a poor performance of resistance to carbonation. Even though, the incorporation of waste glass still contributes to an enhancement of the resistance to carbonation. The uncarbonated area of slag-fly ash mortar (NC1) only accounts for 59.3% after 3 days carbonation curing, and 11.4% for 8 weeks carbonation. After the waste glass added as part of binders, uncarbonated area after 3 days are 83.3%, 73.6%, and 77.6% for NC2, NC3 and NC4, respectively. The incorporation of waste glass enhances the resistance for carbonation significantly at an early age. Furthermore, this enhancement also can be observed at a late age, for example, 8 weeks. The residual uncarbonated area of NC2 is 51.4%, while 43.0% and 48.0% for NC3 and NC4; almost four times the uncarbonated area in waste glass blended binders compared to 11.4% of the slag-fly ash binder (NC1) activated by sodium hydroxide-sodium carbonate.

It is interesting to notice that NaOH activated mortars show a significant better resistance to carbonation compared to samples activated by NaOH/Na_2CO_3 during all 8 weeks of carbonation. However, the NaOH series samples exhibit higher mass loss during shrinkage test and a lower strength, which indicates a more porous microstructure and less hydration products. Generally, these kinds of samples are believed to have a poor resistance to CO_2 penetration for ordinary concrete (Gonen and Yazicioglu, 2007). Nevertheless, the NaOH series mortars still keep more than 70% uncarbonated area after 8 weeks CO_2 penetration as shown in Fig. 8 , while less than 20% for NaOH/Na_2CO_3 slag-fly ash mortar is uncarbonated. This can be explained by several factors. At first, the NaOH type activator shows obviously higher pH than the blended activator, which can provide a high buffer capacity to resist the reduction of pH induced by CO_2 dissolving in the pore solution. It is believed that the decalcification of C-S-H only can be observed at low pH (Bakharev et al., 2003). Secondly, hydrotaclite-like minerals as the main reaction products in alkali activated slag, it has a

layered double hydroxide structure. Generally, the interlayer can incorporate OH^-, NO_3^-, Cl^- and CO_3^{2-} (Costa et al., 2012). In some cases, these anions can be replaced by other ones, which can provide a capacity for hazardous ions storage (Chen et al., 2015). For NaOH activated binders, OH^- can be the mainly anions in this structure, and it is possible that OH^- can be replaced by CO_3^{2-} from CO_2 dissolving. During this process, additional OH^- will be released as the pH buffer. Where as in NaOH-Na_2CO_3 activated binders, OH^- has been partially replaced by the CO_3^{2-} from Na_2CO_3, which results in the limitation of buffer capacity. As a consequence, NaOH activated mortars shows better ability of carbonation resistance.

6.3.4 The effects of recycled waste glass on AAM

- *The influence of waste glass addition on reaction kinetics and mechanical performance*

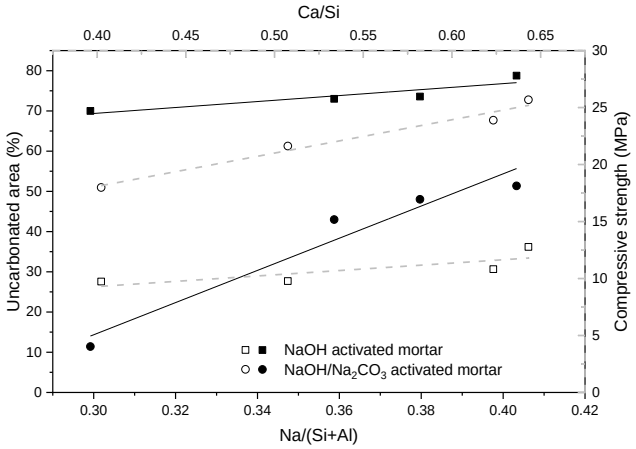

Figure 6.7 The correlation between Na/(Si+Al) and uncarbonated area and between Ca/Si and compressive strength

As detailed above, NaOH/Na_2CO_3 contributes to the higher mechanical performance at the same ages, but lowers the resistance for carbonation compared to NaOH activated samples. The incorporation of waste glass powder as part of the binders induces significant differences of performances, such as reaction kinetics and products. In the present study, waste glass was used as a replacement of slag, fly ash or total binder. From the XRF data as shown in Chapter 4.2.1, high dosage of Na_2O can be identified. When the waste glass was used to replace 20% fly ash in slag-fly ash binder, a higher reaction intensity and shorter induction period were observed. In the previous study, fly ash was identified to show a much slower dissolution rate at ambient temperature, which is caused by a high degree of polymerization of Si and Al in the amorphous phase (Chen-Tan et al., 2009). In the results of the heat flow peak in the present study, the higher reaction rate corresponds to the additional Si and Na dissolution by replacing fly

ash by waste glass compared to the reference sample. However, when waste glass replaces 20% of slag or 20% total binder, the induction period is prolonged, as well as the reaction intensity. This can be explained by the reduced Ca in binders. In slag-fly ash binder systems, higher slag proportion usually induc high reaction intensity and cumulative reaction heat, as well as a reduction of setting time (Puertas et al., 2000). Subsequently, The strength performance of mortars in this study is primarily related to the slag proportion in the mixture and largely unconnected to the activator type. In other words, a higher slag proportion results in the higher mechanical performance of slag-fly ash-waste glass binder system. A slightly lower strength of the waste glass replacing fly ash samples was exhibited at 28 days, which may be caused by the reduction of the formation of C-A-S-H at late age compared to slag-fly ash binder. In addition, the higher Si/Al ratio after the waste glass incorporation may induce the weak peaks of cancrinite (a reaction product in NaOH activated slag/fly ash system (Oh et al., 2010)).

- *The influence of waste glass addition on the carbonation resistance*

The additional Si in the pore solution also can induce changes of microstructure and capillary tension of pore solution. A small pore size and higher capillary force was identified when using additional Si source in binder systems in a previous study (Ye et al., 2017), which contributes to a high shrinkage. This agrees with the observation of drying shrinkage and mass loss in this study. Generally, drying shrinkage contains shrinkage caused by water evaporation and polymerization of reaction. It is interesting to notice that NaOH activated slag/fly ash mortar exhibits the lowest drying shrinkage, which is expected to have the lowest mass loss. However, the lowest mass loss is presented in slag/ (fly ash+waste glass) mortar (NH2 and NC2). At the same time, waste glass replacing slag and total binder mortars exhibit a similar trend of drying shrinkage as for total mass loss. This indicates that, when the waste glass was used as fly ash replacement, the shrinkage caused by chemical reaction is large than the shrinkage induced by water evaporation. However, for other samples, water evaporation dominates the drying shrinkage. When NaOH/Na_2CO_3 was used as activator, the glass replacing fly ash mortar shows the largest drying shrinkage and the lowest mass loss during the test. This proves that the glass as fly ash replacement contributes to a higher shrinkage in NaOH/Na_2CO_3 than in NaOH activated mortars. The higher dissolution rate of glass powder in NaOH/Na_2CO_3 solution than in NaOH solution corresponds to the higher reaction degree (Torres-Carrasco et al., 2014), as a consequence, the shrinkage induced by chemical reaction is higher.

The incorporation of waste glass in slag-fly ash binders shows a positive effect on the resistance to carbonation as shown in Fig. 6.8. The waste glass in binders in general

contributes to a higher carbonation resistance. To investigate the correlation between materials composition and the carbonation resistance, the Na/(Si+Al) ratio was calculated and shown in Fig. 6.7. There is a linear relationship between the Na/(Si+Al) ratio and the uncarbonated area. NaOH and NaOH/Na_2CO_3 activators were designed to contribute the same Na_2O% to binders in this study, but the incorporation of waste glass in binders also brings an additional Na source to the system. By incorporating soda-lime glass, the releasing alkali still can provide or keep a high pore solution alkalinity. This observation agrees with the study of Shi, who presented that the increasing alkali dosage and silicate modulus both result in a high carbonation resistance (Shi et al., 2018). On the other hand, a small average pore size was observed by applying the additional Si source (Ye et al., 2017), which can also provide a positive effect on the resistance to CO_2 penetration. Furthermore, in some studies, waste glass was seen as a sodium silicate based material, that can be used to produce activator in alkali activated concrete (Puertas and Torres-Carrasco, 2014; Torres-Carrasco and Puertas, 2017), and it was identified to show a similar activation mechanism as water glass (Puertas and Torres-Carrasco, 2014). It has been observed that water glass activated concrete shows a better performance of carbonation resistance compared to NaOH and Na_2CO_3 activators (Li et al., 2017). In general, the incorporation of waste glass in alkali activated slag-fly ash binders provides an enhancement of carbonation resistance. Nevertheless, a lower mechanical performance caused by the replacement part was observed in the case of the lower Ca/Si ratio in the binder composition.

6.4 Conclusions

1. Applying waste glass as a 20% replacement of fly ash in ternary alkali activated binders induces a slightly higher reaction heat flow peak and shorter induction period compared to pure slag-fly ash binders. As a consequence, a shorter setting time can be observed. A longer setting period and lower reactivity can be found when the waste glass was used to replace 20% of GGBS in binders.

2. There is no obvious difference in reaction products between waste glass containing samples and slag-fly ash samples. However, the peak shift in FTIR results indicate that the polymerization degree of C-S-H was improved after the waste glass was added.

3. Using the waste glass to replace 20% of GGBS results in the largest drying shrinkage and mass loss of samples activated by NaOH. By activation of NaOH-Na_2CO_3, applying waste glass to replace 20% of fly ash induces the largest drying shrinkage. Overall, both samples containing waste glass contribute to higher drying shrinkage.

4. The application of 20% of waste glass in binders induces an improvement of carbonation resistance, especially for samples activated by NaOH-Na_2CO_3. The resistance to carbonation can be improved by 316% on average after the incorporation of waste glass in slag-fly ash binders activated by NaOH-Na_2CO_3.

Chapter 7 The role of waste glass powder incorporation on the carbonation behaviour of sodium carbonate activated GGBS mortar

This chapter investigates the influences of recycled waste glass powder (RGP) on the carbonation behaviour of sodium carbonate activated ground granulated blast furnace slag (GGBS) mortars. The effect of activator dosages, types and RGP addition on resistance to carbonation are evaluated. The results indicate combining sodium carbonate and water glass in activator always can enhance the resistance to carbonation. Furthermore, the addition of 30% RGP in the GGBS binder system is also beneficial for resistance to carbonation. The carbonation shrinkage is reduced after RGP incorporation; at the same time, a higher strength performance is observed after cabonation. The RGP in sodium carbonate activated GGBS blends shows no influence on the species of reaction products. However, after carbonation, the sample containing RGP promotes the formation of nahcolite ($NaHCO_3$), while less bound water loss and calcium carbonates formation occurs. A high volume of gel pores (<10 nm) is formed in the RGP sample compared to specimens only containing GGBS. These properties contribute to a better resistance to carbonation for RGP containing sodium carbonate activated GGBS mortars.

This chapter is partially published elsewhere:

G. Liu, M.V.A. Florea, H.J.H. Brouwers. The role of recycled waste glass incorporation on the carbonation behaviour of sodium carbonate activated slag mortar (revision submitted).

7.1. Introduction

In Chapter 7, the incorporation of recycled waste glass in AAM that was activated by sodium carbonate resulted in a significant improvement of carbonation resistance. It is well known that the resistance to carbonation is the property of most critical concern for alkali activated concrete. Compared to OPC, due to the absence of portlandite in the alkali activated systems, C-A-S-H is more prone to carbonation as the pH buffer provided by portlandite is absent (Bakharev et al., 2001). Many studies have investigated the mechanisms of alkali activated concrete carbonation. The presented results indicated that the activator types and the chemical composition of binders can result in variable reaction products, porosity, microstructure, cracks development and strength deterioration. Consequently, the resistance to carbonation can be different (Aydın and Baradan, 2014; Bernal et al., 2014, 2013, 2011; Leemann et al., 2015; Shi et al., 2018). The sodium carbonate activated GGBS presents the lowest resistance to carbonation compared to sodium hydroxide and sodium silicate (Bilim and Duran Atiş, 2017), which is probably caused by the low alkalinity environment. For sodium hydroxide/ silicate blended activators, a high modulus of SiO_2/Na_2O was reported to present a high resistance to carbonation of alkali activated slag (Li et al., 2017; Shi et al., 2018). Similarly, the investigation of Chapter 6 indicates that a superior resistance to carbonation was achieved in the waste glass containing GGBS/ fly ash mortars activated by sodium carbonate/hydroxide (Liu et al., 2019). However, the mechanism was not fully explored in the last chapter due to the presence of many influencing factors.

Therefore, in this chapter, only GGBS and recycled waste glass are used for alkali activated composites. In addition, sodium carbonate is used as only activator with different concentrations. Thus, a clear mechanicsm of carbonation resistance can be analysed and discussed. The mechanical performance, reaction products, microstructure and shrinkage during carbonation are also measured and discussed.

7.2. Materials and methods

7.2.1 Characterization of raw materials

The recycled waste glass powder (RGP), ground granulated blast furnace slag (GGBS), and standard sand used in here are same as Chapter 4. The related characterization results have been clearly illustrated in Chapter 4.2.1.

7.2.2 Mortar mix design

The mix design of mortars is shown in Table 7.1. The RGP was used to replace slag in the binder with 0%, 10%, 20% and 30% by mass. The water to binder (GGBS+RGP) ratio was 0.5 for all mixtures. Two different dosages of sodium carbonate were used as activator with an equivalent Na_2O% of 3% and 5%, respectively. In addition, to study the influence of different initial extra silica source, a commercial water glass (modulus Ms = 3.3 and concentration was 36.08%) was used in activator by 5% by mass of binder. Then NC5-SS with an equivalent Na_2O% of 6.16%, while NC3-SS with an equivalent Na_2O% of 4.16% were designed. All activators were prepared as solutions before the mixing of mortars. The mass ratio of fine aggregates (standard sand 0-2 mm) to GGBS/RGP binder was set as 3 for all mortars mixes. In addition, paste samples were prepared according to the same procedure as for the mortars.

7.2.3 Accelerated carbonation test

Mortars after 180 days of curing were moved to a carbonation chamber (AIRTEMP) with a volume of 240 L. A controlled temperature of 25°C and atmospheric pressure were adopted. The relative humidity (RH) in the chamber was kept as 65%, and a circular flow through CO_2 gas with a concentration of 3% by volume of mixed air was applied in the chamber continuously during the test. These parameters have been widely used in previous studies for carbonation resistance evaluation (Bernal et al., 2013b). The cured paste samples were crushed into small fragments (4 mm to 8 mm) and subjected to the same period (56 days) of carbonation test as the mortars.

7.2.4 Test methods

- *Strength performance and carbonation behaviour*

The compressive strength and carbonation depth are determined according to the description in Chapter 6.2.2.

- *Characterization of reaction products before and after carbonation*

X-ray diffraction, the thermo-gravimetry (TG), Fourier transform infrared spectroscopy (FTIR), SEM and N_2 absorption tests and results are described in the Chapter 2.2.2 and Chapter 6.2.2.

- *Carbonation shrinkage*

The carbonation shrinkage tests were conducted using prisms of 40 mm × 40 mm × 160

mm. After 180 days of normal curing, the specimens were moved to the carbonation chamber. Then the length of different mortar samples was measured and recorded for 56 days.

Table 7.1 Mix design of mortars (kg/ m^3)

Sample	GGBS	RGP	Fine aggregates	Water	Sodium carbonate	Sodium silicate	Na_2O %
NC5	501.22	0.00	1503.65	250.61	42.85	0.00	5.00
NC5-G10	449.81	49.98	1499.36	249.89	42.72	0.00	5.00
NC5-G20	398.69	99.67	1495.09	249.18	42.60	0.00	5.00
NC5-G30	347.86	149.08	1490.85	248.47	42.48	0.00	5.00
NC5-SS	501.22	0.00	1503.65	250.61	42.85	25.06	6.16
NC3	501.22	0.00	1503.65	250.61	25.71	0.00	3.00
NC3-G10	449.81	49.98	1499.36	249.89	25.63	0.00	3.00
NC3-G20	398.69	99.67	1495.09	249.18	25.56	0.00	3.00
NC3-G30	347.86	149.08	1490.85	248.47	25.49	0.00	3.00
NC3-SS	501.22	0.00	1503.65	250.61	25.71	25.06	4.16

7.3. Results

7.3.1 Carbonation behaviour

- *Carbonation depth*

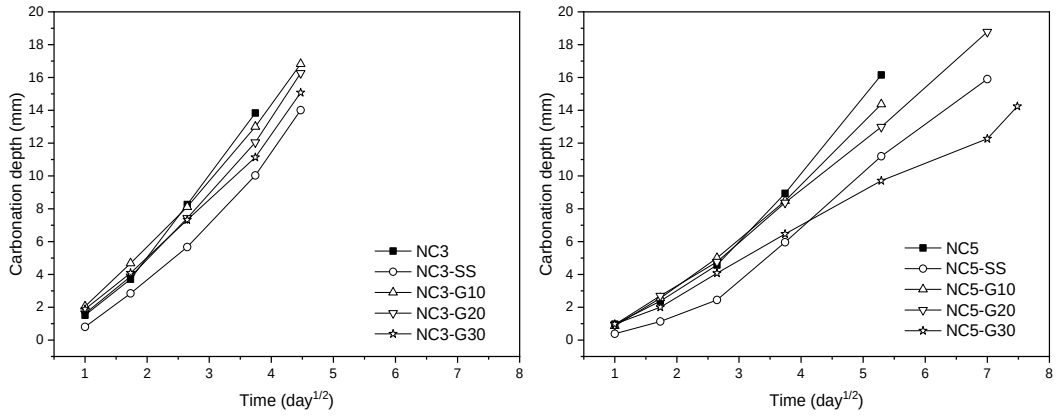

(a) (b)

Figure 7.1 Carbonation depth of different mixtures (a) NC3 series mortars and (b) NC5 series mortars (No data after spot means a full carbonation)

Fig. 7.1 presents the carbonation depth development of sodium carbonate activated mortars during the accelerated carbonation test. The maximum carbonation depth that can be achieved in prepared samples is 20 mm. The close to linear relationship between

depth and square rout of time indicates that the carbonation is a diffusion controlled process. It is clearly shown that different binder systems induced a different carbonation response of the mortars. The RGP proportion, the amount of activator, and water glass addition seem to show significant influence on the resistance to accelerated carbonation.

It can be seen from Fig. 7.1 (a) that sodium carbonate activated mortars with 3% equivalent Na_2O all achieved full carbonation before the 28 days test, which achieve a carbonation depth of 20 mm. NC3 reaches full carbonation at 20 days, however, the addition of RGP in the binder system prolongs the full carbonation duration to 28 days. Furthermore, the RGP blended mortars exhibit a gradually decreasing carbonation depth at 20 days with the increase of RGP proportion. The NC3-SS exhibits the best resistance to carbonation compared to other mortars, which shows the lowest carbonation depth at 20 days. On the other hand, as shown in Fig. 7.1 (b), a better resistance to carbonation of mortars activated by a higher dosage of sodium carbonate activator (with 5% equivalent Na_2O) is observed. NC5 and NC5-G10 exhibit a full carbonation after 49 days, while NC5-G20 and NC-SS reached full carbonation after 56 days. It is noticeable that the carbonation depth of NC5-G30 is only 14 mm after 56 days, which is equal to NC5-G10 at 28 days. It is interesting to notice that NC5-G30 presents a slower carbonation depth development at a later age (after 28 days) compared to NC5-SS. These observations indicate that at first, the high dosage of sodium carbonate activator is beneficial to the resistance of carbonation of mortars. Secondly, the additional water glass incorporation can help to reduce the carbonation depth compared to only using sodium carbonate as activator. Lastly, the incorporation of RGP in the binder system can effectively enhance the carbonation resistance of sodium carbonate activated GGBS mortars.

The above results indicate that the carbonation behaviour of sodium carbonate activated slag mortars depends on the activator type and binder compositions. The addition of water glass as activator also induces an improved performance of resistance to carbonation, which has been widely reported (Shi et al., 2018). On the other hand, the addition of RGP is expected to change the chemical composition of the binder system. A silica-rich material such as fine glass powder addition could modify the alkali activated reaction products and enhance the performance of alkali activated concrete (Coppola et al., 2019; Hajimohammadi et al., 2018). These will cause a variation in mechanical performance and reaction products, as well as resistance to carbonation.

- *Mechanical performance before and after carbonation*

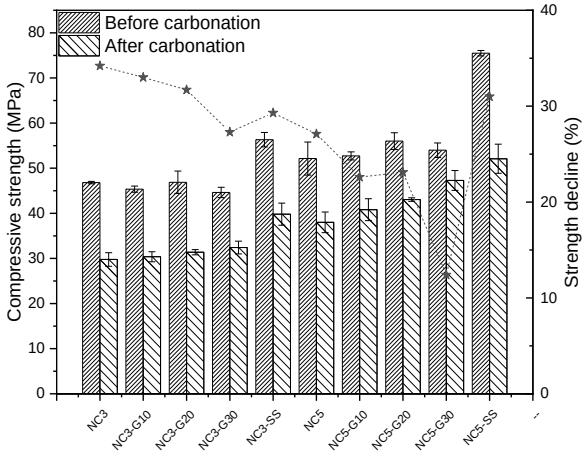

Figure 7.2 The strength performance of AAS mortars before and after 56 days of carbonation

The fact that the mechanical performance of AAS concrete can be influenced after carbonation has been reported in many studies. The decalcification of C-(A)-S-H during carbonation can result in a loss of cohesion, as a consequence, a strength reduction can be observed (Bernal et al., 2010). As it can be seen in Fig. 7.2, the RGP addition in the binder system has a slight effect on the strength performance of mortars before carbonation. The RGP blended mortars present a comparable or slightly higher strength than the reference mortar. After 56 days carbonation, all samples exhibit a variety of strength reduction. However, the NC5 series mortars still present a higher residual strength compared to mortars of the NC3 series. The increase of alkali dosage in activator usually contributes to an increase of strength performance, which is due to the high reaction degree of precursors (Bernal, 2015). Furthermore, the high alkalinity also contributes to the high resistance to carbonation because of the buffer capacity (Shi et al., 2018). These are also confirmed and consistent with the results of this study.

On the other hand, the addition of RGP until 30% shows no strength reduction for all sodium carbonate activated mortars before carbonation. This indicates that the addition of RGP has a limited influence on strength performance for normal curing of samples. After carbonation, it is interesting to see that the residual compressive strength keeps increasing with the RGP proportion in sodium carbonate activated mortars. This indicates a low carbonation degree after RGP incorporation, which agrees with the observation of carbonation depth.

- *Shrinkage behaviour during the carbonation*

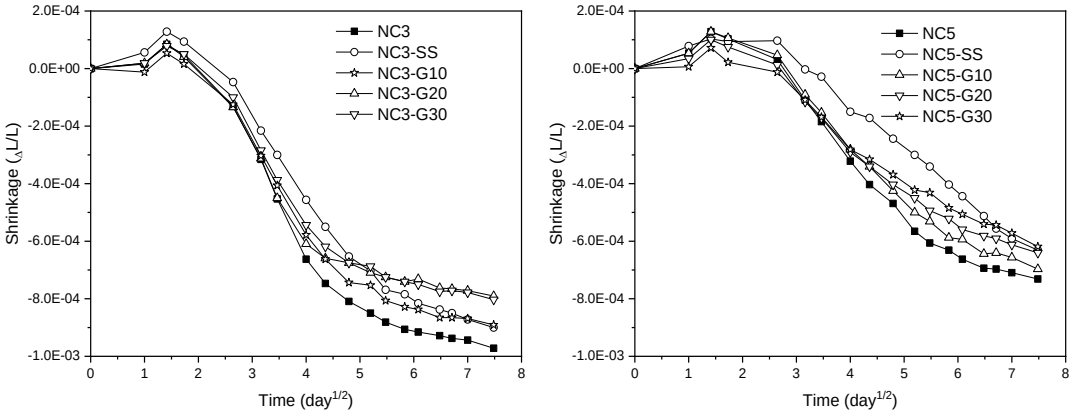

(a) (b)

Figure 7.3 Shrinkage of mortars subjected to accelerate carbonation (a) NC3 series and (b) NC5 series

In previous research, about normal OPC concrete carbonation, after the CH was consumed, the decalcification of C-S-H resulted in a lower Ca/Si ratio. As a consequence, the polymerization of Si-O-T chain can be enhanced. Therefore, an increase of shrinkage of concrete can result during the carbonation (Chen et al., 2006; Matsushita et al., 2004). In the present study, the shrinkage of different mortars during carbonation was monitored and recorded. As it can be seen in Fig. 7.3, the activator dosage and the waste glass incorporation result in different carbonation shrinkage of various specimens. For the high dosage of sodium carbonate activated samples (NC5 series), the maximum shrinkage is observed in NC5, which exhibits a total shrinkage of 7.31×10^{-4}. For low dosage sodium carbonate activated mortars, the maximum shrinkage is found in NC3, which achieves a final carbonation shrinkage of 9.72×10^{-4}. This indicates that a high activator dosage can effectively reduce the shrinkage during carbonation. In other words, the reduced deformation of tested samples also possible to result in fewer cracks or pores in high dosage activator activated samples. This also contributes to better resistance to CO_2 penetration, which also agrees with literature (Shi et al., 2018).

It is clear to see that the RGP addition reduces the shrinkage of all sodium carbonate activated GGBS mortars during the carbonation test period. NC3-G30 and NC5-G30 present a final carbonation shrinkage of 7.9×10^{-4} and 6.18×10^{-4}, respectively, which are reduced by 18.7% and 15.5% compared to the sample without glass powder incorporation. In addition, the waste glass incorporation contributes to a slow shrinkage increase rate. This observation corresponds with the results carbonation depth. The correlation indicates that the fast carbonation shrinkage development induces a fast CO_2 penetration in mortars, which is reflected in a high carbonation depth. Samples activated by sodium carbonate/sodium silicate also present a slow shrinkage increment

during the carbonation test period, which in turn correlates with the high strength performance, the high resistance to deformation. The improvement of carbonation shrinkage after RGP incorporation could be caused by the variation of carbonation products, which will be discussed in the following sections.

7.3.2 Carbonation products

- *XRD analysis*

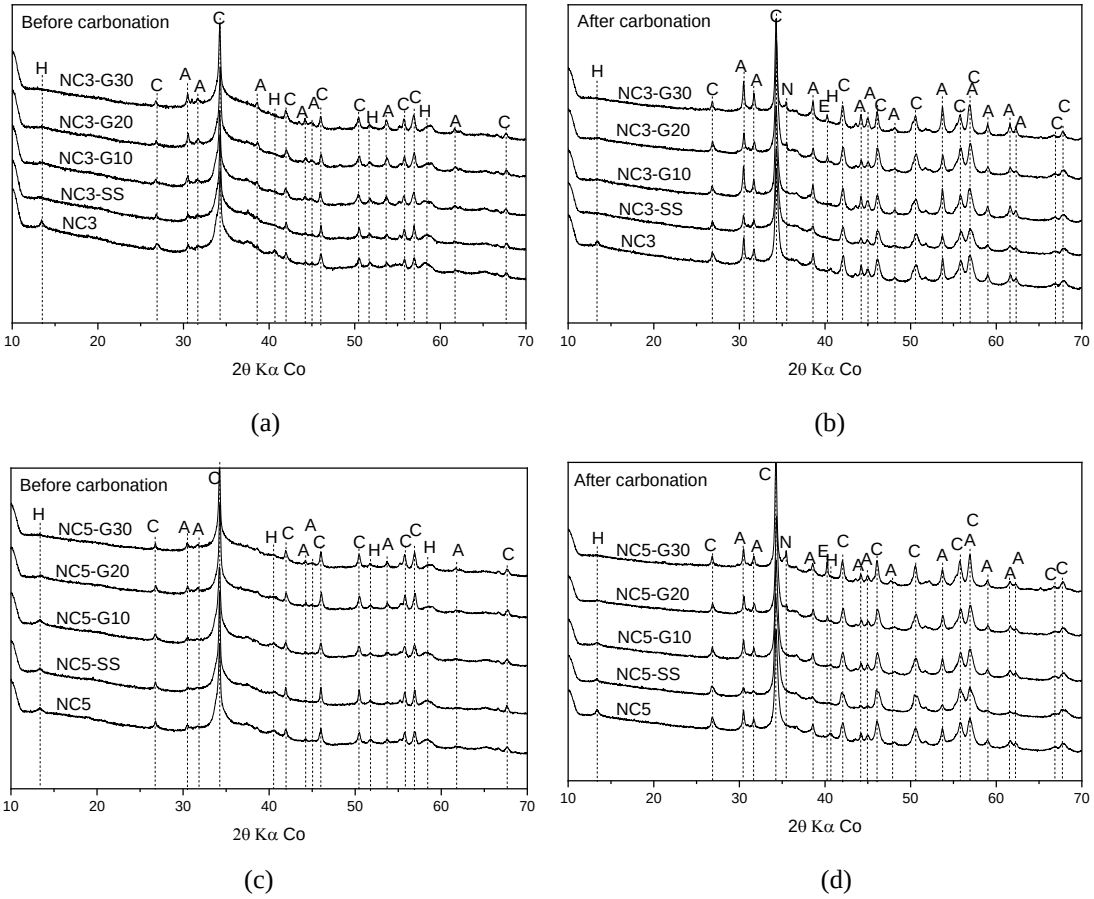

Figure 7.4 XRD patterns of (a) NC3 series samples before carbonation, (b) NC3 series samples after 56 days carbonation, (c) NC5 series samples before carbonation and (d) NC5 series samples after 56 days carbonation (H-hydrotalcite, C- calcite, A- aragonite, N-nahcolite, E- eitelite)

The XRD patterns of different mixtures before and after carbonation are shown in Fig. 7.4. Regarding the working of sodium carbonate in alkali activated slag, calcium carbonates are formed firstly, for instance, calcite and aragonite (Bernal et al., 2015; Kovtun et al., 2015; Yuan et al., 2017). After the consumption of CO_3^{2-}, more OH^- is produced which increases the pH, the slag starts reacting to form hydrotalcite and C-A-S-H. In some reports, gaylusite was also observed in only sodium carbonate or sodium carbonate-based blended activator activated slag (Yuan et al., 2017). However, in the present results, there is no peak of gaylusite, which is because of the long curing age of

samples since gaylusite is not stable and will disappear at later age (Ke et al., 2016). In general, there is no difference between reaction products for samples activated by activator with various concentrations of waste glass incorporation.

However, after 56 days carbonation, new peaks are present in some samples. For sodium carbonate and sodium carbonate/water glass activated slag, the peak of hydrotalcite still exists in carbonated samples. The presence of hydrotalcite indicates that LDH structure are stable over a large range of pH (Zhi and Guo, 2005). The carbonation of C-A-S-H keeps producing calcium carbonates, which explains the sharper and more distinct peaks of calcite and aragonite after carbonation. It is worthwhile to notice that the small addition (10%) of waste glass as binder shows a limited influence on the carbonation products. Nevertheless, when the waste glass proportion reaches 30%, significant peaks of nahcolite ($NaHCO_3$) and eitelite ($Na_2Mg(CO_3)_2$) are present in NC3-G30 and NC5-G30. As in previous investigations, the carbonation products of AAM, calcite, aragonite, vaterite can be formed during the decalcification of C-A-S-H. Furthermore, natron, nahcolite, trona and thermonatrite are formed from Na present in the pore solution in different carbonation conditions (Bernal et al., 2012). The formation of sodium carbonates after carbonation is mainly due to the Na in the pore solution (Eugster, 1966). This indicates that high amount of Na may exist in reaction products and pore solution after RGP addition.

- *FTIR analyses*

The FTIR results of selected samples are shown in Fig. 7.5. The peaks located around 874 cm^{-1} and 1417 cm^{-1} are due to the vibration of υ_3-CO_3^{2-} and υ_2-CO_3^{2-}, respectively (Yuan et al., 2017) . In addition, the peak around 874 cm^{-1} also accounts for the AlO_4^- groups in the unreacted slag particles (García-Lodeiro et al., 2008). The main peaks around 950-970 in mixtures before carbonation are assigned to the formation of C-A-S-H, which is a typical Si-O asymmetric stretching vibration generated by Q_2 units (García Lodeiro et al., 2009). The peak around 1640 represents the chemically bound water (H-O-H) in hydrated mixtures.

It is noticeable that NC5-SS shows the same peak at 953 cm^{-1}, which indicates that combining sodium carbonate with water glass as activator has no influences on the polymerization of Si-O for tested samples. However, a significant shift from 953 cm^{-1} to 963 cm^{-1}, and from 953 cm^{-1} to 967 cm^{-1} are observed after incorporation of RGP in binders. This reveals that the addition of waste glass in binders increases the polymerization degree of Si-O in C-A-S-H, which is also observed in the previous study (Liu et al., 2019). Furthermore, this observation is more significant in the NC5 series than in the NC3 series samples. The high dosage of sodium carbonate in activator is

beneficial to produce more OH^-, which also promotes the reaction of waste glass particles, and then more Si can participate in the formation of C-S-H chains.

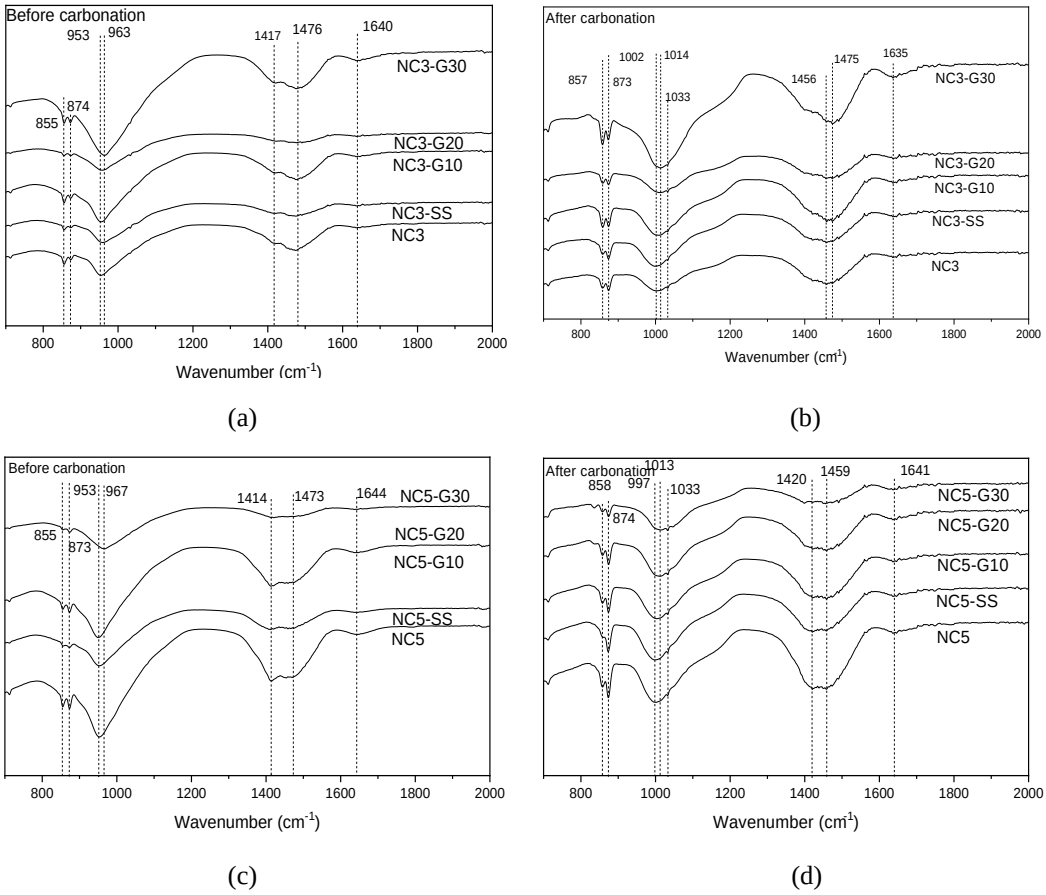

Figure 7.5 FTIR of (a) NC3 series before carbonation, (b) NC5 series before carbonation, (c) NC3 series after carbonation and (d) NC5 series after carbonation

After carbonation, the peaks of Si-O in all samples shift to the higher frequency side. The bands from 997 cm^{-1} to 1014 cm^{-1} in carbonated mixtures are related to a highly polymerized Si-O in C-A-S-H gel. This is attributed to the reduced Ca ratio in C-A-S-H and the formation of amorphous silica gel during the carbonation process. This band shifting also was found in carbonated AAM activated by other kinds of activator, e.g. NaOH and Na_2SiO_3 (Shi et al., 2018). The high polymerization of Si-O in RGP containing samples before and after carbonation indicates a relatively low Ca/Si ratio in reaction products. In some previous research, it has been pointed out that the C-S-H formed around the glass particles was rich in Si and Na (Mejdi et al., 2019).

3.2.3 DTG

In the case of the significantly higher carbonation resistance of sodium silicate activated samples and 30% RGP containing samples, thermogravimetric tests were conducted to investigate the phase transition and evolution before and after carbonation (Fig. 7.6). It

can be seen that for sodium carbonate activated GGBS/RGP blends, several typical decomposition peaks are observed. The first mass loss from 100^{o} C to 300°C is related to the dehydration of C-A-S-H (Burciaga-Díaz and Betancourt-Castillo, 2018). Afterwards, the mass loss between 300-400^{o} C is induced by the decomposition of hydrotalcite (Rey et al., 1992). Following the dehydration of hydrotalcite, a weak and broad peak around 600^{o} C is generated by the decomposition of carbonates, for example, $MgCO_3$, low crystalline calcium carbonate and amorphous calcium carbonate (Dung et al., 2019). The last small mass loss peak around 700^{o} C is due to the decomposition of calcite. These reaction products are also confirmed by XRD (Fig. 7.4).

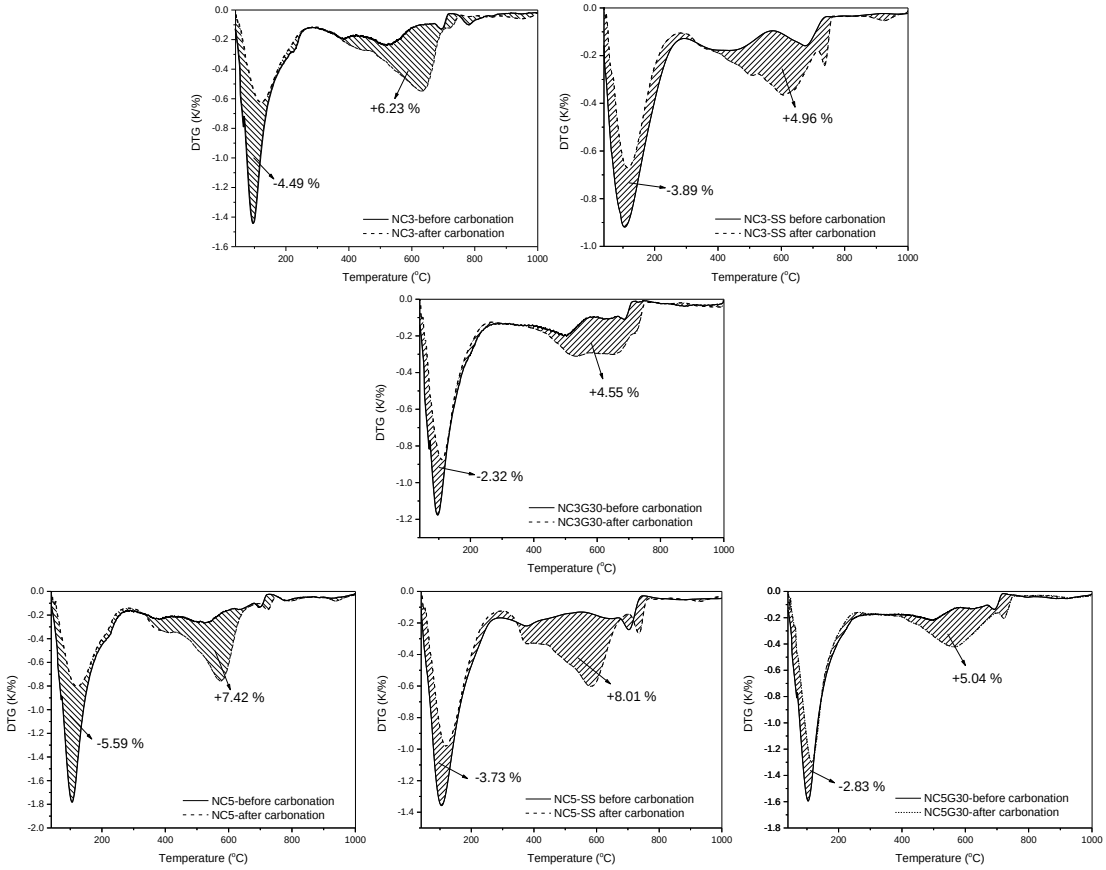

Figure 7.6 DTG of samples before and after carbonation

After carbonation, it is noticeable that the DTG curves of selected mixtures changed significantly. At first, the peaks related to C-A-S-H decomposition in carbonated mixtures all decrease. Especially for pure GGBS mortar only activated by sodium carbonate, such as NC3 and NC5. When water glass was used as activator, this improved slightly. However, the sample containing 30% waste glass exhibits the least change in this range, which indicates that the incorporation of waste glass powder results in more residual molecular water C-A-S-H gel after carbonation. This also explains the higher strength performance of waste glass containing mortar after carbonation compared to the references. Another difference after carbonation is the

formation of the large peak around 600° C. This change is induced by the new formation of calcium carbonates and magnesium carbonates from the decalcification of C-A-S-H during carbonation. These calcium carbonates are more related to the amorphous or low crystalline structure, which is hardly observed in XRD. In addition, the increase of these carbonates in 30% waste glass containing samples is limited compared to sodium carbonate/water glass activated mixtures. This indicates that the waste glass addition may inhibit the formation of calcium carbonates as well as enhancing the resistance to the influence of decalcification of C-A-S-H.

7.3.3 Microstructure

- *SEM*

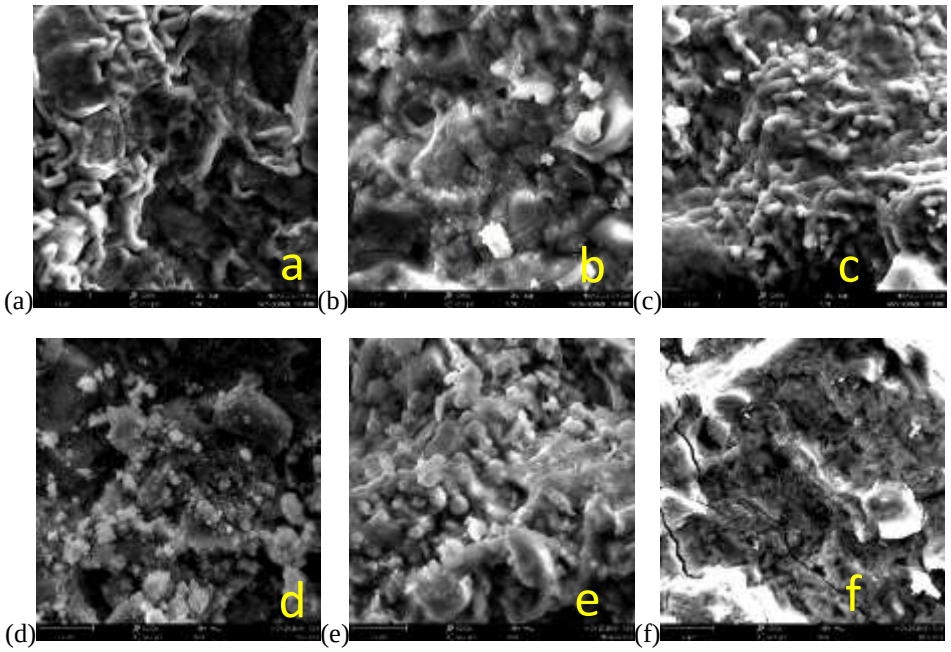

Figure 7.7 SEM images (×5000) of samples before carbonation (a) GGBS (b) GGBS+30%RGP (c) GGBS+water glass and after carbonation (d) GGBS (e) GGBS+30%RGP (f) GGBS+water glass

The microstructure images of selected samples before and after carbonation are shown in Fig. 7.7. It can be seen that the sodium carbonate activated GGBS sample shows a compacted microstructure, as well as the sodium carbonated/silicate activated sample. The morphology of reaction products of them are similar, and this kind of microstructure also was observed in a related study (Ishwarya et al., 2019). After RGP incorporation, the morphology of reaction products exhibits a difference from plain GGBS samples. This may be induced by the increasing Na and Si in the reaction products as discussed in above sections. The carbonation process results in a significantly porous microstructure and cracks in the sodium carbonate activated GGBS samples, and the sample activated by sodium carbonate/silicate activator. This porous

structure could be caused by the decalcification of reaction products. However, for the RGP blended sample, the morphology of reaction products after carbonation is similar to before. This observation confirms the better volume stability of reaction products in RGP blends during carbonation, and in agreement with the high resistance to carbonation.

- *N_2 absorption test*

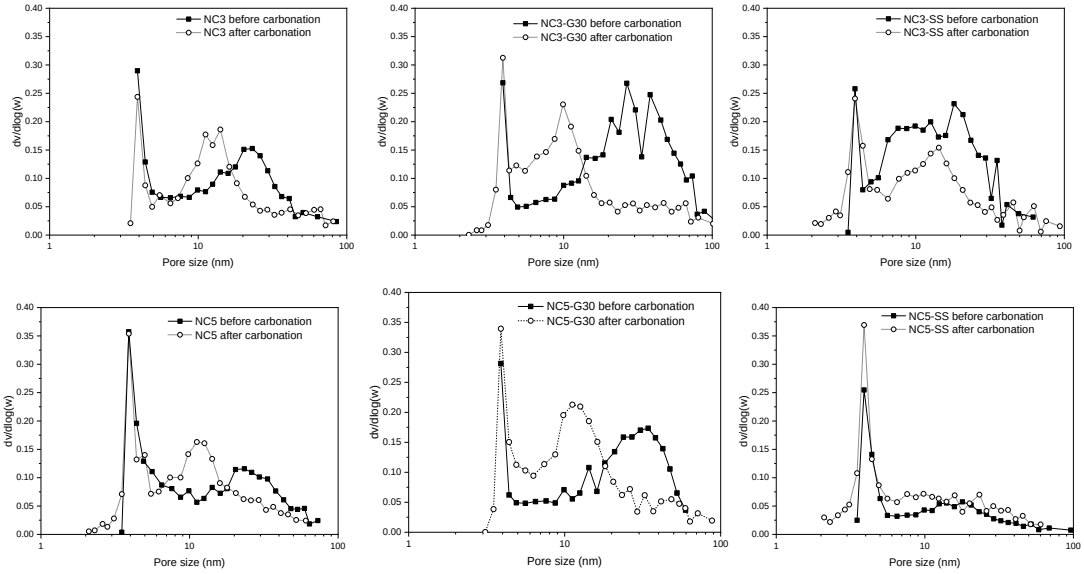

Figure 7.8 Gel pore size distribution by calculation of BJH

The gel pore structures of selected mixtures tested by N_2 absorption are presented in Fig. 7.8. The microstructure of alkali activated materials can be modified during the accelerated carbonation due to the C-A-S-H decalcification and formation of carbonation products. It is clear to see that all selected mixtures exhibit a variation of gel pore volume refinement after carbonation. As illustrated in the previous discussion, the new phases formed in carbonated samples are related to calcium carbonates, for example, calcite and aragonite. These carbonation products could fill the pores and reduce the volume of larger pores in gel, or even block the pore for CO_2 transportation. A linear relationship can be observed between carbonation depth and the square root of carbonation duration (Li et al., 2019; Liu et al., 2019). For samples containing RGP, the peak around 20 nm significantly shifts to 10 nm, which is similar to samples which only contains GGBS. As a consequence, the pore volume less than 10 nm is enhanced obviously after carbonation for RGP blends. This indicates a strong pore modification effect in RGP blends after carbonation compared to sample only containing GGBS, which is due to the formation of nahcolite.

7.4. The role of RGP during carbonation

The presented results of this investigation provide the basis for understanding the role of waste glass on improving the carbonation behaviour of sodium carbonate activated GGBS mortars. The application of RGP results in a comparable strength performance as samples containing GGBS only. The mechanical performance of alkali activated materials before and after carbonation shows a strong correlation to the total pore volume (Gao et al., 2016; Shi et al., 2018). The comparable strength performance indicates that the RGP addition induces no significant increase or decrease of total pore volume before carbonation. In other words, the improvement of resistance to carbonation can be induced only by the variation of reaction products and modification of pore distribution after carbonation. From the XRD results, it can be known that the incorporation of RGP does not change the reaction products species before carbonation. However, it has been reported that the reaction of RGP in an alkaline environments can result in Na-rich C-S-H chains (Mejdi et al., 2019). The FTIR indicates that RGP addition enhances the polymerization of Si-O-T by providing more Si to the C-(N)-A-S-H, while reducing the Ca/Si ratio (Zhang et al., 2017). Therefore, the RGP in sodium carbonate activated GGBS system could promote the formation of Na rich and low Ca/Si C-(N)-A-S-H. On the other hand, the high Na concentration also contributes to a higher alkalinity buffer of the pore solution during carbonation (Nedeljković et al., 2019). At the same time, the carbonation products in RGP blends seem to show more bound water and a lower amount of calcium carbonates from DTG results. This also confirms a higher resistance to carbonation of C-(N)-A-S-H in RGP samples. Furthermore, the nahcolite in carbonated RGP blends has a lower density (2.21g/cm^3) than calcite and aragonite (2.71g/cm^3). Consequently, C-(N)-A-S-H in RGP blends after carbonation exhibits better volume stability than samples only containing GGBS. This is also proved by the decrease of carbonation shrinkage and DTG. On the other hand, a stronger pore refinement occurs promoting the formation of smaller size pores (<10 nm) in RGP blends than in only GGBS sample. At a given RH, the water condensation effect occurs more easily in such a small pore or tunnel sizes. Water easily blocks these small pores, which can further inhibit CO_2 transportation (Nedeljković et al., 2019; Shi et al., 2018). Therefore, less deterioration of microstructure is observed after RGP incorporation in sodium carbonate activated GGBS mortars after carbonation, as well as a higher residual strength.

7.5 Conclusions

1. The resistance to accelerated carbonation of sodium carbonate activated GGBS

mortars is significantly improved by the incorporation of RGP, which is even better than GGBS samples activated by sodium silicate/ sodium carbonate. For sample activated by low concentration of sodium carbonate (3% equivalent Na_2O), the time to full carbonation is extended after incorporation of 30% RGP from 20 days to 28 days. For sample with high concentration of sodium carbonate (5% equivalent Na_2O), the time to full carbonation is extended after incorporation of 30% RGP from 28 days to more than 56 days.

2. The incorporation of up to 30% RGP in alkali activated GGBS mortars causes no obvious strength reduction before the carbonation test. After 56 days of carbonation, all samples reduced in strength. However, waste glass powder containing mortars exhibit a higher residual strength than references.

3. The incorporation of RGP as part of binders significantly reduces the shrinkage compared to reference samples during the carbonation test, which may reduce the potential cracks for CO_2 penetration.

4. After carbonation, the nahcolite formation is only identified in samples containing more than 20% RGP, which may induce more clogging of pore connections compared to calcium carbonate.

5. The DTG results indicate that 30% of RGP incorporation reduces the bound water loss of C-A-S-H gel after carbonation. At the same time, less mass carbonation products are observed after carbonation. This indicates that the intensity of carbonation on gel transformation was mitigated after RGP incorporation.

6. After carbonation, a higher volume of pores smaller than 10 nm is observed in RGP blended samples. These small pores may remain saturated during carbonation, which can effectively prevent CO_2 transportation.

Chapter 8 Sodium silicate precursors from recycled waste glass for one-part aluminosilicate mortars

This chapter investigates the use of recycled waste glass, alkali-thermal treated to prepare one-part aluminosilicate mortars. The recycled waste glass powder (RGP) is treated with NaOH and water at a temperature of 80 °C for 24 hours and then dried at 105 °C for producing a solid activator. Then the treated RGPs are used to prepare ground granulated blast furnace slag-based one-part alkali activated mortars. The treated RGPs and the one part binders are characterized by XRD, FTIR and SEM. Furthermore, a quantitative analysis of the reaction products of RGP after alkali-thermal treatments is conducted by using Rietveld analysis and the PONKCS method. The hydration kinetics and mechanical performance of one-part aluminosilicate mortars are evaluated by calorimetry and compressive strength test. The results indicate that the alkali-thermal treatment of RGPs results in the formation of 2.2% to 45.8% Na_2SiO_3 based on the initial effective modulus (EMs) of SiO_2/Na_2O ranging from 3.0 to 1.0. A low EMs promotes the formation of Na_2SiO_3, with a higher reaction degree of the RGP. The treated RGPs can be used as both solid activator and precursor for one-part slag mortars. Compressive strengths of 55.8 MPa and 54.9 MPa are observed for samples containing RGPs treated with EMs of 1.0 and 1.5, which is comparable to the performance of mortar prepared using CEM I 52.5 R.

This part is partially published elsewhere:

G. Liu, Y.X. Chen, K. Schollbach, M. V. A. Florea, H. J. H. Brouwers. Low temperature synthesis of solid activator from recycled waste glass for one part alkali activated mortars (submitted).

8.1 Introduction

In Chapter 6 and Chapter 7, the application of recycled waste glass as binder in conventional two-part alkali activated materials has been discussed, and it is shown that the recycled waste glass can effectively modify the properties by introducing the additional sodium and silicate to the reaction products. However, the use of highly alkaline activator solutions poses an increased safety risk on construction sites (Kovtun et al., 2015). Therefore, the concept of 'one-part' alkali-activated mortar was proposed to reduce the potential hazards, which means 'just add water' like for an ordinary Portland cement (Duxson and Provis, 2008; Luukkonen et al., 2018; Sturm et al., 2016; Sturm, 2018). Generally, the dry mixtures of one-part binders consist of solid alkali-activator and aluminosilicate precursors, as well as some clay minerals after calcination (Abdel-Gawwad et al., 2019, 2018; Peng et al., 2017). Sodium silicate powder is the most widely used ingredient in the production of one-part alkali-activated concrete (Nematollahi et al., 2015). However, the production of the commercial sodium silicate is energy intensive, because it includes a calcination process at 1300~1600 ℃ where a mixture of quartz and sodium carbonate is heated (Lazaro et al., 2013). Ma et al. investigated the influence of different types of commercial sodium silicate on the performance of one-part geopolymer (Ma et al., 2018). For this reason some investigations were conducted to replace sodium silicate powder with pre-treated solid wastes. Ke et al. investigated thermally treated red mud/NaOH at 800 ℃ for preparation of one-part geopolymer, and a compressive strength of 10 MPa was observed after 7 days curing (Ke et al., 2015). Adesanya et al. reported that alkali-treated paper sludge (95 °C for 48 hours) can effectively function as a solid activator in slag based one-part geopolymer. The maximum strength achieved was 42 MPa (Adesanya et al., 2018). Besides that, by-products rich in silica, such as silica fume and rice husk ash were also used to synthesize one-part alkali-activated concrete to achieve a better mechanical performance (Hajimohammadi and van Deventer, 2017; P. Sturm et al., 2016).

In previous studies, recycled waste glass was treated to prepare a liquid activator by dissolving it in alkaline solutions. Samples activated with material prepared like this exhibited better mechanical performance than those prepared with NaOH only (Puertas and Torres-Carrasco, 2014a). The reaction products of NaOH activated waste glass were mainly sodium silicate gel (Torres-Carrasco and Puertas, 2015). In the alkali environment, the dissolution of RGP can reach a high degree at 80 °C, indicating that recycled waste glass powder after the alkali-treatment has the potential to be an effective silicate precursor to act as activators like solid sodium silicate in one-part

alkali-activated slag concrete. However, the existing studies focused on the liquid activator preparation from RGP, only few studies have reported the application of treated RGP in one-part alkali-activated concrete by using a high temperature fusion pretreatment (Vinai and Soutsos, 2019).

Therefore, in this chapter, recycled waste glass is used as a raw material to produces solid activator for one-part alkali activated building materials. An alkali-thermal treatment of recycled waste glass powder (RGP) at low temperatures (80 °C) is conducted. The effects of the EMs (effective modulus SiO_2/Na_2O ratio) on the reaction products of treated RGPs are investigated by XRD Rietveld analysis combined with the PONKCS method, FTIR, and SEM. Afterwards, the evaluation of treated RGPs in one-part slag mortars is conducted by using calorimetry, thermogravimetry, XRD and compressive strength testing. The results of this research contribute to the novel application of recycled waste glass as a solid activator in one-part alkali-activated concrete.

8.2 Experiments and methodology

8.2.1 Raw materials

The characteristics of recycled waste glass (RGP) and ground granulated blast furnace slag (GGBS) have been illustrated in Chapter 4.2.1.

8.2.2 Methods

- *Pre-treatment of recycled waste glass*

Table 8.1 Mixture design of alkali-thermal treatment

Sample	RGP (g)	NaOH (g)	Water (g)	EMs (SiO_2/Na_2O)	Thermal condition
T1	20	18	10	1.0	80 °C, 24 h
T2	20	12	10	1.5	80 °C, 24 h
T3	20	9	10	2.0	80 °C, 24 h
T4	20	6	10	3.0	80 °C, 24 h

The recipe for alkali-thermal treatment of the as-prepared RGP is shown in Table 8.1. The mass of NaOH was calculated to achieve the different EMs (effective modulus of SiO_2/Na_2O).The Na_2O in waste glass was not taken into account. Firstly, the NaOH pellets and RGP (d_{50} = 10 μm) were weighed and mixed in a plastic bottle. Then the distilled water was added to the mixtures and vibrated until it was homogeneous. Afterwards, the bottle was sealed and placed in a oven for 24 hours at 80 °C for the full reaction of RGP and NaOH. Afterwards, the mixture was removed from the bottle and

dried at 105 °C to remove physical bound water. Finally, the dried mixtures were milled into powder as the solid activator for one-part alkali-activated mortars.

- *Mix design of one-part alkali-activated mortars*

The mixture composition of the one-part mortars is shown in Table 8.2. The treated RGPs were mixed with GGBS for a homogenous one part dry binder. Then the mortars preparation is the same as the normal cement mortars. The water to binder ratio was 0.5 and the sand to binder ratio was 3, which is the same as standard cement mortar. Additionally, an ordinary Portland cement (CEM I 52.5 R) mortar was prepared as reference. The mixing of the mortars was carried out by using a 5-litre mixer. At first, the dry binder and fine aggregates (standard sand) were mixed for 30 s at low speed. Then, water was added and mixed at medium speed for 120 s. Lastly, the fresh mortar was filled into a plastic mold (40 × 40 × 160 mm) and covered with plastic film until demolding (24 hours). Then mortars were covered with plastic film for storage at ambient conditions (25^{o} C) until test.

Table 8.2 Mix design for one-part alkali-activated mortar

Sample	Treated RGP (g)	GGBS (g)	Water (g)	Sand (g)
OPT-1	80 (T1)	320	200	1200
OPT-2	80 (T2)	320	200	1200
OPT-3	80 (T3)	320	200	1200
OPT-4	80 (T4)	320	200	1200

- *Quantification of mineral phases in treated recycled waste glass powder*

Silicon was used as an internal standard (10% by mass) to conduct the Rietveld quantification. The quantification itself was done using TOPAS V5. The PONKCS method was used to build an hkl phase for unreacted RGP, 100% Si was used to determine the normal background. The PONKCS method can be used to distinguish different materials of amorphous structure, which has been used to quantify the amorphous phases (GGBFS and MK) in previous research (Snellings et al., 2014). The methods description has been shown in Chapter 5.2.2.

- *Reaction products characterization*

The related methods of reaction products characterization have been shown in Chapter 2.2.2, and Chapter 6.2.2.

8.3 Results and discussions

8.3.1 Characterization of pre-treated recycled waste glass powder

- *The influence of alkali-thermal treatment on the mineral phases of RGP*

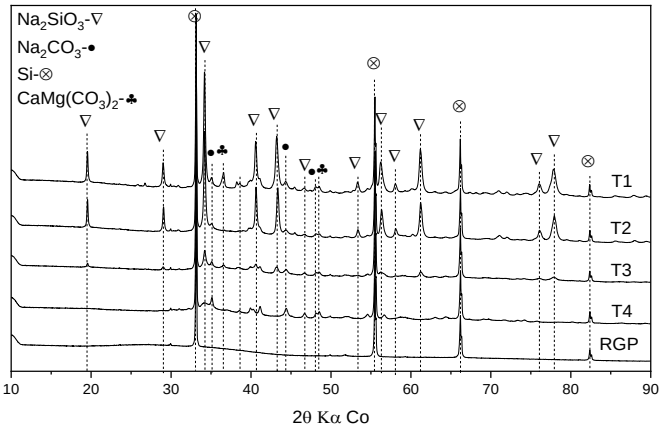

Figure 8.1 XRD patterns of treated RGPs

The XRD patterns of treated RGPs and untreated RGP are shown in Fig. 8.1. It is clear that the RGP is a completely amorphous materials, which shows no significant peak. After alkali-thermal treatments of RGP, several new peaks emerged. The presence of Na_2SiO_3 in samples indicates that the alkali-thermal treatment of RGP is successful. However, the intensity of the Na_2SiO_3 peaks gradually decreases from T1 to T4, which indicates that it is influenced by the EMs during treatment. Na_2CO_3 and $CaMg(CO_3)_2$ are also observed in all samples. It is possible that the carbonation occurred during the sample heating because of contact with the air or because of the presence of impurities in the raw materials.

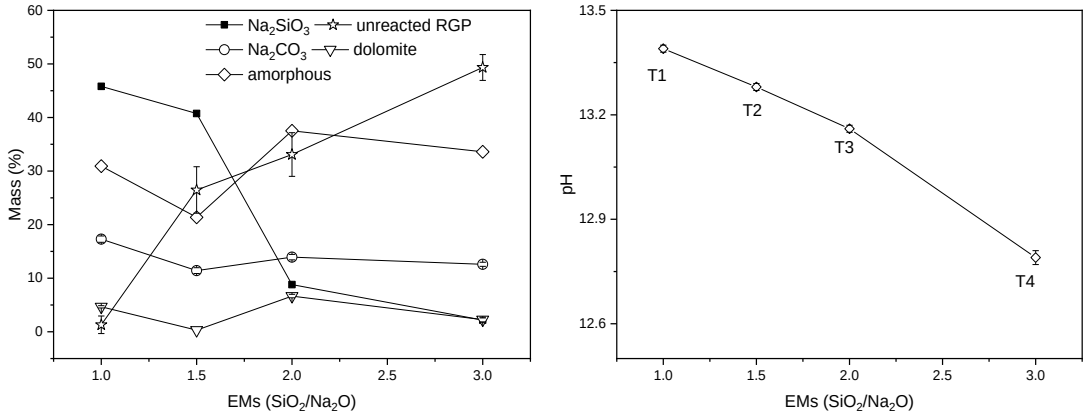

(a) (b)

Figure 8.2 The main reaction products (a) and pH (b) of alkali-thermal treated RGPs

To clearly understand the phase transformation of RGP by the four different alkali treatments, the quantification of XRD was conducted by using TOPAS V5 with Si as the internal standard. The quantifications of Na_2SiO_3, Na_2CO_3, $CaMg(CO_3)_2$, amorphous phase, and unreacted RGP are shown in Fig. 8.2. As observed the difference of EMs during alkali-thermal treatment can significantly influence the reaction of RGP and the formation of Na_2SiO_3. When the EM is 3.0, the unreacted RGP is 49.3%. However, when the EM decreases to 2.0 the unreacted RGP reduces to 33.1%. The unreacted RGP shows a further reduction to 26.5% and 1.31% when the EM decreases to 1.5 and 1.0, respectively. It indicates that the low EMs promote the dissolution and reaction of RGP due to the higher pH of the mixtures, which is also observed in a previous study (Puertas and Torres-Carrasco, 2014). The high initial alkali content also promotes the formation of Na_2SiO_3 in the reacted mixtures. As seen from Fig. 8.2, with the EMs of 3.0 and 2.0, the T4 and T3 samples contain 2.2 and 8.8% Na_2SiO_3, respectively. A significant increase from 8.8 to 40.7% of Na_2SiO_3 in the treated RGP can be found when the EMs decreases from 2.0 to 1.5. It only increases to 45.8% at the ratio of 1.0. Meanwhile, the limited increase of Na_2SiO_3 and the high Na_2CO_3 concentration present in T1 compared to T2 indicates that the alkali dosage is excessive. In addition, the amorphous content in T2 is the lowest among all samples. Therefore, the optimal dosage of NaOH to modify RGP is the T2 group. The amounts of reaction products of RGP also induce the difference in alkalinity as shown in Fig. 8.2 (b). The pH of treated RGP keeps increasing from 12.79 to 13.39 with the decreasing ratio of the EMs. The increase in pH might be controlled by the amount of sodium silicate after alkali treatment. The result indicates that the treated RGPs can not only provide a silicate source but also shows a sufficient pH to alkali-activate slag mortars (Fernández-Jiménez and Puertas, 2003; Živica, 2007).

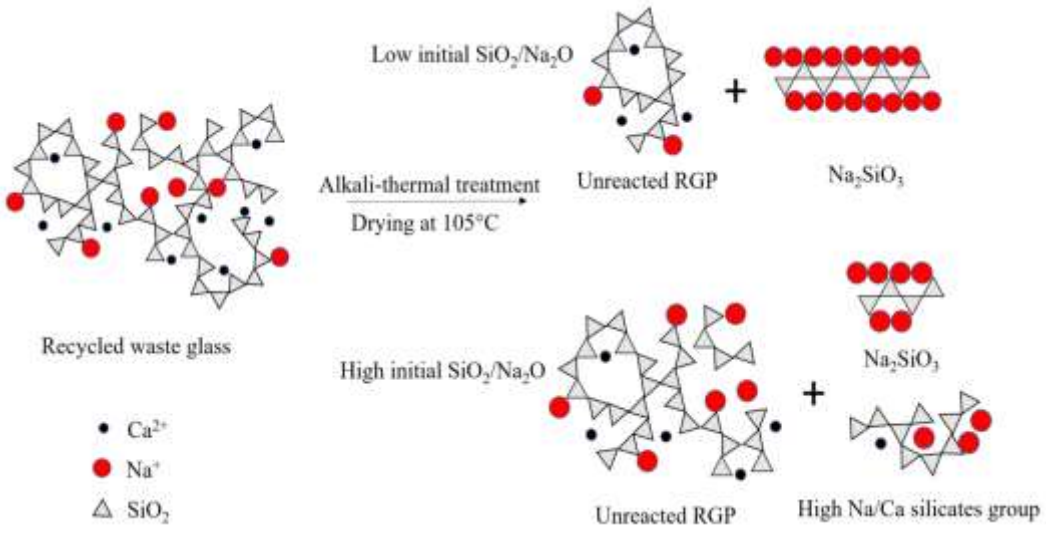

Figure 8.3 Schematic diagram of alkali-thermal treatment of RGP with various initial SiO_2/Na_2O ratios

Table 8.3 The Na_2O from NaOH and RGP in total mass of mixtures (based on Table 8.1)

Sample	EMs	Na_2O from NaOH	Na_2O in original RGP	Released Na_2O from reacted RGP
T1	1.0	14 g	2.9 g	2.9 g (98%)
T2	1.5	9.3 g	2.9 g	2.2 g (74%)
T3	2.0	7.0 g	2.9 g	2.0 g (67%)
T4	3.0	4.7 g	2.9 g	1.5 g (51%)

A schematic diagram of alkali-thermal treatment of RGP with various EMs is shown in Fig. 8.3. The silica network in the amorphous glass structure can be dissolved and destroyed in the presence of hydroxyl anions from NaOH solution at elevated temperatures during the alkali-thermal treatment. A low EMs ratio means large quantities of OH^- can break the silica network in RGP, resulting in a low amount of unreacted RGP. Besides, an adequate amount of sodium is necessary to form Na_2SiO_3 after drying. Conversely, a high EMs yields only a low Na_2SiO_3 content and more unreacted raw RGP. It is worth to notice that an amount of Na also is provided by the reacted RGP as shown in Table 8.3. The lower EMs promotes the higher reaction degree of RGP, as a consequence, Na in the original RGP is released. This Na from RGP also can effectively participate in the formation of reaction products. So, the Na in products derives not only from the initial NaOH but also from reacted RGP. At higher EMs more high Na/Ca ratio silicate species formed, recognized as amorphous phase in samples, showing a possibly low reactivity as activators. The results indicate that the treated RGPs not only can provide a silicate source but also show a sufficient alkalinity as activator in one-part alkali-activated materials (Fernández-Jiménez and Puertas, 2003; Živica, 2007).

- *The influence of alkali-thermal treatments on the silicate network of RGPs*

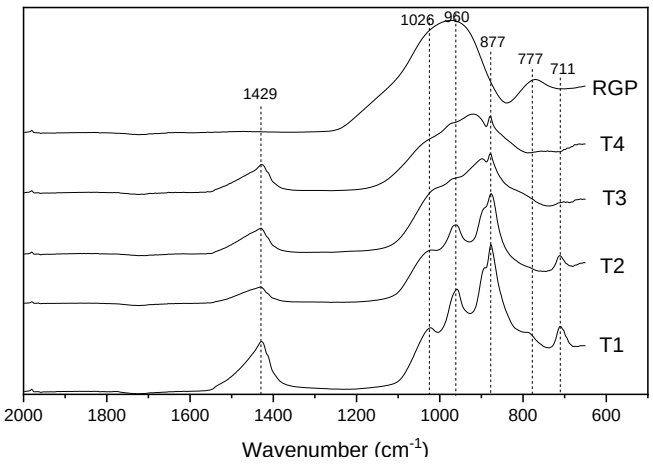

Figure 8.4 FTIR of treated RGPs

The FTIR spectra of RGPs exhibit a significant difference before and after alkali-thermal treatment. The original RGP shows a broad hump between 1000 cm^{-1} and 777 cm^{-1}. The peak at 777 cm^{-1} is attributed to the bridged Si-O-Si bending vibration, while the hump at 1000 cm^{-1} is assigned to the Si-O-Si stretching vibration (Burns et al., 1991). After alkali-thermal treatment, sharp peaks appeared at around 1429 cm^{-1}, 1028 cm^{-1}, 960 cm^{-1}, 877 cm^{-1} and 711 cm^{-1}. Moreover, the intensity of these peaks increases with the increasing EMs during alkali-thermal treatment. The newly formed peak at around 1429 cm^{-1} is related to the asymmetric stretching vibration of CO_3^{2-}, which is due to the presence of Na_2CO_3 and $CaMg(CO_3)_2$ after treatment (Torres-Carrasco et al., 2015). The peaks appearing at 1028 cm^{-1} and 960 cm^{-1} indicate the asymmetric stretching of Si-O-Si (Vafaei and Allahverdi, 2017), corresponding to the unreacted RGP phase. The peak at around 877 cm^{-1} is attributed to Si-O (non-bridging oxygen), which is mainly due to the presence of SiO_4 monomers (Q_0) (Matson et al., 1983). These results are in accordance with XRD results indicating the formation of Na_2SiO_3. Obviously, the alkali-thermal treatment of RGP contributes to the shift of the highest peak from 1000 cm^{-1} to 877 cm^{-1} of RGP. It is evidenced that the alkali-thermal treatment is efficient in rearranging the silicate network of the original RGP from a bridged Si-O-Si network to a non-bridged Si-O-T by alkali attack (Fig 8.3).

- *The influence of alkali-thermal treatments on the morphology of RGPs*

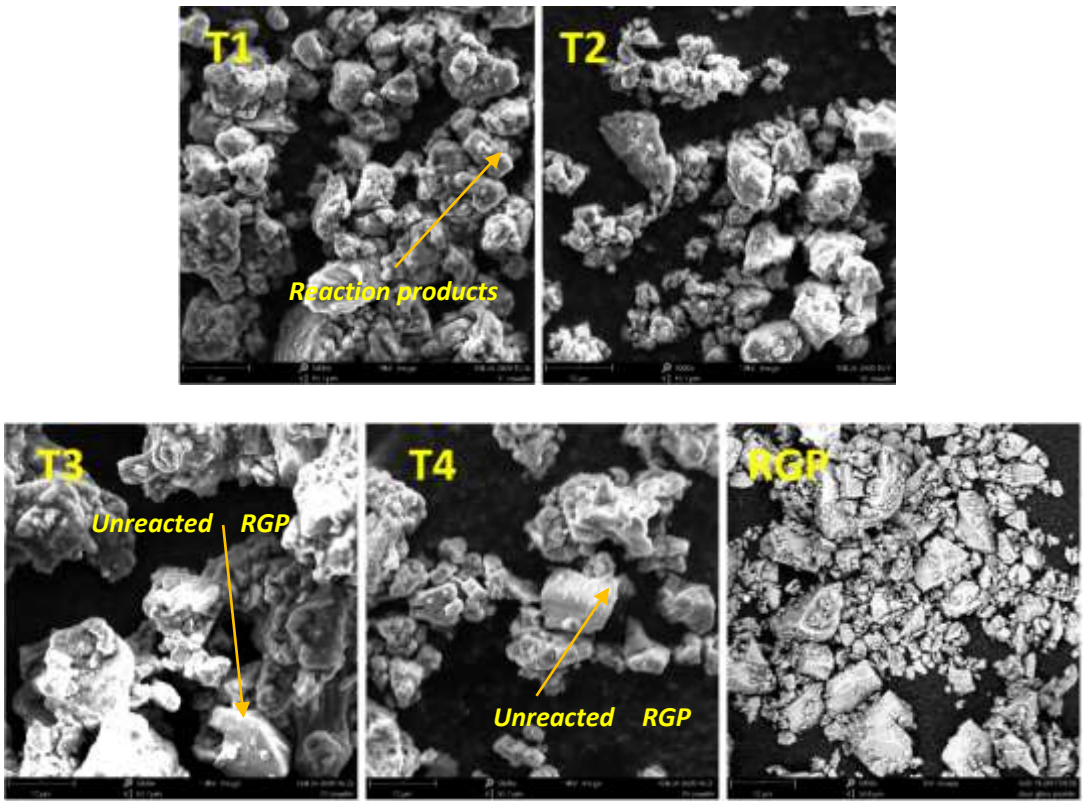

Figure 8.5 SEM images (×5000) of treated RGPs

After the different alkali-thermal treatments of RGPs, the morphology of the RGP particles was investigated by SEM as shown in Fig. 8.5. It is clearly observed that the RGP particles are covered by the reaction products, and consequently, a rough surface can be observed compared to the original RGP. However, there are still some RGP particles in T3 and T4 remaining with a smooth surface and sharp edges, which may be due to the insufficient amount of NaOH and low reaction degree with alkali. On the other hand, almost no smooth surface of unreacted RGP particles can be observed in T1 and T2, This observation is consistent with the quantification results. These rough surface are most likely corresponding to the crystalized Na_2SiO_3 and some other possible amorphous silicate that has a high in Na/Ca ratio based on the XRD results.

8.3.2 Reaction kinetics of one-part alkali-activated slag mortars

- *Calorimetry test*

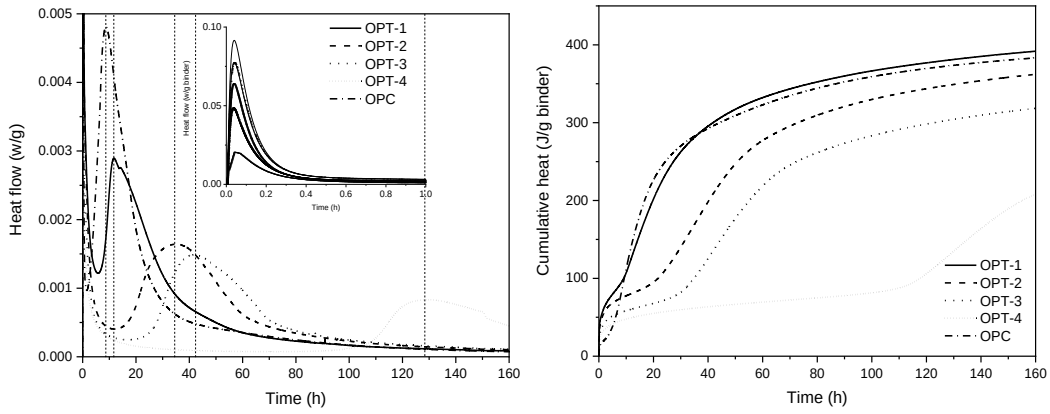

(a) (b)

Figure 8.6 (a) The normalized heat flow and (b) cumulative heat of one-part mixtures and reference OPC

The normalized heat flow and cumulative heat of one-part alkali-activated slag (AAS) paste and normal OPC paste during the first 7-days hydration are illustrated in Fig. 8.6. As observed one-part AAS mixtures exhibit similar hydration stages to OPC. The cumulative heat of OPT-1 is comparable to OPC, while the other AAS samples all present a lower released heat. Two main peaks are observed for all mixtures at the early period. For OPC, the first peak is related to the heat release due to wetting and dissolution of cement clinkers. The following exothermal peak is induced by the formation of C-S-H and AFm during the early hydration of C_3S and C_3A (Jansen et al., 2012). For one-part AAS mixtures, the first peak is caused by the dissolution of sodium silicate from the treated RGP, as well as the dissolution of slag due to the increased alkalinity. The second exothermal peak is attributed to the heat released during the formation of C-A-S-H (Brough and Atkinson, 2002).

It is clear in Fig. 8.6 (a) that the location and intensity of the main exothermal peak of one-part mixtures are different. OPT-1 exhibits the shortest time (11.8 hours) to reach the main heat flow peak, which also has the highest reaction intensity. Meanwhile, OPT-2, OPT-3 and OPT-4 reach the main hydration peak maximum after 34.8, 42.8, and 128.2 hours, respectively, with decreasing reaction intensities and cumulative heat. The different alkali-thermal treatments of RGP affect the hydration behaviour of one-part AAS mixtures. As widely acknowledged, the dosage and type of the activator influences the hydration of alkali- activated materials strongly (Živica, 2007). The higher sodium silicate/ sodium carbonate content and alkalinity of the RGPs treated with lower EMs lead to the increase of hydration rate and intensity of one-part AAS mixtures, which is in agreement with the previous studies (Luukkonen et al., 2018). Therefore, it is demonstrated that the alkali-thermal treated RGPs are effective as a solid activator in the one-part alkali-activated slag.

8.3.3 Reaction products of one-part AAS mixtures

- *XRD analysis*

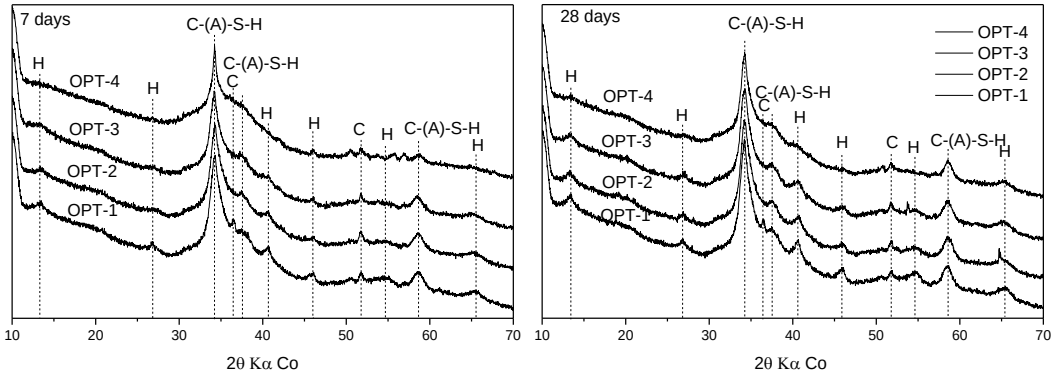

(a) (b)

Figure 8.7 XRD patterns of one-part AAS mixtures (a) after 7 days curing (b) after 28 days curing (H-hydrotalcite, C-(A)-S-H- calcium silicate hydrate, C-calcite)

The reaction products of one-part AAS mixtures after 7 days and 28 days curing are shown in Fig. 8.7. The reaction products of different mixtures are similar but with different peak intensities. Hydrotalcite is a typical reaction product in alkali activated GGBFS, which has a high MgO content. Hydrotalcite is a layered double hydroxide, and can influence the durability of alkali activated slag materials (Bernal et al., 2014). The presence of calcite is caused by the reaction of Na_2CO_3 and GGBFS in treated RGPs, while the carbonation during AAS mortars preparation is also possible (Liu et al., 2019). The broad peak at around 34° is related to the formation of C-(A)-S-H with low crystallinity (Liu et al., 2019). These reaction products are typical mineral phases

in one-part AAS concrete activated by solid sodium silicate (Luukkonen et al., 2018). This indicates that the alkali-thermal treated RGPs can produce the same reaction products, i.e. hydrotalcite and C-(A)-S-H in one-part AAS system as standard sodium silicate. It is noteworthy that the peaks of hydrotalcite and C-S-H in OPT-4 are lower compared to other mixtures. As shown in the characterization of pre-treated RGP, T4 shows the lowest alkalinity and Na_2SiO_3 content among all treated samples. Consequently, the reaction degree was lower at the same curing age.

- *FTIR analysis*

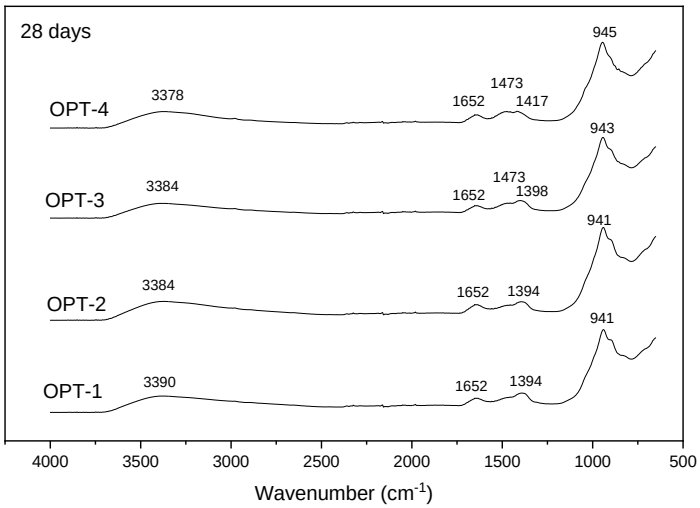

Figure 8.8 FTIR spectra of one-part AAS mixtures after 28 days

The peak from 941~945 cm^{-1} correspond to the asymmetric vibration of Si-O-T (Fernández-Jiménez and Puertas, 2003). The wavenumber of this peak for OPT-1 is 941 cm^{-1}, and gradually shifts to 945 cm^{-1} for OPT-4. The slight increase in the wavenumber indicates the higher degree of the polymerization of Si-O bonds, caused by the formation of C-(A)-S-H that is rich in silica (Liu et al., 2019). However, the extra sodium content in the T1 activator compared to the others, probably modifies the C-(A)-S-H chain, and consequently, induces the variation of Si-O chain structure (García Lodeiro et al., 2009). The bands from 1394~1417 cm^{-1} are related to the symmetric vibration of C-O, which is attributed to the calcium carbonate as shown in XRD. The hump around 1652 cm^{-1} and 3380 cm^{-1} are caused by the H-O-H bands corresponding to bending vibration and stretching vibration of physically bound water that exists in C-(A)-S-H (Tajuelo Rodriguez et al., 2017). Therefore, the higher the alkalinity of treated RGP, the more sodium silicate formed, meaning more polymerized C-(A)-S-H is obtained.

- *Thermal gravimetric analysis*

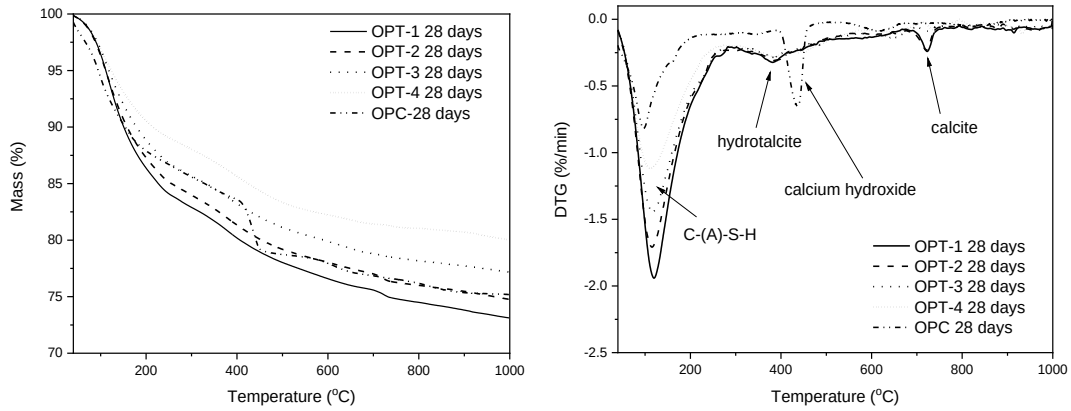

(a) (b)

Figure 8.9 TG analysis of one-part AAS mixtures after 28 days

To further understand reaction products, thermal gravimetric analysis (TGA) was conducted and compared to normal OPC and the results are shown in Fig. 8.9. The OPT-1 shows a total mass loss of 26.88%, while OPT-2, OPT-3 and OPT-4 exhibit a total mass loss of 25.23%, 22.81%, and 19.97%, respectively. Meanwhile, the OPC sample presents a total mass loss of 24.8%. This indicates that the OPT-1 and OPT-2 contained a comparable amount of physical bound water as normal OPC. In the alkali activated slag system, the bound water is mostly incorporated in the C-S-H or C-A-S-H phases (Abdel-Gawwad et al., 2019). As can be seen in Fig. 8.10 (b), where the first peak between 105-300 °C is related to the dehydration of C-(A)-S-H (Tchakouté et al., 2016), The higher the EMs for treating the RGP was, the more C-(A)-S-H seems to be contained in the sample. The following broad peak from 300~400 ℃ is induced by the decomposition of hydrotalcite in the AAS system (Haha et al., 2011). Lastly, a small peak at around 700~800 ℃ indicates the decomposition of calcium carbonate (Yuan et al., 2017), which further confirms the results shown in XRD.

8.3.4 Mechanical performance

The compressive strength of one-part AAS mortars is shown in Fig. 8.10. The standard OPC (CEM I 52.5R) mortar shows a compressive strength of 41.9 MPa at 7-days and then reaches 51.8 MPa at 28-days. OPT-1, OPT-2 and OPT-3 all present a better mechanical performance than OPC mortar at an early age (7 days), reaching 48.2 MPa, 46.3 MPa and 43.9 MPa, respectively. At 28 days only OPT-1 and OPT-2 achieve a compressive strength which is better than the OPC mortar of 55.8 MPa and 54.9 MPa, respectively, These results show that the mixtures of alkali-thermal treated RGP/ GGBS as a one part geopolymer can provide adequate strength at both early age (7 days) and late age (28 days), which is similar or even better than for OPC. The OPT-4 sample has

a lower mechanical performance compared to the other AAS mortars, which is due to the low amount of Na_2SiO_3 in T4.

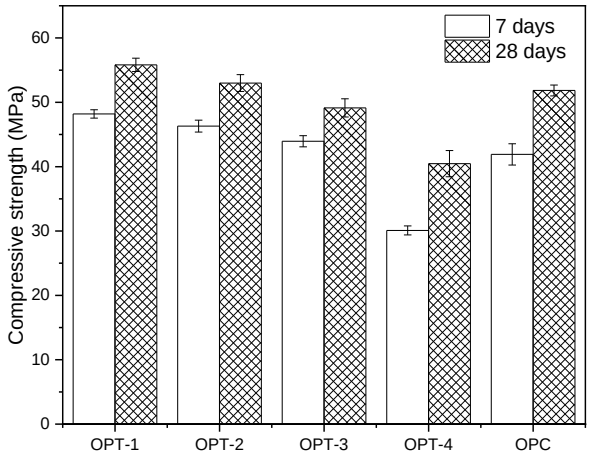

Figure 8.10 Compressive strength of one-part alkali activated slag mortars (see Table 8.2)

8.4 Conclusions

1. The alkali-thermal treatment of recycling waste glass powder (RGP) results in the dissolution of the silica network and the formation of Na_2SiO_3. The EMs strongly affects the amount of Na_2SiO_3 in RGP after treatment. 40.7% to 45.8% of Na_2SiO_3 are produced at EMs of 1.0 and 1.5, respectively, while only 2.2% to 8.3% for EMs of 2.0 and 3.0.

2. The pH of the alkali-thermal treated RGPs increased from 12.79 to 13.39 with the decrease of EMs. High amount of added NaOH during treatment leads to a higher reaction degree of RGP and more products of Na_2SiO_3.

3. The alkali-thermal treated RGPs can be used to produce one-part alkali-activated slag mortar. The treated RGPs play the role of both alkali activator and silicate precursor due to the presence of Na_2SiO_3. The calorimetry results indicate that the prepared one-part AAS binders exhibit a similar heat flow as normal OPC. However, the hydration of sample (OPT-4) containing RGP treated with EMs 3.0 (T4) exhibits a slow reaction compared to others AAS samples, which is due to the low Na_2SiO_3 content and low alkalinity.

4. The reaction products of the prepared one part samples are C-(A)-S-H, hydrotalcite, calcite and amorphous phase. More reaction products were produced by the samples containing RGPs treated at lower EMs.

5. The one-part AAS mortars of OPT-1 and OPT-2 show a compressive strength of 48.2 MPa and 46.3 MPa at 7-days, and 55.8 MPa and 54.9 MPa at 28-days, respectively, indicating equal or superior mechanical properties compared to standard mortar prepared using CEM I 52.5 R.

Chapter 9 Valorization of converter steel slag into eco-friendly ultra-high performance concrete by ambient CO_2 pre-treatment

Converter steel slag is a by-product the steel-making process, which usually can only be used as aggregates or inert filler in road construction due to the relatively low reactivity. However, its mineral composition results in a high reactivity in CO_2 rich environments. From this chapter, applications of converter steel slag in building materials by using CO_2 treatment are illustrated. It shows the modification of converter steel slag by an ambient CO_2 pre-treatment, and the application of modified converter steel slag as a supplementary cementitious material (SCM) in the design of eco-friendly ultra-high performance concrete (UHPC) using a particle packing model. The results show that converter steel slag after ambient CO_2 pre-treatment can be used in eco-friendly UHPC design, achieving a relatively higher compressive strength of over 150 MPa with a cement substitution between 15% to 45% by volume, compared to non-carbonated steel slag. The ambient CO_2 pre-treatment can modify the physical and chemical properties of converter steel slag particles, by producing rough and porous surfaces because of the precipitation of calcium carbonate and amorphous silica gel as carbonation products. Consequently, the incorporation of carbonated steel slag improves the cement hydration, enhance the formation of ettringite and C-S-H, while densifying the microstructure compared to non-carbonated slag in eco-friendly UHPCs. The leaching of potentially hazardous elements, e.g. Cr and V from carbonated steel slag can be efficiently reduced below legal limits in UHPC mixtures.

This chapter is partially published on elsewhere:

G. Liu, K. Schollbach, P. Li, H. J. H. Brouwers. Valorization of converter steel slag into eco-friendly ultra-high performance concrete by ambient CO_2 pre-treatment (submitted).

9.1 Introduction

Ultra-high performance concrete (UHPC) is a type of concrete which shows a high compressive strength (Kang et al., 2018) and an extremely dense microstructure (Verma et al., 2016). As a consequence, excellent durability can be achieved (de Larrard and Sedran, 1994). The high mechanical performance can efficiently reduce the volume and mass of the construction. However, in the UHPC design, to reach an appropriate workability, a large amount of cement (900-1300 kg/m^3) is usually used (Rossi, 2013). This results in a high cost of UHPC compared to normal concrete (Huang et al., 2017). Furthermore, because of the low water-to-binder ratio of UHPC, the hydration degree of cement is limited (Korpa et al., 2009).Thus, a large quantity of cement remains unreacted and acts as micro-filler. For the purpose of reducing costs and increasing sustainability much attention is paid to industrial by-products, for instance, ground granulated blast furnace slag (GGBFS), fly ash, silica fume and recycled waste glass to replace cement in eco-friendly UHPC mixture design (Ambily et al., 2015; Chen et al., 2018; Ghafari et al., 2016; Kim et al., 2016). The Brouwers mix design method was widely applied to optimize low carbon footprint and eco-friendly UHPC (Brouwers, 2006; Brouwers and Radix, 2005; Li et al., 2019, 2017).

Recently, some studies indicated that the carbonation of fine steel slag powder can take place at ambient conditions and, that the finer steel slag can lead to a higher carbonation reactivity (Abdul-baki, 2017; Pang et al., 2016). Furthermore, Huijgen et al. have reported CO_2 sequestration capacities of about 100–150 g CO_2/kg with ground (< 38 μm) steel slag powder (Huijgen, 2005). These results prove that fine steel slag has a potential to store large amounts of CO_2 during ambient pressure carbonation treatment. Furthermore, an ambient carbonation process also provides the possibility to utilize industrial waste gas, which usually contains around 10-20% of CO_2 (Taniguchi and Yamada, 2017). On the other hand, the other carbonation product of steel slag - amorphous silica gel has pozzolanic property and can be the reactive mineral ingredients during cement hydration. As shown in Chapter 3, SCMs addition provide higher mechanical strength in concrete with low water content. Thus, the carbonated steel slag powder has a potential to be a new kind of reactive powder as SCM in UHPC design.

In this chapter, CO_2 is sequestrated in converter steel slag powder by an ambient carbonation pre-treatment. The carbonated and non-carbonated converter steel slag powder is used as cement replacement at different volumes (0-60%) to design a low carbon-footprint eco-friendly UHPC based on a packing model. To clarify the influences of converter steel slag before and after carbonation on the performance of

blended UHPC, workability, reaction kinetics, quantification of reaction products, mechanical performance, microstructure and environmental impact are tested and evaluated. The results from this investigation contribute to improve the high-end application and recycling of converter steel slag in eco-friendly and sustainable ultra-high performance concrete manufacture.

9.2 Materials characterization and test methods

9.2.1 Materials

The cement used in this study was CEM I 52.5 R, which was produced by ENCI, The Netherlands. The raw converter steel slag (with fractions of 0-5.6 mm) was provided by Tata Steel, IJmuiden, Netherlands. Fine sand (0-0.2 mm) and standard sand (0-2 mm) were used as aggregates in UHPC design, and provided by Normensand GmbH. The superplasticizer used in this study was polycarboxylic ether based, with a concentration of 35%, provided by Sika. The chemical components of steel slag and cement were identified by using X-ray fluorescence (XRF. PANalytical Epsilon 3) spectroscopy and are shown in Table 9.1.

Table 9.1 Chemical composition of cement and converter steel slag

Chemical composition (%)	Converter steel slag (%)	CEM I 52.5 R (%)
CaO	41.55	67.97
SiO_2	11.47	16.19
Al_2O_3	2.24	3.79
Fe_2O_3	31.35	3.59
MgO	3.78	1.71
MnO	4.78	0.09
TiO_2	1.56	0.28
P_2O_5	1.30	0.42
SO_3	0.03	4.05
V_2O_5	1.14	/
Cr_2O_3	0.35	0.01
Cl	0.01	0.04
LOI	0.72	0.51

9.2.2 Preparation and characterization of SS & CSS powders

The steel slag (SS) used in UHPC design was prepared by using a disc mill (Retsch, RS 300 XL). Afterwards, the fine steel slag powder was sprayed with distilled water to reach a solid to water ratio of 0.1. Then the pre-wetted steel slag powder was moved to a climate chamber with a volume of 240 L for ambient pressure carbonation at 25 °C for 72 hours. The relative humidity in the chamber was kept at 80%, and circular flow-through CO_2 gas with a concentration of 20% was applied in the chamber continuously. After carbonation for 72 hours, no colour was observed after a 0.5% phenolphthalein

solution was sprayed on the surface of the carbonated steel slag powder. Finally, the carbonated steel slag (CSS) was dried in the oven at 105 °C for 24 hours to remove the free-water, then milled for 5 min to break the agglomeration particles.

9.2.3 Mix design of UHPC mixtures

In the present study, the reference UHPC mixture was designed based on a packing model using the Brouwers method as shown in:

$$P(D) = \frac{D^q - D_{min}^q}{D_{max}^q - D_{min}^q} \quad (9.1)$$

P(D) is the cumulative fractions of all particles less than size of D. Dmax and Dmin are referred to the maximum particle size and minimum particle size in mixture design. q is the distribution modulus.The optimal proportion of each raw material was calculated to achieve an optimum fit between target curve and composed mix according to:

$$RSS = \sum_{i=1}^{n}\left[P_{mix}\left(D_i^{i+1}\right) - P_{tar}\left(D_i^{i+1}\right)\right]^2 \rightarrow min \quad (9.2)$$

Pmix is the designed mix, while Ptar is the target grading calculated from Equation 1. The mass of each material in the designed mix are adjusted till an optimum fit between Pmix and Ptar, an optimization algorithm based on the Least Squares Method (LSM) was conducted during the calculation process. After the optimal design of the reference mixture, 15%, 30%, 45% and 60% of the cement was replaced by SS or CSS by volume. The water amount of the mixtures was adjusted to achieve a similar flow-ability of 30-33 cm for all mixes. Recipes of the UHPC mixtures are shown in Table 9.2.

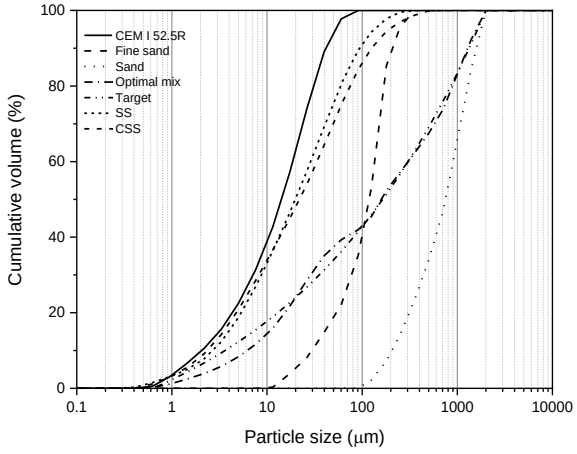

Figure 9.1 Particle size distribution of raw materials and optimal UHPC

The mixing of UHPC was conducted using a 5-liter Hobart mixer. Firstly, the dry powders and aggregates were mixed for 30 s at low speed. Then 70% of the total water

was added and mixed for another 90 s. After that, the remaining water and superplasticizer were added in the mixer for 120 s at low speed and 120 s at medium speed. Lastly, the fresh UHPC mixtures were filled into the steel moulds of 50 mm × 50 mm × 50 mm and covered with a plastic film for 24 hours. After the first 24 h, the UHPC samples were demoulded and cured in lime-saturated water until further testing.

Table 9.2 Mixtures design of UHPC (1 m^3)

Sample	Cement (kg)	SS (kg)	CSS (kg)	Sand 0-0.2 (kg)	Sand 0-2 (kg)	Water (kg)	SP (kg)
OPC	925.0	0.0	0.0	287.9	1028.3	177.2	27.8
SS15	786.3	160.8	0.0	287.9	1028.3	172.2	27.8
SS30	647.5	321.6	0.0	287.9	1028.3	167.2	27.8
SS45	508.8	482.4	0.0	287.9	1028.3	162.2	27.8
SS60	370.0	643.1	0.0	287.9	1028.3	160.9	27.8
CSS15	786.3	0.0	155.5	287.9	1028.3	177.2	27.8
CSS30	647.5	0.0	311.0	287.9	1028.3	177.2	27.8
CSS45	508.8	0.0	466.5	287.9	1028.3	177.2	27.8
CSS60	370.0	0.0	622.0	287.9	1028.3	177.2	27.8

10.2.3 Test methods for the performance of UHPC

- *Characterization of reaction products and performance of UHPC*

The reaction kinetics and products characterization methods have been shown in Chapter 2.2.2 and Chapter 4.2.2. The XRD quantification has been described in Chapter 5.

The compressive strength of UHPC cubes (with a size of 50 mm × 50 mm × 50 mm) was tested after 7 days, 28 days and 91 days curing, which was conform to the EN 12390. An average value was recorded by testing 3 cubes.

The water demand of SS and CSS were evaluated according to the relative slump flow method, which was calculated by using the mini-slump flow test (EN1015-3). Several mixes with various water to powder ratios were measured for obtaining a statistically reliable trend line (Li et al., 2018).

- *Leaching tests*

To evaluate the influence of steel slag and carbonated steel slag UHPC on the environmental impact, a one batch leaching test was performed on the UHPC samples after 28 days curing. The cube was crushed to below 4 mm and leaching test was conducted by using a dynamic shaker, at ambient temperature, and the leaching

conditions were L/S=10, 250 rpm and 24 hours. The leachates were then filtered through a 0.017-0.030 nm membrane filter. After acidifying the leachates with HNO_3, the concentration of elements in the solutions was measured with Inductively Coupled Plasma Atomic Emission Spectrometry (ICP-OES) according to the one batch leaching test protocol, NEN 6966.

9.3 Results and discussion

9.3.1 Characterization of converter steel slag after ambient carbonation

- *Mineral composition*

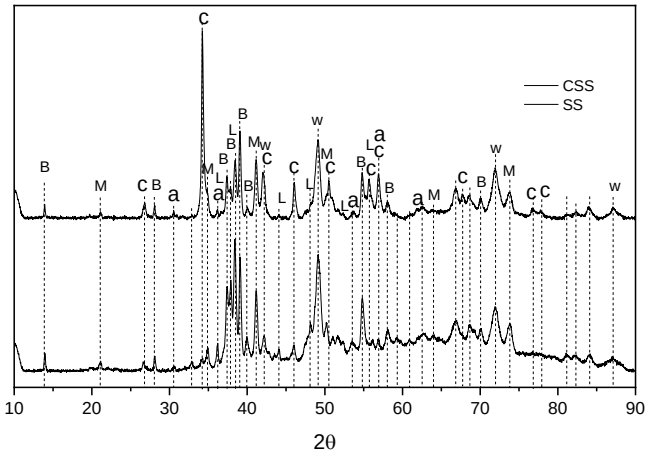

Figure 9.2 XRD patterns of converter steel slag after ambient carbonation treatment (B-brownmillerite, M-magnetite, C-calcite, a-aragonite, L-larnite, W-wustite)

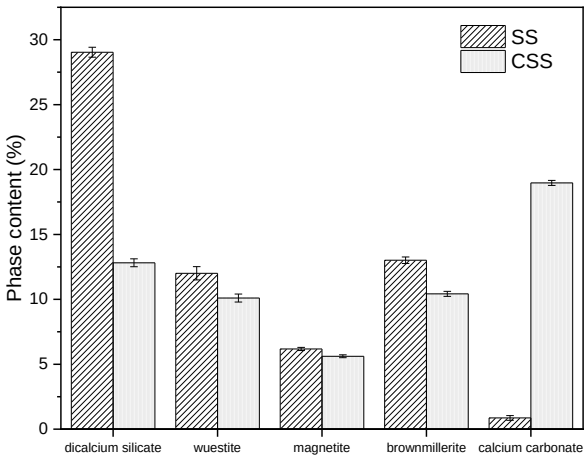

Figure 9.3 The variation of main phases in converter steel slag after ambient carbonation treatment

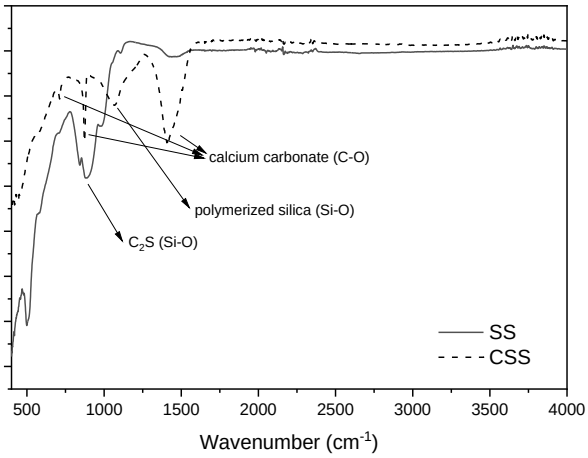

Figure 9.4 FTIR of converter steel slag before and after ambient carbonation treatment

The mineral composition of SS and CSS are shown in Fig. 9.2. The minerals in SS are larnite, magnetite, brownmillerite and wustite, which are typically observed in steel slag (Baciocchi et al., 2015). After ambient carbonation treatment, high intensity calcite peaks can be identified, while a small amount of aragonite is also present in CSS. By using the Rietveld quantification analysis for SS and CSS, the change of main phases before and after ambient carbonation are shown in Fig. 9.3.

It is clear to see a significant reduction of dicalcium silicate from 29% to 12.8% after carbonation, while brownmillerite content decreases from 13% to 10%. At the same time, the calcium carbonate (including calcite and aragonite) increases from 0.86% to 19% after treatment. The other phases such as wuestite and magnetite exhibit a relatively low reactivity at ambient carbonation conditions and remain largely unchanged. Furthermore, the amorphous content increases from 33% to 40% after ambient carbonation.

The reaction of dicalcium silicate is also confirmed in FTIR results in Fig. 9.4. The peak around 878 cm^{-1} is related to the Si-O vibration in dicalcium silicate (larnite) in SS. After carbonation, this signal exhibits a huge reduction, while the location of Si-O shifts to 1070 cm^{-1}. This is induced by the formation of polymerized silica gel after the carbonation reaction of dicalcium silicate phase, which cannot be observed from XRD because of the amorphous structure (Zajac et al., 2020). At the same time, new peaks at 712 cm^{-1}, 873 cm^{-1} and 1401 cm^{-1} occur from the presence of C-O in calcium carbonate (calcite and aragonite) (Siva et al., 2017). These indicate steel slag powder can be carbonated in the ambient temperature and pressure. The Ca-bearing minerals are the main reactive phases in converter steel slag during carbonation, while calcium carbonate and amorphous silica gel are the main reaction products.

- *Physical properties*

Table 9.3 Physical properties of materials

Material	Surface area (m^2/g)	Pore volume (cm^3/g)	Specific density (g/cm^3)	CO_2 uptake (g/kg)
CEM I 52.5R	1.004	0.0089	3.10	/
SS	1.153	0.0068	3.90	/
CSS	21.05	0.0298	3.65	107

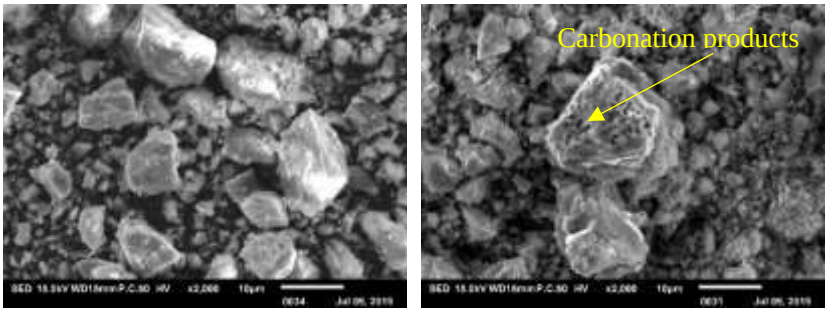

(a) (b)

Figure 9.5 SEM images of (a) SS particles, (b) CSS paticles

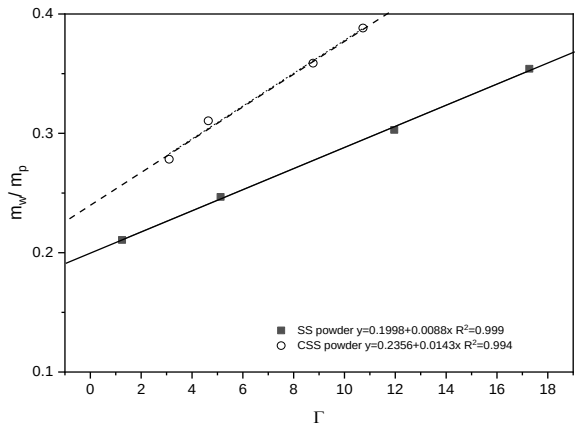

Figure 9.6 Water demand of converter steel slag powder before and after ambient carbonation

The physical properties of components, for example, morphology and water demand, effectively determine the workability and performance of designed UHPC. As can be seen in Table 9.3, the surface area and pore volume of steel slag increased dramatically after ambient carbonation treatment. This is caused by the reaction of Ca-bearing phases such as C_2S, and the presence of carbonation products. In addition, due to the lower density of calcium carbonate compared to dicalcium silicate, the carbonation treatment reduced the specific density of steel slag. Furthermore, the rough and porous surface of steel slag particles after carbonation also indicates the presence of carbonation products as shown in SEM images (Fig. 9.5). Generally, such a porous microstructure and high surface area can result in a high water demand, which can influence the performance of UHPC. To clarify this, the results of water demand of SS and CSS is shown in Fig. 9.6. Indeed, CSS exhibits a higher water demand compared

to SS, which is attributed to the high surface area and porosity. However, in a comparision with our previous research (Li et al., 2018), the water demand of CSS is still lower than cement powder even with such a high surface area. This might be due to the presence of calcium carbonate on the surface of slag particles after ambient carbonation treatment, which can lead to a inter-particle electrostatic replusion in water (Bentz et al., 2017). The results in Table 9.2 (mixdesign) also confirms a satisfactory flowability of CSS blended UHPC mixtures.

9.3.2 Early hydration of SS/CSS-UHPC

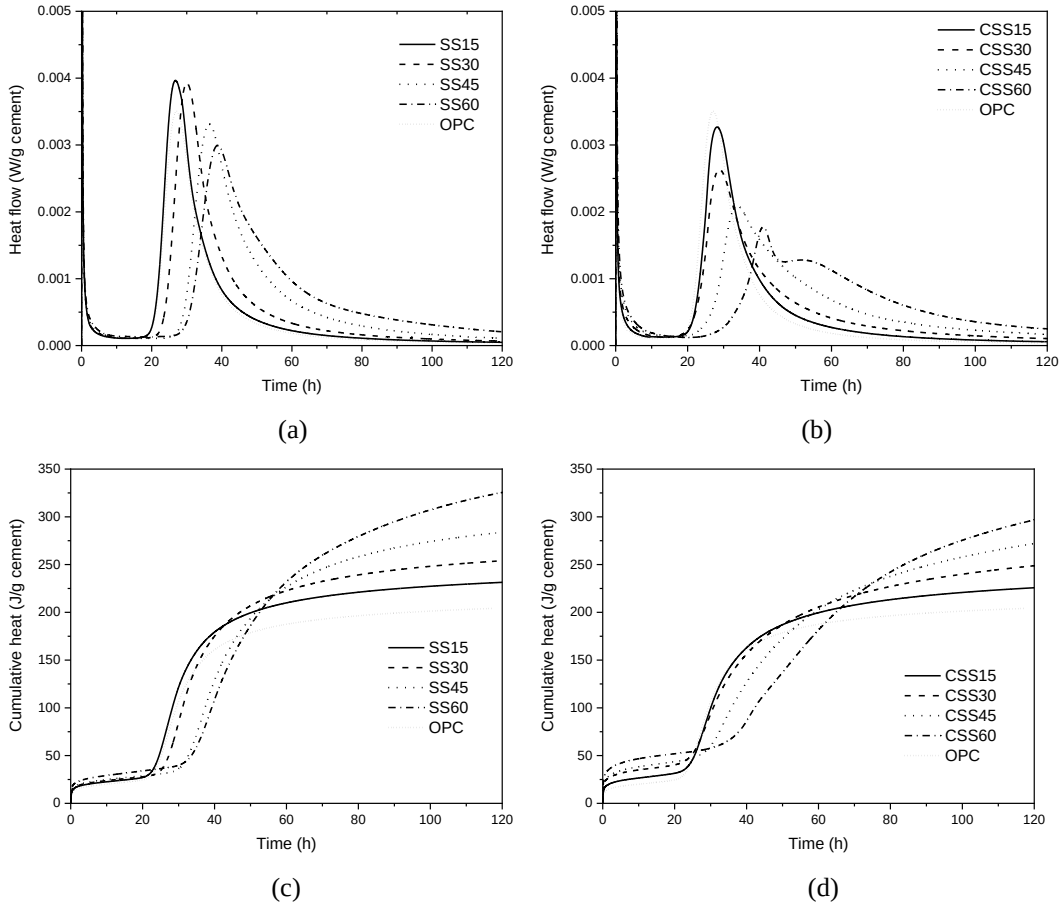

Figure 9.7 The heat flow of (a) SS blended binder and (b) CSS blended binder and the cumulative heat of (c) SS blended UHPC binders and (d) CSS blended UHPC binders

To study the influence of SS and CSS substitution on the hydration of different mixtures, the calorimeter test was conducted and the results are shown in Fig. 9.7 (a)-(d). For steel slag blended UHPC mixtures, SS15 and SS30 present a slight enhancement of the intensity of the main peaks to the OPC. Meanwhile, a reduction of the main peak intensity and a retardation effect can be observed in S45 and S60. Generally, the hydration intensity and the time of the hydration reaction will be influenced by several factors, such as the change of the effective water-to-cement ratio, superplasticizer to

cement ratio, filler effect and nucleation effect (Lawrence et al., 2003). The reduction of the main hydration peak intensity and the increase of time to reach the hydration peak in the blended UHPC mixtures were caused by the higher SP to cement ratio (Yamada et al., 2000; Zhang and Kong, 2015). However, the normalized cumulative heat of SS and CSS blended UHPCs are all higher than OPC after the test period and increase with increasing replacement level. This is induced by the dillution effect, which increases the effective water-to-cement ratio. As a consequence, cement can achieve a higher reaction degree (Shi et al., 2015).

As can be seen from the calorimeter results of blended UHPC mixtures, SS blended samples release slightly more cumulative heat than CSS blends with the same replacement ratio. This limited change can be induced by two factors. Firstly, steel slag is well known as a highly alkaline solid by-product, which is due to the leaching of Ca^{2+} (Gomes et al., 2016). As a consequence, the reaction intensity could be promoted. However, carbonation treatment significantly reduces the larnite content and therefore the Ca^{2+} leaching, as well as the pH (Chang et al., 2018). Secondly, the highly porous CSS also absorbs more water which results in a lower effective water amount for hydration, which slightly reduces the total heat compared to SS blends at early age. It is interesting to notice that the silica gel in CSS shows limited acceleration effect on cement hydration at early age, probably because the amorphous silica gel exists in the inner layer of CSS particles, which is covered by the calcium carbonate (Librandi et al., 2019). Consequently, the reaction between silica gel and cement is limited in the first days. At high volume replacement ratios (60%), CSS blended UHPC also exhibits a clear shoulder after the main hydration peak, which is not present in SS blended samples. The shoulder is possibly caused by the formation of hemicarboaluminate and the transformation of ettringite (Wang et al., 2018).

9.3.3 Performance evaluation of SS/CSS- UHPC

- *Compressive strength*

The compressive strength of UHPC incorporating various percent of SS and CSS after 7, 28 and 91 days curing is shown in Fig. 9.8. It is clearly observed that all samples present sufficient strength to be classified as UHPC after the test period except SS45, SS60 and CSS60.

At the very early age (7 days), all SS and CSS blended UHPC mixtures exhibit a poor strength performance compared to the reference. Gradual strength reduction occurs with increased replacement ratio for both SS and CSS. The lower mechanical performance of UHPC at early ages is commonly observed if cement is replaced by

other low reactivity SCMs or fillers, for example, fly ash and limestone powder (Huang et al., 2017; Zhang et al., 2019). However, Ref, SS15, SS30, CSS15 and CSS30 have reached a strength higher than 145 MPa after 28 days of curing. A further increase of strength occurs after 91 days. CSS15, CSS30 and CSS45 exhibit a strength of 162 MPa, 159 MPa, and 150 MPa, respectively, while the reference mixture reaches 156 MPa. It should be noted that CSS blended UHPCs show an obviously better strength performance than SS blended UHPCs when cement replacement ratios range from 15% to 45%. When the cement substitution achieves 60%, a significant strength reduction can be observed because of the lack of hydration products (Huang et al., 2017).

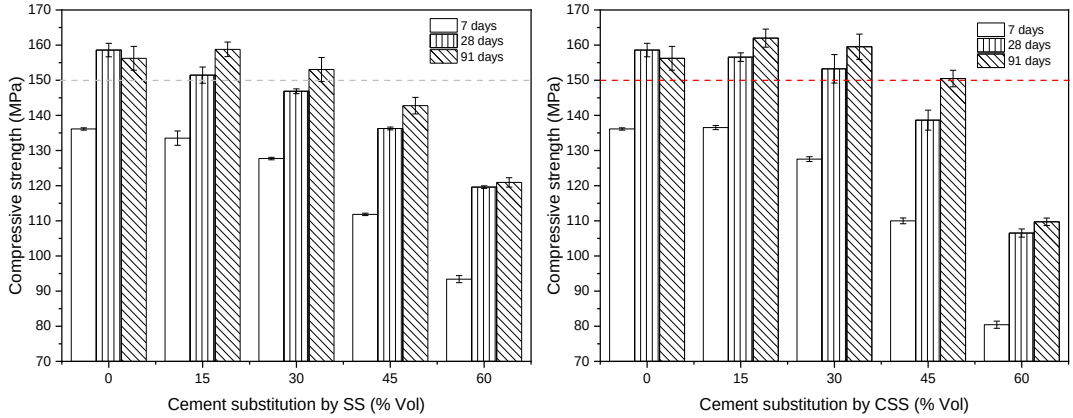

(a) (b)

Figure 9.8 Compressive strength of UHPC mixtures

The above strength results imply that ambient carbonation treatment is effective to improve the feasibility of using steel slag in UHPC. Firstly, CSS has a highly porous structure, rough surface and a subsequent high water demand compared to SS as shown in above results. Therefore, the effective pore water may be reduced, as well as the distance between particles, which causes a denser microstructure. A similar observation also can be found in concrete containing carbonated recycled concrete aggregate (Xuan et al., 2016) and UHPC containing manufactured sand (Yang et al., 2019). On the other hand, the rough surface also can provide a strengthened bonding between CSS particles and cement pastes. In addition, the water absorbed by CSS particles also can be released gradually at a later age and act as an internal curing agent, which can promote the further hydration of cement, especially in UHPC. Afterwards, a further strength development can be observed at later ages. Secondly, the precipitation of carbonation products on the surface of CSS particles also possible serves to enhance the cement reaction and modify the microstructure of blended UHPC, which will be discussed in the following sections.

- *Reaction products- Quantification of hydration products*

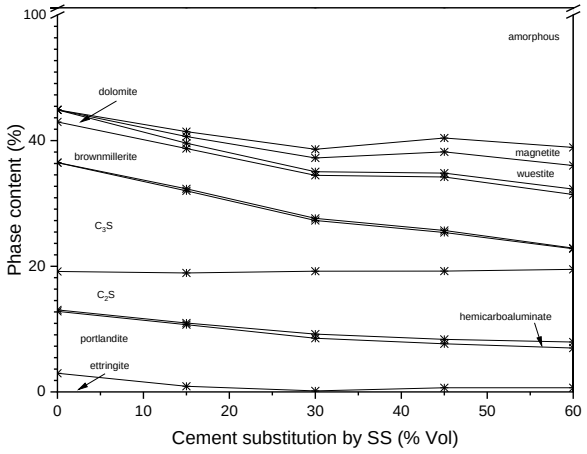

(a)

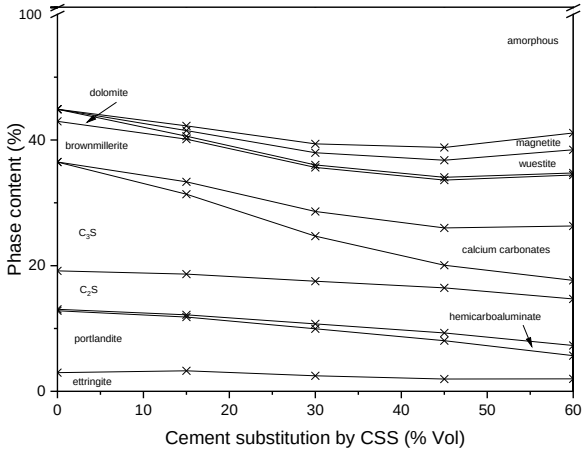

(b)

Figure 9.9 Quantification of phases by mass in mixtures (a) SS UHPC pastes and (b) CSS UHPC pastes after 28 days curing

The evolution of mineral phases with various cement substitution in the SS and CSS UHPC pastes after 28 days hydration is shown in Fig. 9.9. In the SS samples the amount of magnetite, wuestite, brownmillerite and C_2S increases with the cement substitution ratio, because uncarbonated converter slag is composed of these minerals (Fig. 9.2). The residual C_3S keeps decreasing at the same time, because the samples contain less cement, while the enhanced effective water to cement ratio also promotes the hydration of cement particles. As a consequence, more C_3S phase reacts at higher substitution levels as can be seen in Fig. 9.10 (a), where the amount of C_3S is normalized by the overall amount of cement in the sample. Due to the increase of reaction degree of C_3S, the portlandite content also increases proportionally as shown in Fig. 9.10 (b). For CSS mixtures, the magnetite, wuestite, brownmillerite and carbonate contents increase with increasing substitution levels, as these are the major phases of carbonated converter slag (Fig. 9.3). The amount of ettringite is overall higher than in the SS samples. This

can be explained by the existence of large amounts of calcium carbonate from CSS in the hydration system, which can promote the formation of ettringite (Lothenbach et al., 2008). A similar observation was also reported in the hydration system of OPC-limestone (Kakali et al., 2000). The second peak in the calorimeter measurement of CSS60 also supports this observation.

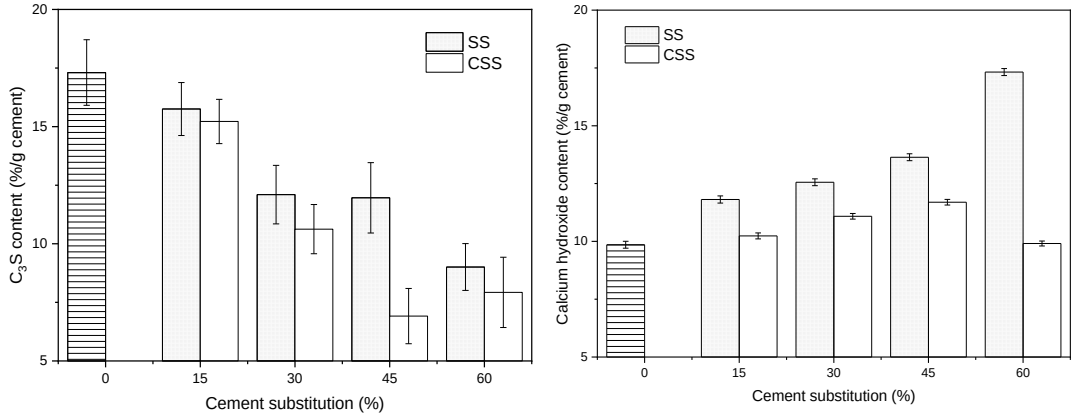

(a) (b)

Figure 9.10 Normalized content of (a) unreacted C_3S and (b) calcium hydroxide by mass of cement

It is interesting to notice that the unreacted C_3S in SS and CSS UHPC pastes all keep decreasing according to the increase of cement substitution in Fig. 9.10, which is due to the dilution effect after SS/CSS incorporation. However, the incorporation of CSS in UHPC mixtures results in a lower C_3S content compared to SS. This is likely due to the higher water content in the CSS samples compared to SS samples. The porous carbonated slag might even act as internal curing. Then the hydration of the cement part can be more advanced. In this case a greater amount of portlandite could have been expected in the CSS samples compared to SS, but this is not the case. Instead the portlandite content shows a limited increase and even a decrease at high substitution level, for example 60% in CSS samples compared to SS as shown in Fig. 9.10 (b). This indicates that portlandite in CSS samples is consumed in the system and that the consumed amount seems to increase with the substitution level. In FTIR result, a polymerized silica gel is identified in CSS, which can show a high pozzolanic reactivity (Zajac et al., 2020). Consequently, when CSS was incorporated in cement based UHPC mixtures, calcium hydroxide from cement hydration can be consumed by the presence of amorphous silica gel. Furthermore, the secondary C-S-H can be formed to fill the void, this also agrees with the results of compressive strength.

- *TG analysis*

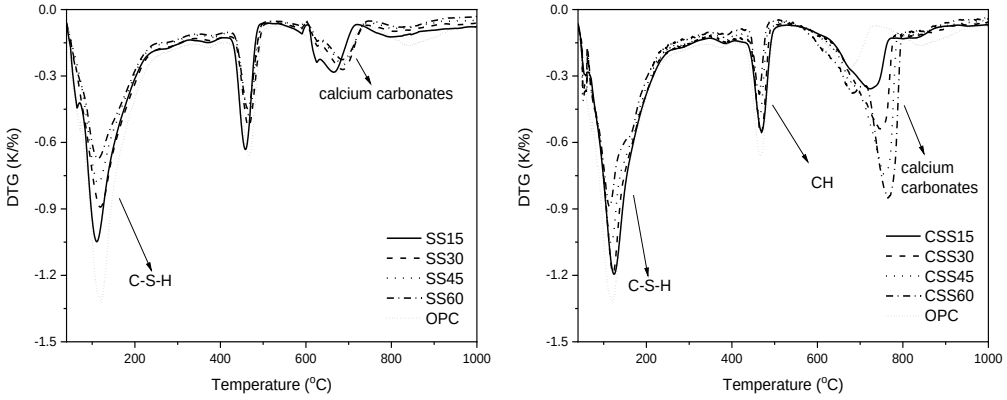

(a) (b)

Figure 9.11 TG results of UHPC mixtures (a) SS blended samples, (b) CSS blended samples after 28 days

The thermogravimetric analysis results for the different mixtures is shown in Fig. 9.11. For all UHPC pastes after 28 days curing, three significant decomposition stages can be observed. These stages are mainly related to the dehydration of C-S-H, decomposition of calcium hydroxide, and decomposition of calcium carbonate (Stepkowska et al., 2004).

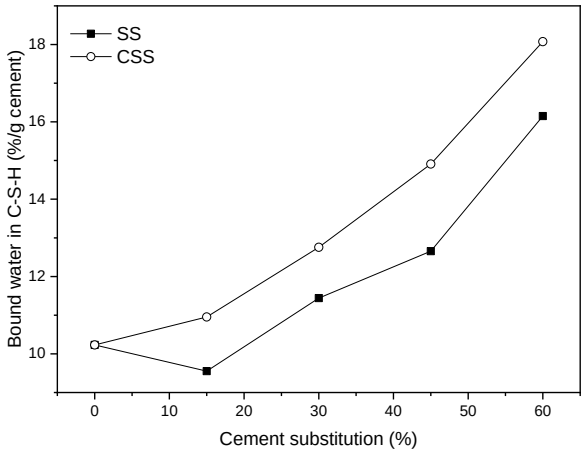

Figure 9.12 Bound water in C-S-H as determined by TG between 105°C to 400°C

To clarify the influences of SS and CSS on C-S-H formation, the amount of bound water in CSH was plotted normalized by mass of cement (Fig. 9.12). It is clear that the increase of cement substitution in the SS samples promotes cement hydration, which is reflected by the increase of bound water in C-S-H, as well as the formation of portlandite and consumption of C_3S as discussed in above. The more bound water in C-S-H gel in CSS samples compared to SS is observed. This indicates that CSS mixtures produced more C-S-H by consuming portlandite. The likely reason for this is the fact

that the carbonation of C_2S in CSS does not only produce calcite, but also amorphous silica gel (Huijgen and Comans, 2006). The amorphous silica can exhibits pozzolanic reactivity in OPC based UHPC concrete and increase the formation of secondary C-S-H, which also increases the total amount of water bound in C-S-H (Li et al., 2019; Schöler et al., 2015; Yu et al., 2014) and consumes portlandite.

- *Microstructure*

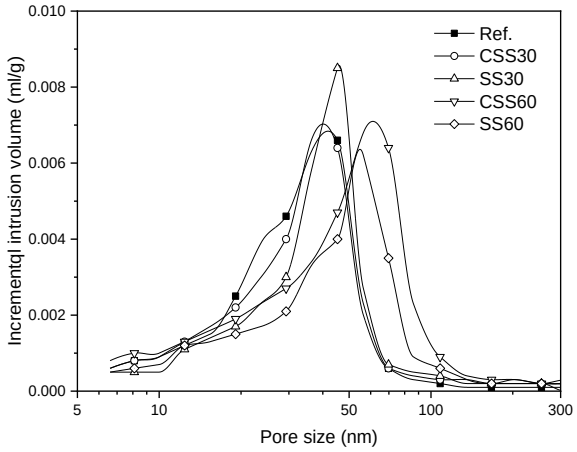

Figure 9.13 Pore size distribution of blended UHPC

Fig. 9.13 exhibits the pore size distribution of selected UHPC samples after 28 days. The pore sizes from 5 nm to 300 nm are presented for selected mixtures. The critical pore diameter (the peak on the pore size curve, defined as the pore size when reaching the highest intrusion rate) of the reference mixture without steel slag occurs at around 40 nm. When 30% steel slag is utilized to replace cement (SS30), the peak of the critical pore diameter is higher, because the dilution effect increases the effective water to cement ratio and promotes the formation of porous structures. However, UHPC incorporating 30% carbonated steel slag (CSS30) shows a very similar pore size distribution to the reference only containing cement, which indicates that the dilution effect does not have any negative effect on pore structure, because it will be compensated or overcome by the formation of secondary C-S-H from the pozzolanic reaction of amorphous silica gel (Li et al., 2019). In other words, the steel slag, especially carbonated steel slag could be successfully used to substitute cement in UHPC system. However, too much addition of either steel slag or carbonated steel slag, e.g. 60%, will significantly weaken the microstructure, by greatly shifting the critical pore diameter to larger values (around 50 - 60 nm) due to the lack of cement hydration products.

9.3.4 Leaching property of SS/CSS-UHPC

The leaching results of raw steel slags and UHPC mixtures are shown in Table 9.4. The leaching of B, Ba, Cr and V are different before and after carbonation of steel slag. B leaching increased from 0.199 mg/L to 0.417 mg/L after carbonation, while Cr and V leaching increased from below the detection limit to 0.047 mg/L and 12.11 mg/L, respectively. On the contrary, the leaching of Ba decreased from 0.236 mg/L to non-detectable. Thus, the carbonation treatment of steel slag dramatically increases Cr and V leaching. C_2S in converter slag contains V and Cr (van Hoek et al., 2016), which reacts during carbonation and decreases the pH overall, and causes higher V and Cr leaching. The newly formed carbonates seem not able to incorporate the V and Cr, either.

Table 9.4 Leaching of raw materials and UHPC samples

	B (mg/L)	Ba (mg/L)	Cr (mg/L)	V (mg/L)
Limit in SQD	N.A.	2.2	0.063	0.18
Carbonated steel slag	0.417	L.D.	0.047	12.11
Steel slag	0.199	0.236	L.D.	0.005
OPC	L.D.	0.585	0.016	L.D.
S15	L.D.	0.668	0.006	L.D.
S30	L.D.	0.549	0.004	L.D.
S45	L.D.	0.515	0.002	L.D.
S60	L.D.	0.523	0.001	L.D.
CS15	L.D.	0.532	0.008	L.D.
CS30	L.D.	0.413	0.005	L.D.
CS45	L.D.	0.419	0.004	L.D.
CS60	L.D.	0.290	0.003	L.D.

L.D. – lower than the detection limit. SQD – Soil quality decree in Netherlands (L/S=10)

For the leaching of blended UHPCs, it can be observed that when steel slag and carbonated steel slag are used as cement replacement, Ba, Cr and V leaching are significantly reduced to below the legislative limit of the Dutch SQD (Soil Quality Decree). Generally, ordinary Portland cement can be used to stabilize harmful ions in practical constructions. As reported in a previous study of cement based materials, the Cr and V can be absorbed in cement hydration products, for example AFt and AFm phases (Bonen and Sarkar, 1995). The high pH in concrete pore solution also keeps Cr and V in a less soluble state (Santos et al., 2012; van Zomeren et al., 2011). However, the concentration of Ba was increased for steel slag and carbonated steel slag blended UHPC mixtures, which is higher than that of the raw materials. This indicates that the Ba leaching is mostly contributed by the cement (Caprai et al., 2018). This observation agrees with the previous investigation that application of carbonated steel slag as aggregates in concrete (Bodor et al., 2016).

9.4 Conclusions

1. The dicalcium silicate (C_2S) and browmillerite in SS powder are observed to show reactivity during ambient carbonation. The CO_2 uptake achieves 107 g/kg steel slag. The consequent carbonation products – calcium carbonate and amorphous silica gel are identified by using XRD and FTIR, respectively. The CSS forms a rough and porous surface as presented in SEM image, which is due to the presence of calcium carbonate and silica gel as carbonation products. Therefore, CSS powder exhibits a 23.5% higher water demand than SS powder. However, CSS and SS blended UHPC samples still have a better flow ability than that of the reference OPC sample.

2. The UHPCs incorporating CSS present a higher compressive strength than SS samples when the replacement ratio is below 60%. When cement was substituted by 15% -45% CSS, compressive strengths between 150 MPa and 162 MPa can be obtained. For SS samples, only 15% - 30% steel slag can be applied, which present a compressive strength between 150 MPa and 158 MPa.

3. The XRD quantification results of reaction products indicate that CSS powder addition can improve the cement clinker hydration, compared to SS powder. At the same time, the reduction of calcium hydroxide content in CSS samples is observed, which is due to its reaction with ambient carbonation product- amorphous silica gel. The enhanced bound water in hydration products in CSS samples also confirms the formation of secondary C-S-H by the pozzolanic reaction of silica gel.

4. The pore size distribution indicates that CSS contributes to a denser microstructure and a smaller critical pore size than SS in UHPCs due to the additional C-S-H formation. However, high replacement ratios, e.g. 60% exhibit a negative effect on the microstructure development by increasing the critical pore size, which is due to the lack of hydration products.

5. The ambient carbonation treatment of SS powder results in a high leaching of V and Cr of CSS due to the decomposition of C_2S phase. However, the hydration products and dense structure of UHPC can effectively immobilize V and Cr, therefore, the leaching results of CSS blended UHPC satisfies the requirement of Soil Quality Decree (SQD) in Netherlands.

Chapter 10 Recycling and utilization of high volume converter steel slag into CO_2 activated mortars – the role of slag particle size

In this chapter, a low carbon footprint binders consisting of mass of converter steel slag powder (80%) of varying fineness, and normal cement (20%) are applied to produce mortars under ambient carbonation. The results indicate that the variation of steel slag particle size influences gas transport and CO_2 uptake of carbonated steel slag blended mortars during the curing period, which affects microstructure, strength, and leaching. The application of optimal size range of steel slag (21.75 to 24.13 μm) in blended mortars leads to a higher compressive strength (31.21 MPa), CO_2 uptake (15.9%), faster carbonation rate as well as sustainability efficiency (0.486 MPa/(kg/m^3)), which is obviously superior compared to the mortars with larger or smaller size of steel slags. The leaching properties, especially V and Ca leaching of steel slag blended mortars are observed to be strongly influenced by the CO_2 uptake, rather than steel slag particle size. A green binder system is achieved by both the reduction of cement content and the high CO_2 uptake by mass of binder.

This chapter is partially published elsewhere:

G. Liu, K. Schollbach, S. van der Laan, P. Tang, M.V.A. Florea, H.J.H. Brouwers. Recycling and utilization of high volume converter steel slag into CO_2 activated mortars – The role of slag particle size. Resources, Conservation and Recycling, 2020, Volume 160, Page 1-9.

10.1 Introduction

In Chapter 9, the potential of converter steel slag as binder after ambient carbonation treatment in normal blended UHPC has been discussed. Since the carbonation process of converter steel slag results in a reduction of true density, however, the volume expansion from the carbonation and hydration of calcium silicate and the precipitation of calcite were observed to reduce porosity and increase the bulk density thereby contributing to a significant strength development after pressurized CO_2 curing (Moon and Choi, 2018). In Shao's study, a combination of poorly crystalline $CaCO_3$ and C-S-H was confirmed after steel slag carbonation, which also has a potential to provide strength (Shao et al., 2013). Furthermore, the hydration products of cement, such as calcium silicate hydrates, calcium hydroxide, and ettringite were also identified to be reactive with CO_2 even at ambient conditions (Jang et al., 2016). Most of the previous investigations were carried out using a pressurized and pure CO_2 environment for fast strength development of steel slag concrete, conditions which add to the embodied energy of the products. On the other hand, the carbonation of steel slag is also confirmed to take place at ambient pressure and temperature in Chapter 9. This provides a possible eco-treatment to activate steel slag blended concrete at ambient condition using CO_2.

At ambient temperature and pressure, the dissolution rate of CO_2 is lower and the CO_2 transportation mostly relies on the gas permeability and humidity (Fernández Bertos et al., 2004). This process can be influenced by the mix design of the concrete and binder, and their particle sizes. It has been confirmed that steel slag particle size controls the CO_2 uptake ability (Baciocchi et al., 2009). By selecting the optimal steel slag size in slurry carbonation, Polettini et al. reported a CO_2 uptake of 465 kg/t (Polettini et al., 2016). As a consequence, the produced carbonation products dominate the pore volume development, as opposed to the cement binder hydration. They also control the CO_2 diffusion (Kashef-Haghighi et al., 2015), and influence the strength performance and microstructure development. Therefore, a variation of steel slag particle size should affect the strength evolution of CO_2 activated steel slag concrete, the amount of reaction products and leaching properties. However, the particle size effect of steel slag carbonation was only investigated in thin-film and steel slag slurries (Polettini et al., 2016). There is no report related to the steel slag particle size selection in CO_2 activated production of green concrete building materials available yet.

Therefore, the objective of this chapter is to manufacture a potential green converter steel slag-cement based building material by ambient CO_2 curing (298K, 0.2 CO_2 atm, 1 bar, and 65% RH). To this end, different particle sizes of converter steel slag are investigated. The optimal selection of steel slag particle size and applying of ambient

carbonation help to design concrete with high sustainability efficiency and low energy consumption.

10.2 Materials and methods

10.2.1 Materials

The converter steel slag, cement and standard sand have been described in the Chapter 3.2.1 and Chapter 9.2.1.

For the purpose of cement replacement the as-received converter steel slag was milled into powder using a disc milling (Retsch, RS 300 XL) with a power of 2200W. In order to create different particle size distributions the milling durations were varied from 7, 9, and 11 to 13 minutes (labelled as D1, D2, D3, D4), the particle size distributions are shown in Fig. 10.1.

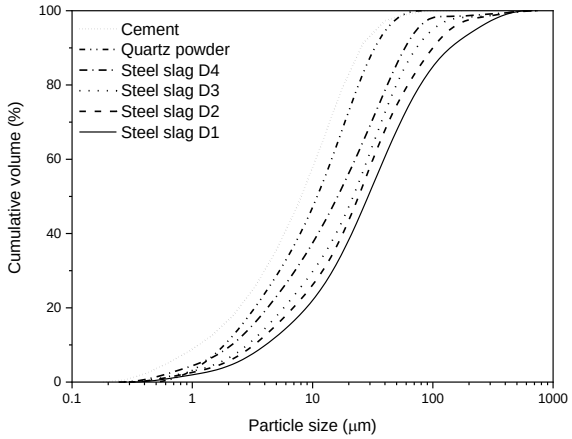

Figure 10.1 Particle size distributions of cement, quartz powder, and milled slags

10.2.2 Application of convert steel slag in sustainable mortars

The milled slags were used as cement replacement (80% wt.) in mortars and then their influence on mortar properties under different curing conditions was evaluated. The mixture design and labels of the mortars are shown in Table 10.1. The water to binder ratio of the mortars was kept at 0.4, and a standard sand (DIN EN 196-1) with a particle size of 0-2 mm was used as aggregate (sand to binder ratio was 3). In the reference mortar (QP), quartz powder was used to replace 80% wt. cement.

10.2.3 Mortar preparation and curing conditions

The milled slag (or quartz powder) was mixed with cement in a Hobart mixer for 30 s,

and then sand was added followed by 30 s mixing. Water was then added to the dry mixture and everything mixed for 30 s at medium speed. The fresh mixture was cast into moulds (40 mm × 40 mm × 160 mm) and then covered with plastic film for 24 hours before demoulding.

Table 10.1. Mixture design of mortars with milled slags (kg/m^3)

Samples	d_{50} of steel slag or quartz powder	Cement	Quartz powder	Steel slag	Sand	Water
QP	10.00 μm	100.78	403.12	0	1511.70	201.56
D1	28.98 μm	106.34	0	425.37	1595.12	212.68
D2	24.13 μm	106.34	0	425.37	1595.12	212.68
D3	21.75 μm	106.34	0	425.37	1595.12	212.68
D4	16.17 μm	106.34	0	425.37	1595.12	212.68

There were two types of curing conditions applied on the mortar samples: normal humidity curing and ambient CO_2 curing.

One batch of mortar samples after demoulding was cured sealed by covering it with plastic film and storing it at room temperature before further tests.

The second batch of mortar samples was cured in a climate chamber at a temperature of 25 °C. The relative humidity (RH) in the chamber was kept at 65% with a circular flow-through and a concentration of 20% CO_2 was applied in the chamber continuously for the tests.

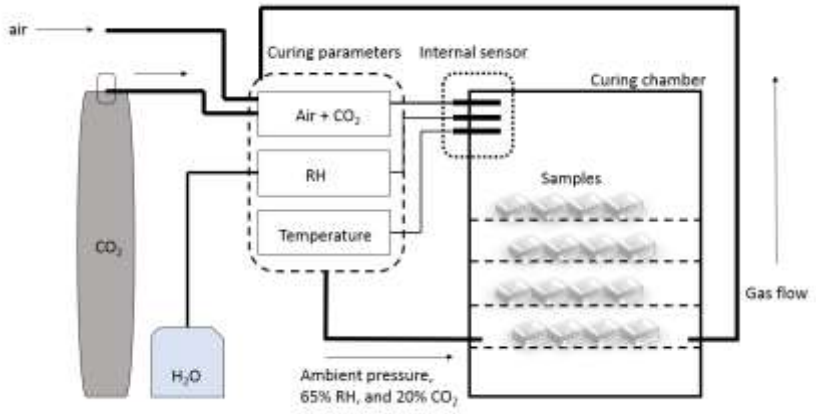

Figure 10.2 Schematic of carbonation chamber

10.2.4 Mechanical property and hydration/carbonation products

The strength performance test has been shown in Chapter 3.2.2. The TG, MIP, one batch leaching tests have been described in Chapter 9.2.2.

10.2.5 Evaluation of total CO_2 emission and sustainability efficiency

The CO_2 emission of energy consumption during converter steel slag milling process was calculated by the power of disc mill and milling duration according CO_2 emissions from public electricity production (295.8 g/kWh) in EU. The energy consumption of the CO_2 inlet was selected as 80.7 kWh/ton (Monkman and Shao, 2010). The CO_2 emission from cement, sand, and water production are set as 930 kg/ton, 4 kg/ton and 0.196 kg/ton, respectively (Li et al., 2019a). The calculation of sustainability efficiency was done according to a previous study (Damineli et al., 2010).

10.3 Results and discussion

10.3.1 Mechanical properties of mortars

Table 10.2 Compressive strengths of mortars

Sample	Compressive strength (MPa)				
	After demoulding	3 days CO_2	7 days CO_2	14 days CO_2	14 days hydration
QP	5.90±0.98	8.91±0.44	10.46±0.49	11.25±0.40	16.68±0.51
D1 (28.98 μm)	0.20±0.02	3.73±0.22	10.44±1.27	25.44±0.89	10.12±0.32
D2 (24.13 μm)	0.51±0.02	5.59±1.4	14.99±1.48	30.30±1.25	11.22±1.05
D3 (21.75 μm)	0.89±0.11	5.46±0.25	13.57±0.97	31.21±1.71	11.35±0.46
D4 (16.17 μm)	1.26±0.02	6.04±0.35	12.62±1.24	23.41±0.89	16.19±0.66

The compressive strengths of all mortars are shown in Table 10.2. For all the mortar samples cured sealed in plastic, the strength increased with curing time. The mortars containing slags showed much lower strength after demolding. Mortars with D1, D2, and D3 showed around 30% lower compressive strength after 14 days hydration compared to the mortar with inert quartz powder, while D4 was only 3% lower than the reference mortar. This result demonstrates that steel slag has very low hydraulic reactivity, which is consistent with previous findings (Qiang et al., 2016). It is also noticed that the strength of mortars containing steel slag increased with the decrease of slag particle size in hydration mortar samples. This may be due to the promotion of cement hydration due to the nucleation function of smaller particles (Lawrence et al., 2003).

Regarding the mortars cured under CO_2 conditions, it can be seen that all mortars showed increased compressive strength with increased curing time, and the mortars with steel slags achieved higher compressive strength after 7 days CO_2 curing than the 14 days normal cured samples. In addition, the compressive strength of mortars after 7 days CO_2 curing with steel slags is higher than the one with quartz powder, and their 14 days carbonated compressive strength is more than 2 times that of reference mortar. This observation indicates the specific contribution of steel slag during CO_2 curing for strength development, implying that steel slag blended mortars can be effectively activated under CO_2 curing conditions.

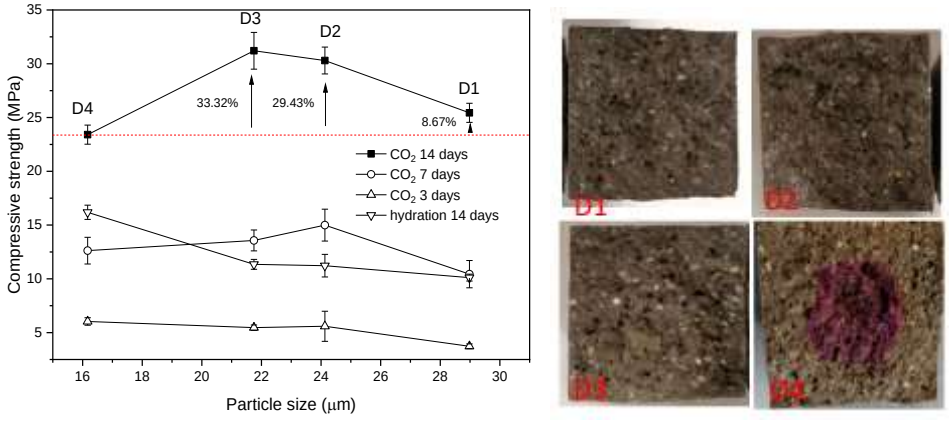

(a) (b)

Figure 10.3. (a) Influence of steel slag particle size on mortar strength and (b) phenolphthalein test of mortars after 14 days CO_2 curing

Fig. 10.3 also shows that the effect of the steel slag particle size on strength performance at various curing ages. As previously stated, in the hydrated mortar samples, the compressive strength of mortar decreased with the increase of slag particle size (Qiang et al., 2016) that finer steel slag particles exhibited higher reactivity, while in carbonated mortar samples, the mortar strength after 7 days firstly increased and then decreased with the increase of particle size. An optimal steel slag particle size value can be identified from the correlation between steel slag particle size and compressive strength. In comparison with D4 (23.41MPa), D3 exhibits an increase of 33.3% in compressive strength after 14 days carbonation, while it is 29.4% and 8.8% for D2 and D1, respectively. To further explain the contribution of steel slag and influence of its particle size on mortar properties, hydration and carbonation products and microstructures of mortars are studied in the followed sections.

10.3.2 Determination of hydration and carbonation products

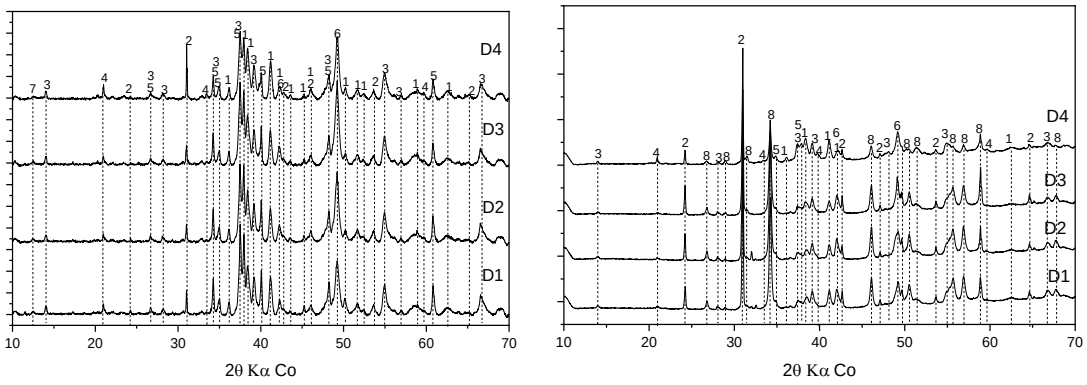

(a) (b)

Figure 10.4. XRD patterns of samples (a) before carbonation, and (b) after 14 days carbonation (1-larnite, 2-quartz, 3-brownmillerite, 4-portlandite, 5-C_3S, 6-wustite, 7-LDH like structure, 8-calcite)

It can be seen in Fig. 10.4 (a), that there is no significant difference in XRD patterns between steel slag blended mixtures after 24 hours hydration. The presence of CH is mainly due to the cement hydration (Shi, 2002). The larnite, brownmillerite, and wustite are related to the minerals in the unhydrated steel slag. Fig. 10.4 (b) shows the XRD patterns of samples after 14 days carbonation curing. Calcite is observed in all carbonated samples, while peaks of calcium hydroxide are only present in D4, indicating an incomplete carbonation, which is confirmed by the phenolphthalein test as shown in Fig. 10.3 (b). The detected calcite in carbonated samples demonstrates the activation of steel slag and its carbonation products under CO_2 curing conditions.

10.3.3 Mass change of samples during carbonation

The mass development of different mortars was measured and is shown in Fig. 10.5. It can be seen that the mass development of the reference sample (quartz powder blended) consists of two stages. The first stage is related to a high decrease of total mass, then the second stage corresponds to a stable period. However, the mass variation of the steel slag blended mortars consists of three stages. At first, there is a rapid decrease in mass (stage I), after that, a mass increase period can be observed (stage II), that gradually reaches a stable period (stage III).

Once mortars were moved to the carbonation chamber, pore water kept evaporating due to the difference of humidity between the inside and the outside of the mortar resulting in the mass decrease during the initial several days (stage I), Once the CO_2 uptake exceeds the water evaporation, the mass change of the mortars shows the profile of stage II. In stage II, mineral phases in the blended mortars, such as dicalcium silicate, calcium silicate, tricalcium silicate, and C-S-H react with CO_2 to form calcium

carbonate, amorphous silica gel, or CSH with low calcium content, and new free water (Humbert and Castro-Gomes, 2019), which resulted in an increase of mass of the sample.

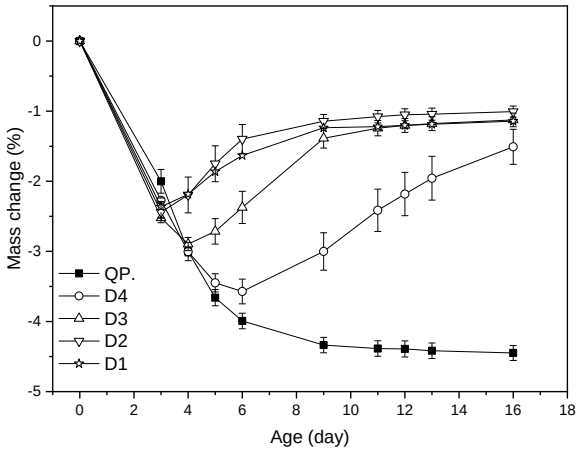

Figure 10.5. Mass change of mortars during the carbonation curing

Generally, these two processes are simultaneous. During the initial days of carbonation, the water evaporation process dominates the mass decrease. After that the sample is less saturated and connected pores become available for CO_2 diffusion. Consequently, more carbonation products are formed. The mass increase by carbonation gradually exceeds the mass loss by water evaporation. As a result, a turning point is observed, and the total mass starts to increase. In other words, the turning point reflects the speed of mortar carbonation. As can be seen from Fig. 10.5, the turning points for steel slag blended mortars containing slags of larger particle size occurs earlier than those with finer slags. Additionally, they reached a stable stage earlier (stage III). This demonstrates that a larger particle size of steel slag benefits the carbonation speed during CO_2 curing of mortar samples.

The contribution of the different particle sizes of steel slag to the carbonation speed can be explained by the initial porosity of mortar samples, and a subsequent decrease in the evaporation speed of pore water during the CO_2 curing. Moreover, the small pores were filled by the newly formed carbonation products. Then the route for CO_2 transportation was blocked. Thus, CO_2 took a longer time to reach the inside of the mortar samples containing fine size steel slag.

10.3.4 CO_2 uptake ability

The thermogravimetric results of the different carbonated samples are illustrated in Fig. 10.6. The sharp decline of mass in the temperature interval of 550 °C to 800 °C in the TG curve is corresponding to the decomposition of calcium carbonates and is used to

quantify the carbonation degree of the steel slag samples (Mo et al., 2016). Furthermore, there is a minor peak between 400-500 °C for D4, which is related to the decomposition of calcium hydroxide. This indicates that residual calcium hydroxide is present. This observation agrees with the XRD analysis (almost no calcium hydroxide in D1, D2, and D3) and the phenolphthalein test (Fig 10.3b).

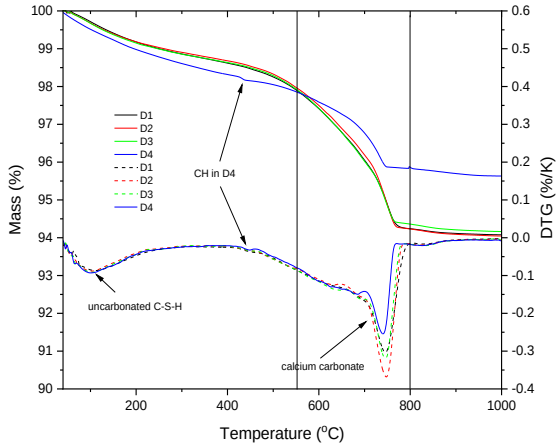

Figure 10.6 TG results of samples after 14 days CO_2 curing

To evaluate the carbonation rate at different ages, the CO_2 uptake was calculated and shown in Figure 10.7. The results showed that all samples exhibit an increasing CO_2 uptake with the increase of CO_2 curing duration. In addition, the CO_2 absorption occurs at a constant rate.

The constant carbonation rate is consistent with the mass loss and subsequent gain shown in Fig. 10.7 (b), and confirms that water evaporation dominates over the mass gain from carbonation at first. This also agrees with the previous discussion of total mass change where D2 reaches the turning point faster. It is clear to see that D4 presents a slower CO_2 uptake during the whole CO_2 curing period. A smaller slag particle size shows no positive effect on the CO_2 uptake below 24.13 μm for a carbonation duration of 14 days. This result may be due to the slow CO_2 diffusion in fine steel slag blended samples.

Generally, the carbonation rates of normal concrete exhibit a linear relationship between carbonation depth and the square root of time. However, in the present study, the carbonation shows a constant rate for all blended mortars even when it has reached the sample core. This indicates that CO_2 diffusion alone does not control the carbonation rate of these steel slag blended mortars.

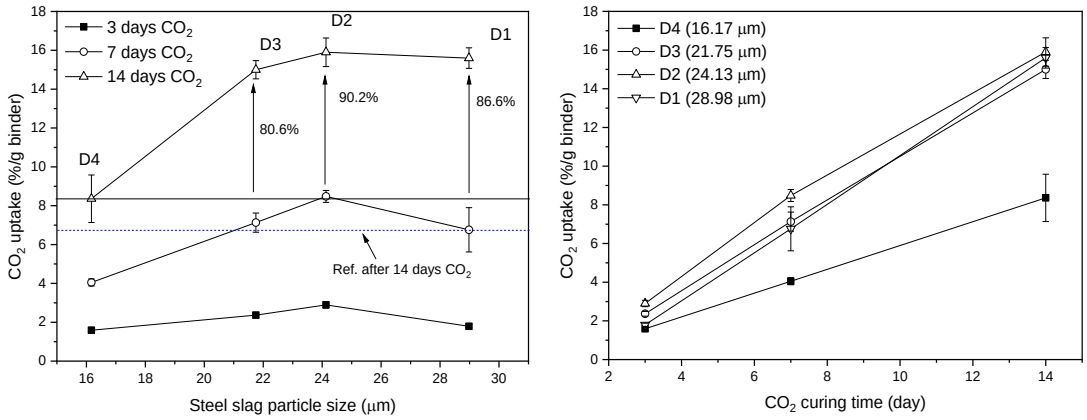

(a) (b)

Figure 10.7. CO_2 uptake of different cement-steel slag binders

The CO_2 permeability in the concrete sample is dominated by several factors, such as humidity, temperature, and pore structure. During early age, free water evaporation provides more and more unsaturated pores, which effectively promote CO_2 transportation as a gas. As a consequence, a constant carbonation rate was observed. In addition, the reaction of steel slag carbonation needs appropriate internal humidity and a necessary water film on the slag surface (Baciocchi et al., 2011). Even though the fast water evaporation could provide more pathways for CO_2 diffusion, a lack of water on the slag surface would slow the carbonation rate. On the other hand, slow water evaporation could inhibit CO_2 penetration, as well as the carbonation. These observations are consistent with the results in Chapter 10.3.3. It is confirmed again that the optimal steel slag particle size is a critical factor for the CO_2 uptake ability of steel slag blended mortars.

Table 10.3 CO_2 emisssion of carbonated steel slag-cement concrete (kg/m^3)

CO_2 emission	OPC[a]	D1	D2	D3	D4
Cement	495.59	98.89	98.89	98.89	98.89
Steel slag (milling)	0	32.24	41.52	50.74	59.97
Sand	6.39	6.38	6.38	6.38	6.38
Water	0.04	0.04	0.04	0.04	0.04
CO_2 uptake	/	-82.95	-84.54	-79.75	-44.45
CO_2 for curing	/	0.025	0.025	0.024	0.013
Total emisssion	502.02	54.63	62.31	76.32	120.84
Sustainbility efficiency (MPa/(kg/m^3))	0.112	0.466	0.486	0.409	0.194

a- normal cement mortar from previous study (Liu et al., 2019)

The CO_2 footprints of normal cement mortar and converter steel slag blended mortars are evaluated and shown in Table 10.3. The energy of steel slag milling and CO_2 gas preparation are included. It can be seen that the increase of milling intensity contributes

to a gradually increased CO_2 emission due to higher energy consumption. This increases the total CO_2 emission from 54.63 kg/m^3 to 120.84 kg/m^3. However, the CO_2 uptake ability of steel slag and the high volume cement replacement results in a lower footprint of blended mortars than for normal OPC. As a the building material, sustainability efficiency reflects the correlation between strength and CO_2 emission (Damineli et al., 2010). As can be seen, the sustainability efficiency of carbonated blended mortars is obviously higher than for normal OPC concrete. D2 shows the highest sustainability efficiency of all samples. This indicates that the optimal selection of converter steel slag particle size can efficiently help to enhance the sustainability of carbonated blends by enhancing strength and CO_2 uptake of samples.

10.3.5 Microstructural property

To further explain the observed mechanical properties of the CO_2-cured mortar samples, their microstructures were investigated with SEM and MIP, and the results are shown in Fig. 10.8.

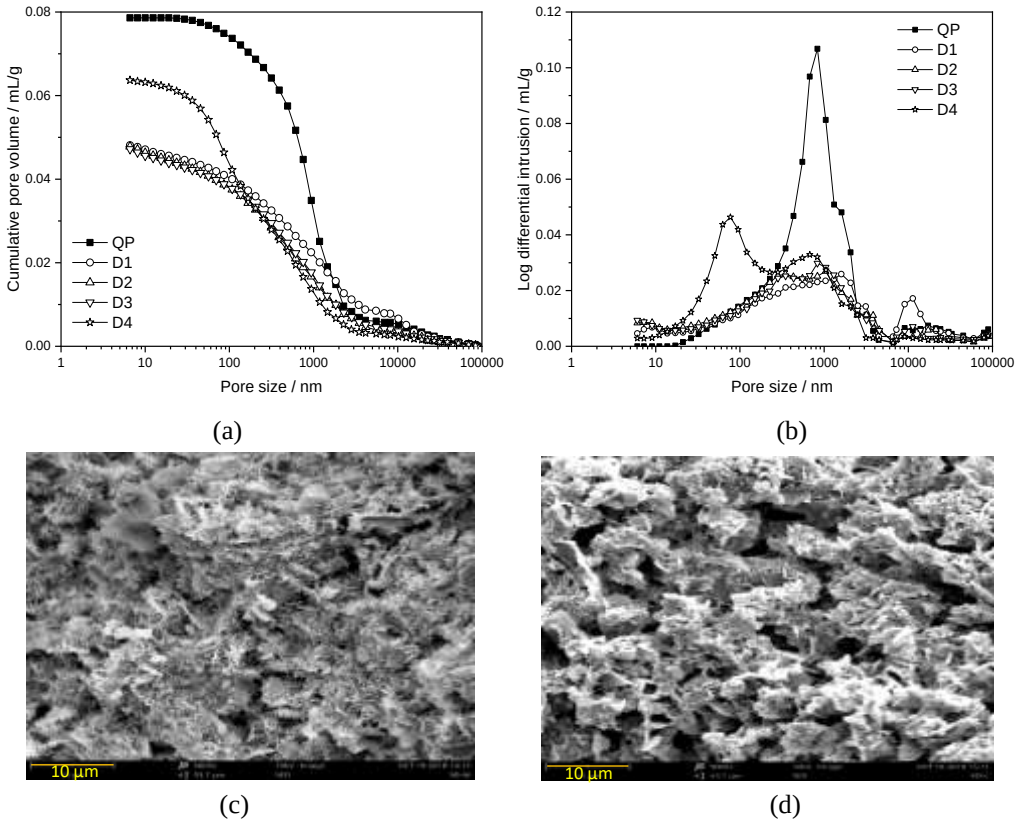

(a) (b)

(c) (d)

Figure 10.8. Pore size distribution and SEM of mortars after 14 days carbonation curing (a) cumulative pore volume (b) pore size distribution (c) hydrated area (d) carbonated area

As it can be seen from the MIP results, sample QP shows the highest total pore volume (0.0786 ml/g) of all samples, which is due to the fact that quartz powder cannot be

carbonated, while steel slag does carbonate, filling in the pores (Zhan et al., 2013). Comparing the total pore volume of mortar samples with steel slag, it can be seen that the sample D4 had the highest total pore volume and the other three showed a slight decrease with the increase of slag particle size.

The pore size distribution of different carbonated mortars is shown in Fig. 10.8 (b). It is noticed that there is an additional peak at around 100 nm in D4 (16.17 μm) that is not present in the other steel slag samples. This peak is usually observed in cement samples, and is characteristic for capillary pores of C-S-H in cement based concrete (Liu et al., 2019). The presence in D4 indicates that there likely is a coexistence of C-S-H-hydration and carbonation products, as already identified in Section 9.3.2. In addition, the pore volume in this range (around 100 nm) is dramatically reduced in samples with a higher carbonation degree, such as D1 and D2. It appears that capillary pores were partially refined by the carbonation products in D1-D3. However, when the steel slag particle size increased from 21.75 μm (D3) to 28.98 μm (D1), the location of the main peak gradually shifts to the larger value. In addition, a small peak was present at 28.98 μm (D1) steel slag blended mortar. This gradual increase of pore may be caused by the poor particle packing of the mixtures. The increase of pore size also correlates with the mechanical performance of D1, D2, and D3. The mechanical performance is not only controlled by the amount of reaction products but also influenced by the packing of mixtures (Brouwers and Radix, 2005).

10.3.6 Evaluation of leaching properties

To study the leaching properties of steel slag blended mortars after carbonation a leaching test was conducted after 3 days, 7 days and 14 days. The results are shown in Table 10.4 and Figure 10.9.

It can be seen that for all steel slag samples, the leaching of Mg keeps increasing with progressive carbonation. At the same time, Ca concentration decreases gradually concurrent with the appearance of V in the leachate and a drop in pH. The Al and Cr concentration of D1, D2 and D3 also increase until 7 days carbonation. For D4, the Al concentration keeps increasing during the whole test duration.

The correlation between pH and leaching of steel slag blended mortars is shown in Fig. 10.9, which indicates that the leaching behaviour of samples relies on the pH variation and phase assemblage rather than the steel slag particle size difference. In addition, the carbonation degree controls the leaching properties by changing the pH. Since portlandite and free-lime exist in the binder system before carbonation, a high pH can be kept during early carbonation. During the carbonation process, the portlandite from

cement and steel slag hydration can serve as a pH buffer, and keep Ca leaching at a high level for the first 7 days. On the other hand, the leaching of Mg is limited under these condition (Huijgen and Comans, 2006). Regarding further carbonation, once the residual portlandite is carbonated and cannot contribute to Ca leaching anymore, the pH drops significantly. At the same time, the Mg leaching increases (Baciocchi et al., 2015). So, the decrease of Ca leaching corresponds with the increase of Mg leaching.

Table 10.4 One batch leaching results of converter steel slag blended mortars

Sample		Leaching ions (mg/L)					
		Al	Ca	Mg	Cr	V	pH
D1	Before CO_2	0.363	156.7	L.D.	0.007	0.006	12.4
	3 days CO_2	0.449	157.7	0.002	0.018	0.004	12.47
	7 days CO_2	0.671	166.8	0.006	0.069	0.047	12.28
	14 days CO_2	0.104	68.6	0.466	0.06	5.522	10.85
D2	Before CO_2	0.334	156.5	L.D.	0.005	0.005	12.4
	3 days CO_2	0.442	159.5	0.001	0.02	0.012	12.43
	7 days CO_2	0.624	124.7	0.038	0.081	0.753	11.9
	14 days CO_2	0.100	64.9	0.547	0.052	6.278	10.7
D3	Before CO_2	0.312	156.5	L.D.	0.006	0.005	12.46
	3 days CO_2	0.427	160.1	0.003	0.022	0.013	12.45
	7 days CO_2	0.462	163.3	0.004	0.049	0.024	12.39
	14 days CO_2	0.099	68.2	0.476	0.05	5.251	10.83
D4	Before CO_2	0.221	156.4	L.D.	0.013	0.001	12.55
	3 days CO_2	0.311	159.0	0.005	0.01	0.005	12.5
	7 days CO_2	0.264	156.5	0.003	0.034	0.003	12.56
	14 days CO_2	0.634	122.7	0.056	0.087	0.447	11.91

L.D. – below the detection limit.

The leaching of both Al and Cr increase at first and then decrease with the lowering of the pH. The increase of Al leaching can be attributed to the carbonation of AFt and AFm formed from cement hydration, while the Cr leachingbehaves like Al. However, the leaching of Cr and Al decreases after the pH drops to below 12, which is related to the identical amphoteric behavior. A similar result also was observed in previous research (Baciocchi et al., 2015). The leaching of V also exhibits a strong correlation with pH, being mainly driven by the dissolution behaviour of C_2S in steel slag. During the early carbonation, the portlandite saturation induces a high Ca concentration and high pH in the pore solution. At these conditions of portlandite saturated pore solution, the dissolution of C_2S is inhibited and the leaching of the V hosted by C_2S limited (Santos et al., 2012). The increasing CO_2 uptake correlates with a decrease of pH as shown in Fig. 9. With more advanced carbonation, pH decreases and C_2S dissolution starts to increase, corresponding with a significant rise in V leaching. This observation

agrees with previously published results (Costa et al., 2016). Furthermore, the V leaching of crushed mortars after 14 days carbonation in the present study is higher than the limit set in the Dutch Soil Quality Decree (1.8 mg/kg). However, the leaching properties are influenced by many factors, such as mix design, curing strategy and porosity. For example, D4 still exhibits a low V leaching (due to its still high pH), which meets the requirement of SQD. So, in future research the influence of mix design and porosity on V leaching will be investigated to solve this problem. It is possible to improve the V leaching using optimal concrete mix design, as well as the CO_2 curing process to satisfy the regulation. This should also be investigated in future research.

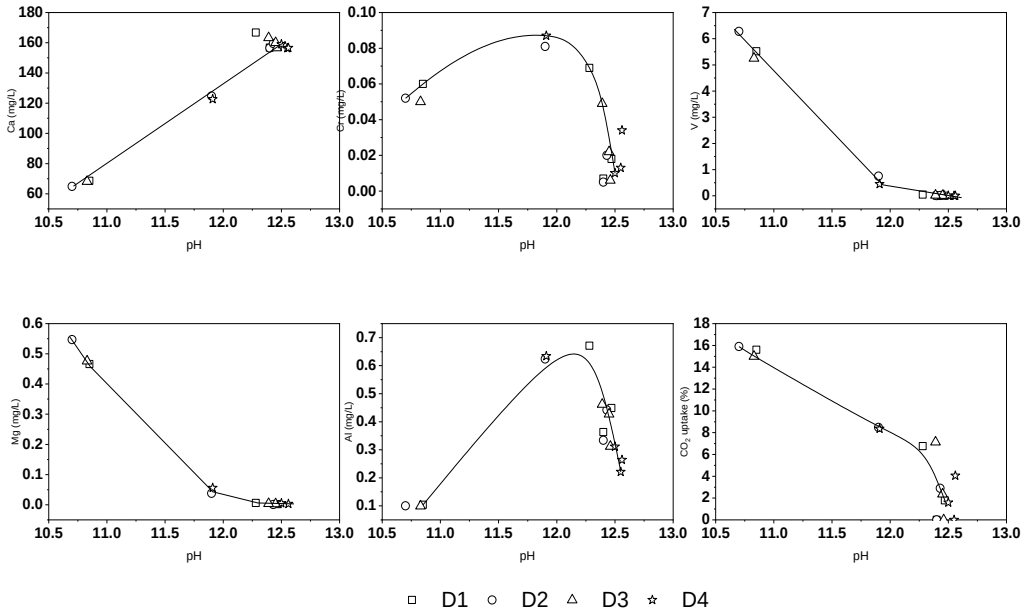

Figure 10.9. The ions leaching and CO_2 uptake versus pH of different converter slag blended mortars

10.4 Conclusions

1. Ambient CO_2 curing is more effective than using normal, humid curing of converter steel slag blended mortars in terms of strength development.

2. There is an optimal mean particle size of 21.75 μm (D3) for steel slag in the present study based on strength performance after 14 days carbonation. The compressive strength and sustainability coefficiency are found to decrease for both larger and smaller steel slag particle sizes.

3. The mass development of steel slag blended mortars during CO_2 curing showed three stages. A turning point at the transition from stage I to stage II could be defined, which reflects the carbonation speed. The finer the converter steel slag was, the longer the

blended mortars needed to reach the turning point.

4. Between 8 to 15.9% of CO_2 can be taken up by the cement - steel slag binder due to carbonation, with the slag size of 24.13 μm (D2) showing the highest CO_2 uptake after 14 days CO_2 curing. Less carbonation is observed when the slag particle size is finer or larger than D2.

5. The leaching properties of steel slag blended mortars are controlled by the CO_2 uptake, and only indirectly by steel slag particle size. The Cr and V leaching increased with progressing carbonation once the pH and Ca concentration of the leachate dropped. The highest V leaching was related to the steel slag D2 (24.13 μm), which correlated with the highest CO_2 uptake and lowest leachate pH after 14 days CO_2 curing.

Chapter 11 Cement-free steel slag mortars activated by ambient CO_2/alkali activation

This chapter illustrates the development of cement-free steel slag based green binder mortars treated with a combination of alkali activation and CO_2 activation. GGBS accounts for 10%, 20%, 30%, 40% and 50% in steel slag based mortars by mass, while sodium hydroxide solution (2M) is used as activator in the preparation of mortars. The results indicate that the cement free steel slag mortars exhibit a quick development of strength during 14 days of CO_2 activation. The GGBS part provides an initial strength of 1.5 to 8.1 MPa after 24 hours alkali activation. The final strength is 37.5 to 44 MPa after 14 days CO_2 activation. The results of XRD and TG tests reveals that the reaction products after the combination of alkali/CO_2 are related to different forms of calcium carbonates, hydrotalcite and C-S-H. Moreover, the amount of GGBS in the binder system contributes to formation of the calcium carbonates with a poor crystallization degree, while steel slag prefers to form crystalline calcite after carbonation. The investigation in this chapter contributes to the high-end application of steel slag in low carbon footprint building materials.

This chapter is reproduced from:

G. Liu, K. Schollbach, H.J.H. Brouwers. Application of converter steel slag for CO_2 sequestration in alkali activated materials (in preparation).

11.1 Introduction

In Chapter 10, high volume converter steel slag application is investigated in the manufacturing of building materials by combining it with normal OPC. It is shown that the small amount of OPC can produce an adequate early strength for demoulding. However, the calcium hydroxide from the hydration of cement can reduce the C-S-H carbonation rate due to its pH buffer capacity, consequently, a slow strength development can be observed during carbonation as found in Chapter 10. Compared to traditional OPC based building materials, AAM (alkali activated material) exhibits a faster hardening behaviour, higher mechanical performance and significantly lower carbon footprint (Puertas et al., 2018). Ground granulated blast furnace slag (GGBS) is widely used as binder with alkali activation process because of its reactive amorphous calcium aluminosilicate structure (Shi et al., 2018). The main reaction product of GGBS after alkali activation is C-(A)-S-H (Bernal et al., 2013), which also shows a CO_2 binding capacity during carbonation. Furthermore, compared to hydrated OPC, alkali activated GGBS exhibits a low resistance to accelerated carbonation due to the absence of calcium hydroxide as shown in previous studies (Chapter 6, Chapter 7 and Li et al., 2017). In addition, a recent studies reported that accelerated carbonation causes no strength reduction when NaOH was used to activate GGBS mortars (Li et al., 2017; Shi et al., 2018). Therefore, the NaOH activated GGBS is expected to be an ideal blended component to produce cement free mortars for CO_2 sequestration.

As investigated in Chapter 9 and Chapter 10, converter steel slag powder can be carbonated at ambient conditions. However, its low hydration reactivity hampers the development of green strength as has been confirmed. in order to design a cement-free binder for CO_2 sequestration, the early hardening behaviour before carbonation should be considered for demoulding and transportation. Since alkali activated GGBS exhibits a faster hardening process and high strength at early ages, combining alkali activation and CO_2 activation in a GGBS/steel slag binder deserves to be investigated to produce a new cement-free green binder system.

Therefore, in this chapter, a combined application of alkali activation and CO_2 activation on GGBS/steel slag mortars is investigated. The GGBS is used in the converter steel slag based binder in a range of 10% to 50% by mass. The mechanical performance, carbonation rate, reaction products, CO_2 binding capacity are evaluated and discussed. The aim of this chapter is to propose a new method for the utilization of converter steel slag in cement-free building materials.

11.2 Materials and methods

11.2.1 Materials

The chemical and physical properties of used converter steel slag and standard sand have been shown in Chapter 9.2.1. The characterization of GGBS and preparation of activator have been described in Chapter 6.2.1 and Chapter 7.2.1.

11.2.2 Methods

- *Preparation of cement free GGBS/steel slag binders for carbonation*

The GGBS and converter slag are used for preparation of cement free binders. The amount of GGBS in the binder system is from 10% to 50% labelled G10 to G50 (pure steel slag samples cannot be demoulded after 24 hours normal curing, so it is only used as a reference sample G0 for reaction products analysis). The water to binder ratio is selected as 0.4, while the aggregate to binder ratio is 3. The used activator is 2 M NaOH solution. The mix design is shown in Table 11.1. The carbonation conditions are the same as described in Chapter 10.2.2.

Table 11.1 Mix design of cement free steel slag mortars

Sample	GGBS / kg	Steel slag / kg	Sand / kg	Activator / kg
G0	0	532.72	1598.17	230.14
G10	53.27	479.45	1598.17	230.14
G20	106.16	424.63	1592.35	229.30
G30	158.66	370.20	1586.56	228.46
G40	210.78	316.16	1580.81	227.64
G50	262.52	262.52	1575.11	226.82

Activator- 2M NaOH solution

- *Characterization of reaction products and performance evaluation*

The mechanical performance determination of samples has been shown in Chapter 3.2.2. Carbonation depth identification has been shown in Chapter 6.2.2. The XRD, TG and FTIR tests have been described in Chapter 2.2.2 and Chapter 3.2.2.

11.3 Results and discussion

11.3.1 Mechanical performance

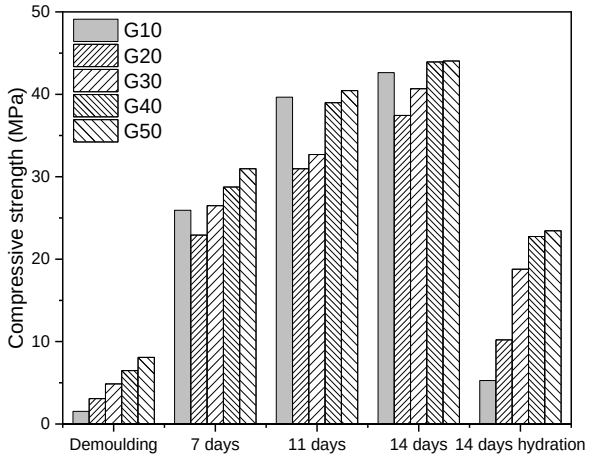

Figure 11.1 Compressive strength of cement-free steel slag mortars at different ages

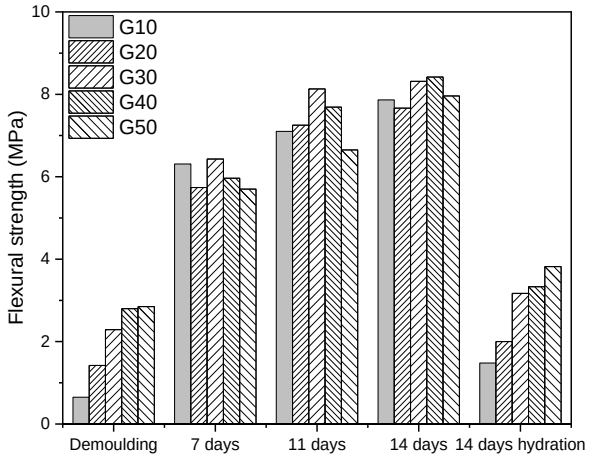

Figure 11.2 Flexural strength of cement-free steel slag mortars

The compressive strength of cement-free steel slag mortars is shown in Fig. 11.1. After the first 24 hours normal curing, the compressive strength ranges from 1.5 MPa to 8.0 MPa with different GGBS/steel slag ratios. The increase of the GGBS proportion in mortars contributes to a higher initial strength after demoulding. In the following CO_2 activation, the cement-free mortars exhibit a fast compressive strength development. After 7 days of CO_2 activation, a compressive strength of 23 MPa to 31 MPa can be observed. With prolongued CO_2 curing, the compressive strength of mortars shows further development. G10, G40 and G50 achieve almost full carbonation after 11 days, with a compressive strength up to 39.6 MPa, 38.9 MPa and 40.4 MPa, respectively. The compressive strength of mortars reaches 42.6 MPa, 43.9 MPa and 44.0 MPa at 14 days.

It is interesting that the flexural strength development differs from the compressive strength during CO_2 activation as shown in Fig. 11.2. While G30 develops the highest flexural strength compared to the other mixtures, however, at the same time, G30, together with G20, stay behind in their compressive strength development. This is possible induced by a lower amount of micro cracks from carbonation shrinkage as shown in Chapter 7. In comparison to mortars with normal curing, CO_2 activated mortars exhibit an obviously better mechanical performance after 14 days. It can be concluded that the combination of alkali/CO_2 activated GGBS/steel slag binder is feasible to produce building materials with a satisfactory strength performance, and that this treatment is more efficient than normal curing by a faster strength development. Moreover, these systems show a higher strength compared to the mixtures of Chapter 10.

11.3.2 Carbonation depth

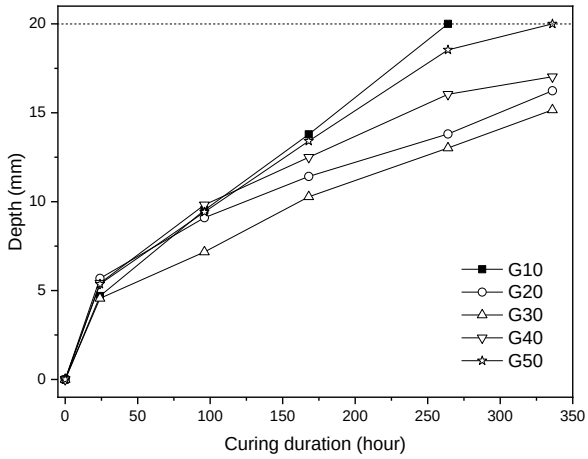

Figure 11.3 The carbonation depth at different curing ages

The carbonation depths of mortars were determined by using the phenolphthalein test and the results are presented in Fig. 11.3. It is clear that the mix design of mortars strongly influences the penetration of CO_2. All samples exhibit an increase of carbonation depth with the carbonation time. G10 and G50 nearly achieve full carbonation after 11 days CO_2 activation, while G20, G30 and G40 only carbonate to depth of 13.8 mm to 16.0 mm. After 14 days, these mortars still remain only partially carbonated, with a carbonation depth from 16.2 mm to 17.0 mm. The development of carbonation depth indicates that G30 is the mixture subject to the slowest carbonation process among all samples. This indicates that G30 may form the most dense pore structure after first 24 hours alkali activation, which inhibits the CO_2 transportation. As mentioned in Chapter 10, the degree of carbonation relates to the strength development, and the steel slag is the main reactive component during the CO_2 curing. Furthermore,

this observation is also in agreement with the results in Chapter 11.3.2. Consequently, the G20 and G30 exhibit a slow increase of strength during activation. However, prolongued duration of CO_2 activation after 14 days could still enhance the strength of partially carbonated samples, for example G20 to G40. In order to clearly understand the final CO_2 uptake potential of various mixtures, crushed pastes samples subjected to 14 days carbonation will be discussed in the following sections.

11.3.3 Reaction products evolution

- *XRD*

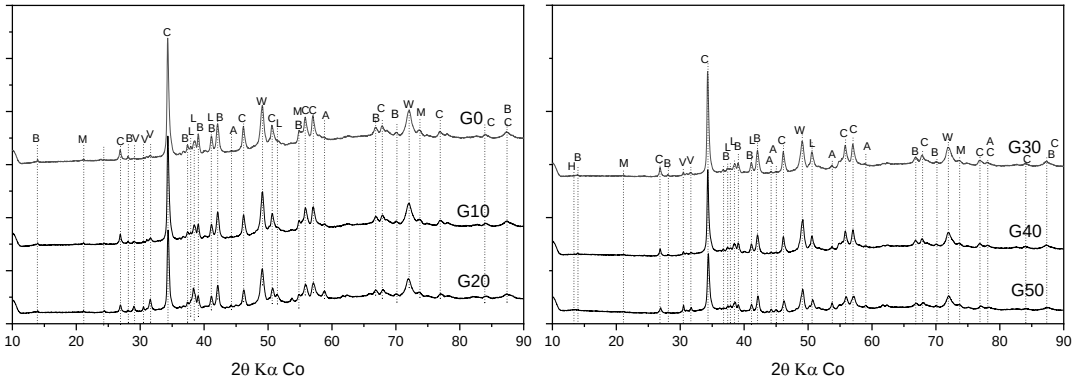

(a) (b)

Figure 11.4 Reaction products of cement-free steel slag binders after 14 days carbonation (B- brownmillerite, M- magnetite, C-calcite, L-larnite, V-vaterite, W-wuestite, H- hydrotalcite)

The characterization of the mineral composition of different mixtures after full carbonation is shown in Fig. 11.4. It can be seen that the increase of GGBS proportions in the binder system influences the reaction products. For the pure steel slag sample G0, the main identified peaks are related to brownmillerite, magenetite, larnite and wuestite, which are the unreacted phases of the original steel slag. At the same time, carbonation products, for example, calcite and vaterite are observed. After GGBS was introduced in the system, peaks of aragonite, and hydrotalcite can be observed. It is well known that, alkali activated GGBS is vulnerable to aggressive carbonation due to the absence of portlandite compared to normal OPC sample. As the main alkali activation products of GGBS activated by NaOH, layered double hydroxide (LDH) can keep a stable structure during the carbonation, however, the OH- between the layers can be replaced by CO_3^{2-}, leading to the formation of hydrotalcite (Costa et al., 2012). On the other hand, the C-A-S-H from alkali activation can be transformed to calcium carbonate, alumina-silica gel and free water (Shi et al., 2018). For the converter steel slag in the binder system, a limited hydration can take place, at the expense of C_2S, and the formed C-S-H can be carbonated producing calcium carbonate and silica gel and water. At the

same time, C_2S also directly shows a high reactivity in the CO_2 rich environment to form calcium carbonate and amorphous silica gel. This indicate that the products from alkali activated GGBS also can play a role of CO_2 uptake and that they may contribute to strength development at early ages.

- *FTIR*

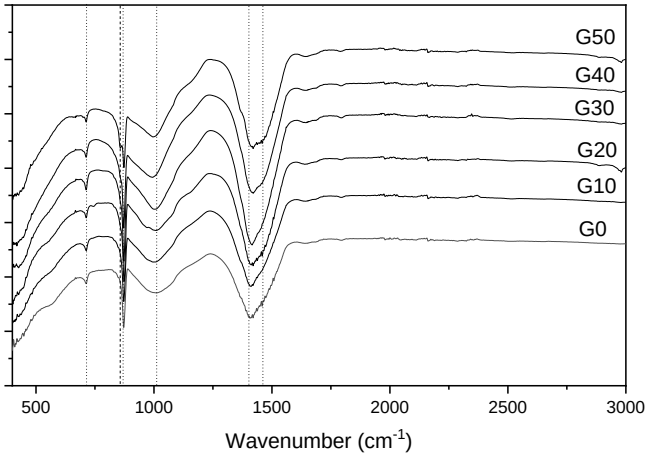

Figure 11. 5 FTIR of different mixtures after 14 days carbonation

To examine the variation in reaction products after CO_2 activation, FITR spectrometry test was conducted, with results as shown in Fig. 11.5. The peaks related to the reaction products are located at 997-1013 cm^{-1}, 714 cm^{-1}, 872 cm^{-1}, 858 cm^{-1} and 1404-1459 cm^{-1}. Peaks in the range of 997-1013 cm^{-1} are induced by the vibration of Si-O in reaction products, for example, C-(A)-S-H and amorphous alumina silica gel. It can be seen that the increased GGBS in mixtures results in a shift of Si-O to smaller wavenumber. This indicates a decrease of polymerization degree of silicate chains with the increase of GGBS proportion, which is due to more GGBS becomes less alkali activated, and as a consequence less carboanated. On the other hand, a gradually increased intensity of peak at 858 cm^{-1} after carbonation is observed in the samples containing higher GGBS after carbonation, which is related to the C-O in aragonite. This observation is in agreement with the XRD results. Several calcium carbonate polymorphs can co-exist in mixtures, while aragonite is mainly from the carbonation of C-A-S-H.

- *TG and CO_2 uptake*

The thermal gravimetric results of selected mixtures are shown in Fig. 11.6. The first mass loss before 300^{o}C is caused by the dehydration of uncarbonated and partially carbonated C-(A)-S-H. Then a second mass loss can be observed from 550 ^{o}C to 850 ^{o}C, which is related to the decomposition of various calcium carbonates: calcite, aragonite, vaterite and amorphous calcium carbonate (Mo et al., 2016). It is interesting

to notice that the increased GGBS proportion in mixtures results in a decomposition of calcium carbonates at lower temperature compared to the pure steel slag sample (G0). As it is well known, the aragonite and vaterite decompose at lower temperature (550-680 °C) compared to calcite (Borges et al., 2009). This indicates that the increase of GGBS amount in mixtures promotes the formation of aragonite and vaterite compared to pure steel slag sample after carbonation. Additionally, the decomposition of calcium carbonates even start from 450 °C in G50, which may be induced by the existing of amorphous calcium carbonate and poorly crystallized calcium carbonate polymorphs.

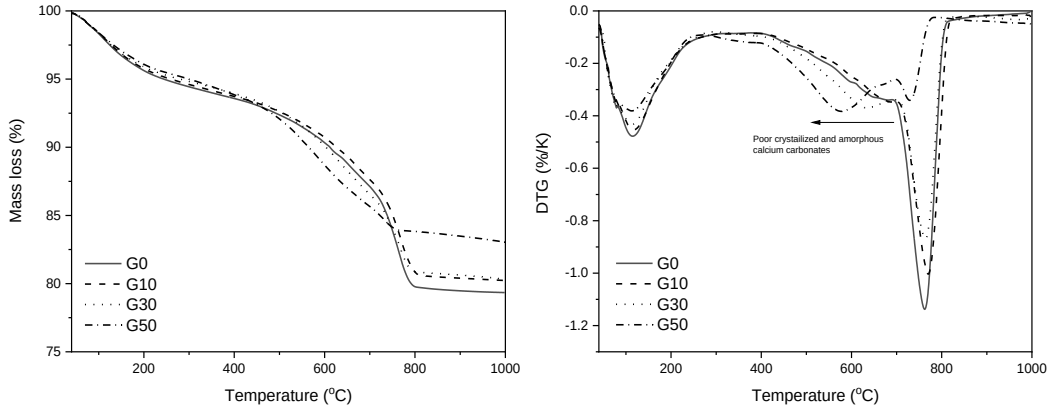

(a) (b)

Figure 11. 6 Results of thermo-gravimetric test after 14 days carbonation

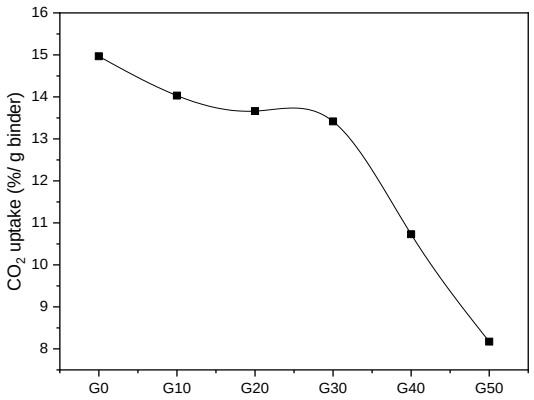

Figure 11. 6 The TGA-based estimated CO_2 uptake of different mixtures after 14 days

The CO_2 uptake of different GGBS/steel slag mixtures is calculated from the mass loss between 550 to 850 °C and shown in Fig. 11.6. It is clear that the progressive incorporation of GGBS keeps reducing the CO_2 uptake of mixtures. The highest CO_2 uptake is observed in G0, which accounts for 15% per gram of dry binder. Then it decreases to 13.4% after 30% GGBS was incorporated. A significant decline is observed if more GGBS is used (40% and 50%). This correlates with the reduction of the steel slag proportion, but it can also be influenced by the reaction products from activated GGBS.

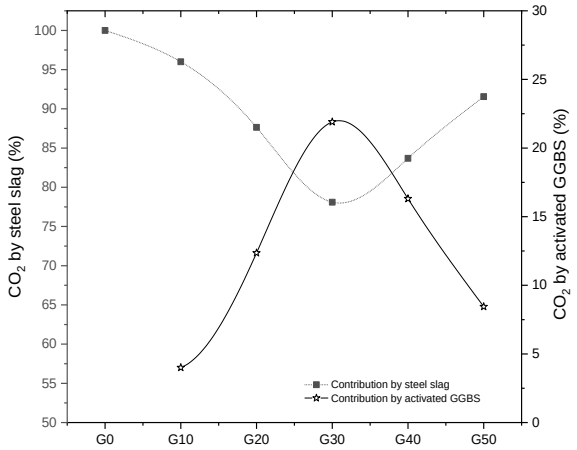

Figure 11. 7 CO_2 uptake by steel slag and activated GGBS after 14 days carbonation

To investigate the contribution of CO_2 uptake ability from GGBS and steel slag, it is assumed that the carbonation degree of steel slag in different mixtures is same as in G0, then the CO2 uptake by alkali activated GGBS can be roughly estimated and shown in Fig. 11.7. It can be seen that the steel slag accounts for the most of CO_2 uptake in blended mixtures, between 78% to 96%. On the other hand, the CO_2 uptake by GGBS gradually increases from 4% to 22% with a GGBS proportion from 10% to 30%, then it decreases to 8% when 50% of GGBS was used. This is caused by the different alkali activation reaction degree of GGBS, as well as the carbonation degree of activated GGBS.

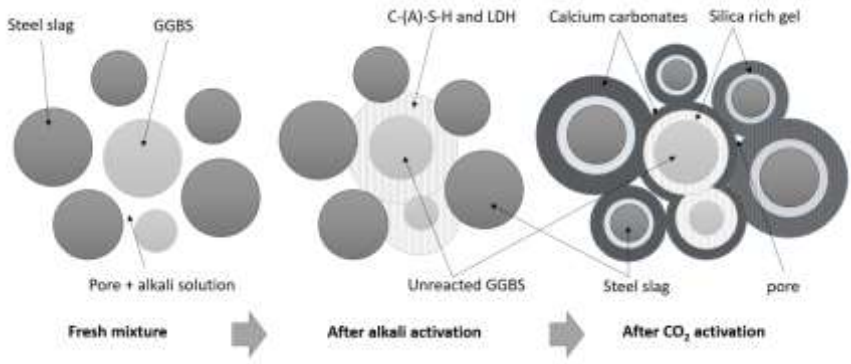

Figure 11.8 Reaction process of combining alkali activation and CO_2 activation

The reaction process of combining alkali activation and CO_2 activation in GGBS/steel slag based green binders is shown in Fig. 11.8. The fresh mixtures contains steel slag and GGBS particles, as well as a large volume of pore saturated with alkali solution. After the first 24 hours alkali activation, the reaction products such as C-A-S-H and LDH from reacted GGBS fill the pores, binding the particles and resulting in the early strength of the specimens. However, during this period, the reaction of steel slag is

relatively limited. Afterwards, the samples are moved to the carbonation chamber for CO_2 activation. As shown in Chapter 9 and Chapter 11, the converter steel slag exhibits a high reactivity in a CO_2 rich environment, so the C_2S phase in converter steel slag starts to react with CO_2 dissolved in pore solution. Consequently, the carbonation of the C_2S phase produces a silica rich inter layer and calcium carbonates outer layer. During this process, the pore volume is further decreased and the mechanical performance is enhanced. At the same time, the reaction products from alkali activated GGBS also start to carbonate. The LDH absorbs CO_3^{2-} into the layer and releases OH^- to the pore solution to form hydrotalcite, which acts as a buffer for pH change. However, after the LDH is saturated with CO_3^{2-}, the dissolution of CO_2 in the pore solution keeps decreasing its pH, so the C-(A)-S-H gel starts to decalcify and forms calcium carbonates on the outer layer of alkali activated products.

Therefore, the amount of CO_2 sequestrated by GGBS can be controlled by the reaction of GGBS in previous normal curing period, as well as the GGBS proportion in mixtures. The decreased CO_2 uptake by GGBS in G40 and G50 indicates a limited reaction degree compared the GGBS in other samples. This is probably induced by the low activator concentration (2M), which cannot provide enough alkali for the reaction of GGBS. At last, the limited reaction degree of GGBS only provides low amounts of C-A-S-H and LDH for carbonation.

11.4 Conclusions

1. The incorporation of GGBS provides cement-free mortars with a sufficient early strength for demoulding after the first 24 hours of activated curing. The steel slag powder contributes to a fast strength development during CO_2 activation. The compressive strength of cement-free mortars reaches 37.4 MPa to 44 MPa after 14 days CO_2 activation.

2. The reaction products of mixtures after alkali/CO_2 activation are aragonite, vaterite, calcite and amorphous alumina silica gel. In samples containing high amount of GGBS, the hydrotalcite can also be observed.

3. The TG results indicate that the incorporation of GGBS results in the formation of poorly crystalized calcium carbonates and possibly amorphous calcium carbonate from the carbonation process of C-A-S-H of activated GGBS.

4. The CO_2 uptake of achieved with these cement-free binders is 8% to 14%. The steel slag carbonation contributes to over 79% of CO_2 binding capacity andless than 21%

CO_2 binding capacity comes from reacted GGBS. The reaction degree of GGBS may influence the CO_2 uptake ability of the mixtures. Furthermore, for the cement-free mortars both the strength performance of cement-free mortars is better and the carbonation speed higher than of the OPC-steel slag mortars of in Chapter 10.

Chapter 12 Conclusions and recommendations

12.1 Conclusions

Cement is the most widely used material for the production of buildings worldwide. Huge energy and natural resources are consumed by the cement industry. Due to these environmental and sustainability concerns, blended cement containing supplementary cementitious materials (SCMs) is getting much more attention in recent years. The incorporation of SCMs in the production of building materials can effectively reduce the dependence on normal cement, at the same time, SCMs from industrial and domestic wastes are also recycled in a high-end application. Furthermore, other methods for producing cement-free and low carbon footprint building materials have been developing for years, for example, alkali activated and CO_2 activated materials. Cement-free and low carbon footprint building materials even provide a chance to totally replace cement-based materials in some cases. Solid wastes can be effectively utilized as building materials provided appropriate methods are applied such as hydration, alkali activation and carbonation, depending on the chemical and physical chacter of the waste material. Recycled waste glass is mostly generated from domestic waste, processing a highly amorphous structure and high content of SiO_2 as well as Na. These characteristics make it feasible to be an SCM in blended cement due to its pozzolanic reactivity. On the oppsite end, steel slag is a highly crystalline material with a well-crystallized structure drived during its solidification process. The existence of calcium silicate phases, mainly C_2S, give it some hydraulic reactivity. However, the relatively high reactivity of calcium silicate phases in a CO_2 rich environment provides a more suitable application by using CO_2 activation rather than normal hydration for production of low carbon footprint materials. The main conclusions from this thesis and the recommendations for future research and study are summarized as follows:

12.1.1 Recycled waste glass as an ingredient in blended cement hydration

Chapter 2 to Chapter 5 focus on the recycled waste glass powder (RGP) as SCM with high volume replacement in normal cement and blended cement-based materials. The reaction kinetics, reaction products, microstructure and durability are evaluated and discussed. The recycled waste glass blended cement exhibits better workability due to the morphology of the glass powder particles. The dissolution of waste glass can release Na in the pore solution, consequently, the hydration of clinker can be enhanced. However, a longer setting time for recycled waste glass blended cement is noticed related to the limited reaction of recycled waste glass at early ages. Therefore, high

volume recycled waste glass blended cement mortars exhibit a lower compressive strength compared to pure cement samples. Nevertheless, the highly effective water to cement ratio and the pozzolanic reaction of recycled waste glass contributes to a further strength development at later ages in these blended cement mortars. By reducing the initial water in the mixtures, the compressive strength contribution from recycled waste glass can be significantly enhanced. On the other hand, the weak structure at early ages is accompanied by a higher drying shrinkage. Due to the pozzolanic reaction of recycled waste glass in hydrated cement samples, the microstructure and even ITZ of mortars are observed to be modified in blends with high volume SCMs (GGBS and FA).

The incorporation of recycled waste glass in high volume GGBS or FA blended cement can effectively improve the resistance to rapid chloride migration and mechanical performance of ternary cement blends. The Na dissolution from recycled waste glass can result in an increase of pH, of which, in turns, the reaction of GGBS and FA benefit. On the other hand, the high SiO_2 content in waste glass promotes secondary C-S-H formation via pozzolanic reaction, as a consequence, the volume of pores between 10 – 100 nm can be densified, restricting the transport properties, resulting in an enhanced resistance to chloride penetration. By using PONKCS and Rietveld methods, it is found that the reaction degree of recycled waste glass in blended cement is controlled by the cement replacement ratio. The theoretical Ca/Si and (Na+Ca)/Si ratio in the reaction products are influenced by the reaction degree. A higher reaction degree of glass particles seems to induce a low Ca/Si and (Na+Ca)/Si ratio. We find that an amount of 0.38 to 0.62 mole of calcium hydroxide is consumed by every mole of waste glass, while 1 to 2.5 mole water is combined in the reaction products in the presented results.

12.1.2 Recycled waste glass as a binder in alkali activated materials

From Chapter 6 to Chapter 8, the recycled waste glass forms part of an alkali activated binders systems in blends containing GGBS and FA. As a silica-rich material, RGP can play a role as the amorphous silica source to form (N)-C-(A)-S-H during alkali activation. The addition of recycled waste glass in GGBS/FA systems usually increases the avilaiable silica in raw mixtures, while at the same time, the Ca/(Si+Al) ratio in reaction products can be decreased. This change is accompanied by increased of Si-O polymerization during alkali activation, observed as a shift to higher wavenumbers in the FTIR spectra. In addition, the incorporation of recycled waste glass is accompanied by an increase in total shrinkage for $NaOH/Na_2CO_3$ activated GGBS/FA binder systems with a slight decrease in the strength performance at 28 days. However, a significant improvement of resistance to aggressive carbonation.

A reaction between alkali activated materials and CO_2 is of much concern because the

carbonation reaction can directly modify the C-(A)-S-H and cause the deterioration of strength and durability. As noticed, after activation by a nearly neutral activator such as Na_2CO_3, GGBS samples exhibit a poorer resistance to carbonation compared to NaOH activation due to the lower alkalinity and presence of CO_3^{-2} instead of OH^- in LDH. The addition of recycled waste glass in Na_2CO_3 activated GGBS mortars enhances the resistance to carbonation by modifying reaction products and microstructures without strength reduction. The resistance is even better than for commercial water glass incorporation. The carbonation shrinkage is reduced after RGP incorporation; at the same time, a higher strength performance is observed. The RGP in sodium carbonate activated GGBS blends shows no influence on the species of reaction products. However, after carbonation, the sample containing RGP promotes the formation of nahcolite, while less bound water loss and calcium carbonates formation are found. A high volume of gel pores (<10 nm) is formed in the RGP sample compared to specimens only containing GGBS. These properties contribute to a better resistance to carbonation for RGP containing sodium carbonate activated GGBS mortars.

Based on the alkali activation products (similar to sodium silicates) of recycled waste glass, an alkali-thermal pretreatment at low temperature is conducted. Afterwards, the treated waste glass is successfully applied as one part solid activator and binder in alumina-silicate mortars with GGBS. The mechanical performance of prepared mortars is comparable to cement mortar made using CEM I 52.5 R at both early and late ages. It is interesting to notice that the main reaction product of recycled waste glass after alkali-thermal treatment is Na_2SiO_3, which is the main component of commercial water glass. The various initial effective modulus (EMs) in treatment results in the formation of different products, for example, the amount of Na_2SiO_3 in treated blends. A low EMs promotes the formation of Na_2SiO_3, with a higher reaction degree of the recycled waste glass. The compressive strength of one part mortar containing treated blends with EMs 1.0 achieves 55.8 MPa after 28 days. The treated recycled waste glass can be a low price and low energy consumption alternatives for commercial water glass in one part concrete preparation.

12.1.3 Converter steel slag composites in CO_2 activation

Chapter 9 to Chapter 11 focus on the application of converter steel slag in sustainable and low carbon footprint building materials by CO_2 pre-treatment and CO_2 activation. The carbonation products of converter steel slag at ambient conditions are various calcium carbonate polymorphs: calcite, aragonite, vaterite and even amorphous calcium carbonate. Besides these carbonates, as part of the carbonation reaction of the calcium silicate phases in steel slag, a silica gel forms poessing an amorphous structure and

presenting a highly pozzolanic reactivity similar to nano-silica and silica fume. This makes carbonated converter steel slag an attractive option as SCMs in eco-ultra high performance concrete (UHPC) design, with additional bonus of sequestrated CO_2 in addition to cement replacement as part of eco-UHPC.

Due to the precipitation of calcium carbonates and silica gel on the surface of CO_2 treated steel slag particles, clinker phase hydration, for example, C_3S, can be improved. In addition, the formation of ettringite is promoted. Furthermore, the silica gel can react with calcium hydroxide from cement hydration, forming secondary C-S-H, which improves the binding between the hydrated cement and carbonated steel slag particles. As a consequence, 45% of cement can be replaced by carbonated steel slag in eco-UHPC, and the strength achieved can still be more than 150 MPa. Particularly, the V and Cr leaching from carbonated converter steel slag can be effectively remediated with the C-S-H and AFm from cement hydration. It can be concluded that converter steel slag after carbonation treatment exhibits a better performance than before in eco-UHPC.

The CO_2 not only can improve the properties of steel slag powder but can also activate high volume steel slag based mortars at ambient curing conditions. By combining 20% of OPC and 80% of steel slag as binder, green mortars can be produced for CO_2 activation. However, the steel slag particle size effectively influences the performance of these green mortars by affecting the CO_2 penetration and controlling carbonation process. The application of optimal size ranges of steel slag (21.75 to 24.13 μm) in blended mortars leads to a higher compressive strength (31.21 MPa), CO_2 uptake (15.9%), faster carbonation rates as well as sustainability efficiency (0.486 MPa/(kg/m^3)), which is superior compared to the use of larger or smaller size steel slags in mortars. To achieve fast carbonation at ambient conditions, the OPC component even can be replaced by alkali activated GGBS to provide the necessary early age strength before carbonation. A faster carbonation rate and strength development are observed in alkali/CO_2 activated GGBS/steel slag mortars. The highest compressive strength achieved 44 MPa and full carbonation can be observed after only 11 days CO_2 activation. The reaction products from alkali activated GGBS are also identified to contribute CO_2 uptake ability. Thus, cement-free steel slag based mortars based on combined alkali/CO_2 activation can be developed, making feasible the manufacturing of low carbon footprint building materials.

12.2 Recommendations for future studies

This thesis investigates the high-end application of two by-products – recycled waste glass and converter steel slag in the manufacture of sustainable building materials.

Based on the chemical compositions and character of these secondary raw materials, different activation methods are selected for optimal utilization in building materials, for example, as SCMs in cement-based system, as a binder in alkali activation and as components in CO_2 activation. The presented results can be used for an optimal design of sustainable building materials to achieve properties of excellent durability, low costs and low emissions. Nevertheless, some open questions are remaining for future research:

1. The application of recycled waste glass as SCM in blended cement results in the modification of reaction products by introducing more sodium and silica. Consequently, the properties of the related microstructure could be changed, as well as the durability performance. As shown in this thesis, the resistance to chloride penetration is enhanced even when recycled waste glass is introduced as high volume cement replacement. However, the high volume of recycled waste glass in blended cement can result in a significant decrease of Ca/(Si+Al) and increase of Na/Ca. As a consequence, ASR expansion is possibly induced posing a potential risk. Therefore, the mechanism of potential ASR expansion should be studied in high volume recycled waste glass blended cement concrete.

2. The carbonation behaviour of alkali activated materials is getting intense scrutiny in recent years. The carbonation conditions such as CO_2 dosage, temperature and humidity can strongly influence the reaction products, as well as the carbonation process of related samples. The carbonation behaviour of recycled waste glass containing mortars in this thesis is studied at a high CO_2 dosage, which could be different from the practical situation. Also, the activator type seems to affect the carbonation of alkali activated materials. So, further investigation for a better understanding of the performance of recycled waste glass in alkali activated materials should be undertaken.

3. The production of sodium silicate precursor from the recycled waste glass at low temperature is successfully achieved in this thesis. However, the reaction process can still be optimized to produce lower costs precursors, regarding temperature, duration, drying conditions and alkali compositions. Furthermore, the application of alkali-thermal treated recycled waste glass in one part concrete may result in a different reaction mechanism from commercial water glass, and the shrinkage and carbonation behaviour could be modified, which also need further investigation.

4. The converter steel slag after CO_2 pre-treatment shows better feasibility as SCMs in eco-UHPC design. A more detailed study should be conducted to address the correlation between carbonation degree and potential pozzolanic reactivity, as well as leaching behaviour.

5. The activation performance of CO_2 with converter steel slag based building materials at ambient conditions mostly depends on the CO_2 diffusion and dissolution in the pore fluid of specimen. Therefore, the initial boundary conditions, for instance, porosity, pore size distribution, reaction products and pore solution chemistry need to be considered for the optimization of green concrete design and curing strategy.

Bibliography

Abdel-Gawwad, H.A., Heikal, E., El-Didamony, H., Hashim, F.S., Mohammed, A.H., 2018. Recycling of concrete waste to produce ready-mix alkali activated cement. Ceram. Int. 44, 7300–7304. https://doi.org/10.1016/j.ceramint.2018.01.042

Abdel-Gawwad, H.A., Rashad, A.M., Heikal, M., 2019. Sustainable utilization of pretreated concrete waste in the production of one-part alkali-activated cement. J. Clean. Prod. 232, 318–328. https://doi.org/10.1016/j.jclepro.2019.05.356

Abdul-baki, G., 2017. Development of vacuum carbonation curing technology for concrete at ambient conditions. McGill University.

Adesanya, E., Ohenoja, K., Luukkonen, T., Kinnunen, P., Illikainen, M., 2018. One-part geopolymer cement from slag and pretreated paper sludge. J. Clean. Prod. 185, 168–175. https://doi.org/10.1016/j.jclepro.2018.03.007

Ahmad, S., Assaggaf, R.A., Maslehuddin, M., Al-Amoudi, O.S.B., Adekunle, S.K., Ali, S.I., 2017. Effects of carbonation pressure and duration on strength evolution of concrete subjected to accelerated carbonation curing. Constr. Build. Mater. 136, 565–573. https://doi.org/10.1016/j.conbuildmat.2017.01.069

Alarcon-Ruiz, L., Platret, G., Massieu, E., Ehrlacher, A., 2005. The use of thermal analysis in assessing the effect of temperature on a cement paste. Cem. Concr. Res. 35, 609–613. https://doi.org/10.1016/j.cemconres.2004.06.015

Alderete, N., Villagrán, Y., Mignon, A., Snoeck, D., De Belie, N., 2017. Pore structure description of mortars containing ground granulated blast-furnace slag by mercury intrusion porosimetry and dynamic vapour sorption. Constr. Build. Mater. 145, 157–165. https://doi.org/10.1016/j.conbuildmat.2017.03.245

Aliabdo, A.A., Abd Elmoaty, A.E.M., Aboshama, A.Y., 2016. Utilization of waste glass powder in the production of cement and concrete. Constr. Build. Mater. 124, 866–877. https://doi.org/10.1016/j.conbuildmat.2016.08.016

Ambily, P.S., Umarani, C., Ravisankar, K., Prem, P.R., Bharatkumar, B.H., Iyer, N.R., 2015. Studies on ultra high performance concrete incorporating copper slag as fine aggregate. Constr. Build. Mater. 77, 233–240. https://doi.org/10.1016/j.conbuildmat.2014.12.092

Andrew, R.M., 2018. Global CO_2 emissions from cement production. Earth Syst. Sci. Data 10, 195–217. https://doi.org/10.5194/essd-10-195-2018

Atahan, H.N., Oktar, O.N., Taşdemir, M.A., 2009. Effects of water-cement ratio and curing time on the critical pore width of hardened cement paste. Constr. Build. Mater. 23, 1196–1200. https://doi.org/10.1016/j.conbuildmat.2008.08.011

Ataie, F.F., Juenger, M.C.G., Taylor-Lange, S.C., Riding, K.A., 2015. Comparison of the retarding mechanisms of zinc oxide and sucrose on cement hydration and interactions with supplementary cementitious materials. Cem. Concr. Res. 72, 128–136. https://doi.org/10.1016/j.cemconres.2015.02.023

Aydın, S., Baradan, B., 2014. Effect of activator type and content on properties of alkali-activated slag mortars. Compos. Part B Eng. 57, 166–172. https://doi.org/10.1016/j.compositesb.2013.10.001

Baciocchi, R., Costa, G., Di Bartolomeo, E., Polettini, A., Pomi, R., 2011. Wet versus slurry carbonation of EAF steel slag. Greenh. Gases Sci. Technol. 1, 312–319. https://doi.org/10.1002/ghg.38

Baciocchi, R., Costa, G., Di Gianfilippo, M., Polettini, A., Pomi, R., Stramazzo, A., 2015. Thin-film versus slurry-phase carbonation of steel slag: CO_2 uptake and effects on mineralogy. J. Hazard. Mater. 283, 302–313. https://doi.org/10.1016/j.jhazmat.2014.09.016

Baciocchi, R., Costa, G., Polettini, A., Pomi, R., 2015. Effects of thin-film accelerated carbonation on steel slag leaching. J. Hazard. Mater. 286, 369–378. https://doi.org/10.1016/J.JHAZMAT.2014.12.059

Baciocchi, R., Costa, G., Polettini, A., Pomi, R., 2009. Influence of particle size on the carbonation of stainless steel slag for CO_2 storage. Energy Procedia 1, 4859–4866. https://doi.org/10.1016/j.egypro.2009.02.314

Bakharev, T., Sanjayan, J., Cheng, Y.-B., 2003. Resistance of alkali-activated slag concrete to acid attack. Cem. Concr. Res. 33, 1607–1611. https://doi.org/10.1016/S0008-8846(03)00125-X

Bakharev, T., Sanjayan, J.G., Cheng, Y.B., 2001. Resistance of alkali-activated slag concrete to carbonation. Cem. Concr. Res. 31, 1277–1283. https://doi.org/10.1016/S0008-8846(01)00574-9

Ballekere Kumarappa, D., Peethamparan, S., Ngami, M., 2018. Autogenous shrinkage of alkali activated slag mortars: Basic mechanisms and mitigation methods. Cem. Concr. Res. 109, 1–9. https://doi.org/10.1016/j.cemconres.2018.04.004

Barrett, E.P., Joyner, L.G., Halenda, P.P., 1951. The Determination of Pore Volume and Area Distributions in Porous Substances. I. Computations from Nitrogen Isotherms. J. Am. Chem. Soc. 73, 373–380. https://doi.org/10.1021/ja01145a126

Ben Haha, M., Le Saout, G., Winnefeld, F., Lothenbach, B., 2011. Influence of activator type on hydration kinetics, hydrate assemblage and microstructural development of alkali activated blast-furnace slags. Cem. Concr. Res. 41, 301–310. https://doi.org/10.1016/j.cemconres.2010.11.016

Bentz, D.P., 2006. Influence of water-to-cement ratio on hydration kinetics: Simple models based on spatial considerations. Cem. Concr. Res. 36, 238–244. https://doi.org/10.1016/j.cemconres.2005.04.014

Bentz, D.P., Ferraris, C.F., Jones, S.Z., Lootens, D., Zunino, F., 2017. Limestone and silica powder replacements for cement: Early-age performance. Cem. Concr. Compos. 78, 43–56. https://doi.org/10.1016/j.cemconcomp.2017.01.001

Bernal, S.A., 2015. Effect of the activator dose on the compressive strength and accelerated carbonation resistance of alkali silicate-activated slag/metakaolin blended materials. Constr. Build. Mater. 98, 217–226. https://doi.org/10.1016/j.conbuildmat.2015.08.013

Bernal, S.A., de Gutierrez, R.M., Provis, J.L., Rose, V., 2010. Effect of silicate modulus and metakaolin incorporation on the carbonation of alkali silicate-activated slags. Cem. Concr. Res. 40, 898–907. https://doi.org/10.1016/j.cemconres.2010.02.003

Bernal, S.A., Provis, J.L., Brice, D.G., Kilcullen, A., Duxson, P., Van Deventer, J.S.J., 2012. Accelerated carbonation testing of alkali-activated binders significantly underestimates service life: The role of pore solution chemistry. Cem. Concr. Res. 42, 1317–1326. https://doi.org/10.1016/j.cemconres.2012.07.002

Bernal, S.A., Provis, J.L., Myers, R.J., San Nicolas, R., van Deventer, J.S.J., 2015. Role of carbonates in the chemical evolution of sodium carbonate-activated slag binders. Mater. Struct. 48, 517–529. https://doi.org/10.1617/s11527-014-0412-6

Bernal, S.A., Provis, J.L., Rose, V., Mejía de Gutierrez, R., 2011. Evolution of binder structure in sodium silicate-activated slag-metakaolin blends. Cem. Concr. Compos. 33, 46–54. https://doi.org/10.1016/j.cemcomcomp.2010.09.004

Bernal, S.A., Provis, J.L., Walkley, B., San Nicolas, R., Gehman, J.D., Brice, D.G., Kilcullen, A.R., Duxson, P., van Deventer, J.S.J., 2013. Gel nanostructure in alkali-activated binders based on slag and fly ash, and effects of accelerated carbonation. Cem. Concr. Res. 53, 127–144. https://doi.org/10.1016/j.cemconres.2013.06.007

Bernal, S.A., San Nicolas, R., Myers, R.J., Mejía de Gutiérrez, R., Puertas, F., van Deventer, J.S.J., Provis, J.L., 2014. MgO content of slag controls phase evolution and structural changes induced by accelerated carbonation in alkali-activated binders. Cem. Concr. Res. 57, 33–43. https://doi.org/10.1016/j.cemconres.2013.12.003

Bignozzi, M.C., Saccani, A., Barbieri, L., Lancellotti, I., 2015. Glass waste as supplementary cementing materials:

The effects of glass chemical composition. Cem. Concr. Compos. 55, 45–52. https://doi.org/10.1016/j.cemconcomp.2014.07.020

Bijen, J., 1996. Benefits of slag and fly ash. Constr. Build. Mater. 10, 309–314. https://doi.org/10.1016/0950-0618(95)00014-3

Bilim, C., Duran Atiş, C., 2017. Carbonation resistance of slag mortars activated by different alkali activators. Turkey Turkish J. Eng. 1, 1–4. https://doi.org/10.31127/tuje.315227

Bishop, M., Barron, A.R., 2006. Cement Hydration Inhibition with Sucrose , Tartaric Acid , and Lignosulfonate : Analytical and Spectroscopic Study 7042–7049. https://doi.org/10.1021/ie060806t

Boddy, A.M., Hooton, R.D., Thomas, M.D.A., 2003. The effect of the silica content of silica fume on its ability to control alkali-silica reaction. Cem. Concr. Res. 33, 1263–1268. https://doi.org/10.1016/S0008-8846(03)00058-9

Bodor, M., Santos, R.M., Cristea, G., Salman, M., Cizer, O., Iacobescu, R.I., Chiang, Y.W., Van Balen, K., Vlad, M., Van Gerven, T., 2016. Laboratory investigation of carbonated BOF slag used as partial replacement of natural aggregate in cement mortars. Cem. Concr. Compos. 65, 55–66. https://doi.org/10.1016/j.cemconcomp.2015.10.002

Bonen, D., Sarkar, S.L., 1995. The effects of simulated environmental attack on immobilization of heavy metals doped in cement-based materials. J. Hazard. Mater. 40, 321–335. https://doi.org/10.1016/0304-3894(94)00091-T

Borges, P.H.R., Costa, J.O., Milestone, N.B., Lynsdale, C.J., Streatfield, R.E., 2009. Carbonation of CH and C-S-H in composite cement pastes containing high amounts of BFS. Cem. Concr. Res. 40, 284–292. https://doi.org/10.1016/j.cemconres.2009.10.020

Bouikni, A., Swamy, R.N., Bali, A., 2009. Durability properties of concrete containing 50% and 65% slag. Constr. Build. Mater. 23, 2836–2845. https://doi.org/10.1016/j.conbuildmat.2009.02.040

Brough, A.R., Atkinson, A., 2002. Sodium silicate-based, alkali-activated slag mortars: Part I. Strength, hydration and microstructure. Cem. Concr. Res. 32, 865–879. https://doi.org/10.1016/S0008-8846(02)00717-2

Brouwers, H.J.H., 2016. Packing fraction of particles with a Weibull size distribution. Phys. Rev. E 94, 12905. https://doi.org/10.1103/PhysRevE.94.012905

Brouwers, H.J.H., 2006. Particle-size distribution and packing fraction of geometric random packings. Phys. Rev. E 74. https://doi.org/10.1103/PhysRevE.74.031309

Brouwers, H. J.H., Radix, H.J., 2005. Self-compacting concrete: Theoretical and experimental study. Cem. Concr. Res. 35, 2116–2136. https://doi.org/10.1016/j.cemconres.2005.06.002

Brouwers, H.J.H., van Eijk, R.J., 2003. Alkali concentrations of pore solution in hydrating OPC. Cem. Concr. Res. 33, 191–196. https://doi.org/10.1016/S0008-8846(02)01022-0

Brunauer, S., Emmett, P.H., Teller, E., 1938. Adsorption of Gases in Multimolecular Layers. J. Am. Chem. Soc. 60, 309–319. https://doi.org/10.1021/ja01269a023

BS EN, 2005. Methods of testing cement —Part 1: Determination of strength 3.

Bueno, E.T., Paris, J.M., Clavier, K.A., Spreadbury, C., Ferraro, C.C., Townsend, T.G., 2020. A review of ground waste glass as a supplementary cementitious material: A focus on alkali-silica reaction. J. Clean. Prod. https://doi.org/10.1016/j.jclepro.2020.120180

Bullard, J.W., Jennings, H.M., Livingston, R.A., Nonat, A., Scherer, G.W., Schweitzer, J.S., Scrivener, K.L., Thomas, J.J., 2011. Mechanisms of cement hydration. Cem. Concr. Res. 41, 1208–1223. https://doi.org/10.1016/j.cemconres.2010.09.011

Burciaga-Díaz, O., Betancourt-Castillo, I., 2018. Characterization of novel blast-furnace slag cement pastes and mortars activated with a reactive mixture of MgO-NaOH. Cem. Concr. Res. 105, 54–63.

https://doi.org/10.1016/j.cemconres.2018.01.002

Burns, A., Brack, H.P., Risen, W.M., 1991. Dielectric and infrared reflectance studies of inorganic oxide glasses. J. Non. Cryst. Solids 131–133, 994–1000. https://doi.org/10.1016/0022-3093(91)90714-H

Caprai, V., Schollbach, K., Brouwers, H.J.H., 2018. Influence of hydrothermal treatment on the mechanical and environmental performances of mortars including MSWI bottom ash. Waste Manag. 78, 639–648. https://doi.org/10.1016/j.wasman.2018.06.030

Chang, J., Wang, D., Fang, Y., 2018. Effects of mineralogical changes in BOFS during carbonation on pH and Ca and Si leaching. Constr. Build. Mater. 192, 584–592. https://doi.org/10.1016/j.conbuildmat.2018.10.057

Cheah, C.B., Ramli, M., 2012. Mechanical strength , durability and drying shrinkage of structural mortar containing HCWA as partial replacement of cement. Constr. Build. Mater. 30, 320–329. https://doi.org/10.1016/j.conbuildmat.2011.12.009

Chen-Tan, N.W., van Riessen, A., LY, C. V., Southam, D.C., 2009. Determining the Reactivity of a Fly Ash for Production of Geopolymer. J. Am. Ceram. Soc. 92, 881–887. https://doi.org/10.1111/j.1551-2916.2009.02948.x

Chen, J.J., Thomas, J.J., Jennings, H.M., 2006. Decalcification shrinkage of cement paste. Cem. Concr. Res. 36, 801–809. https://doi.org/10.1016/j.cemconres.2005.11.003

Chen, T., Gao, X., Ren, M., 2018. Effects of autoclave curing and fly ash on mechanical properties of ultra-high performance concrete. Constr. Build. Mater. 158, 864–872. https://doi.org/10.1016/j.conbuildmat.2017.10.074

Chen, W., Brouwers, H.J.H., 2010. Alkali binding in hydrated Portland cement paste. Cem. Concr. Res. 40, 716–722. https://doi.org/10.1016/j.cemconres.2009.12.007

Chen, W., Brouwers, H.J.H., 2007. The hydration of slag, part 2: reaction models for blended cement. J. Mater. Sci. 42, 444–464. https://doi.org/10.1007/s10853-006-0874-1

Chen, Y., Shui, Z., Chen, W., Chen, G., 2015. Chloride binding of synthetic Ca–Al–NO_3 LDHs in hardened cement paste. Constr. Build. Mater. 93, 1051–1058. https://doi.org/10.1016/j.conbuildmat.2015.05.047

Cheyrezy, M., Maret, V., Frouin, L., 1995. Microstructural analysis of RPC (Reactive Powder Concrete). Cem. Concr. Res. 25, 1491–1500. https://doi.org/10.1016/0008-8846(95)00143-Z

Collins, F., Sanjayan, J.., 2000. Effect of pore size distribution on drying shrinking of alkali-activated slag concrete. Cem. Concr. Res. 30, 1401–1406. https://doi.org/10.1016/S0008-8846(00)00327-6

Cook, R.A., Hover, K.C., 1999. Mercury porosimetry of hardened cement pastes. Cem. Concr. Res. 29, 933–943. https://doi.org/10.1016/S0008-8846(99)00083-6

Coppola, B., Palmero, P., Montanaro, L., Tulliani, J.M., 2019. Alkali-activation of marble sludge: Influence of curing conditions and waste glass addition. J. Eur. Ceram. Soc. https://doi.org/10.1016/j.jeurceramsoc.2019.11.068

Costa, D.G., Rocha, A.B., Souza, W.F., Chiaro, S.S.X., Leitão, A.A., 2012. Comparative Structural, thermodynamic and electronic analyses of ZnAlAn− hydrotalcite-like compounds (An $^{-}Cl^{-}$, F^{-}, Br^{-}, OH^{-}, CO_3^{2-} or NO_3^{-}): An ab initio study. Appl. Clay Sci. 56, 16–22. https://doi.org/10.1016/J.CLAY.2011.11.014

Costa, G., Polettini, A., Pomi, R., Stramazzo, A., 2016. Leaching modelling of slurry-phase carbonated steel slag. J. Hazard. Mater. 302, 415–425. https://doi.org/10.1016/j.jhazmat.2015.10.005

Crossin, E., 2015. The greenhouse gas implications of using ground granulated blast furnace slag as a cement substitute. J. Clean. Prod. 95, 101–108. https://doi.org/10.1016/j.jclepro.2015.02.082

Damineli, B.L., Kemeid, F.M., Aguiar, P.S., John, V.M., 2010. Measuring the eco-efficiency of cement use. Cem. Concr. Compos. 32, 555–562. https://doi.org/10.1016/j.cemconcomp.2010.07.009

De Larrard, F., Sedran, T., 1994. Optimization of ultra-high-performance concrete by the use of a packing model.

Cem. Concr. Res. 24, 997–1009. https://doi.org/10.1016/0008-8846(94)90022-1

Dembovska, L., Bajare, D., Pundiene, I., Vitola, L., 2017. Effect of Pozzolanic Additives on the Strength Development of High Performance Concrete. Procedia Eng. 172, 202–210. https://doi.org/10.1016/J.PROENG.2017.02.050

Deschner, F., Winnefeld, F., Lothenbach, B., Seufert, S., Schwesig, P., Dittrich, S., Goetz-Neunhoeffer, F., Neubauer, J., 2012. Hydration of Portland cement with high replacement by siliceous fly ash. Cem. Concr. Res. 42, 1389–1400. https://doi.org/10.1016/j.cemconres.2012.06.009

DIN E N, 2007. Methods of Test for Mortar for Masonry—Part 3: Determination of Consistence of Fresh Mortar (by Flow Table) 1–11.

Du, H., Tan, K.H., 2017. Properties of high volume glass powder concrete. Cem. Concr. Compos. 75, 22–29. https://doi.org/10.1016/j.cemconcomp.2016.10.010

Du, H., Tan, K.H., 2014. Effect of particle size on alkali-silica reaction in recycled glass mortars. Constr. Build. Mater. 66, 275–285. https://doi.org/10.1016/j.conbuildmat.2014.05.092

Du, H., Tan, K.H., 2014. Waste Glass Powder as Cement Replacement in Concrete. J. Adv. Concr. Technol. 12, 468–477. https://doi.org/10.3151/jact.12.468

Du, H., Tan, K.H., 2013. Use of waste glass as sand in mortar: Part II - Alkali-silica reaction and mitigation methods. Cem. Concr. Compos. 35, 109–117. https://doi.org/10.1016/j.cemconcomp.2012.08.029

Dung, N.T., Hooper, T.J.N., Unluer, C., 2019. Accelerating the reaction kinetics and improving the performance of Na_2CO_3-activated GGBS mixes. Cem. Concr. Res. 126, 105927. https://doi.org/10.1016/j.cemconres.2019.105927

Duxson, P., Provis, J.L., 2008. Designing Precursors for Geopolymer Cements. J. Am. Ceram. Soc. 91, 3864–3869. https://doi.org/10.1111/j.1551-2916.2008.02787.x

El-Naas, M.H., El Gamal, M., Hameedi, S., Mohamed, A.M.O., 2015. CO_2 sequestration using accelerated gas-solid carbonation of pre-treated EAF steel-making bag house dust. J. Environ. Manage. 156, 218–224. https://doi.org/10.1016/j.jenvman.2015.03.040

EN, D., 2009. Methods of testing cement – Part 3: Determination of setting times and soundness.

Eugster, H.P., 1966. Sodium carbonate-bicarbonate minerals as indicators of P CO_2 . J. Geophys. Res. 71, 3369–3377. https://doi.org/10.1029/jz071i014p03369

EUROFER, 2018. European Steel in Figures 2018. https://doi.org/10.1016/S0008-8846(99)00213-6

Fang, G., Bahrami, H., Zhang, M., 2018. Mechanisms of autogenous shrinkage of alkali-activated fly ash-slag pastes cured at ambient temperature within 24 h. Constr. Build. Mater. 171, 377–387. https://doi.org/10.1016/j.conbuildmat.2018.03.155

Federico, L.M., Chidiac, S.E., 2009. Waste glass as a supplementary cementitious material in concrete - Critical review of treatment methods. Cem. Concr. Compos. 31, 606–610. https://doi.org/10.1016/j.cemconcomp.2009.02.001

Feiz, R., Ammenberg, J., Eklund, M., Helgstrand, A., Marshall, R., 2015. Improving the CO_2 performance of cement, part I: utilizing life-cycle assessment and key performance indicators to assess development within the cement industry. J. Clean. Prod. 98, 272–281. https://doi.org/10.1016/J.JCLEPRO.2014.01.083

Fernández-Jiménez, A., Palomo, J.G., Puertas, F., 1999. Alkali-activated slag mortars: Mechanical strength behaviour. Cem. Concr. Res. 29, 1313–1321. https://doi.org/10.1016/S0008-8846(99)00154-4

Fernández-Jiménez, A., Puertas, F., 2003. Effect of activator mix on the hydration and strength behaviour of alkali-activated slag cements. Adv. Cem. Res. 15, 129–136. https://doi.org/10.1680/adcr.2003.15.3.129

Fernández-Jiménez, A., Puertas, F., Sobrados, I., Sanz, J., 2003. Structure of Calcium Silicate Hydrates Formed in Alkaline-Activated Slag: Influence of the Type of Alkaline Activator. J. Am. Ceram. Soc. 86, 1389–1394.

https://doi.org/10.1111/j.1151-2916.2003.tb03481.x

Fernández Bertos, M., Simons, S.J.R., Hills, C.D., Carey, P.J., 2004. A review of accelerated carbonation technology in the treatment of cement-based materials and sequestration of CO_2. J. Hazard. Mater. 112, 193–205. https://doi.org/10.1016/j.jhazmat.2004.04.019

Fernandez, R., Martirena, F., Scrivener, K.L., 2011. The origin of the pozzolanic activity of calcined clay minerals: A comparison between kaolinite, illite and montmorillonite. Cem. Concr. Res. 41, 113–122. https://doi.org/10.1016/j.cemconres.2010.09.013

Filipponi, P., Polettini, A., Pomi, R., Sirini, P., 2003. Physical and mechanical properties of cement-based products containing incineration bottom ash. Waste Manag. 23, 145–156. https://doi.org/10.1016/S0956-053X(02)00041-7

Gao, X., Yu, Q.L., Brouwers, H.J.H., 2016. Assessing the porosity and shrinkage of alkali activated slag-fly ash composites designed applying a packing model. Constr. Build. Mater. 119, 175–184. https://doi.org/10.1016/j.conbuildmat.2016.05.026

Gao, X., Yu, Q.L., Brouwers, H.J.H., 2015. Reaction kinetics, gel character and strength of ambient temperature cured alkali activated slag–fly ash blends. Constr. Build. Mater. 80, 105–115. https://doi.org/10.1016/j.conbuildmat.2015.01.065

Gao, X., Yu, Q.L., Lazaro, A., Brouwers, H.J.H., 2017. Investigation on a green olivine nano-silica source based activator in alkali activated slag-fly ash blends: Reaction kinetics, gel structure and carbon footprint. Cem. Concr. Res. 100, 129–139. https://doi.org/10.1016/j.cemconres.2017.06.007

Garbev, K., Beuchle, G., Bornefeld, M., Black, L., Stemmermann, P., 2008. Cell dimensions and composition of nanocrystalline calcium silicate hydrate solid solutions. Part 1: synchrotron-based x-ray diffraction. J. Am. Ceram. Soc. 91, 3005–3014. https://doi.org/10.1111/j.1551-2916.2008.02484.x

Garci Juenger, M.C., Jennings, H.M., 2002. New insights into the effects of sugar on the hydration and microstructure of cement pastes. Cem. Concr. Res. 32, 393–399. https://doi.org/10.1016/S0008-8846(01)00689-5

Garci Juenger, M.C., Jennings, H.M., 2002. Examining the relationship between the microstructure of calcium silicate hydrate and drying shrinkage of cement pastes. Cem. Concr. Res. 32, 289–296. https://doi.org/10.1016/S0008-8846(01)00673-1

Garci Juenger, M.C., Jennings, H.M., 2001. The use of nitrogen adsorption to assess the microstructure of cement paste. Cem. Concr. Res. 31, 883–892. https://doi.org/10.1016/S0008-8846(01)00493-8

García-Lodeiro, I., Fernández-Jiménez, A., Blanco, M.T., Palomo, A., 2008. FTIR study of the sol-gel synthesis of cementitious gels: C-S-H and N-A-S-H. J. Sol-Gel Sci. Technol. 45, 63–72. https://doi.org/10.1007/s10971-007-1643-6

García Lodeiro, I., Macphee, D.E., Palomo, A., Fernández-Jiménez, A., 2009. Effect of alkalis on fresh C-S-H gels. FTIR analysis. Cem. Concr. Res. 39, 147–153. https://doi.org/10.1016/j.cemconres.2009.01.003

Ghacham, A. Ben, Pasquier, L.C., Cecchi, E., Blais, J.F., Mercier, G., 2016. CO_2 sequestration by mineral carbonation of steel slags under ambient temperature: parameters influence, and optimization. Environ. Sci. Pollut. Res. 23, 17635–17646. https://doi.org/10.1007/s11356-016-6926-4

Ghafari, E., Arezoumandi, M., Costa, H., Júlio, E., 2015. Influence of nano-silica addition in the durability of UHPC. Constr. Build. Mater. 94, 181–188. https://doi.org/10.1016/j.conbuildmat.2015.07.009

Ghafari, E., Ghahari, S.A., Costa, H., Júlio, E., Portugal, A., Durães, L., 2016. Effect of supplementary cementitious materials on autogenous shrinkage of ultra-high performance concrete. Constr. Build. Mater. 127, 43–48. https://doi.org/10.1016/j.conbuildmat.2016.09.123

Gholampour, A., Ozbakkaloglu, T., 2017. Performance of sustainable concretes containing very high volume

Class-F fly ash and ground granulated blast furnace slag. J. Clean. Prod. 162, 1407–1417. https://doi.org/10.1016/j.jclepro.2017.06.087

Gomes, H.I., Mayes, W.M., Rogerson, M., Stewart, D.I., Burked, I.T., 2016. Alkaline residues and the environment: A review of impacts, management practices and opportunities. J. Clean. Prod. https://doi.org/10.1016/j.jclepro.2015.09.111

Gonen, T., Yazicioglu, S., 2007. The influence of compaction pores on sorptivity and carbonation of concrete. Constr. Build. Mater. 21, 1040–1045. https://doi.org/10.1016/j.conbuildmat.2006.02.010

Goñi, S., Frias, M., Vegas, I., García, R., Vigil De La Villa, R., 2012. Effect of ternary cements containing thermally activated paper sludge and fly ash on the texture of C-S-H gel. Constr. Build. Mater. 30, 381–388. https://doi.org/10.1016/j.conbuildmat.2011.12.002

Haha, M. Ben, Lothenbach, B., Le Saout, G., Winnefeld, F., 2011. Influence of slag chemistry on the hydration of alkali-activated blast-furnace slag - Part I: Effect of MgO. Cem. Concr. Res. 41, 955–963. https://doi.org/10.1016/j.cemconres.2011.05.002

Hajimohammadi, A., Ngo, T., Kashani, A., 2018. Glass waste versus sand as aggregates: The characteristics of the evolving geopolymer binders. J. Clean. Prod. 193, 593–603. https://doi.org/10.1016/j.jclepro.2018.05.086

Hajimohammadi, A., van Deventer, J.S.J., 2017. Solid Reactant-Based Geopolymers from Rice Hull Ash and Sodium Aluminate. Waste and Biomass Valorization 8, 2131–2140. https://doi.org/10.1007/s12649-016-9735-6

Häkkinen, T., 1993. The influence of slag content on the microstructure, permeability and mechanical properties of concrete Part 1 Microstructural studies and basic mechanical properties. Cem. Concr. Res. 23, 407–421. https://doi.org/10.1016/0008-8846(93)90106-J

Hong, H., Xiao-dong, S., 2014. Interaction effect of triisopropanolamine and glucose on the hydration of Portland cement. Constr. Build. Mater. 65, 360–366. https://doi.org/10.1016/j.conbuildmat.2014.04.077

Hong, S.-Y., Glasser, F.P., 1999. Alkali binding in cement pastes: Part I. The C-S-H phase. Cem. Concr. Res. 29, 1893–1903. https://doi.org/10.1016/S0008-8846(99)00187-8

Hu, C., 2014. Microstructure and mechanical properties of fly ash blended cement pastes. Constr. Build. Mater. 73, 618–625. https://doi.org/10.1016/j.conbuildmat.2014.10.009

Huang, W., Kazemi-Kamyab, H., Sun, W., Scrivener, K., 2017. Effect of cement substitution by limestone on the hydration and microstructural development of ultra-high performance concrete (UHPC). Cem. Concr. Compos. 77, 86–101. https://doi.org/10.1016/j.cemconcomp.2016.12.009

Hui, Z., Poon, C.S., Ling, T.C., 2013. Properties of mortar prepared with recycled cathode ray tube funnel glass sand at different mineral admixture. Constr. Build. Mater. 40, 951–960. https://doi.org/10.1016/j.conbuildmat.2012.11.102

Huijgen, W.J.J., 2005. Mineral CO_2 Sequestration by Steel Slag Carbonation. Environ. Sci. Technol. 39, 9676–9682. https://doi.org/10.1021/es050795f

Huijgen, W.J.J., Comans, R.N.J., 2006. Carbonation of steel slag for CO_2 sequestration: Leaching of products and reaction mechanisms. Environ. Sci. Technol. 40, 2790–2796. https://doi.org/10.1021/es052534b

Humbert, P.S., Castro-Gomes, J., 2019. CO2 activated steel slag-based materials: A review. J. Clean. Prod. 208, 448–457. https://doi.org/10.1016/j.jclepro.2018.10.058

Hwang, C.L., Shen, D.H., 1991. The effects of blast-furnace slag and fly ash on the hydration of portland cement. Cem. Concr. Res. 21, 410–425. https://doi.org/10.1016/0008-8846(91)90090-5

Idir, R., Cyr, M., Tagnit-Hamou, A., 2010. Use of fine glass as ASR inhibitor in glass aggregate mortars. Constr. Build. Mater. 24, 1309–1312. https://doi.org/10.1016/j.conbuildmat.2009.12.030

Isaia, G., Gastaldini, A.L., Moraes, R., 2003. Physical and pozzolanic action of mineral additions on the

mechanical strength of high-performance concrete. Cem. Concr. Compos. 25, 69–76. https://doi.org/10.1016/S0958-9465(01)00057-9

Ishwarya, G., Singh, B., Deshwal, S., Bhattacharyya, S.K., 2019. Effect of sodium carbonate/sodium silicate activator on the rheology, geopolymerization and strength of fly ash/slag geopolymer pastes. Cem. Concr. Compos. 97, 226–238. https://doi.org/10.1016/j.cemconcomp.2018.12.007

Ismail, I., Bernal, S.A., Provis, J.L., San Nicolas, R., Hamdan, S., van Deventer, J.S.J., 2014. Modification of phase evolution in alkali-activated blast furnace slag by the incorporation of fly ash. Cem. Concr. Compos. 45, 125–135. https://doi.org/10.1016/j.cemconcomp.2013.09.006

Jain, J.A., Neithalath, N., 2010. Chloride transport in fly ash and glass powder modified concretes – Influence of test methods on microstructure. Cem. Concr. Compos. 32, 148–156. https://doi.org/10.1016/j.cemconcomp.2009.11.010

Jang, J.G., Kim, G.M., Kim, H.J., Lee, H.K., 2016. Review on recent advances in CO_2 utilization and sequestration technologies in cement-based materials. Constr. Build. Mater. 127, 762–773. https://doi.org/10.1016/j.conbuildmat.2016.10.017

Jani, Y., Hogland, W., 2014. Waste glass in the production of cement and concrete - A review. J. Environ. Chem. Eng. 2, 1767–1775. https://doi.org/10.1016/j.jece.2014.03.016

Jansen, D., Goetz-Neunhoeffer, F., Lothenbach, B., Neubauer, J., 2012. The early hydration of Ordinary Portland Cement (OPC): An approach comparing measured heat flow with calculated heat flow from QXRD. Cem. Concr. Res. 42, 134–138. https://doi.org/10.1016/j.cemconres.2011.09.001

Jeon, D., Jun, Y., Jeong, Y., Oh, J.E., 2015. Microstructural and strength improvements through the use of Na_2CO_3 in a cementless $Ca(OH)_2$-activated Class F fly ash system. Cem. Concr. Res. 67, 215–225. https://doi.org/10.1016/j.cemconres.2014.10.001

Jeong, Y., Park, H., Jun, Y., Jeong, J.H., Oh, J.E., 2015. Microstructural verification of the strength performance of ternary blended cement systems with high volumes of fly ash and GGBFS. Constr. Build. Mater. 95, 96–107. https://doi.org/10.1016/j.conbuildmat.2015.07.158

Jun-yuan, H., Scheetz, B.E., Roy, D.M., 1984. Hydration of fly ash-portland cements. Cem. Concr. Res. 14, 505–512. https://doi.org/10.1016/0008-8846(84)90126-1

Kakali, G., Tsivilis, S., Aggeli, E., Bati, M., 2000. Hydration products of C_3A, C_3S and Portland cement in the presence of $CaCO_3$. Cem. Concr. Res. 30, 1073–1077. https://doi.org/10.1016/S0008-8846(00)00292-1

Kang, S.-H., Hong, S.-G., Moon, J., 2018. The use of rice husk ash as reactive filler in ultra-high performance concrete. Cem. Concr. Res. 1–0. https://doi.org/10.1016/j.cemconres.2018.09.004

Kashef-Haghighi, S., Shao, Y., Ghoshal, S., 2015. Mathematical modeling of CO_2 uptake by concrete during accelerated carbonation curing. Cem. Concr. Res. 67, 1–10. https://doi.org/10.1016/j.cemconres.2014.07.020

Kayali, O., Sharfuddin Ahmed, M., 2013. Assessment of high volume replacement fly ash concrete – Concept of performance index. Constr. Build. Mater. 39, 71–76. https://doi.org/10.1016/j.conbuildmat.2012.05.009

Ke, X., Bernal, S.A., Provis, J.L., 2016. Controlling the reaction kinetics of sodium carbonate-activated slag cements using calcined layered double hydroxides. Cem. Concr. Res. 81, 24–37. https://doi.org/10.1016/j.cemconres.2015.11.012

Ke, X., Bernal, S.A., Ye, N., Provis, J.L., Yang, J., 2015. One-Part Geopolymers Based on Thermally Treated Red Mud/NaOH Blends. J. Am. Ceram. Soc. 98, 5–11. https://doi.org/10.1111/jace.13231

Khatib, J.M., 2008. Metakaolin concrete at a low water to binder ratio. Constr. Build. Mater. 22, 1691–1700. https://doi.org/10.1016/j.conbuildmat.2007.06.003

Khokhar, M.I.A., Roziere, E., Turcry, P., Grondin, F., Loukili, A., 2010. Mix design of concrete with high content

of mineral additions: Optimisation to improve early age strength. Cem. Concr. Compos. 32, 377–385. https://doi.org/10.1016/j.cemconcomp.2010.01.006

Kim, H., Koh, T., Pyo, S., 2016. Enhancing flowability and sustainability of ultra high performance concrete incorporating high replacement levels of industrial slags. Constr. Build. Mater. 123, 153–160. https://doi.org/10.1016/j.conbuildmat.2016.06.134

Kim, H.K., Lee, H.K., 2013. Effects of High Volumes of Fly Ash , Blast Furnace Slag , and Bottom Ash on Flow Characteristics , Density , and Compressive Strength of High-Strength Mortar. J. Mater. Civ. Eng. 25, 662–665. https://doi.org/10.1061/(ASCE)MT.1943-5533.0000624.

Kochova, K., Schollbach, K., Gauvin, F., Brouwers, H.J.H., 2017. Effect of saccharides on the hydration of ordinary Portland cement. Constr. Build. Mater. 150, 268–275. https://doi.org/10.1016/j.conbuildmat.2017.05.149

Korpa, A., Kowald, T., Trettin, R., 2009. Phase development in normal and ultra high performance cementitious systems by quantitative X-ray analysis and thermoanalytical methods. Cem. Concr. Res. 39, 69–76. https://doi.org/10.1016/j.cemconres.2008.11.003

Kourounis, S., Tsivilis, S., Tsakiridis, P.E., Papadimitriou, G.D., Tsibouki, Z., 2007. Properties and hydration of blended cements with steelmaking slag. Cem. Concr. Res. 37, 815–822. https://doi.org/10.1016/j.cemconres.2007.03.008

Kourounis, S., Tsivilis, S., Tsakiridis, P.E., Papadimitriou, G.D., Tsibouki, Z., 2007. Properties and hydration of blended cements with steelmaking slag. Cem. Concr. Res. 37, 815–822. https://doi.org/10.1016/j.cemconres.2007.03.008

Kovtun, M., Kearsley, E.P., Shekhovtsova, J., 2015. Chemical acceleration of a neutral granulated blast-furnace slag activated by sodium carbonate. Cem. Concr. Res. 72, 1–9. https://doi.org/10.1016/j.cemconres.2015.02.014

Kumar, A., Walder, B.J., Kunhi Mohamed, A., Hofstetter, A., Srinivasan, B., Rossini, A.J., Scrivener, K., Emsley, L., Bowen, P., 2017. The Atomic-Level Structure of Cementitious Calcium Silicate Hydrate. J. Phys. Chem. C 121, 17188–17196. https://doi.org/10.1021/acs.jpcc.7b02439

Kurda, R., Silvestre, J.D., de Brito, J., Ahmed, H., 2018. Optimizing recycled concrete containing high volume of fly ash in terms of the embodied energy and chloride ion resistance. J. Clean. Prod. 194, 735–750. https://doi.org/10.1016/j.jclepro.2018.05.177

Lam, C.S., Poon, C.S., Chan, D., 2007. Enhancing the performance of pre-cast concrete blocks by incorporating waste glass - ASR consideration. Cem. Concr. Compos. 29, 616–625. https://doi.org/10.1016/j.cemconcomp.2007.03.008

Lam, L., Wong, Y., Poon, C., 1998. Effect of Fly Ash and Silica Fume on Compressive and Fracture Behaviors of Concrete. Cem. Concr. Res. 28, 271–283. https://doi.org/10.1016/S0008-8846(97)00269-X

Lam, L., Wong, Y.L., Poon, C.S., 2000. Degree of hydration and gel/space ratio of high-volume fly ash/cement systems. Cem. Concr. Res. 30, 747–756. https://doi.org/10.1016/S0008-8846(00)00213-1

Lavergne, F., Ben Fraj, A., Bayane, I., Barthélémy, J.F., 2018. Estimating the mechanical properties of hydrating blended cementitious materials: An investigation based on micromechanics. Cem. Concr. Res. 104, 37–60. https://doi.org/10.1016/j.cemconres.2017.10.018

Lawrence, P., Cyr, M., Ringot, E., 2003. Mineral admixtures in mortars: Effect of inert materials on short-term hydration. Cem. Concr. Res. 33, 1939–1947. https://doi.org/10.1016/S0008-8846(03)00183-2

Lazaro, A., Quercia, G., Brouwers, H.J.H., Geus, J.W., 2013. Synthesis of a Green Nano-Silica Material Using Beneficiated Waste Dunites and Its Application in Concrete. World J. Nano Sci. Eng. 03, 41–51. https://doi.org/10.4236/wjnse.2013.33006

Lee, G., Ling, T.C., Wong, Y.L., Poon, C.S., 2011. Effects of crushed glass cullet sizes, casting methods and pozzolanic materials on ASR of concrete blocks. Constr. Build. Mater. 25, 2611–2618. https://doi.org/10.1016/j.conbuildmat.2010.12.008

Lee, N.K., Jang, J.G., Lee, H.K., 2014. Shrinkage characteristics of alkali-activated fly ash/slag paste and mortar at early ages. Cem. Concr. Compos. 53, 239–248. https://doi.org/10.1016/j.cemconcomp.2014.07.007

Leemann, A., Moro, F., 2017. Carbonation of concrete: the role of CO_2 concentration, relative humidity and CO_2 buffer capacity. Mater. Struct. Constr. 50, 1–14. https://doi.org/10.1617/s11527-016-0917-2

Leemann, A., Nygaard, P., Kaufmann, J., Loser, R., 2015. Relation between carbonation resistance, mix design and exposure of mortar and concrete. Cem. Concr. Compos. 62, 33–43. https://doi.org/10.1016/j.cemconcomp.2015.04.020

Leng, F., Feng, N., Lu, X., 2000. An experimental study on the properties of resistance to diffusion of chloride ions of fly ash and blast furnace slag concrete. Cem. Concr. Res. 30, 989–992. https://doi.org/10.1016/S0008-8846(00)00250-7

Li, G., Zhao, X., 2003. Properties of concrete incorporating fly ash and ground granulated blast-furnace slag. Cem. Concr. Compos. 25, 293–299. https://doi.org/10.1016/S0958-9465(02)00058-6

Li, J., Yao, Y., 2001. A study on creep and drying shrinkage of high performance concrete. Cem. Concr. Res. 31, 1203–1206. https://doi.org/10.1016/S0008-8846(01)00539-7

Li, K., Zeng, Q., Luo, M., Pang, X., 2014. Effect of self-desiccation on the pore structure of paste and mortar incorporating 70% GGBS. Constr. Build. Mater. 51, 329–337. https://doi.org/10.1016/j.combuildmat.2013.10.063

Li, N., Farzadnia, N., Shi, C., 2017. Microstructural changes in alkali-activated slag mortars induced by accelerated carbonation. Cem. Concr. Res. 100, 214–226. https://doi.org/10.1016/j.cemconres.2017.07.008

Li, N., Shi, C., Zhang, Z., 2019. Understanding the roles of activators towards setting and hardening control of alkali-activated slag cement. Compos. Part B Eng. 171, 34–45. https://doi.org/10.1016/j.compositesb.2019.04.024

Li, P.P., Cao, Y.Y.Y., Brouwers, H.J.H., Chen, W., Yu, Q.L., 2019. Development and properties evaluation of sustainable ultra-high performance pastes with quaternary blends. J. Clean. Prod. 240, 118124. https://doi.org/10.1016/j.jclepro.2019.118124

Li, P.P., Yu, Q.L., Brouwers, H.J.H., 2018. Effect of coarse basalt aggregates on the properties of Ultra-high Performance Concrete (UHPC). Constr. Build. Mater. 170, 649–659. https://doi.org/10.1016/j.conbuildmat.2018.03.109

Li, P.P., Yu, Q.L., Brouwers, H.J.H., 2017. Effect of PCE-type superplasticizer on early-age behaviour of ultra-high performance concrete (UHPC). Constr. Build. Mater. 153, 740–750. https://doi.org/10.1016/j.conbuildmat.2017.07.145

Li, P.P., Yu, Q.L., Brouwers, H.J.H., Chen, W., 2019. Conceptual design and performance evaluation of two-stage ultra-low binder ultra-high performance concrete. Cem. Concr. Res. 125, 105858. https://doi.org/10.1016/j.cemconres.2019.105858

Li, Y., Bao, J., Guo, Y., 2010. The relationship between autogenous shrinkage and pore structure of cement paste with mineral admixtures. Constr. Build. Mater. 24, 1855–1860. https://doi.org/10.1016/j.conbuildmat.2010.04.018

Librandi, P., Nielsen, P., Costa, G., Snellings, R., Quaghebeur, M., Baciocchi, R., 2019. Mechanical and environmental properties of carbonated steel slag compacts as a function of mineralogy and CO_2 uptake. J. CO_2 Util. 33, 201–214. https://doi.org/10.1016/j.jcou.2019.05.028

Lin, X., Silsbee, M.R., Roy, D.M., Kessler, K., Blankenhorn, P.R., Materials, I., 1994. Approaches to improve the

properties of wood fiber reinforced cementitious composites. Cem. Concr. Res. 24, 1558–1566.

Liu, G., Florea, M.V.A., Brouwers, H.J.H., 2019. Performance evaluation of sustainable high strength mortars incorporating high volume waste glass as binder. Constr. Build. Mater. 202, 574–588. https://doi.org/10.1016/j.cobuildmat.2018.12.110

Liu, G., Florea, M.V.A., Brouwers, H.J.H., 2019. Waste glass as binder in alkali activated slag–fly ash mortars. Mater. Struct. Constr. 52. https://doi.org/10.1617/s11527-019-1404-3

Liu, G., Florea, M.V.A., Brouwers, H.J.H., 2019. Characterization and performance of high volume recycled waste glass and ground granulated blast furnace slag or fly ash blended mortars. J. Clean. Prod. 235, 461–472. https://doi.org/10.1016/j.jclepro.2019.06.334

Liu, J., Wang, X., Qiu, Q., Ou, G., Xing, F., 2017. Understanding the effect of curing age on the chloride resistance of fly ash blended concrete by rapid chloride migration test. Mater. Chem. Phys. 196, 315–323. https://doi.org/10.1016/j.matchemphys.2017.05.011

Lothenbach, B., Le Saout, G., Gallucci, E., Scrivener, K., 2008. Influence of limestone on the hydration of Portland cements. Cem. Concr. Res. 38, 848–860. https://doi.org/10.1016/j.cemconres.2008.01.002

Luukkonen, T., Abdollahnejad, Z., Yliniemi, J., Kinnunen, P., Illikainen, M., 2018. One-part alkali-activated materials: A review. Cem. Concr. Res. https://doi.org/10.1016/j.cemconres.2017.10.001

Luukkonen, T., Abdollahnejad, Z., Yliniemi, J., Kinnunen, P., Illikainen, M., 2018. Comparison of alkali and silica sources in one-part alkali-activated blast furnace slag mortar. J. Clean. Prod. 187, 171–179. https://doi.org/10.1016/j.jclepro.2018.03.202

M.V.A. Florea, H.J.H. Brouwers, 2012. Chloride binding related to hydration products part I: Ordinary Portland cement. Cem. Concr. Res. 3, 125–131. https://doi.org/10.1007/978-94-007-2703-8_13

Ma, C., Long, G., Shi, Y., Xie, Y., 2018. Preparation of cleaner one-part geopolymer by investigating different types of commercial sodium metasilicate in China. J. Clean. Prod. 201, 636–647. https://doi.org/10.1016/j.jclepro.2018.08.060

Marjanović, N., Komljenović, M., Baščarević, Z., Nikolić, V., Petrović, R., 2015. Physical–mechanical and microstructural properties of alkali-activated fly ash–blast furnace slag blends. Ceram. Int. 41, 1421–1435. https://doi.org/10.1016/j.ceramint.2014.09.075

Martinez-Lopez, R., Ivan Escalante-Garcia, J., 2016. Alkali activated composite binders of waste silica soda lime glass and blast furnace slag: Strength as a function of the composition. Constr. Build. Mater. 119, 119–129. https://doi.org/10.1016/j.conbuildmat.2016.05.064

Matson, D.W., Sharma, S.K., Philpotts, J.A., 1983. The structure of high-silica alkali-silicate glasses. A Raman spectroscopic investigation. J. Non. Cryst. Solids 58, 323–352. https://doi.org/10.1016/0022-3093(83)90032-7

Matsushita, F., Aono, Y., Shibata, S., 2004. Calcium silicate structure and carbonation shrinkage of a tobermorite-based material. Cem. Concr. Res. 34, 1251–1257. https://doi.org/10.1016/j.cemconres.2003.12.016

Mejdi, M., Wilson, W., Saillio, M., Chaussadent, T., Divet, L., Tagnit-Hamou, A., 2019. Investigating the pozzolanic reaction of post-consumption glass powder and the role of portlandite in the formation of sodium-rich C-S-H. Cem. Concr. Res. 123, 105790. https://doi.org/10.1016/j.cemconres.2019.105790

Mikhail, R.S., Copeland, L.E., Brunauer, S., 1964. Pore structures and surface areas of hardened Portland cement pastes by nitrogen adsorption. Can. J. Chem. 42, 426–438. https://doi.org/10.1139/v64-060

Mo, K.H., Johnson Alengaram, U., Jumaat, M.Z., Yap, S.P., 2015. Feasibility study of high volume slag as cement replacement for sustainable structural lightweight oil palm shell concrete. J. Clean. Prod. 91, 297–304. https://doi.org/10.1016/j.jclepro.2014.12.021

Mo, L., Zhang, F., Deng, M., 2016. Mechanical performance and microstructure of the calcium carbonate binders

produced by carbonating steel slag paste under CO_2 curing. Cem. Concr. Res. 88, 217–226. https://doi.org/10.1016/j.cemconres.2016.05.013

Monkman, S., Shao, Y., 2010. Integration of carbon sequestration into curing process of precast concrete. Can. J. Civ. Eng. 37, 302–310. https://doi.org/10.1139/L09-140

Moon, E.J., Choi, Y.C., 2018. Development of carbon-capture binder using stainless steel argon oxygen decarburization slag activated by carbonation. J. Clean. Prod. 180, 642–654. https://doi.org/10.1016/j.jclepro.2018.01.189

Moon, H.Y., Kim, H.S., Choi, D.S., 2006. Relationship between average pore diameter and chloride diffusivity in various concretes. Constr. Build. Mater. 20, 725–732. https://doi.org/10.1016/j.conbuildmat.2005.02.005

Moorehead, D.R., 1986. Cementation by the carbonation of hydrated lime. Cem. Concr. Res. 16, 700–708. https://doi.org/10.1016/0008-8846(86)90044-X

Mostafa, N.Y., Brown, P.W., 2005. Heat of hydration of high reactive pozzolans in blended cements: Isothermal conduction calorimetry. Thermochim. Acta 435, 162–167. https://doi.org/10.1016/j.tca.2005.05.014

Naber, C., Stegmeyer, S., Jansen, D., Goetz-Neunhoeffer, F., Neubauer, J., 2019. The PONKCS method applied for time resolved XRD quantification of supplementary cementitious material reactivity in hydrating mixtures with ordinary Portland cement. Constr. Build. Mater. 214, 449–457. https://doi.org/10.1016/j.conbuildmat.2019.04.157

Nedeljković, M., Ghiassi, B., van der Laan, S., Li, Z., Ye, G., 2019. Effect of curing conditions on the pore solution and carbonation resistance of alkali-activated fly ash and slag pastes. Cem. Concr. Res. 116, 146–158. https://doi.org/10.1016/j.cemconres.2018.11.011

Nematollahi, B., Sanjayan, J., Shaikh, F.U.A., 2015. Synthesis of heat and ambient cured one-part geopolymer mixes with different grades of sodium silicate. Ceram. Int. 41, 5696–5704. https://doi.org/10.1016/j.ceramint.2014.12.154

Neubauer, C.M., Yang, M., Jennings, H.M., 1998. Interparticle potential and sedimentation behavior of cement suspensions: Effects of admixtures. Adv. Cem. Based Mater. 8, 17–27. https://doi.org/10.1016/S1065-7355(98)00005-4

Nocuò-Wczelik, W., 1999. Effect of Na and Al on the phase composition and morphology of autoclaved calcium silicate hydrates. Cem. Concr. Res. 29, 1759–1767. https://doi.org/10.1016/S0008-8846(99)00166-0

Odler, I., Rößler, M., 1985. Investigations on the relationship between porosity, structure and strength of hydrated Portland cement pastes. II. Effect of pore structure and of degree of hydration. Cem. Concr. Res. 15, 401–410. https://doi.org/10.1016/0008-8846(85)90113-9

Ogawa, K., Uchikawa, H., Takemoto, K., Yasui, I., 1980. The mechanism of the hydration in the system C_3S-pozzolana. Cem. Concr. Res. 10, 683–696. https://doi.org/10.1016/0008-8846(80)90032-0

Oh, J.E., Monteiro, P.J.M., Jun, S.S., Choi, S., Clark, S.M., 2010. The evolution of strength and crystalline phases for alkali-activated ground blast furnace slag and fly ash-based geopolymers. Cem. Concr. Res. 40, 189–196. https://doi.org/10.1016/j.cemconres.2009.10.010

Omran, A., Tagnit-Hamou, A., 2016. Performance of glass-powder concrete in field applications. Constr. Build. Mater. 109, 84–95. https://doi.org/10.1016/j.conbuildmat.2016.02.006

Paiva, H., Silva, A.S., Velosa, A., Cachim, P., Ferreira, V.M., 2017. Microstructure and hardened state properties on pozzolan-containing concrete. Constr. Build. Mater. 140, 374–384. https://doi.org/10.1016/j.conbuildmat.2017.02.120

Pane, I., Hansen, W., 2005. Investigation of blended cement hydration by isothermal calorimetry and thermal analysis. Cem. Concr. Res. 35, 1155–1164. https://doi.org/10.1016/j.cemconres.2004.10.027

Pang, B., Zhou, Z., Cheng, X., Du, P., Xu, H., 2016. ITZ properties of concrete with carbonated steel slag

aggregate in salty freeze-thaw environment. Constr. Build. Mater. 114, 162–171. https://doi.org/10.1016/j.conbuildmat.2016.03.168

Pang, B., Zhou, Z., Hou, P., Du, P., Zhang, L., Xu, H., 2016. Autogenous and engineered healing mechanisms of carbonated steel slag aggregate in concrete. Constr. Build. Mater. 107, 191–202. https://doi.org/10.1016/j.conbuildmat.2015.12.191

Parrott, L.J., Geiker, M., Gutteridge, W.A., Killoh, D., 1990. Monitoring Portland cement hydration: Comparison of methods. Cem. Concr. Res. 20, 919–926. https://doi.org/10.1016/0008-8846(90)90054-2

Pehanich, J.L., Blankenhorn, P.R., Silsbee, M.R., 2004. Wood fiber surface treatment level effects on selected mechanical properties of wood fiber-cement composites. Cem. Concr. Res. 34, 59–65. https://doi.org/10.1016/S0008-8846(03)00193-5

Peng, M.X., Wang, Z.H., Xiao, Q.G., Song, F., Xie, W., Yu, L.C., Huang, H.W., Yi, S.J., 2017. Effects of alkali on one-part alkali-activated cement synthesized by calcining bentonite with dolomite and Na_2CO_3. Appl. Clay Sci. 139, 64–71. https://doi.org/10.1016/j.clay.2017.01.020

Peterson, V.K., Garci Juenger, M.C., 2006. Hydration of tricalcium silicate: Effects of $CaCl_2$ and sucrose on reaction kinetics and product formation. Chem. Mater. 18, 5798–5804. https://doi.org/10.1021/cm061724y

Plowman, C., Cabrera, J.G., 1984. Mechanism and kinetics of hydration of C3A and C4AF. Extracted from cement. Cem. Concr. Res. 14, 238–248. https://doi.org/10.1016/0008-8846(84)90110-8

Polettini, A., Pomi, R., Stramazzo, A., 2016. Carbon sequestration through accelerated carbonation of BOF slag: Influence of particle size characteristics. Chem. Eng. J. 298, 26–35. https://doi.org/10.1016/j.cej.2016.04.015

Poon, C.S., Lam, L., Wong, Y.L., 2000. A study on high strength concrete prepared with large volumes of low calcium fly ash. Cem. Concr. Res. 30, 447–455. https://doi.org/10.1016/S0008-8846(99)00271-9

Powers, T.C., 1958. Structure and Physical Properties of Hardened Portland Cement Paste. J. Am. Ceram. Soc. 41, 1–6. https://doi.org/10.1111/j.1151-2916.1958.tb13494.x

Provis, J.L., 2014. Geopolymers and other alkali activated materials: Why, how, and what? Mater. Struct. Constr. 47, 11–25. https://doi.org/10.1617/s11527-013-0211-5

Puertas, F., Fernández-Jiménez, A., 2003. Mineralogical and microstructural characterisation of alkali-activated fly ash/slag pastes. Cem. Concr. Compos. 25, 287–292. https://doi.org/10.1016/S0958-9465(02)00059-8

Puertas, F., González-Fonteboa, B., González-Taboada, I., Alonso, M.M., Torres-Carrasco, M., Rojo, G., Martínez-Abella, F., 2018. Alkali-activated slag concrete: Fresh and hardened behaviour. Cem. Concr. Compos. 85, 22–31. https://doi.org/10.1016/j.cemconcomp.2017.10.003

Puertas, F., Martínez-Ramírez, S., Alonso, S., Vázquez, T., 2000. Alkali-activated fly ash/slag cements: Strength behaviour and hydration products. Cem. Concr. Res. 30, 1625–1632. https://doi.org/10.1016/S0008-8846(00)00298-2

Puertas, F., Torres-Carrasco, M., 2014. Use of glass waste as an activator in the preparation of alkali-activated slag. Mechanical strength and paste characterisation. Cem. Concr. Res. 57, 95–104. https://doi.org/10.1016/j.cemconres.2013.12.005

Qiang, W., Mengxiao, S., Jun, Y., 2016. Influence of classified steel slag with particle sizes smaller than 20 μm on the properties of cement and concrete. Constr. Build. Mater. 123, 601–610. https://doi.org/10.1016/j.conbuildmat.2016.07.042

Ramakrishnan, K., Pugazhmani, G., Sripragadeesh, R., Muthu, D., Venkatasubramanian, C., 2017. Experimental study on the mechanical and durability properties of concrete with waste glass powder and ground granulated blast furnace slag as supplementary cementitious materials. Constr. Build. Mater. 156, 739–749. https://doi.org/10.1016/j.conbuildmat.2017.08.183

Ranjbar, N., Behnia, A., Alsubari, B., Moradi Birgani, P., Jumaat, M.Z., 2016. Durability and mechanical properties of self-compacting concrete incorporating palm oil fuel ash. J. Clean. Prod. 112, 723–730. https://doi.org/10.1016/j.jclepro.2015.07.033

Rashad, A.M., 2015. An investigation of high-volume fly ash concrete blended with slag subjected to elevated temperatures. J. Clean. Prod. 93, 47–55. https://doi.org/10.1016/j.jclepro.2015.01.031

Reddy, K.R., Chetri, J.K., Kumar, G., Grubb, D.G., 2019. Effect of basic oxygen furnace slag type on carbon dioxide sequestration from landfill gas emissions. Waste Manag. 85, 425–436. https://doi.org/10.1016/j.wasman.2019.01.013

Rey, F., Fornés, V., Rojo, J.M., 1992. Thermal decomposition of hydrotalcites. An infrared and nuclear magnetic resonance spectroscopic study. J. Chem. Soc. Faraday Trans. 88, 2233–2238. https://doi.org/10.1039/FT9928802233

Ribeiro, A.C.F., Barros, M.C.F., Lobo, V.M.M., Sobral, A.J.F.N., Fangaia, S.I.G., Nicolau, P.M.G., Guerra, F.A.D.R.A., Esteso, M.A., 2011. Interaction between calcium chloride and some carbohydrates as seen by mutual diffusion at 25 °C and 37 °C. Food Chem. 124, 842–849. https://doi.org/10.1016/j.foodchem.2010.07.005

Richardson, I.G., Groves, G.W., 1993. Microstructure and microanalysis of hardened ordinary Portland cement pastes. J. Mater. Sci. 28, 265–277. https://doi.org/10.1007/BF00349061

Rodger, S.A., Groves, G.W., 1989. Electron Microscopy Study of Ordinary Portland Cement and Ordinary Portland Cement–Pulverized Fuel Ash Blended Pastes. J. Am. Ceram. Soc. 72, 1037–1039. https://doi.org/10.1111/j.1151-2916.1989.tb06265.x

Rossi, P., 2013. Influence of fibre geometry and matrix maturity on the mechanical performance of ultra high-performance cement-based composites. Cem. Concr. Compos. 37, 246–248. https://doi.org/10.1016/j.cemconcomp.2012.08.005

Rostami, V., Shao, Y., Boyd, A.J., He, Z., 2012. Microstructure of cement paste subject to early carbonation curing. Cem. Concr. Res. 42, 186–193. https://doi.org/10.1016/j.cemconres.2011.09.010

Santos, R.M., Ling, D., Sarvaramini, A., Guo, M., Elsen, J., Larachi, F., Beaudoin, G., Blanpain, B., Van Gerven, T., 2012. Stabilization of basic oxygen furnace slag by hot-stage carbonation treatment. Chem. Eng. J. 203, 239–250. https://doi.org/10.1016/j.cej.2012.06.155

Scarlett, N.V.Y., Madsen, I.C., 2006. Quantification of phases with partial or no known crystal structures. Powder Diffr. 21, 278–284. https://doi.org/10.1154/1.2362855

Schöler, A., Lothenbach, B., Winnefeld, F., Zajac, M., 2015. Hydration of quaternary Portland cement blends containing blast-furnace slag, siliceous fly ash and limestone powder. Cem. Concr. Compos. 55, 374–382. https://doi.org/10.1016/j.cemconcomp.2014.10.001

Schwarz, N., Neithalath, N., 2008. Influence of a fine glass powder on cement hydration: Comparison to fly ash and modeling the degree of hydration. Cem. Concr. Res. 38, 429–436. https://doi.org/10.1016/j.cemconres.2007.12.001

Shao, Y., Lefort, T., Moras, S., Rodriguez, D., 2000. Studies on concrete containing ground waste glass. Cem. Concr. Res. 30, 91–100. https://doi.org/10.1016/S0008-8846(99)00213-6

Shao, Y., Liu, M., He, Z., Yang, H., 2013. Early carbonation behaviour of no-clinker steel slag binder. Adv. Cem. Res. 25, 342–351. https://doi.org/10.1680/adcr.12.00054

Shayan, A., Xu, A., 2006. Performance of glass powder as a pozzolanic material in concrete: A field trial on concrete slabs. Cem. Concr. Res. 36, 457–468. https://doi.org/10.1016/j.cemconres.2005.12.012

Shayan, A., Xu, A., 2004. Value-added utilisation of waste glass in concrete. Cem. Concr. Res. 34, 81–89. https://doi.org/10.1016/S0008-8846(03)00251-5

Shehata, M.H., Thomas, M.D.A., Bleszynski, R.F., 1999. The effects of fly ash composition on the chemistry of pore solution in hydrated cement pastes. Cem. Concr. Res. 29, 1915–1920. https://doi.org/10.1016/S0008-8846(99)00190-8

Shi, C., 2004. Effect of mixing proportions of concrete on its electrical conductivity and the rapid chloride permeability test (ASTM C1202 or ASSHTO T277) results. Cem. Concr. Res. 34, 537–545. https://doi.org/10.1016/j.cemconres.2003.09.007

Shi, C., 2002. Characteristics and cementitious properties of ladle slag fines from steel production. Cem. Concr. Res. 32, 459–462. https://doi.org/10.1016/S0008-8846(01)00707-4

Shi, C., He, F., Wu, Y., 2012. Effect of pre-conditioning on CO_2 curing of lightweight concrete blocks mixtures. Constr. Build. Mater. 26, 257–267. https://doi.org/10.1016/j.conbuildmat.2011.06.020

Shi, C., Wu, Y., Riefler, C., Wang, H., 2005. Characteristics and pozzolanic reactivity of glass powders. Cem. Concr. Res. 35, 987–993. https://doi.org/10.1016/j.cemconres.2004.05.015

Shi, C., Wu, Z., Xiao, J., Wang, D., Huang, Z., Fang, Z., 2015. A review on ultra high performance concrete: Part I. Raw materials and mixture design. Constr. Build. Mater. 101, 741–751. https://doi.org/10.1016/j.conbuildmat.2015.10.088

Shi, Z., Shi, C., Wan, S., Li, N., Zhang, Z., 2018. Effect of alkali dosage and silicate modulus on carbonation of alkali-activated slag mortars. Cem. Concr. Res. 113, 55–64. https://doi.org/10.1016/j.cemconres.2018.07.005

Siad, H., Lachemi, M., Sahmaran, M., Mesbah, H.A., Hossain, K.M.A., 2018. Use of recycled glass powder to improve the performance properties of high volume fly ash-engineered cementitious composites. Constr. Build. Mater. 163, 53–62. https://doi.org/10.1016/j.conbuildmat.2017.12.067

Siva, T., Muralidharan, · S, Sathiyanarayanan, · S, Manikandan, · E, Jayachandran, · M, Manikandan, E., Muralidharan, S., Sathiyanarayanan, S., Jayachandran, M., 2017. Enhanced Polymer Induced Precipitation of Polymorphous in Calcium Carbonate: Calcite Aragonite Vaterite Phases. J. Inorg. Organomet. Polym. Mater. 27, 770–778. https://doi.org/10.1007/s10904-017-0520-1

Skibsted, J., Snellings, R., 2019. Reactivity of supplementary cementitious materials (SCMs) in cement blends. Cem. Concr. Res. 124, 105799. https://doi.org/10.1016/j.cemconres.2019.105799

Škvára, F., Kopecký, L., Šmilauer, V., Bittnar, Z., 2009. Material and structural characterization of alkali activated low-calcium brown coal fly ash. J. Hazard. Mater. 168, 711–720. https://doi.org/10.1016/j.jhazmat.2009.02.089

Smith, B.J., Roberts, L.R., Funkhouser, G.P., Gupta, V., Chmelka, B.F., 2012. Reactions and Surface Interactions of Saccharides in Cement Slurries 28, 14202–14217. https://doi.org/10.1021/la3015157

Snellings, R., Salze, A., Scrivener, K.L., 2014. Use of X-ray diffraction to quantify amorphous supplementary cementitious materials in anhydrous and hydrated blended cements. Cem. Concr. Res. 64, 89–98. https://doi.org/10.1016/j.cemconres.2014.06.011

Soliman, N.A., Tagnit-Hamou, A., 2016. Development of ultra-high-performance concrete using glass powder – Towards ecofriendly concrete. Constr. Build. Mater. 125, 600–612. https://doi.org/10.1016/j.conbuildmat.2016.08.073

Song, S., Jennings, H.M., 1999. Pore solution chemistry of alkali-activated ground granulated blast-furnace slag. Cem. Concr. Res. 29, 159–170. https://doi.org/10.1016/S0008-8846(98)00212-9

Spiesz, P., Brouwers, H.J.H., 2012. Influence of the applied voltage on the Rapid Chloride Migration (RCM) test. Cem. Concr. Res. 42, 1072–1082. https://doi.org/10.1016/j.cemconres.2012.04.007

Spiesz, P., Rouvas, S., Brouwers, H.J.H., 2016. Utilization of waste glass in translucent and photocatalytic concrete. https://doi.org/10.1016/j.conbuildmat.2016.10.063

Stepkowska, E.T., Blanes, J.M., Franco, F., Real, C., Pérez-Rodríguez, J.L., 2004. Phase transformation on heating of an aged cement paste, in: Thermochimica Acta. pp. 79–87. https://doi.org/10.1016/j.tca.2003.11.057

Stetsko, Y.P., Shanahan, N., Deford, H., Zayed, A., 2017. Quantification of supplementary cementitious content in blended Portland cement using an iterative Rietveld-PONKCS technique. J. Appl. Crystallogr. 50, 498–507. https://doi.org/10.1107/S1600576717002965

Sturm, P., 2018. Hardening, high-temperature resistance and acid resistance of one-part geopolymers. PhD thesis, Eindhoven University of Technology.

Sturm, P., Gluth, G.J.G., Brouwers, H.J.H., Kühne, H.-C., 2016. Synthesizing one-part geopolymers from rice husk ash. Constr. Build. Mater. 124, 961–966. https://doi.org/10.1016/j.conbuildmat.2016.08.017

Sugama, T., Brothers, L.E., Van de Putte, T.R., 2005. Acid-resistant cements for geothermal wells: sodium silicate activated slag/fly ash blends. Adv. Cem. Res. 17, 65–75. https://doi.org/10.1680/adcr.2005.17.2.65

Tajuelo Rodriguez, E., Garbev, K., Merz, D., Black, L., Richardson, I.G., 2017. Thermal stability of C-S-H phases and applicability of Richardson and Groves' and Richardson C-(A)-S-H(I) models to synthetic C-S-H. Cem. Concr. Res. 93, 45–56. https://doi.org/10.1016/j.cemconres.2016.12.005

Taniguchi, I., Yamada, T., 2017. Low Energy CO_2 Capture by Electrodialysis, in: Energy Procedia. Elsevier Ltd, pp. 1615–1620. https://doi.org/10.1016/j.egypro.2017.03.1902

Tchakouté, H.K., Rüscher, C.H., Kong, S., Kamseu, E., Leonelli, C., 2016. Geopolymer binders from metakaolin using sodium waterglass from waste glass and rice husk ash as alternative activators: A comparative study. Constr. Build. Mater. 114, 276–289. https://doi.org/10.1016/j.conbuildmat.2016.03.184

Thomas, J.J., Allen, A.J., Jennings, H.M., 2009. Hydration Kinetics and Microstructure Development of Normal and $CaCl_2$ -Accelerated Tricalcium Silicate Pastes. J. Phys. Chem. C 113, 19836–19844. https://doi.org/10.1021/jp907078u

Thomas, N.L., Birchall, J.D., 1983. The retarding action of sugars on cement hydration. Cem. Concr. Res. 13, 830–842. https://doi.org/10.1016/0008-8846(83)90084-4

Toniolo, N., Rincón, A., Roether, J.A., Ercole, P., Bernardo, E., Boccaccini, A.R., 2018. Extensive reuse of soda-lime waste glass in fly ash-based geopolymers. Constr. Build. Mater. 188, 1077–1084. https://doi.org/10.1016/j.conbuildmat.2018.08.096

Topçu, İ.B., Canbaz, M., 2004. Properties of concrete containing waste glass. Cem. Concr. Res. 34, 267–274. https://doi.org/10.1016/j.cemconres.2003.07.003

Torres-Carrasco, M., Palomo, J.G., Puertas, F., 2014. Sodium silicate solutions from dissolution of glass wastes . Statistical analysis. Mater. construcción 64, 1–14. https://doi.org/10.3989/mc.2014.05213

Torres-Carrasco, M., Puertas, F., 2017. Waste glass as a precursor in alkaline activation: Chemical process and hydration products. Constr. Build. Mater. 139, 342–354. https://doi.org/10.1016/j.conbuildmat.2017.02.071

Torres-Carrasco, M., Puertas, F., 2015. Waste glass in the geopolymer preparation. Mechanical and microstructural characterisation. J. Clean. Prod. 90, 397–408. https://doi.org/10.1016/j.jclepro.2014.11.074

Torres-Carrasco, M., Rodríguez-Puertas, C., Del Mar Alonso, M., Puertas, F., 2015. Alkali activated slag cements using waste glass as alternative activators. Rheological behaviour. Bol. la Soc. Esp. Ceram. y Vidr. 54, 45–57. https://doi.org/10.1016/j.bsecv.2015.03.004

Vafaei, M., Allahverdi, A., 2017a. High strength geopolymer binder based on waste-glass powder. Adv. Powder Technol. 28, 215–222. https://doi.org/10.1016/j.apt.2016.09.034

Vaitkevičius, V., Šerelis, E., Hilbig, H., 2014. The effect of glass powder on the microstructure of ultra high performance concrete. Constr. Build. Mater. 68, 102–109. https://doi.org/10.1016/j.conbuildmat.2014.05.101

Van Hoek, C., Small, J., van der Laan, S., 2016. Large-Area Phase Mapping Using PhAse Recognition and

Characterization (PARC) Software. Micros. Today 24, 12–21. https://doi.org/10.1017/S1551929516000572

Van Zomeren, A., van der Laan, S.R., Kobesen, H.B.A., Huijgen, W.J.J., Comans, R.N.J., 2011. Changes in mineralogical and leaching properties of converter steel slag resulting from accelerated carbonation at low CO_2 pressure. Waste Manag. 31, 2236–2244. https://doi.org/10.1016/J.WASMAN.2011.05.022

Verma, M., Prem, P.R., Rajasankar, J., Bharatkumar, B.H., 2016. On low-energy impact response of ultra-high performance concrete (UHPC) panels. Mater. Des. 92, 853–865. https://doi.org/10.1016/j.matdes.2015.12.065

Vinai, R., Soutsos, M., 2019. Production of sodium silicate powder from waste glass cullet for alkali activation of alternative binders. Cem. Concr. Res. 116, 45–56. https://doi.org/10.1016/j.cemconres.2018.11.008

Wan, S., Zhou, X., Zhou, M., Han, Y., Chen, Y., Geng, J., Wang, T., Xu, S., Qiu, Z., Hou, H., 2018. Hydration characteristics and modeling of ternary system of municipal solid wastes incineration fly ash-blast furnace slag-cement. Constr. Build. Mater. 180, 154–166. https://doi.org/10.1016/J.CONBUILDMAT.2018.05.277

Wang, D., Shi, C., Farzadnia, N., Shi, Z., Jia, H., Ou, Z., 2018. A review on use of limestone powder in cement-based materials: Mechanism, hydration and microstructures. Constr. Build. Mater. 181, 659–672. https://doi.org/10.1016/j.conbuildmat.2018.06.075

Wang, Q., Yan, P., 2010. Hydration properties of basic oxygen furnace steel slag. Constr. Build. Mater. 24, 1134–1140. https://doi.org/10.1016/j.conbuildmat.2009.12.028

Wang, Q., Yang, J., Yan, P., 2013. Cementitious properties of super-fine steel slag. Powder Technol. 245, 35–39. https://doi.org/10.1016/j.powtec.2013.04.016

Wang, Q., Yang, J., Yan, P., 2012. Influence of initial alkalinity on the hydration of steel slag. Sci. China Technol. Sci. 55, 3378–3387. https://doi.org/10.1007/s11431-012-4830-9

Wei, Y.M., Zhou, Y.G., Tomita, B., 2000. Hydration behavior of wood cement-based composite (I): evaluation of wood species effects on compatibility and strength with ordinary portland cement. J. Wood Sci. 46, 296–302. https://doi.org/10.1007/BF00766220

Wongkeo, W., Thongsanitgarn, P., Ngamjarurojana, A., Chaipanich, A., 2014. Compressive strength and chloride resistance of self-compacting concrete containing high level fly ash and silica fume. Mater. Des. 64, 261–269. https://doi.org/10.1016/j.matdes.2014.07.042

Wu, K., Shi, H., Xu, L., Ye, G., De Schutter, G., 2016. Microstructural characterization of ITZ in blended cement concretes and its relation to transport properties. Cem. Concr. Res. 79, 243–256. https://doi.org/10.1016/j.cemconres.2015.09.018

Xie, Z., Xi, Y., 2002. Use of recycled glass as a raw material in the manufacture of Portland cement. Mater. Struct. 35, 510–515. https://doi.org/10.1007/BF02483139

Xu, G., Tian, Q., Miao, J., Liu, J., 2017. Early-age hydration and mechanical properties of high volume slag and fly ash concrete at different curing temperatures. Constr. Build. Mater. 149, 367–377. https://doi.org/10.1016/j.conbuildmat.2017.05.080

Xuan, D., Zhan, B., Poon, C.S., 2016. Assessment of mechanical properties of concrete incorporating carbonated recycled concrete aggregates. Cem. Concr. Compos. 65, 67–74. https://doi.org/10.1016/j.cemconcomp.2015.10.018

Yamada, K., Takahashi, T., Hanehara, S., Matsuhisa, M., 2000. Effects of the chemical structure on the properties of polycarboxylate-type superplasticizer. Cem. Concr. Res. 30, 197–207. https://doi.org/10.1016/S0008-8846(99)00230-6

Yang, J., Su, Y., He, X., Tan, H., Jiang, Y., Zeng, L., Strnadel, B., 2018. Pore structure evaluation of cementing composites blended with coal by-products: Calcined coal gangue and coal fly ash. Fuel Process. Technol. 181, 75–90. https://doi.org/10.1016/j.fuproc.2018.09.013

Yang, R., Yu, R., Shui, Z., Guo, C., Wu, S., Gao, X., Peng, S., 2019. The physical and chemical impact of manufactured sand as a partial replacement material in Ultra-High Performance Concrete (UHPC). Cem. Concr. Compos. 99, 203–213. https://doi.org/10.1016/j.cemconcomp.2019.03.020

Yazıcı, H., 2007. The effect of curing conditions on compressive strength of ultra high strength concrete with high volume mineral admixtures. Build. Environ. 42, 2083–2089. https://doi.org/10.1016/j.buildenv.2006.03.013

Ye, H., Cartwright, C., Rajabipour, F., Radlińska, A., 2017. Understanding the drying shrinkage performance of alkali-activated slag mortars. Cem. Concr. Compos. 76, 13–24. https://doi.org/10.1016/j.cemconcomp.2016.11.010

Young, J.F., 1972. A review of the mechanisms of set-retardation in portland cement pastes containing organic admixtures. Cem. Concr. Res. 2, 415–433. https://doi.org/10.1016/0008-8846(72)90057-9

Yu, B., Bian, H., Plank, J., 2010. Self-assembly and characterization of Ca-Al-LDH nanohybrids containing casein proteins as guest anions. J. Phys. Chem. Solids 71, 468–472. https://doi.org/10.1016/j.jpcs.2009.12.013

Yu, R., Spiesz, P., Brouwers, H.J.H., 2014. Effect of nano-silica on the hydration and microstructure development of Ultra-High Performance Concrete (UHPC) with a low binder amount. Constr. Build. Mater. 65, 140–150. https://doi.org/10.1016/j.conbuildmat.2014.04.063

Yu, X., Tao, Z., Song, T.-Y., Pan, Z., 2016. Performance of concrete made with steel slag and waste glass. Constr. Build. Mater. 114, 737–746. https://doi.org/10.1016/j.conbuildmat.2016.03.217

Yu, Z., Ma, J., Ye, G., van Breugel, K., Shen, X., 2017. Effect of fly ash on the pore structure of cement paste under a curing period of 3 years. Constr. Build. Mater. 144, 493–501. https://doi.org/10.1016/j.conbuildmat.2017.03.182

Yu, Z., Ye, G., 2013. The pore structure of cement paste blended with fly ash. Constr. Build. Mater. 45, 30–35. https://doi.org/10.1016/j.conbuildmat.2013.04.012

Yuan, B., Yu, Q.L., Brouwers, H.J.H., 2017. Assessing the chemical involvement of limestone powder in sodium carbonate activated slag. Mater. Struct. 50, 136. https://doi.org/10.1617/s11527-017-1003-0

Yuan, B., Yu, Q.L., Brouwers, H.J.H., 2017. Time-dependent characterization of Na_2CO_3 activated slag. Cem. Concr. Compos. 84, 188–197. https://doi.org/10.1016/j.cemconcomp.2017.09.005

Zajac, M., Skocek, J., Durdzinski, P., Bullerjahn, F., Skibsted, J., Ben Haha, M., 2020. Effect of carbonated cement paste on composite cement hydration and performance. Cem. Concr. Res. 134, 106090. https://doi.org/10.1016/j.cemconres.2020.106090

Zeng, Q., Li, K., Fen-chong, T., Dangla, P., 2012. Pore structure characterization of cement pastes blended with high-volume fly-ash. Cem. Concr. Res. 42, 194–204. https://doi.org/10.1016/j.cemconcomp.2011.09.012

Zhan, B., Poon, C., Shi, C., 2013. CO2 curing for improving the properties of concrete blocks containing recycled aggregates. Cem. Concr. Compos. 42, 1–8. https://doi.org/10.1016/j.cemconcomp.2013.04.013

Zhang, D., Ghouleh, Z., Shao, Y., 2017. Review on carbonation curing of cement-based materials. J. CO2 Util. 21, 119–131. https://doi.org/10.1016/j.jcou.2017.07.003

Zhang, M.H., Tam, C.T., Leow, M.P., 2003. Effect of water-to-cementitious materials ratio and silica fume on the autogenous shrinkage of concrete. Cem. Concr. Res. 33, 1687–1694. https://doi.org/10.1016/S0008-8846(03)00149-2

Zhang, P., Qian, G., Cheng, H., Yang, J., Shi, H., Frost, R.L., 2011. Near-infrared and mid-infrared investigations of Na-dodecylbenzenesulfate intercalated into hydrocalumite chloride (CaAl-LDH-Cl). Spectrochim. Acta - Part A Mol. Biomol. Spectrosc. 79, 548–553. https://doi.org/10.1016/j.saa.2011.03.031

Zhang, S., Keulen, A., Arbi, K., Ye, G., 2017a. Waste glass as partial mineral precursor in alkali-activated slag/fly ash system. Cem. Concr. Res. 102, 29–40. https://doi.org/10.1016/j.cemconres.2017.08.012

Zhang, X., Zhao, S., Liu, Z., Wang, F., 2019. Utilization of steel slag in ultra-high performance concrete with

enhanced eco-friendliness. Constr. Build. Mater. 214, 28–36. https://doi.org/10.1016/j.conbuildmat.2019.04.106

Zhang, Y., Kong, X., 2015. Correlations of the dispersing capability of NSF and PCE types of superplasticizer and their impacts on cement hydration with the adsorption in fresh cement pastes. Cem. Concr. Res. 69, 1–9. https://doi.org/10.1016/j.cemconres.2014.11.009

Zheng, K., 2016. Pozzolanic reaction of glass powder and its role in controlling alkali-silica reaction. Cem. Concr. Compos. 67, 30–38. https://doi.org/10.1016/j.cemconcomp.2015.12.008

Zhi, P.X., Guo, Q.L., 2005. Hydrothermal synthesis of layered double hydroxides (LDHs) from mixed MgO and Al_2O_3: LDH formation mechanism. Chem. Mater. 17, 1055–1062. https://doi.org/10.1021/cm048085g

Zingg, A., Winnefeld, F., Holzer, L., Pakusch, J., Becker, S., Figi, R., Gauckler, L., 2009. Interaction of polycarboxylate-based superplasticizers with cements containing different C_3A amounts. Cem. Concr. Compos. 31, 153–162. https://doi.org/10.1016/j.cemconcomp.2009.01.005

Živica, V., 2007. Effects of type and dosage of alkaline activator and temperature on the properties of alkali-activated slag mixtures. Constr. Build. Mater. 21, 1463–1469. https://doi.org/10.1016/j.conbuildmat.2006.07.002

Zong, L., Fei, Z., Zhang, S., 2014. Permeability of recycled aggregate concrete containing fly ash and clay brick waste. J. Clean. Prod. 70, 175–182. https://doi.org/10.1016/j.jclepro.2014.02.040

Zuquan, J., Wei, S., Yunsheng, Z., Jinyang, J., Jianzhong, L., 2007. Interaction between sulfate and chloride solution attack of concretes with and without fly ash. Cem. Concr. Res. 37, 1223–1232. https://doi.org/10.1016/j.cemconres.2007.02.016

List of publications

Peer-reviewed journal papers

1. **G. Liu**, K. Schollbach, S. van der Laan, P. Tang, M.V.A. Florea, H.J.H. Brouwers. Recycling and utilization of high volume converter steel slag into CO_2 activated mortars – The role of slag particle size. Resources, Conservation and Recycling, 2020, Volume 160, page 1-9.
2. **G. Liu**, M.V.A. Florea, H.J.H. Brouwers. Characterization and performance of high volume recycled waste glass and ground granulated blast furnace slag or fly ash blended mortars. Journal of Cleaner Production, 2019, Volume 235, page 461-472.
3. **G. Liu**, M.V.A. Florea, H.J.H. Brouwers. Waste glass as binder in alkali activated slag–fly ash mortars. Materials and Structures, 2019, Volume 52, page 1-12.
4. **G. Liu**, M.V.A. Florea, H.J.H. Brouwers. Performance evaluation of sustainable high strength mortars incorporating high volume waste glass as binder. Construction and Building Materials, 2019, Volume 202, page 574-588.
5. **G. Liu**, M.V.A. Florea, H.J.H. Brouwers. The hydration and microstructure characteristics of cement pastes with high volume organic-contaminated waste glass powder. Construction and Building Materials, 2018, Volume 187, page 1177-1189.
6. Y.Y.Y. Cao, **G. Liu**, H.J.H. Brouwers, Q. Yu. Enhancing the low-velocity impact resistance of Ultra-High Performance Concrete by an optimized layered-structure concept. Composites Part B (accepted).
7. **G. Liu**, M.V.A. Florea, H.J.H. Brouwers. The role of recycled waste glass incorporation on the carbonation behaviour of sodium carbonate activated slag mortar (submitted).
8. **G. Liu**, K. Schollbach , P. Li, H.J.H. Brouwers. Valorization of converter steel slag into eco-friendly ultra-high performance concrete by ambient CO_2 pre-treatment (submitted).
9. **G. Liu**, Y.X. Chen, K. Schollbach, H.J.H. Brouwers. Low temperature synthesis of solid activator from recycled waste glass for one part alkali activated mortars (submitted).
10. **G. Liu**, M.V.A. Florea, H.J.H. Brouwers. The role of Na from recycled waste glass on the carbonation behaviour of alkali activated materials (in preparation).

Conference proceedings

1. **G. Liu**, M.V.A. Florea, H.J.H. Brouwers. Characterization and treatment of contaminated glass fractions as building materials. 6th International Conference on Non-Traditional Cement & Concrete . editor / E.V. Bílek ; Z. Keršner ; H. Šimonová. Brno, Czech Republic : NOVPRESS, 2017.
2. **G. Liu**, M.V.A. Florea, H.J.H. Brouwers. The hydration and micro-structure characteristics of cement replaced by high volume of an organic-contaminated waste glass fraction. The 9th International Symposium on Cement and Concrete (ISCC 2017), 31 October - 3 November 2017, Wuhan, China. 2017.
3. **G. Liu**, M.V.A. Florea, H.J.H. Brouwers. Sodium hydroxide/carbonate activated GGBS-fly ash mortars incorporating recycled waste glass. The 2nd International Conference of Sustainable Building Materials (ICSBM 2019), 12-15 August, Eindhoven, The Netherlands. 2019.

Curriculum vitae

Gang Liu was born in Shaanxi Province, China in July 21, 1988. After finishing his primary middle and high school educations in Xi'an, he started to study at Northwest Agriculture and Forestry University (NWAFU) in Xi'an in September 2006. In June 2010, he received his Bachelor's degree. In September 2013, he started to study at the College of Water Resource and Architectural Engineering (NWSUAF) as a master student supervised by Prof. Henghui Fan, majoring in Geotechnical Engineering and receiving his Master degree in June 2016. His research interests included the engineering properties of contaminated soil, deformation characters of dispersive soil and solidification methods of loess. In October 2016, he began his PhD study under the supervision of Prof. H.J.H. (Jos) Brouwers, Dr. M.V.A. (Miruna) Florea and Dr. K. (Katrin) Schollbach at Eindhoven University of Technology (TU/e), Eindhoven, the Netherlands. His PhD research includes application of recycled waste glass in sustainable building materials, and high-end application of converter steel slag in building materials.

The demand for solid wastes disposal such as industrial and domestic wastes, has gradually increased in recent years. As inorganic by-products, waste glass and steel slag cannot be used for energy recovery but only disposed in a landfill or p artially a pplied a s aggregates in road constructions. However, they can be utilized more valuable and eco-friendly in innovative building materials for a purpose of high-end application. Owing to the amorphous silicate structure of recycled waste glass, it can be used as the pozzolanic addition in conventional cement concrete and as the precursor in alkali activated geopolymer concrete, while converter steel slag exhibits a high reactivity in CO_2 environment. These properties provide the possibilities to design building materials with better performance and lower CO_2 emission compared to traditional concrete. This thesis aims to provide new application methods for innovative building materials by using recycled waste glass and converter steel slag as ingredients.

DEPARTMENT OF THE BUILT ENVIRONMENT

TU/e EINDHOVEN UNIVERSITY OF TECHNOLOGY